Université de Montréal

Catalytic Copolymerization of Ethylene with Various Olefins in Solution and in Emulsion

par
Kirill Skupov

Département de chimie
Faculté des arts et des sciences

Thèse présentée à la Faculté des études supérieures
en vue de l'obtention du grade de Philosophiae Doctor (Ph.D.)
en Chimie

Juin, 2009

Université de Montréal

Faculté des études supérieures

Cette thèse intitulée :

Catalytic Copolymerization of Ethylene with Various Olefins in Solution and in Emulsion

présentée par :

Kirill Skupov

a été évaluée par un jury composé des personnes suivantes :

Dr. William G. Skene, président-rapporteur

Dr. Françoise M. Winnik, directrice de recherche

Dr. Jérôme P. Claverie, co-directeur

Dr. Frank Schaper, membre du jury

Dr. Sandro Gambarotta, examinateur externe

Dr. Richard Leonelli, représentant du doyen de la FES

Résumé

Les copolymères d'éthylène avec des oléfines polaires et non-polaires ont été obtenus par polymérisation catalytique en solution et en émulsion en utilisant des catalyseurs à base de Ni et Pd. Des latexes des copolymères d'éthylène avec l'hexadécène ou undécénol ont été preparés par polymérisation en émulsion en utilisant un catalyseur à base de Ni formé *in situ*. Ces latexes peuvent former des revêtements par évaporation d'eau. L'adhesion des revêtements est améliorée par introduction d'unités d'undécénol. Le norbornène a été copolymérisé en présence d'éthylène en solution organique et en émulsion aqueuse, en utilisant des systèmes catalytiques mal définis à base de Pd et de phosphine d'aryl sulfoné. L'incorporation de norbornène peut atteindre 45 mol. %, ce qui produit des copolymères alternés. Les copolymères comportant plus de 15 mol. % de norbornène peuvent être utilisés pour la formation de revêtements à partir de formulation à base de solvants non aqueux. Les propriétés anticorrosives de ces revêtements ont été évaluées par EIS après le traitement dans une chambre Q-Fog.

Plusieurs catalyseurs bien définis à base de Pd ont été préparés pour la copolymérisation de l'éthylène avec des comonomères polaires. La réaction de l'acide 2-[bis-(2-méthoxyphényl)phosphanyl]-4-méthylbenzènesulfonique et de l'acide 2-[bis-(2',6'-diméthoxybiphényl-2-yl)phosphanyl]benzènesulfonique avec le diméthyl(N,N,N',N'-tétraméthyléthylènediamine) palladium(II), $PdMe_2$(TMEDA), mêne à la formation de catalyseurs à base de Pd, pontés par le TMEDA. Dans le cas des réactions avec la pyridine,

deux catalyseurs mononucléaires ont été isolés. Ces catalyseurs homocopolymérisent l'éthylène et copolymérisent l'éthylène avec les acrylates ou avec le norbornène. Des copolymères à hauts poids moléculaires ont été formés avec de hauts rendements en utilisant l'acide 2-[bis-(2',6'-diméthoxybiphényl-2-yl)phosphanyl]benzènesulfonique comme ligand. Des incorporations de comonomère plus hautes ont été obtenues en utilisant l'acide 2-[bis-(2-méthoxyphényl)phosphanyl]-4-méthylbenzènesulfonique.

Des copolymères d'éthylène avec la N-vinyl-2-pyrrolidinone (NVP) ou le N-isopropylacylamide (NIPAM) ont été preparés directement à partir des comonomères correspondants. La microstructure des copolymères obtenus a été characterisée par ^{1}H RMN et ^{13}C RMN, IR et DSC. Les copolymères linéaires possèdant un point de fusion élevé et leurs films ont un angle de contact faible pour l'eau. Ces propriétés pourraient être utiles pour les applications du polyétylène linéaire en peinture.

En utilisant le même catalyseur, l'éthylène a été copolymerisé avec des acrylates en solution et en émulsion. Les cinétiques de copolymérisation de C_2H_4 et de l'acrylate de méthyle en solution sont limitées par la réaction de substitution de la pyridine et par la σ-coordination de l'acrylate avec le Pd. La substitution de la pyridine par elle-même procède par un mécanisme d'association, avec des paramètres d'activation $\Delta H^{\neq}$ = 16.8 kJ/mol et $\Delta S^{\neq}$ = -98 J/(mol K). Les paramètres pour la substitution de pyridine par l'acrylate de méthyle sont $\Delta H^{\neq}$ = 18.1 kJ/mol and $\Delta S^{\neq}$ = - 87 J/(mol K). En utilisant ces catalyseurs à base de Pd dans des processus de polymérisation en émulsion, il a été possible d'obtenir

des latexes de copolymères d'éthylène avec des différents acrylates ayant des diamètres autour de 200 nm. Leurs contenus solides ne dépassent pas 5 %, à cause de la faible activité du catalyseur résultant de la coordination de l'eau et de la décomposition par l'eau du site actif du catalyseur.

Mots-clés : copolymérisation, catalyseur organometallique, polyéthylène, polyoléfines, polymérisation catalytique, polymérisation en émulsion, revêtements polymériques, latex, revêtements anticorrosifs, copolymères d'acrylates, copolymères de norbornène.

Abstract

The copolymers of ethylene with both, polar and non-polar olefins were obtained in solution and in emulsion catalytic polymerizations, using Ni- and Pd-based catalysts. Latexes of copolymers of hexadecene or undecenol and ethylene were prepared by emulsion polymerization using a Ni-based catalyst formed in-situ. These latexes may form polymeric films upon evaporation of water. Film adhesion may be improved by introducing undecenol units. Norbornene was copolymerized with ethylene in organic solution and in aqueous emulsion using ill-defined Pd-based sulfonated arylphophine catalytic systems. Norbornene incorporation could be as high as 45 mol. %, leading to copolymers which are alternating. The copolymers with > 15 mol. % of norbornene were suitable for the formation of solvent-based coatings. The resulting films were assessed for anticorrosion properties by EIS after treatment in a Q-Fog chamber.

Several well-defined Pd-based catalysts were prepared for the copolymerization of ethylene with polar monomers. Reaction of (2-[bis-(2-methoxy-phenyl)-phosphanyl]-4-methyl-benzenesulfonic acid and 2-[bis-(2',6'-dimethoxy-biphenyl-2-yl)-phosphanyl]-benzenesulfonic acid with dimethyl(*N,N,N',N'*-tetramethylethylenediamine)-palladium(II), $PdMe_2$(TMEDA) led to the formation of TMEDA bridged palladium based polymerization catalysts. Upon reaction with pyridine, two mononuclear catalysts were isolated. These catalysts were found to homopolymerize ethylene and also copolymerize ethylene with acrylates or with norbornenes. With the ligand 2-[bis-(2',6'-dimethoxy-biphenyl-2-yl)-

phosphanyl]-benzenesulfonic acid, high molecular weight polymers were formed in high yield. Higher comonomer incorporations were obtained with catalyst having the (2-[bis-(2-methoxy-phenyl)-phosphanyl]-4-methyl-benzenesulfonic acid ligand.

With this catalyst in hand, copolymers of ethylene with either N-vinyl-2-pyrrolidinone (NVP) or N-isopropylacrylamide (NIPAM) were prepared directly from the corresponding comonomers. The microstructure of the copolymers was characterized by ^{1}H and ^{13}C NMR, IR and differential scanning calorimetry. These linear copolymers are shown to combine a high melting point with a low contact angle with water – a fact which could potentially open the door to a directly paintable linear polyethylene.

Using the same catalyst, ethylene was copolymerized with acrylates in solution and in emulsion. The kinetics of the solvent based copolymerization of C_2H_4 and methyl acrylate were found to be limited by the reaction of pyridine substitution and by the σ-coordination of the acrylate on Pd. The substitution of pyridine by itself was shown to proceed via an associative mechanism with activation parameters $\Delta H^{\neq}$ = 16.8 kJ/mol and $\Delta S^{\neq}$ = -98 J/(mol K), whereas the activation parameters for the substitution of pyridine by methyl acrylate were found to be $\Delta H^{\neq}$ = 18.1 kJ/mol and $\Delta S^{\neq}$ = - 87 J/(mol K). Using these Pd-based catalysts in an emulsion polymerization process, latexes of copolymers of ethylene with various acrylates having particle diameters ~200 nm were obtained. Their solid contents did not exceed 5 % because of the low activity of the catalyst resulting from

the coordination of water and resulting from the slow decomposition of the active site by water.

Keywords: copolymerization, organometallic catalysts, polyethylene, polyolefins, catalytic polymerization, miniemulsion polymerization, polymer films, latex, anticorrosion coating, acrylate copolymers, norbornene copolymers.

Table of Contents

Chapter Two

Chapter Four

List of Tables

List of Figures

List of abbreviations

Ac	acetate
AC	alternating current
ADMET	acyclicdiene metathesis
AIBN	azobisisobutyronitrile
AN	acrylonitrile
ANSI	American National Standards Institute
ASTM	American Society for Testing and Materials
ATR	attenuated total reflectance
BA	butyl acrylate
BBN	9-borabicyclo[3.3.1]nonane
BF	bright field
BHT	butylated hydroxytoluene
BnA	benzyl acrylate
BP	bound pyridine
CA	contact angle
CA	cetyl alcohol
cat	catalyst
CCDC	Cambrige Crystallographic Data Center
CGC	constrained geometry catalyst
CHDF	capillary hydrodynamic fractionation
CMC	critical micelle concentration

COD	cyclooctadiene
CONTIN	constrained regularization method for inverting data
CTMA-Cl	cetyltrimethylammonium chloride
cp	cyclopentadiene
DAAA	diacetone acrylamide
DAB	1,4-diazobutadiene
dba	dibenzylideneacetone
DCBQ	dichlorobenzoquinone
DDM	dodecyl mercaptane
DF	dark field
DFT	density functional theory
DLS	dynamic light scattering
DMSO	dimethyl sulfoxide
DP	degree of polymerization
DSC	differential scanning calorimetry
EB	ethyl benzoate
EHA	2-ethylhexyl acrylate
E	ethylene
EIS	electrochemical impedence spectroscopy
EPDM	ethylene propylene diene M-class rubber

EPR	ethylene-propylene rubber
expt.	experiment
FID	free induction decay
Fig.	figure
FR	free radical polymerization
FP	free pyridine
FT	Fourier transformation
FTIR	Fourier transform infrared spectroscopy
GPC	gel permeation chromatography
HD	hexadecene
HDPE	high-density polyethylene
HMBC	heteronuclear multiple bond correlation
HT	high temperature
IMR	Instrumentation for Materials Research
ICI	Imperial Chemical Industries
IR	infrared spectroscopy
L	ligand
LALS	low angle light scattering detector
LCB	long chain branch
LDPE	low density polyethylene
LLDPE	linear low density polyethylene

LTM	late transition metal
MAO	methylalumoxane
MFFT	minimum film formation temperature
mDSC	modulated differential scanning calorimetry
MMA	methyl methacrylate
mon.	monomer
N, NB or NBE	norbornene
nsc	not completely soluble
n/d	not determined
NIPAM	N-isopropylacrylamide
NIST	National Institute of Standards and Thechnology
nm	not measured
NMR	nuclear magnetic resonance
NOE	nuclear Overhauser effect
NSERC	Natural Science and Engineering Research Council of Canada
NSF	National Science Foundation
NVP	N-vinyl-2-pyrrolidinone
ODCB	o-dichlorobenzene
OEM	original equipment manufacturer

P or p	pressure
PAFARC	Programme d'aide financière à la recherche et à la création
PDI	polydispersity index
PE	polyethylene
PEA	2-phenoxyethyl acrylate
PMMA	polymethylmethacrylate
PNBE	polynorbornene
PP	polypropylene
pol.	polymer
PS	polystyrene
py	pyridine
QELS	quasi-elastic light scattering
R	substituent
ref.	reference
RI	refractive index detector
ROMP	ring opening metathesis polymerization
R_p	polarization resistance
rpm	rounds per minute
rms	root mean square
RT	room temperature

S	solution
SAD	selective area difraction
SC	solid content
SDS	sodium dodecyl sulfate
SHOP	Shell Higher Olefin Process
SLS	static light scattering
SMA	stearyl methacrylate
T	temperature
tBA	tert-butyl acrylate
TEM	transmission electron microscopy
TEMPO	2,2,6,6-tetramethylpiperidine 1-oxyl
T_g	glass transition temperature
THF	tetrahydrofurane
T_m	melting temperature
TMEDA	N,N,N',N'-tetramethylethylenediamine
TO	turnover
TOF	turnover frequency
TON	turnover number
tol.	toluene
TPPTS	3,3',3''-phosphinidinetris(benzenesulfonic

	acid) trisodium salt
TriCBQ	trichlorobenzoquinone
UHMWPE	ultra-high molecular weight polyethylene
UQAM	University of Quebec at Montreal
UNH	University of New Hampshire
UV	ultraviolet spectroscopy
VC	vinyl chloride
VE	vinyl ether
VEOVA	vinyl versatate
VF	vinyl fluoride
VOC	volatile organic compounds
WCA	weekly coordinating anion
WinDNMR	Windows Dynamic Nuclear Magnetic Resonance
X	halogen

Things shoud be made as simple as possible,
but not any simpler

Albert Einstein

Aknowledgements

I would like to thank my advisors Françoise Winnik and Jérôme Claverie with whom I was working during my PhD studies at UdeM, UQAM and UNH.

I would like to thank Professor Jérôme Claverie with whom I was working the longer part of my PhD studies at UNH and UQAM, for his dynamism and a lot of help he provided me, especially at the beginning of my studies when it was extremely important. Professor Jerome Claverie encouraged me for deep studies of many domains of chemistry. The frequent discussions were very helpful for the progress of my project.

I would like to thank Professor Françoise Winnik with whom I was working under direct supervision at UdeM during the last year, for her high motivation, very helpful advises, and accessibility for discussions, which helped me to continue my project. I appreciate her ability to encourage me for finding solutions and possible ways of further developing my research.

I also would like to thank our collaborators from Rohm and Haas company: Brian Goodall, Lester McIntosh, David Conner, Nathan Allen, Suzanne Golisz for theoretical and practical help.

I am very thankful to my colleagues who worked on this project: Jason Hobbs, Pooja Marella, Laurence Piché, Jean-Christophe Daigle and Vladimir Kryuchkov who were always accessible for the help.

I also want to thank all the members of the research groups at UdeM, UQAM and UNH I worked with for their friendship and collaboration.

Finally, I want to thank my parents, Mikhail Skupov and Lyubov Skupova for their constant support and care given during my studies.

Chapter 1

General Introduction

A general overview on the polyethylene based polymers and its copolymers with polar and non-polar comonomers, their types of synthesis, preparation of their aqueous dispersions, their characterization, the usage of early and late transition metal complexes as the catalysts for olefin copolymerization.

1.1 Polyethylene

Historical overview. Polyethylene (PE) was synthesized for the first time by the German chemist Hans von Pechmann[1] in 1898, and he was then followed by Bamberger and Tschirner[2] in 1900. In both cases PE was produced by heating diazomethane, yielding what is strictly speaking polymethylene. In 1930, the unexpected polymerization of ethylene was reported by Friedrich and Marvel.[3] Later in the 1930s, Koch[4] and Carothers[5] reported the production of what might be PE by the action of sodium on decamethylene bromide followed by Fischer-Tropsch reduction of CO by hydrogen. In both cases the oligomers were obtained in the form of paraffin wax with a molecular weight lower than 2000 g/mol. The existence of PE was correctly recognized for the first time when Fawcett and Gibson obtained a waxy solid by reaction of ethylene with benzaldehyde.[6] The reaction was irreproducible until Perrin established the right set of conditions and thus obtained a polymer with a melting point of ~115 °C. Finally, the British company Imperial Chemical Industries (ICI) was awarded the first patent for ethylene production, and industrial production was started in the mid-thirties.[7] This polymer played a pivotal role in the development of dielectric materials used in radar manufacturing.

The catalytic polymerization of olefins has significantly simplified polyolefin production. Various novel polyolefin materials with tailored structures have been produced by advancing polymer processing technologies, reaction engineering and catalyst design. The latest point is important since changing the catalyst structure leads to drastically different product properties.

Up to 1953, ethylene was only polymerized by free radical process at high temperature (150 – 230 °C) and high pressure (1000 – 3000 atm). The resulting polymer was highly branched with broad molecular weight distributions.[8] In 1953 Ziegler found that ethylene could be polymerized at atmospheric pressure and room temperature using metal alkyls and transition metal salts such as ($AlEt_3$ + $TiCl_4$).[9] A year later Natta demonstrated the possibility of α-olefin catalytic polymerization with the production of isotactic polypropylene.[10] Despite the vast usage of this process, the mechanism of this heterogeneous polymerization is still unclear. It is believed that the polymerization proceeds according to the Cossee-Arlman mechanism in which the monomer coordinates to a vacant transition metal site *cis* to a metal alkyl bond, followed by insertion of the metal-alkyl bond across the double-bond, to regenerate a metal alkyl.

Ziegler-Natta catalysts are heterogeneous. In some cases a support, often based on anhydrous $MgCl_2$, is used for these catalysts.[11] It has been shown that $MgCl_2$ is an efficient support because of the similar coordination number and atomic size between Mg and Ti.[12] A typical recipe of a Ziegler-Natta catalyst contains the support ($MgCl_2$), the metal source ($TiCl_4$, etc.), one or two Lewis bases, called internal and external Lewis bases (siloxanes, phthalates, piperidines for example), and an alkyl aluminum.

Phillips catalysts, Cr/SiO_2, are heterogeneous catalysts for ethylene polymerization which were patented by Banks and Hogan in 1958.[13] Phillips catalysts are able to make more than 50 different types of high density and linear low density polyethylene.

Furthermore, the catalyst preparation and production process is simplified by the fact that these systems do not require activators.[14]

The evolution of Ziegler-Natta calalysis drastically changed with the discovery of metallocene catalysis. In 1980, Kaminski *et al.*[15] found that metallocenes, such as $ZrCp_2Cl_2$, activated by MAO, can polymerize ethylene with high activity. It was also shown that it is possible to prepare high molecular weight copolymers of ethylene and other α-olefins. The metallocene catalysis opened the door to the preparation of a wide variety of stereoregular and partially regular polymers and copolymers. Several, among those, are now industrially produced, such as syndiotactic polypropylene and syndiotactic polystyrene.[16, 17]

Constrained geometry catalysts (CGC) are hemimetallocenes which are active in incorporation of bulky olefins into polyethylene chain, for example, norbornene. For example, the titanium based catalyst $(Me_4Cp)(N\textit{t}Bu)TiCl_2$, when activated with MAO shows high activity in catalytic copolymerization of ethylene with norbornene.[18]

Although it is only seventy years-old, PE is the most important synthetic material, with a total production of approximately 70 million tons per year, whereas synthetic polymeric materials reach approximately 150 million tons per year.[19] There exist many different types of PE depending on the type and amount of branching, which affect the density, degree of crystallinity, melting point, processability and other physical properties of the polymer.

Early attempts to copolymerize ethylene and polar olefins. Early attempts to copolymerize ethylene with polar monomers (such as acrylates) using early transition metal catalysts were often unsuccessful.[20]. For example, the metallocene $Et[Ind]_2ZrCl_2$ could only copolymerize ethylene and 10-undecene-1-ol when the comonomer was pretreated with MAO.[21] Often the protection of the polar group was required, for example, oxygen-functionalized comonomers can be copolymerized with propylene with zirconocene catalyst when the atom of oxygen is shielded with alkyl groups. A long spacer between the double bond and functional group enhances the polymerizability of the comonomer.[22] Oftenly comonomers containing keto- or methyl ester groups were found to poison the zirconocene more effectively than alcohols.[23, 24]

The high pressures required and large excess of the Lewis acid used to overcome the "polymer backbiting" problem (backbiting refers to a process in which the carbonyl function of the last inserted acrylate unit chelates the catalyst center and thereby inhibits further monomer coordination and insertion) represents only a minor advance over work more than 30 years old in which 2 mol. % of acrylic acid was incorporated into isotactic polypropylene by protecting it with a readily available Lewis acid (diethylaluminum chloride).[25]

Because of high water-sensitivity of early transition metal complexes to water, the catalytic aqueous emulsion polymerization of ethylene with these systems seems unreachable. However, styrene polymerization was performed with a Ti-based metallocene catalyst in aqueous emulsion.[26] For that purpose, a prepolymerization was run for 30

seconds and then the prepolymerization solution contaning the catalyst the fluorinated borate activator, styrene and toluene was added to water with emulsifier. The authors claim that the catalyst is protected from water by the presence of crystalline syndiotactic polystyrene, but details about the polymer microstructure and the catalyst activity are not provided.

1.2 Late transition metal catalysts

Early catalysts (prior 1995). Besides early transition metals, late transition metal complexes, particularly complexes of Ni, Pd, Co and Fe are also known to catalyze ethylene polymerization.[27] There is a long history of Ni-based catalysts for ethylene oligomerization. For example, one can cite the Dimersol process,[28] where a nickel-based catalyst catalyzes the dimerization of propene and butene to hexenes and octenes. More sophisticated catalysts which do not require Lewis acid activation and are able to function in polar solvents such as butanediol, were prepared by Keim.[29, 30] These catalysts, based on chelating P,O-ligands, (complexes 1 and 2) generate very low molecular weight products (M_n up to 400 g/mol).[31] Complex 2 is commercially used in the Shell Higher Olefin Process (SHOP) for the synthesis of α-olefins from ethylene.[32]

If the phosphine from complex 1 is abstracted by a phosphine sponge such as $Ni(COD)_2$ or $Rh(acetylacetonate)(C_2H_4)_2$,[33] the catalyst can switch from oligomerization to polymerization. Accordingly, Klabunde[34] and Ostoja-Starzewski[35, 36] prepared a series of triphenylphosphine free catalysts and found that they promote polymerization versus

oligomerization (complexes 1(D), 3 and 4). At the time Klabunde and Ostoja-Starzewski reported their findings, no definite explanation was offered to shed light on the increase in molecular weight resulting from the removal of phosphine. In fact, the original intent of Klabunde was to remove the phosphine in order to increase activity, since both phosphine and ethylene compete for the coordination site *cis* to the alkyl group.

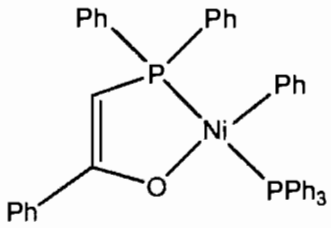

Complex 1

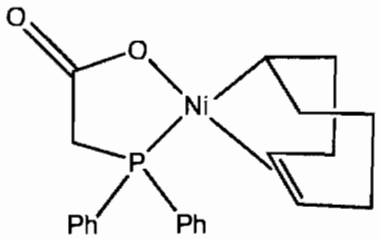

Complex 2

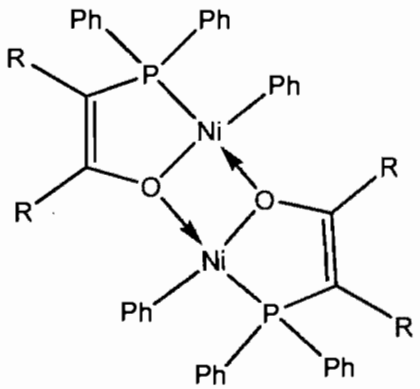

Complex 1(D)

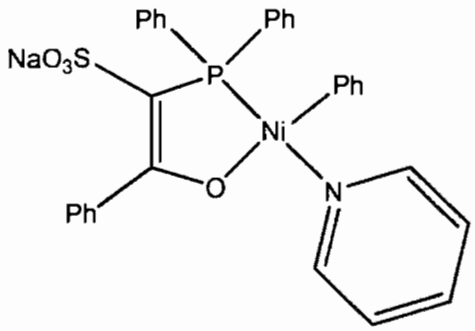

Complex 3

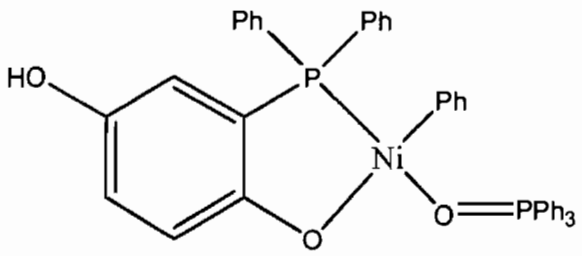

Complex 4

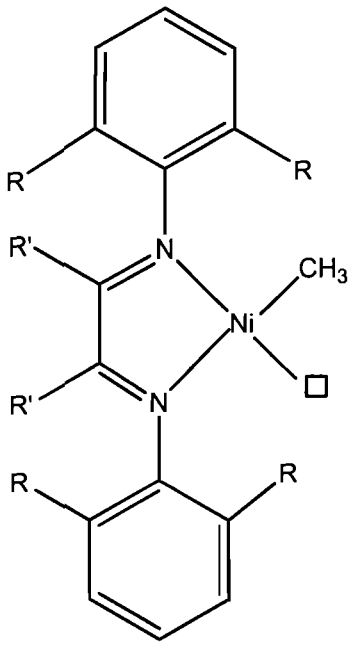

Complex 5

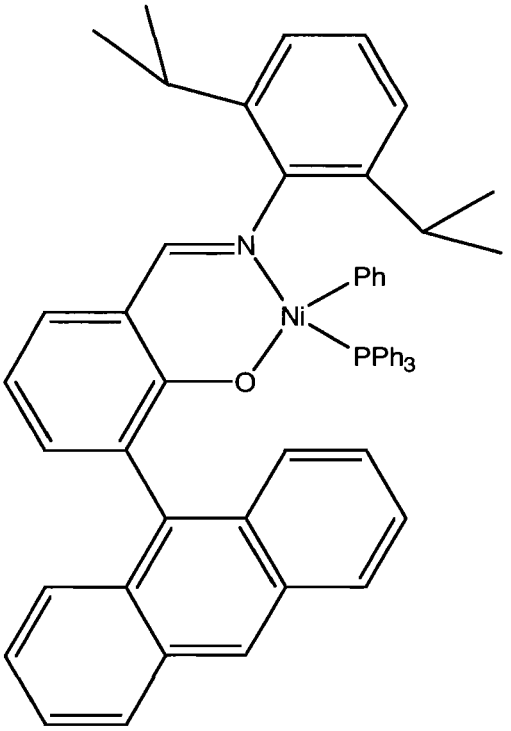

Complex 6

Brookhart and Grubbs systems. A possible explanation of molecular weight increase was provided by Brookhart with the discovery in 1995 of cationic N,N-diimine Pd- and Ni-based catalysts (complex 5).[37] These square planar catalysts yield high molecular weight polyethylene when their axial faces are sterically hindered. Brookhart indeed demonstrated that the chain transfer reaction occurs via an associative mechanism involving the axial coordination site: when it is not accessible, the rate of chain transfer decreases and molecular weight increases. For the Keim complexes, the axial faces are totally accessible, resulting in low molecular weight products.

Preparation and activation of the Grubbs and Brookhart catalysts. Grubbs reported a series of highly active sterically-hindered N,O-ligand based catalysts (Complex 6) generating high molecular weight polyethylenes. Unlike the Brookhart cationic diimines complexes, the N,O-chelated salicylaldimine nickel complexes need a phosphine scavenger ($Ni(COD)_2$) in order to be active.[38, 39] For the N,N-α-diimine complexes, several situations arise. They can be formed by reaction of the nickel dibromide precursor and an alkylating agent such as MAO (in an excess of 100 to 1000), yielding a catalyst which is active at 35 °C.[40] Alternatively, a precursor of the catalyst, obtained by directly reacting the ligand and $NiBr_2$, can be alkylated with $MgMe_2$, and activated with MAO.[40]

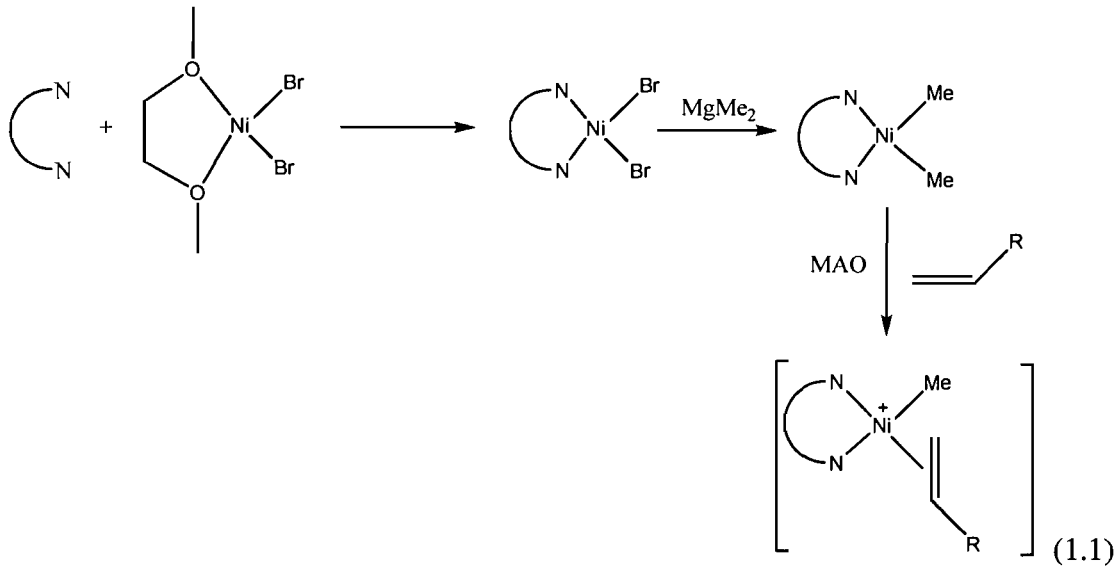

(1.1)

Well-defined catalysts have been isolated for palladium diimines (see below). In this case, it is necessary to use a weakly coordinating anion (WCA) as counter ion in order to increase the electrophilicity of the catalyst, increase the catalytic activity, and improve

the accessibility of the olefin to the active site.[37]. Introduction of the WCA can be achieved by anion metathesis on the monohalogenated complex[41] or protonolysis of the dimethylated complex. [42]

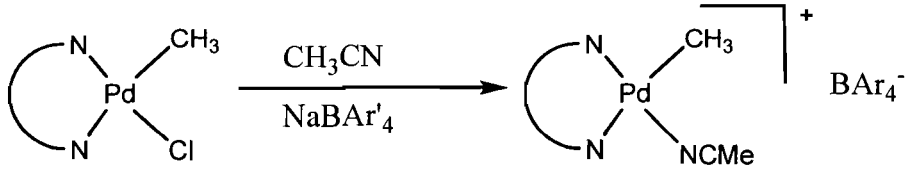

(1.2)

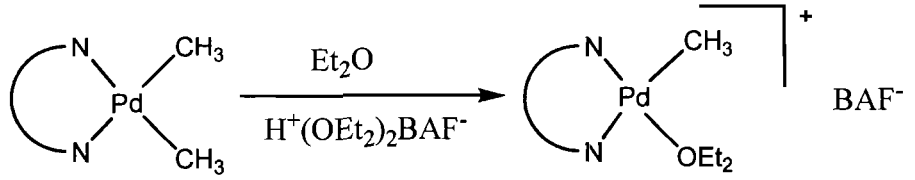

(1.3)

Both complexes above are stabilized by a Lewis base (ether, acetonitrile), but is possible to isolate the catalyst without it. For example, in the presence of methylacrylate, a chelate complex can be readily isolated and used as catalyst.[42]

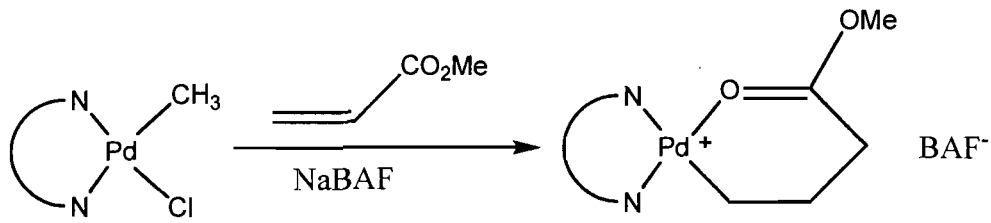

(1.4)

Allyl forms of the catalyst can also be formed from [(DAB)Ni(η^3-allyl)]$^+$. [42]

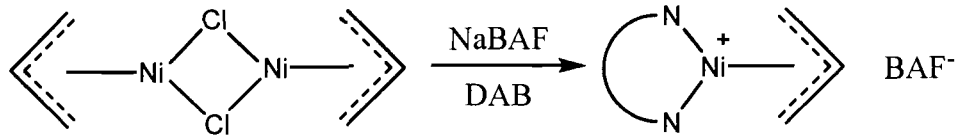

(1.5)

Polymerization mechanism. The polymerization mechanism by cationic palladium diimines was extensively studied, both experimentally (mostly by low temperature NMR),[43] and theoretically (mostly by DFT[44] calculations).[45, 46] (Figure 1.1) When weakly coordinating anions are used, the rate limiting step is the insertion of the ethylene-bound complex to Pd – C bond, which translates into a zero order kinetics of polymerization in ethylene. The chain grows by the usual sequence of ethylene coordination followed by migratory insertion. The resulting Pd-alkyl complex is stabilized by a strong β-agostic effect. It is in equilibrium with the Pd-hydride complex formed by β-hydride elimination. However, the Pd-hydride complex may reinsert, either to regenerate the initial Pd-alkyl complex, or to form a branched Pd-alkyl complex. The sequence of β-hydride eliminations and reinsertion steps are the basis of the chain walking reactions which in effect 'reorganize' the architecture of the polymer chain, creating branches along the backbone. These branches are randomly distributed along the polymer chain, shorter branches being always more frequent than longer ones (C1 > C2 > C3...).[47] Branching of polyethylene made by Ni-based Brookhart catalysts was analyzed by the Monte-Carlo simulations.[48] The activation barriers for migratory insertion of cationic Pd diimines are in the range of 17-18 kcal/mol,[49] whereas they are in the range of 13-14 kcal/mol for Ni catalysts,[50] which accounts for the higher activity of Ni-based catalysts and also for the fact that Ni catalysts yield less branched and more crystalline polymers. Very often, Pd-based catalysts produce amorphous and highly branched polymers with glass transition temperatures in the range of -60 to -70 °C.[51]

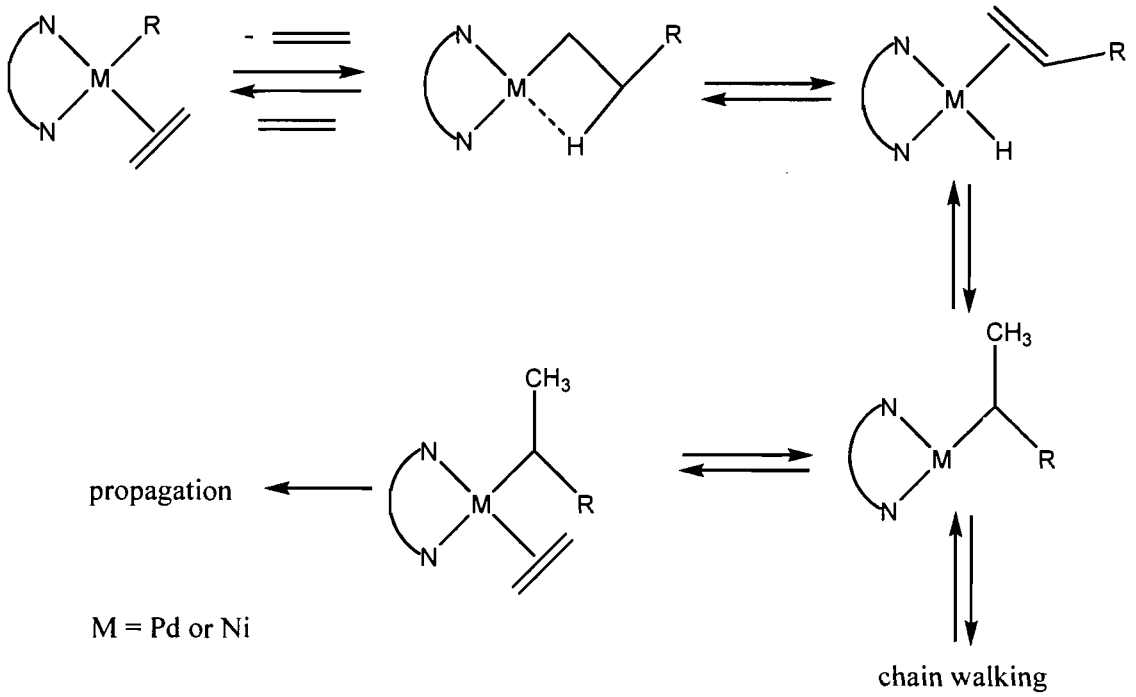

Figure 1.1: Mechanism of ethylene polymerization and branch formation as a result of chain walking for N,N-α-diimine Pd and Ni catalysts.

As stated above, the main process regulating chain transfer, and therefore the molecular weight distribution, is the steric hindrance in the axial sites of the metal. As shown by X-Ray diffraction, these α-diimine complexes are square planar with aromatic rings placed perpendicular to this plane.[52] The ortho-substituents of these aromatic rings are located directly above and below the metal atom, creating steric bulk hindrance in the axial position. Two possible modes of chain transfer have been postulated for α-diimine complexes: associative displacement and direct β-hydride transfer to the monomer (Figure 1.2), both of which involve a penta-coordinate transition state. Calculations for the Ni-

system indicate that chain transfer occurs through direct β-hydride transfer to monomer from the alkyl-olefin resting state,[53] however, for Pd-systems, associative displacement seems to be more favorable (Figure 1.2).[45] Depending on the catalyst and reaction conditions, oligomers up to high molecular weight polymers (M_w > 1 000 000 g/mol) can be obtained with Ni and Pd based diimines.[52, 54]

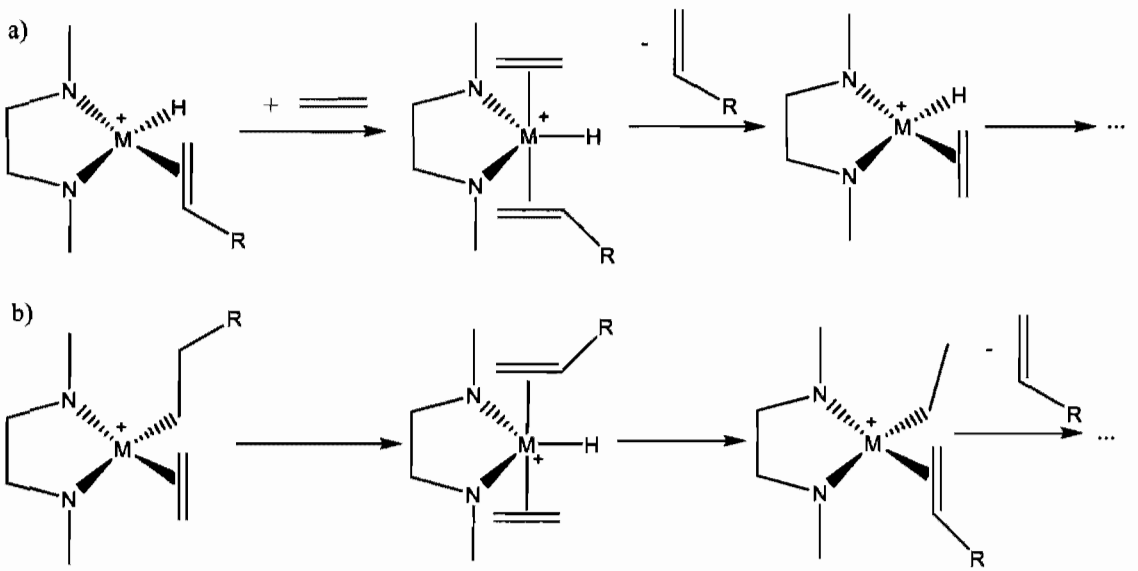

Figure 1.2: Two routes of chain transfer. a) associative displacement; b) direct β-hydride transfer to monomer.[55]

The cationic Brookhart Pd(II) and Ni(II) α-diimine catalysts are not only active for the polymerization of ethylene, but they can also be used to incorporate α-olefins,[37] norbornenes,[56] and even internal olefins.[57] For the polymerization of the internal olefins, the catalyst 'rectifies' the structure via chain-walking, producing lower and shorter branching than expected.[58]

The Grubbs Ni(II) catalyst yields a polymer which is quite linear (< 50 br/1000 C), indicating that chain-walking is not important for this catalyst.[38] It can copolymerize norbornene and functionalized norbornenes (with $-OC(O)CH_3$ or –OH groups) with ethylene.[39]

Iron and cobalt based catalysts. Brookhart and Gibson independently found that Fe and Co pyridine-diimine complexes produce highly linear high density polyethylene (Complex 7).[59, 60] Molecular weights of polyethylene were reported to be in the range of 14 000 – 611 000 g/mol. The Fe-based catalyst was an order of magnitude more active than the Co-based one.[61] These catalysts have several advantages due to their lower toxicity and lower cost comparatively to Ni and Pd-based systems. By reducing the bulk on this type of catalysts, polymerization can be switched to oligomerization with high selectivity.[62] However, these catalysts are only active in the presence of large excesses of MAO. Gibson *et al.* proposed that dicationic Fe(III) alkyl species $[LFe - R]^{2+}$ or chloro, alkyl species of Fe (III) $[LFe(Cl)(R)]^{+}$ could be the active species for these catalysts.[63] Now it is generally accepted that the trialkylaluminium and MAO bind Fe to give catalytically neutral species.[64]

Other Ni and Pd based catalysts. Numerous other Ni and Pd-based catalysts for ethylene polymerization have been described, but within studies which are less exhaustive than for the Grubbs and Brookhart's catalysts. Some of them are presented below. Branched olefins $C_8 - C_{24}$ were obtained with the cationic complex 8, $(B(C_6F_5)_4^-$ was used as a counterion), with an average of 1 branch per 20 carbons when the polymerization was carried out at 1 atm at 23 °C.[65] Using Complex 10 (R is *o*-tolyl and L is PPh_3) oligomers of ethylene were produced.[66] Ethylene was also polymerized with complex 11, yielding a completely amorphous polymer with 70 Me branches per 1 000 C and M_n = 1500 g/mol.[67] Complex 12, when activated with 200 equivalents of MAO, produces polyethylene with M_n 15 000 – 40 000 g/mol when reaction is carried out at pressure 1 – 50 bars and temperature 25 – 50 °C.[68]

Some of these complexes are also able to insert higher olefins. For example, 3,3-dialkylcyclopropenes can be polymerized with complex 9, producing a polymer with M_n > 10 000 g/mol.[69]

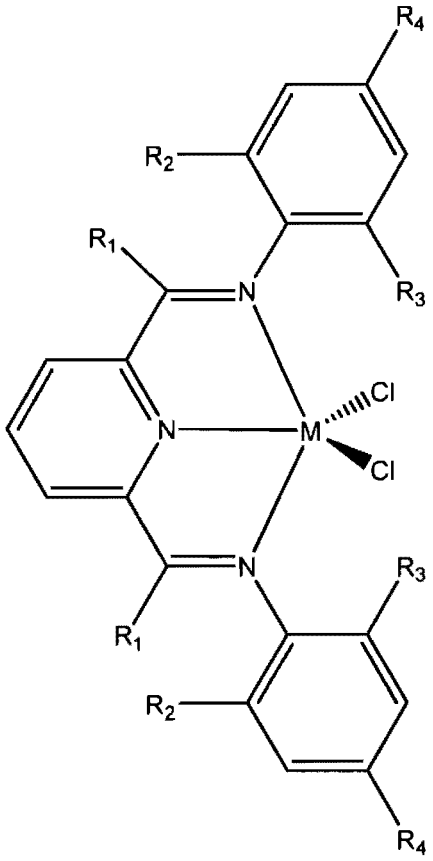

M = Co, Fe

R_1, R_4 = Me or H
R_2, R_3 = Me or i-Pr

Complex 7.

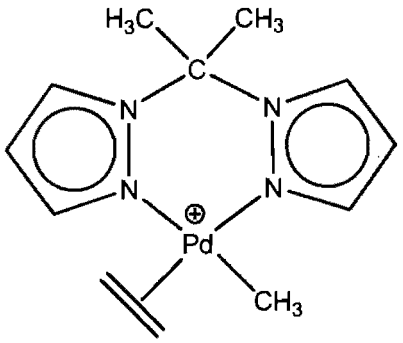

Complex 8

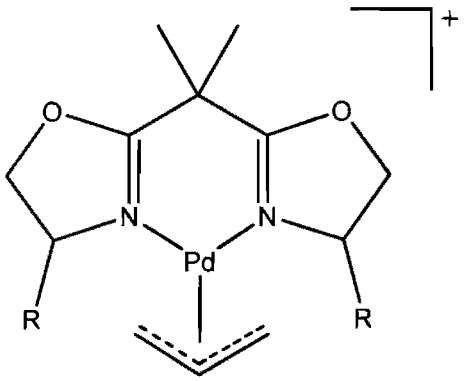

SbF_6^-

Complex 9

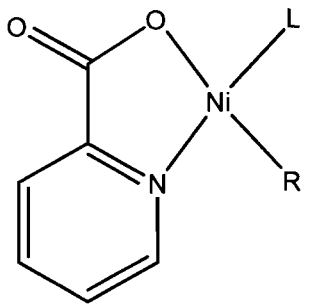

Complex 10

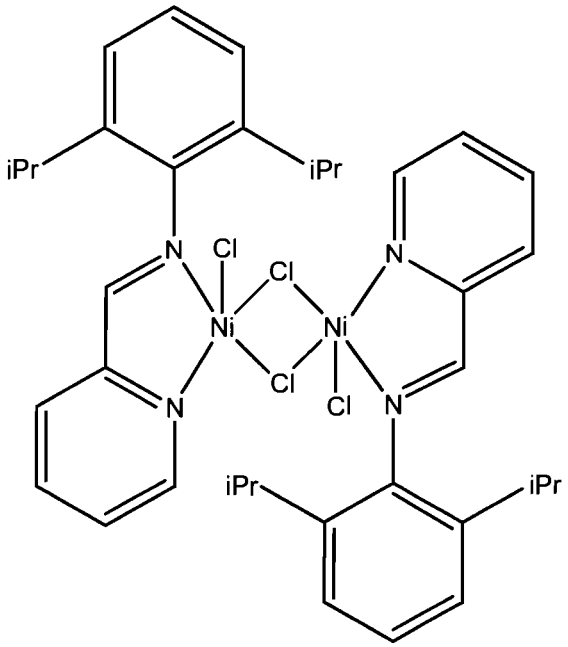

Complex 11

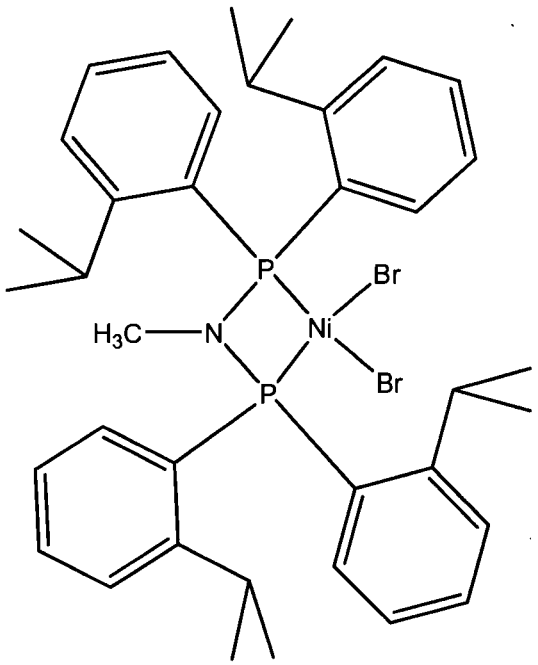

Complex 12

1.3 Catalytic copolymerization of ethylene with vinyl polar monomers

Usually vinyl substituted polar monomers $H_2C=CHX$, such as acrylates, vinyl acetate and acrylonitrile, are homo- and copolymerized by radical route. The use of transition metal complexes as catalysts for copolymerization of polar monomers with ethylene is of high importance since polar groups impart to the polymer properties such as solvent resistance, adhesion, toughness, paintability, rheological properties, etc. Catalytic copolymerization would allow control over polymer architecture and molecular weight distribution and it would open the door to a series of novel materials.

In 1987, a Ni-based catalyst (Complex 3) capable to copolymerize ethylene with olefins was reported.[34] It could tolerate esters, trimethylsilyl – protected acids, fluoro substituents and ketones. However, for the copolymerization to occur, the functional group had to be placed in a position remote from the double bond: vinyl acetate and methyl methacrylate were not inserted by this catalyst. Gibson *et al.*[70] found that the P,O-chelated Ni-based Catalyst 13 is able to incorporate methyl methacrylate in the reaction of propylene polymerization, producing a polymer (M_n = 3 800 g/mol, PDI = 2.3) with a MMA group as chain end.

A breakthrough in the field happened in the mid 1990s when Brookhart *et al.* discovered Ni^{II}- and Pd^{II}-based α-diimine complexes for olefin polymerization,[37] and for copolymerizing olefins with various acrylates. [43]

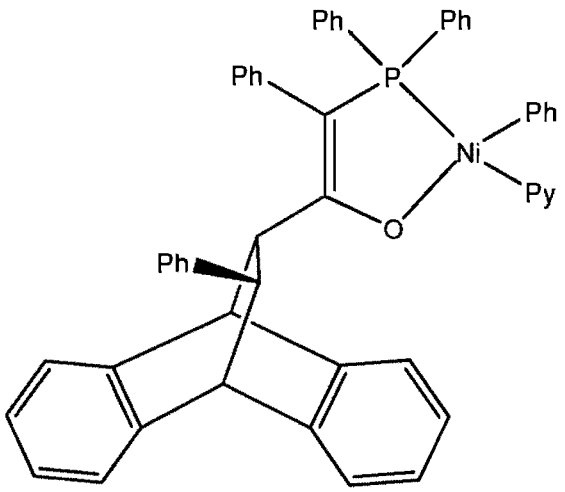

Complex 13.

Due to the mechanism of "chain walking", the polymer is highly branched and amorphous. It was also found that these catalysts place the acrylate moiety predominantly on a branch or on the main chain end.[43] In principle, polymerization with (N^N)NiR$^+$ may lead to linear E-MA copolymers, however, this reaction is slow and proceeds only at high temperatures.[71] The possibility of silyl vinyl ethers incorporation was shown with (N^N)PdMe$^+$ catalyst,[72] after it was found that the N,N-α-diimine catalyst is capable to insert up to 3 sequential units of $CH_2CHOSiPh_3$. At the same time, other important monomers such as vinyl acetate, acrylonitrile or vinyl chloride cannot be copolymerized with these cationic organometallic complexes. For vinyl chloride (VC) it likewise that the catalyst is capable to insert VC, but β-Cl elimination prevents the polymerization.[73] β-Acetate elimination occurs after the insertion of vinyl acetate.[74] The high stability of the M – O and M – Cl adducts is the most likely driving force for this process.[75] For

acrylonitrile, the catalyst becomes poisoned via formation of N-bound complex, with no further insertion occurs at 23 °C.[76] Insertion of one acrylonitrile molecule was observed also with Pd-based N,O-chelated salicylaldiminato complexes.[77] For the N,N-chelated Brookhart catalysts which may insert acrylonitrile, theoretical studies by the DFT method were performed.[78] Furthermore, some recent NMR studies of cationic species of (N^N)PdMe$^+$ with polar monomers have unveiled possible mechanisms to account for the difficulties of polar monomer copolymerization.[74] In this mechanism (Figure 1.3), the first step is π-coordination of the carbon-carbon double bond (either of ethylene or of the polar monomer). This reaction competes with the coordination of the polar group, blocking further polymerization. In terms of π-coordination, binding of ethylene is more favorable, compared to binding of the polar olefin because of its stronger π-donating capability and lower steric demand. However, polar monomers undergo insertion more easily than ethylene ($k_1 > k_2$) because of the electron-poor nature of the first double bond in the polar monomers (destabilization of the ground state). In general, the interplay of these factors determines the final copolymer composition. For acrylonitrile the significant σ-X coordination of the nitrile group predominates over π-coordination of the olefinic double bond. According to Ziegler,[46, 79] it was found using the DFT method that more electrophilic metal centers, (N^N)NiMe$^+$, undergo formation of σ -X coordination of polar olefin, which is slightly more favourable (the difference in binding energies between C=C π-binding and O σ-binding (ΔE(C=C) - ΔE(O)) was 0.68 kcal/mol). For the Pd-catalyst the π-complex

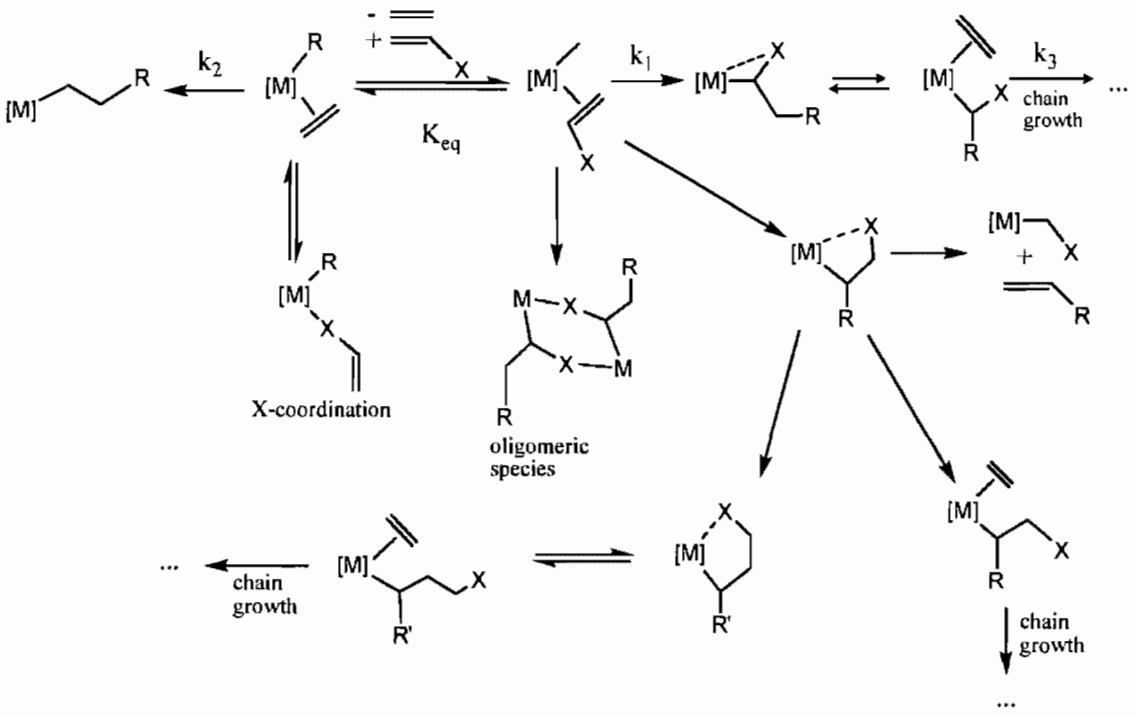

Figure 1.3: Reaction steps in the copolymerization of ethylene with polar-substituted olefins $H_2C=CHX$.[75]

with the olefin was found to be more stable than for the Ni-based one($\Delta E(C=C) - \Delta E(O)$ was -5.16 kcal/mol).

In the experiments with vinyl acetate,[74] σ-X coordination and π-coordination were observed approximately in equal extent with slight disfavour of O-coordinated complex for (N^N)$NiMe^+$ catalyst (by 0.7 kcal/mol). After 2,1-insertion of the polar olefin, further insertion and chain growth (k_3) can become difficult because of the presence of the polar unit X on the α-carbon atom which impedes sterically the approach of another monomer and can even form a stable chelate with the metal. In the latter case, β-hydride elimination and olefin reinsertion may place the polar X-groups on β- and γ-carbons, as in the case of acrylate polymerization.

Pugh *et al.*[80] discovered the first catalytic system capable to incorporate methyl acrylate in the main chain. It is formed *in situ* from $Pd_2(dba)_3$ or $Pd(OAc)_2$ and a sulfonated phosphine ($Ar_2PC_6H_4SO_3H$) and yields linear methyl acrylate – ethylene copolymers (absence of chain walking). The catalysts based on sulfonated phosphines are now studied very intensively. Since the beginning of my PhD research in 2004, many new articles have appeared on this type of catalysts. DFT studies of the catalyst show that the complex is prone to catalyze the formation of linear chains due to the high barrier for the formation of secondary alkyl-Pd intermediates.[81] The first well defined catalyst of this type was prepared by Rieger *et al.*[82] in 2005 (Figure 1.4), and it was used for copolymerization of ethylene with CO. Jordan showed that the catalyst may exist as a dimer, which may form as a result of the reaction of the catalyst with $B(C_6F_5)_3$ (Figure 1.5). The dimer is formed as a result of

pyridine abstraction and Pd – O coordination.[83] In 2006 Nozaki published an anionic form of the same catalyst used for the copolymerization of ethylene with MA.[84] The general structure of a well-defined catalyst of this type with various possible substitutes (including those developed by us) is shown on Figure 1.4.

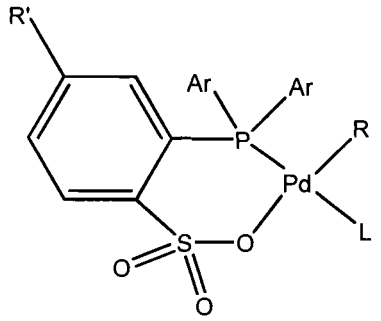

Ar = 2-$MeOC_6H_4$; 2,6-$(MeO)_2C_6H_3$; Ph;
R' = H, Me
R = Me, CH_2Ph, CH_2t-Bu, CH_2SiMe_3
L = pyridine, lutidine, 1/2 $Me_2NCH_2CH_2NMe_2$, DMSO; piridazine, PPh_3,
R,L = 6,7-tricyclo[5.2.1.$0^{5,9}$]-deca-6-ene-3-ethoxy-2-yl;
C,O-coordinated *C*(Et)OC(*O*)Me; allyl

General structure of the catalyst[75, 82, 83, 85-88]

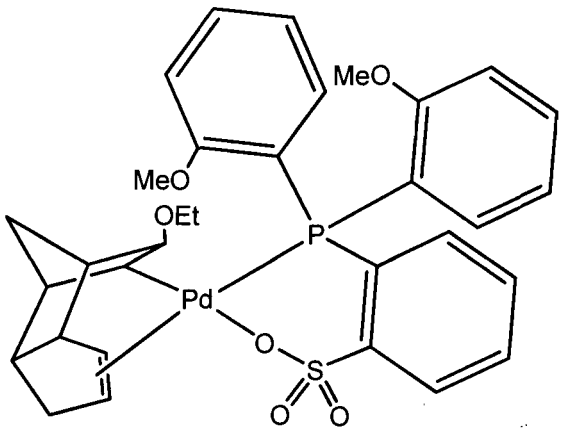

Rieger's catalyst

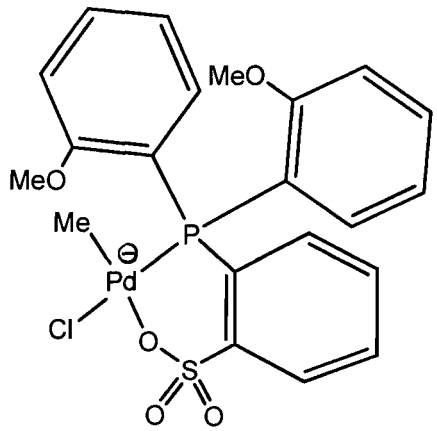

Nozaki's catalyst

Figure 1.4: Structures of the Pd-based sulphonated arylphosphine catalysts.

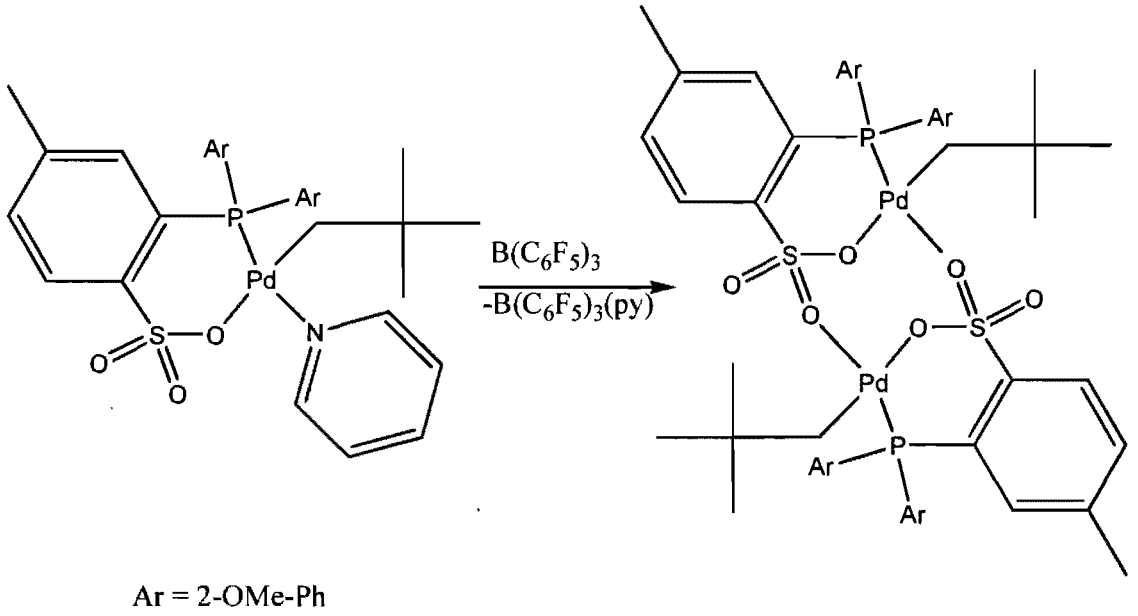

Ar = 2-OMe-Ph

Figure 1.5: Dimer formation and general structure of well-defined Pd-based P,O-chelated catalyst.[83]

Copolymerization of functionalized norbornenes with ethylene, with up to 40 mol. % of incorporation, was reported by Sen[88] in 2007 using *in situ* catalyst, formed from $Pd(dba)_2$ and P-O sulfonated aryl phosphine ligand.

Ni-based sulphonated aryl phosphine P,O-chelated complexes are also known for the synthesis of polyethylene. [P^O]Ni(η^3-benzyl) base free complexes may function as single component ethylene polymerization catalysts.[89] Linear polymers (~10 br / 1 000 C) with M_n of 1 000 – 2 000 were produced.

The catalytic polymerization of ethylene with acrylonitrile using Pd-based catalyst was reported recently.[86] The units of AN are distributed both along the polymer chain and on the end groups. Polymers contained up to 9 mol. % of AN with M_n of $10^3 - 10^4$ g/mol. It was suggested that chain transfer occurs after the insertion of AN unit which results in a decrease of molecular weight. Under the employed conditions for this process (100 °C, 30 atm, 120 h) the reaction was slow with the average activity ~10 TO/h. The decrease in the reaction rate was probably due to σ-coordination of AN with the catalyst. Vinyl ethers (VE) can be also incorporated with up to 6 mol. % of incorporation.[90] The M_n of the copolymer reached 5 000 g/mol with average activity of the catalyst 350 TO/h. Even challenging monomers such as vinyl fluoride can be incorporated in an amount of incorporation as 0.5 mol. %.[91] Block copolymers of ethylene and CO, $[(CH_2CH_2)_x$-*block*-$(CH_2CH_2CO)_y]$ can be also produced. By changing the monomer ratio during polymerization, non-alternating ethene/CO copolymers with CO content < 50 mol. % were produced at 70 °C, 60 atm with an activity of 20 TO/h.[92]

1.4 Miniemulsion polymerization

Types of emulsion polymerization. Emulsion polymerization is widely used industrially because it offers many advantages, the main one being the use of environmentally-friendly water as dispersing phase. Additionally, the high heat capacity of water provides effective heat transfer during polymerizations which are exothermic. The viscosity of latex is very low in comparison to the viscosity of a polymer dissolved in a solvent. The use of latexes is a convenient method to handle sticky and tacky polymers (i.e. polymers having T_gs below room temperature), since the tackiness only appears once the water is evaporated. Accordingly, latexes are widely used in the coatings and adhesives application sectors.

At least three types of emulsion polymerization are known, which are named macro-, mini- and microemulsion polymerization.[93] Macroemulsion polymerization is the conventional emulsion polymerization process which starts with large monomer droplets generated upon stirring. The monomer diffuses from monomer droplets to micelles through the aqueous phase during polymerization. With this technique, polymer particles having a diameter of 50-500 nm are obtained.

Another type of heterophase process is microemulsion polymerization.[94] In this case, all the monomer is initially located into micelles. High amounts of surfactant are necessary for their preparation, since the loading capacity of micelles is limited. The polymerization results in particles with a size of 5 – 50 nm, most often in coexistence with empty micelles.[95]

In miniemulsion polymerization, the polymerization occurs in relatively stable droplets, 50-500 nm in size.[96] These droplets can be polymerized and the diffusion of monomer through the water phase can be lowered by adding a hydrophobe (see below). Unlike microemulsions which are thermodynamically stable, miniemulsions are only metastable. In conventional (macro)emulsion polymerization, once the particles are nucleated the monomer has to diffuse through the aqueous phase to sustain polymerization. This precludes the polymerization of very hydrophobic monomers, for example vinyl versatate (VEOVA).[97] The necessity of mass diffusion can be eliminated if a large fraction of the monomer droplets are nucleated. This situation may happen if the total surface area of the monomer droplets is very large as in the case of submicron size monomer droplets, which is the basis for miniemulsion polymerization.

Two mechanisms of miniemulsion destabilization exist: Ostwald ripening (τ_1-process) which cannot be totally suppressed and the collisions of droplets (τ_2-process).[98] The collision process is accelerated when miniemulsions are stirred for prolonged periods.

Stabilization by surfactants. Ugelstad[99] was the first to demonstrate that by using the surfactant and cosurfactant mixture of cetyl alcohol and SDS at 60 °C, a miniemulsion of styrene in water could be formed, which could then be polymerized. This miniemulsion was found to be stable for two weeks. In general, miniemulsions are stable for several weeks.[100] Miniemulsions can be prepared with a variety of surfactants.[101, 102] The amount of surfactant required for miniemulsion stabilization is lower than for microemulsions.[93]

Increasing the amount of surfactant allows the formation of droplet with smaller size. The influence of different surfactants on the emulsion droplet size is shown on a Figure 1.6.

After polymerization it was found that a large number of polymer particles were produced by droplet nucleation. The reason for the droplet stability in this system still remains unclear. Droplets stabilized by SDS alone are not stable because surfactant molecules adsorbed on the droplet are exchanging rapidly with surfactant in the aqueous phase. This exchange process is due to the strong electrostatic repulsion between tightly packed anionic SDS end-groups at the water-droplet interface.

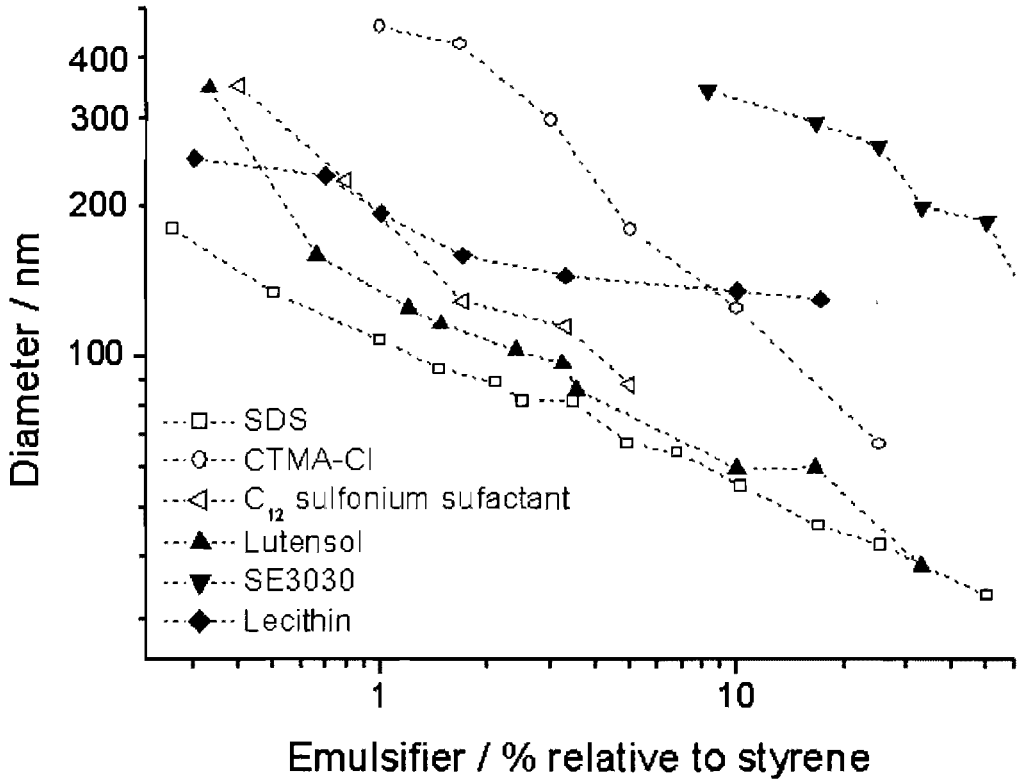

Figure 1.6: Surfactants for the formulation of miniemulsions. (According to[101, 102].)

Effect of hydrophobe on miniemulsion stability. Ostwald ripening is the phenomenon whereby smaller droplets disappear whereas larger ones increase in size. Addition of small amounts of a water-insoluble compound such as hexadecane will stop the Ostwald ripening (Figure 1.7). Indeed, if allowed to proceed, this would result in the formation of droplets of pure hexadecane (which does not diffuse through aqueous phase) and large droplets of emulsified liquid. The stabilization is achieved due to osmotic pressure which would force back the emulsified liquid (which is diffusing through the aqueous phase) into the droplet of pure hexadecane in order to lower hexadecane concentration in the droplet.

This low molecular weight water-insoluble compound is called a hydrophobe, and sometimes it is wrongly referred as a cosurfactant.

Cetyl alcohol (linear alcohol in C_{16}) is believed to intercalate in between SDS molecules at the interface, thus attenuating these anionic repulsions, and allowing the formation of smaller droplets.[103] Davis and Smith[104] found that emulsions of light petroleum and benzene stabilized by a surfactant can be rendered stable by addition of small amounts of hexadecane. It was suggested by Higuchi[105] that hexadecane may prevent Ostwald ripening - the process by which emulsions separate into two separate phases. Various hydrophobes can be used, being of low molecular weight (for example hexadecane, fluorinated compounds, silanes) or high molecular weight (for example polystyrene, polyesters), as long as they are soluble in the emulsified phase.[103] Chern and Chen prepared styrene miniemulsions using four different costabilizers: hexadecane, stearyl methacrylate

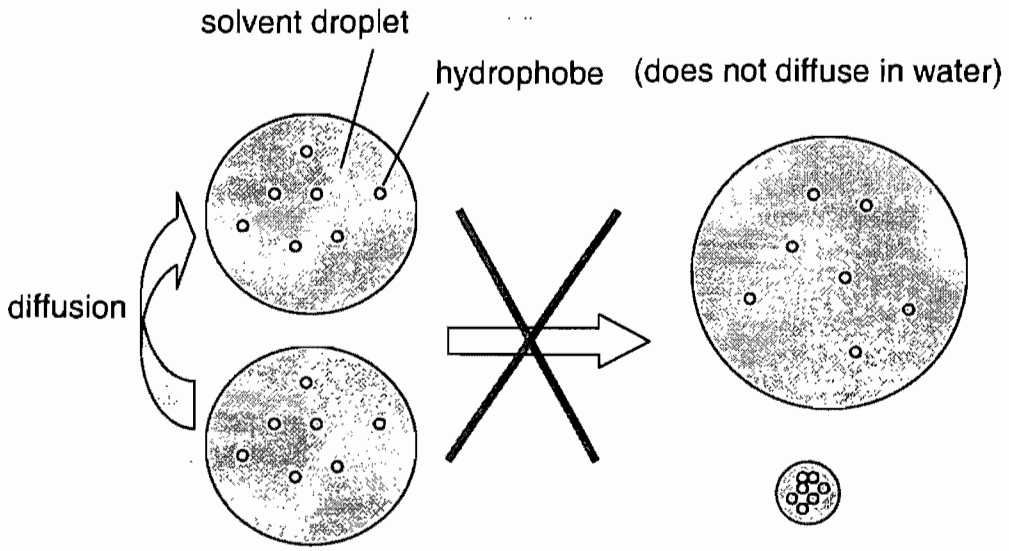

Figure 1.7: Scheme of the use of hydrophobe in the suppression of Ostwald ripening.

(SMA), dodecyl methacrylate (DMA) and cetyl alcohol (CA).[106] The effectiveness of the hydrophobe depends on its solubility in water. The less hydrophobic CA and DMA show droplet and homogeneous nucleation in styrene polymerization, while the more hydrophobic SMA and hexadecane show predominantly droplet nucleation. The solubilities in water of the hydrophobes were found to be: CA ($5.77 \cdot 10^{-8}$ mL/mL) > DMA($1.38 \cdot 10^{-8}$ mL/mL) > SMA($3.23 \cdot 10^{-9}$ mL/mL) > hexadecane ($1.14 \cdot 10^{-9}$ mL/mL).

It was found that when the chain length of the hydrophobe increases, the miniemulsion stability also increases.[107] Polymers also can be used as hydrophobes in the case when they are soluble in emulsified liquid ant insoluble in water.[108] Molecules such as dodecyl mercaptane (DDM) also can be used as hydrophobe yielding miniemulsions that are stable for periods of 17 h to 3 months.[100] Relatively stable miniemulsions of styrene can be prepared by using water-insoluble low molecular weight blue dye (Blue 70) as a hydrophobe.[109]

Miniemulsion formation. Unlike a microemulsion, which is formed spontaneously, the formation of miniemulsion requires a large input of energy to the system, usually under the form of mechanical agitation. Two main mechanical devices are used for this purpose: the ultrasonicator and the microfluidizer. The ultrasonicator is a sonic probe of high power. During the sonication, the sound waves propagate into the liquid. This results in alternating high-pressure (compression) and low-pressure (rarefaction) cycles, which apply mechanical stress on attracting electrostatic forces (e.g. van der Waals forces).[110]

The mechanical stress creates small size miniemulsion droplets. In a microfluidizer,[111] the emulsion is condensed at very high pressure (up to 40 000 psi sustained) using the same device as a milk homogenizer. In a conventional laboratory setup, it is easier to use a sonicator because small volumes (5 – 1 000 mL) can be processed.

The miniemulsion technique allows in principle the polymerization of all kinds of monomers that have no water solubility. Each droplet may be considered as a small nanoreactor for polymerization. The miniemulsion process is also extensively used for the encapsulation of hydrophobic compounds and inorganic solids. For example, Erdem described the encapsulation of TiO_2 particles via miniemulsion polymerization of styrene.[112] In our case (see below), a miniemulsion will be used to encapsulate the catalyst in a minimum amount of organic solvent, in order to trigger the polymerization.

1.5 Catalytic olefin copolymerization in aqueous emulsion

A catalyst tolerant to polar functionalities and to water may allow olefin copolymerization in aqueous emulsion or miniemulsion, enabling the production of polymer latexes with regulated properties. Early transition metal complexes are highly water-sensitive and cannot be used in aqueous emulsions. Late transition metal complexes are less oxophilic and can be used in polymerizations in aqueous medium.[113] The field of catalytic olefin polymerization in water has been reviewed.[113-115] The catalyst not only must be tolerant to water, but also able to be active without Lewis acid activation. The

aforementioned Fe- and Co-based tridentate N,N,N-chelated catalysts require MAO for activation and cannot be used in water.

Hydrosoluble catalysts. $[(N,N,N\text{-ligand})RhMe(OH_2)(OH)]^+$ complex where N,N,N-ligand is 1,4,7-trimethyl-1,4,7-triazacyclononane was reported for ethylene polymerization in water, but the reaction was very slow (0.04 TO/h).[116] This catalyst is hydrosoluble and polymerization may proceed in water until the polymer chain crystallizes or precipitates out of the aqueous phase.

The majority of the organometallic catalysts are not soluble in water. However, the P,O-chelated Ni-based Complex 14 (Figure 1.8) is soluble in water when Na^+ is used as a counter ion,[117] but a very small amount of water-miscible organic solvent (acetone) is still required.

The activity of the Complex 14 decreased almost two orders of magnitude upon changing the solvent from 100 % acetone to a mixture of 5 % of acetone in water (15 220 vs 360 TO/h). The decrease in activity was one order of magnitude when toluene, was used instead of acetone (13 340 vs 1 180 TO/h).[117] This decrease of activity was explained by diffusion limitations of solubilized ethylene and by water poisoning of the catalyst.

Another water soluble N,N-α-diimine ligand, $ArN=C(Me)–C[(CH_2)_4SO_3Li]=NAr$ where Ar is 2,6-$(i\text{-}Pr)_2$-Ph,[118] turned out to decompose in the presence of ethylene. This was explained by the need of the catalyst for acid stabilization in order to avoid the decomposition of Pd – H species which may decompose giving Pd(0) and H^+.

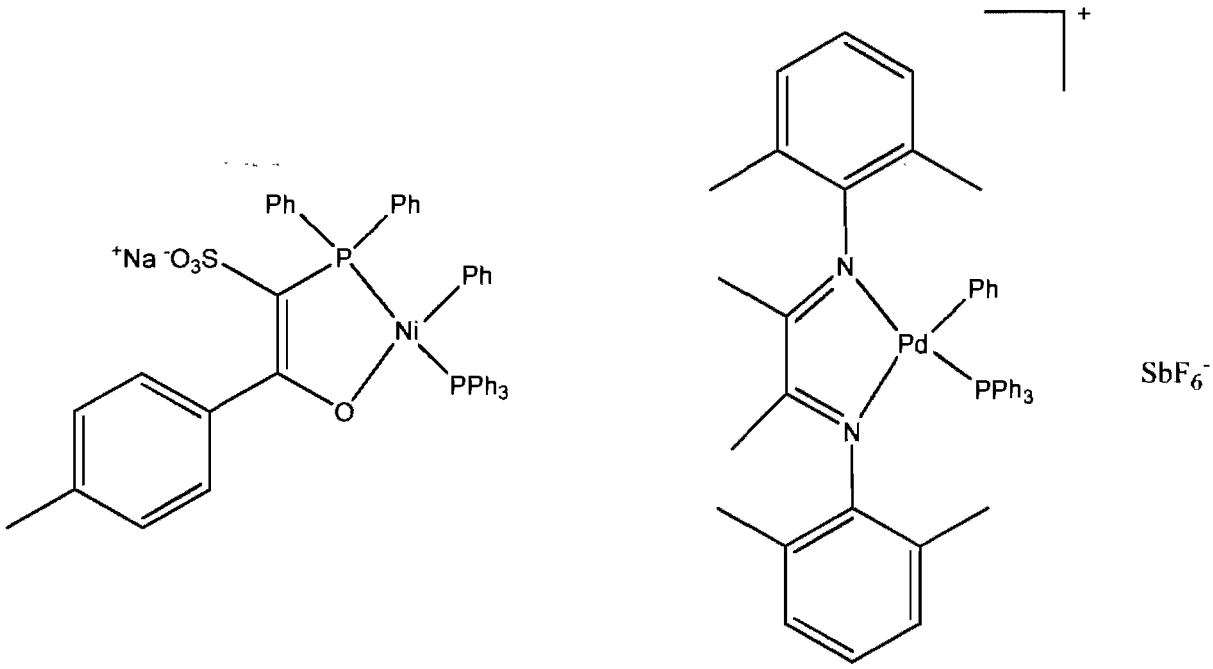

Complex 14 Complex 15

Figure 1.8: Catalysts for aqueous ethylene polymerization.

Polymerization with suspended catalysts. The N,N-α-diimine complex (Complex 15) was able to polymerize ethylene when suspended in water. A polymer of M_n $6{\cdot}10^4$ - $8{\cdot}10^4$ g/mol with a PDI of 2-3 was obtained at a pressure of 40 psi.[117]The activity of this complex in suspension is very close to the activity of the complex solubilized in CH_2Cl_2 (400 vs. 600 TO/h) at a pressure 50 bar at room temperature. The polymer obtained in CH_2Cl_2 was more branched and had a lower molecular weight compared with the polymer obtained when the catalyst was suspended in water (109 vs. 83 br / 1 000 C, M_n 14 500 vs 77 700 g/mol). Thus, the catalyst ability for isomerization and chain walking seems to be higher when the catalyst is solubilized.

Emulsion polymerization with organosoluble catalysts. There exist only a limited number of catalysts affording ethylene polymerization in water. Mecking demonstrated that Brookhart type of catalysts,[118] generate polymer in water in low yields even at high pressure such as 50 bar.

Benzoquinone-based catalysts, formed *in situ* were reported for aqueous polymerization.[119] The mechanism of this formation is shown in Figure 1.9.

Another two systems which were found to be highly active in ethylene aqueous emulsion polymerization are nickel(II)-based phosphinoenolato complexes and nickel(II)-based salicylaldiminato complexes. The Ni-phosphinoenolato fluorinated complex was used by Claverie[120] to produce a polyethylene latex with a reasonably high solid content (Figure 1.10). The possibility of copolymerization of ethylene with α-olefins in the aqueous medium was also demonstrated using the same catalytic system.[121] The CF_3 groups make the ligand electron-deficient, with the consequence that the resulting catalyst is very active (likely via the destabilization of the metal carbon bond). The first step in the synthesis of the catalyst is the complexation of $Ni(COD)_2$ with the keto-ylide $CF_3C(O)C(PPh_3)COOEt$, which is more difficult to accomplish than in the case of the more electron-rich keto-ylides used by Klabunde.[122] Thus, the catalyst was formed directly *in situ* (Complex 16), and the group of Claverie was never able to isolate it. Phosphinoenolate complexes convert ethylene in a low molecular weight polymers ($M_n < 10^4$ g/mol), forming linear semicrystalline polymer. Salicylaldiminato complexes can yield polymerization with

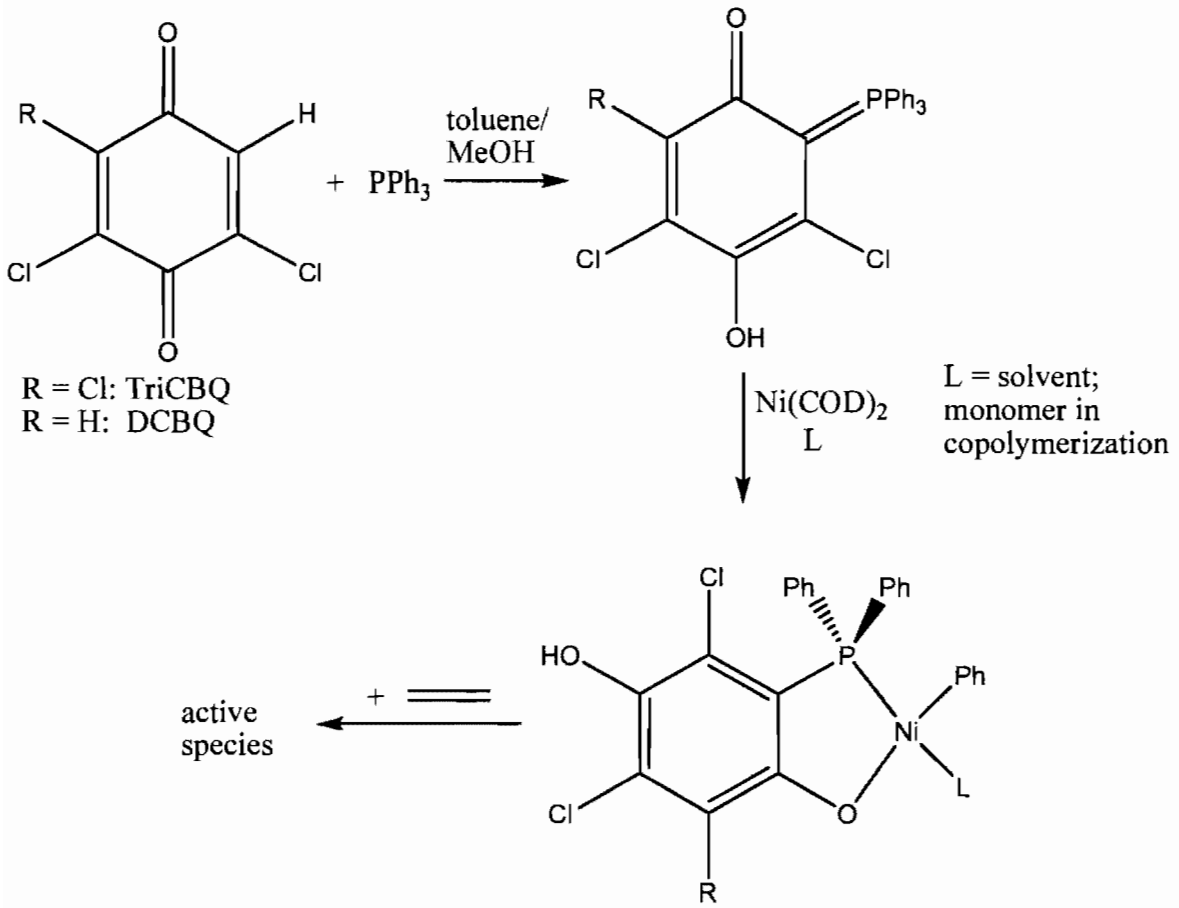

Figure 1.9: General scheme of benzoquinone catalyst formation.

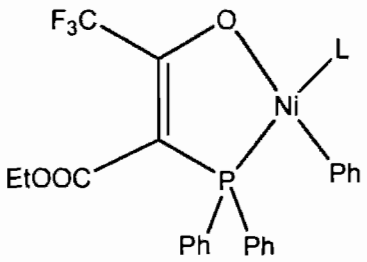

Ni-phosphinoenolato catalyst (Complex 16)

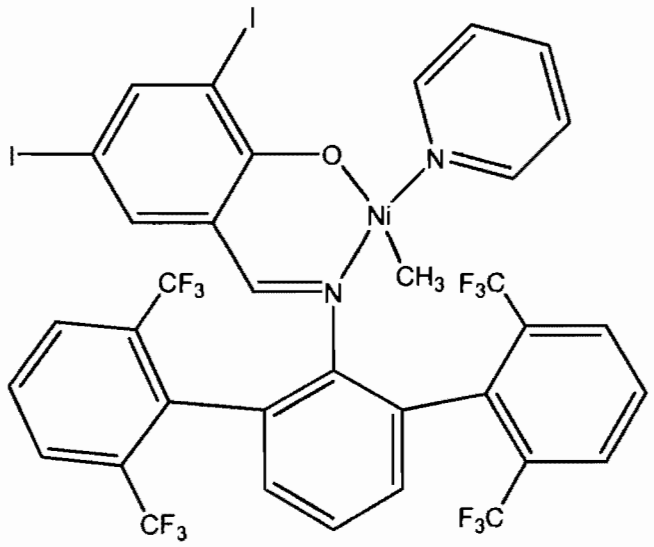

Ni-salicylaldiminato catalyst (Complex 17)

Figure 1.10: Structures of Ni-based complexes, used in olefin emulsion polymerization.

M_n up to 10^3 g/mol. The reaction is carried out at a pressure of 10 – 40 atm and a temperature of 25 – 80 °C.[119]

Polymerization inhibition by water. One of the major reasons for the use of miniemulsions is the high degree of dispersion of water-insoluble catalyst in the reaction mixture.[123] However, water reacts as a poison to the catalyst. DeKock reported that water hydrolyzes Pd-alkyl bond in the presence of ethylene, leading to the catalyst decomposition via a Wacker-type reaction .[124] The scheme of decomposition is shown in Figure 1.11. For the N,O-chelated salicylaldiminate Ni-based complexes the decomposition was reported via the substitution of ethylene by water.[125] For both nickel(II)-based phosphinoenolato complexes and nickel(II)-based salicylaldiminato complexes (Figure 1.10; Complexes 16, 17), water was found to lower the catalytic activity, and latexes can only be obtained when very active catalysts are used.

Latexes obtained by catalytic emulsion polymerization. In general, the average particle size of the dispersions is usually in the range of 100 – 500 nm, with solid contents up to 30 %.[119, 121]

A latex with 28 % of solid content was obtained using a dichlorobenzoquinone-based catalyst formed *in situ*.[119] (Figure 1.9) This catalyst is stable in water and led to the formation of the latexes with polyethylene with of M_n $8.3 \cdot 10^2$ g/mol, M_n/M_w 2.9 and T_m 118 °C. Tetra- and trichlorobenzoquinone were also used in aqueous polymerization of ethylene, yielding latexes of solid content which depends on conditions.

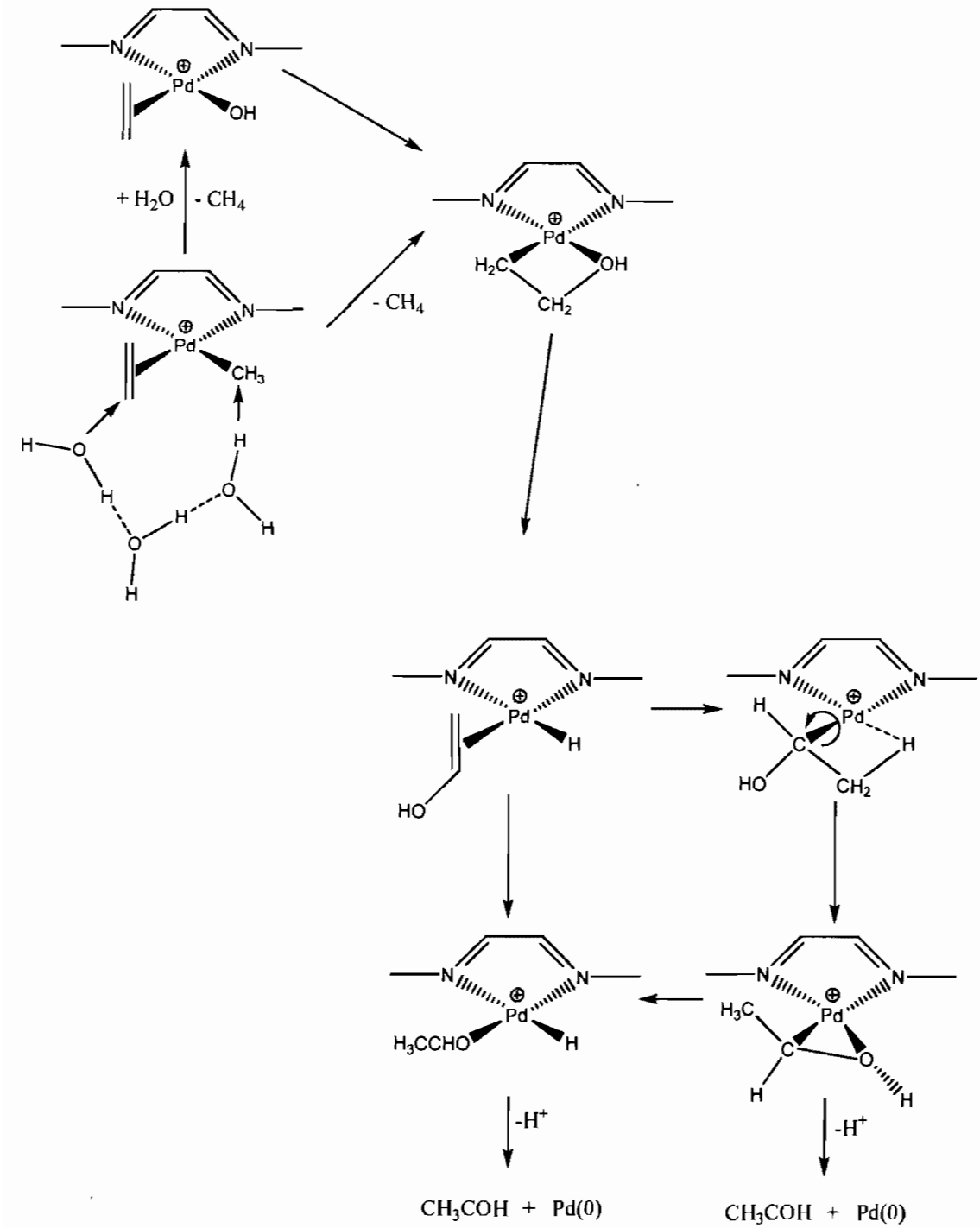

Figure 1.11: The suggested mechanism for catalyst decomposition via a Wacker-type reaction.[124]

For tetrachlorobenzene-based catalysts, the values of M_n were in the range $1.7 \cdot 10^3$ – $3.1 \cdot 10^3$ g/mol and the crystallinity was in range 70-80 % as expected for linear polyethylene. HDPE polymer particles have an irregular shape, which is indication of the crystallinity of the polymer, probably because the rate of PE crystallization is faster than the speed of particle growth. The latexes of ethylene-α-olefin copolymers have a smoother and nearly spherical shape due to decreased percentage of crystallinity of these copolymers.[121] Ni-based salicylaldiminato complexes were used also by Mecking for the synthesis of polymer dispersions.[126] Stable latexes of a high molecular weight semicrystalline polymer were obtained[127] with control over the branching and crystallinity of the polymer in the range from linear semicrystalline PE (5 br/1000 C, $M_n > 10^4$ g/mol, $T_m = 127$ °C) to highly branched amorphous one (80 br/ 1000 C, M_n $2 \cdot 10^3$ g/mol).[128]

Very low particle size latexes. The control of the particle sizes of latexes is of interest, in particular, the achievement of the particle size < 30 nm is a challenging task. Mecking reported the synthesis of very small polyethylene particles by catalytic microemulsion polymerization.[129] For example, a microemulsion of a toluene catalyst solution with surfactant SDS/pentanol afforded PE particles 26 nm in size using N,O-salicylaldiminato complexes.[130] Stereoregular 1,2-polybutadiene was also polymerized producing particles of size < 30 nm.[123]

Ethylene-norbornene latexes. Copolymerization of ethylene with norbornene was investigated with P,O-chelated catalyst (Complex 14), and N,O-chelated catalyst, using a low amount of toluene (~10 %) for solubilization of norbornene. The comonomer

incorporations ranged from 6 to 25 mol. % (T_g -4 – 25 °C). In the case of high incorporation the polymer was amorphous.[126] At the same time when our article on miniemulsion polymerization of ethylene with norbornene (Chapter 3) was published, Mecking reported the formation of a latex of E-NB copolymer using N,O-salicylaldiminato complexes.[131] Norbornene incorporation reached up to 6 mol. %. When the copolymer contained 3 mol. % of NB, the coalescence took place; particles obtained with a polymer containing 6 mol. % of NB, formed continuous film as observed by TEM.

Examples of the other latexes. Catalytic emulsion polymerization yields very different polymer dispersions. For example, a syndiotactic 1,2-polybutadiene dispersion was obtained by reduction of cobalt(II)octanoate with $NaBH_4$ in the presence of butadiene in a small amount of toluene. This solution was miniemulsified and added to a macroemulsion of butadiene in water which contained CS_2. Polymerization produced latex with 150-200 nm particle size and 8 % solid content was obtained. The polymer formed predominantly by 1,2-insertion was quite crystalline, with a melting point of 190 °C. Modification of the catalyst with organic compounds that contained electrophilic carbon atoms, such as aromatic formamides, aldehydes or nitriles, decreases the crystallinity of the polymer (T_m < 100 °C). In some cases amorphous polybutadiene was obtained. The crystallinity decrease correlates with the increase of 1,4-insertion of butadiene.[132] Butadiene dispersions of size as small as 14 nm were obtained by microemulsion using the same catalyst, producing a dispersion of 6 % solid content (M_w $2 \cdot 10^5$ g/mol; M_w/M_n 2.3).[130] Norbornene also can be polymerized in emulsion by the catalytic route to produce

polynorbornene. When the emulsion is stabilized by SDS and $PdCl_2$ is used as the precatalyst, the norbornene oligomers (DP $\approx$ 10) are formed. The particle size of the resulting polymer dispersion was found to be 10 – 20 nm.[133] The precatalyst [(η^3-allyl)Pd(PCy_3)Cl] when activated with lithium tetraarylborate can form catalytically active cationic species and provide polymerization of norbornene in miniemulsion. The number average particle size was 40 – 80 nm, as determined by dynamic light scattering and broad particle size distributions were obtained from TEM.[134] Interestingly, no T_g was observed. Suspension-type polymerization of 5-butylnorbornene was carried out yielding high molecular weight polymer M_n $4 \cdot 10^5$ g/mol (M_w/M_n = 2.7) using the same catalyst.[135]

Polyketones were obtained by catalytic copolymerization of olefins with CO, alternating copolymers are formed.[136] For example, polyketones were obtained in emulsion using a P,P-chelated catalyst $[(Ph_2P(CH_2)_3PPh_2)PdMe(NCCH_3)]^+SbF_6^-$, to produce a polymer latex with M_n $5.7 \cdot 10^4$ g/mol and M_w/M_n 4.4. Incorporation of undecenoic acid into polyketones increases colloidal stability of the latexes which have a size of 30 – 500 nm. Copolymers of α-olefins, ranging from propene to octadecene, with CO were produced by polymerization at 80 °C and pressure of CO 60 bar. The T_g values of the copolymers were in the range of -55 – 10 °C and solid contents of the latexes reached 12 %. The M_w values were about $2 \cdot 10^4$ g/mol (M_w/M_n 3).[137] Dispersions of conjugated polymers such as aqueous dispersions of polyacetylene were obtained using the a catalyst $Pd(OAc)_2$/t-$Bu_2P(CH_2)_3$Pt-Bu_2, and SDS as a surfactant with a final solid content of 7 %.[138] TEM pictures revealed an unexpectedly small particle size (~20 nm). The explanation

proposed could be that polyacetylene is highly insoluble and precipitates rapidly during polymerization forming the particles.

Another type of polynorbornene was synthesized by ROMP in emulsion when ruthenium alkylidenes as catalysts yielding particles of 150 nm in size and polymers of extremely high molecular weights M_n 10^5 – 10^6 g/mol, with high solid content up to 46 %.[139] In the same study 1,5-cyclooctadiene and cyclooctene were homopolymerized by ROMP using a commercially available catalyst [$(PCy_3)_2Cl_2Ru$=CHPh] producing dispersions of high molecular weight polymers (M_n 10^5 g/mol; M_w/M_n 1.6).

In summary, latexes of polymers such as polyethylene, polybutadiene, polyketones, polyacetylene, etc can be prepared,[140] ranging in crystallinities, from highly crystalline to completely amorphous and in T_g from -80 °C to 170 °C.

1.6 Application of polyolefin latexes to coatings formation

Latex particles are usually held apart in suspension due to electrostatic or steric stabilizing forces resulting from adsorbed surfactants or polymer chains. A latex film forms as a result of compaction, deformation and polymer interdiffusion of the latex particles. This process of coalescence can be initiated by evaporation of the continuous phase of the latex (water). The process of continuous phase evaporation from the latex is schematized by a sigmoidal curve (Figure 1.12) which can be divided into three different regions.[141] During the first stage, the latex is concentrated by water evaporation. In this stage the water evaporation rate is not very different from the one of pure water.

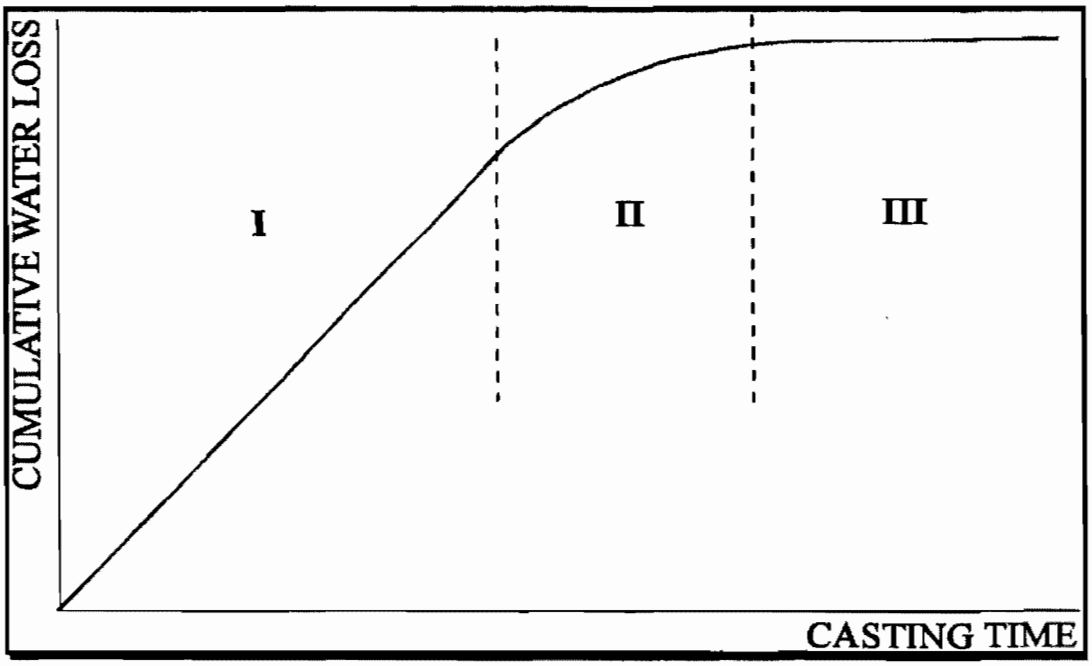

Figure 1.12: Schematic plot of water loss occurring during latex drying. 1. Water evaporation, particle concentration and ordering. 2. Particle deformation. 3. Polymer chain diffusion across particle boundaries.[141]

This stage is the longest and is continuing until the volume fraction reaches 60 – 70 %. The second stage starts when particles come into irreversible contact. The overall rate of water evaporation greatly reduces, leaving enough time for the organization of particles into ordered structures (beehive like). The completion of coalescence or particle deformation indicates the end of second stage. The third stage starts with the formation of a continuous film. Polymer chains interdiffuse through particles. The film properties in the second and third stages are very different from each other, as the initially brittle particles become more ductile due to the development of polymer chain entanglements.

At temperatures higher than the minimum film formation temperature (MFFT) coalescence and film formation can proceed. At temperatures lower than MFFT, a discontinuous, cracked film or even powder is obtained and the resulting 'films' are typically opaque due to the presence of light-scattering voids. However, when the temperature is much above MFFT, the process can result in a tacky film that is more suited for adhesive applications.[142]

The formation of a transparent and crack-free continuous film only occurs for temperatures above MFFT, which is assessed visually by using a metallic bar[143] with a temperature gradient which depends, in turn on the resistance of particles deformation (elastic modulus). The MFFT tends to be close to the T_g of the polymer, since both values are governed by the chain mobility of the polymer. However, it was reported in some cases that MFFT is above or below T_g. For example, it was considered that comonomers which impart hydrophilic properties to PE, such as methyl or ethyl acrylates, may decrease MFFT

below T_g in the case of wet film (as opposed to the properties measured for a dry film), allowing water to act as plasticizer.[144] In the same way, a surfactant which is compatible with the polymer may act as a plasticizer and decrease MFFT or T_g, or both.[145] MFFT is an empirical value which depends on many parameters. For example, Eckersley[146] found that MFFT depends on the latex particle size but changing the latex diameter from 150 to 1200 nm only changes the MFFT by 5 K. Sperry[147] explained this effect by suggesting the explanation that for larger particles, it is difficultt to fill the larger interstitial voids during particle deformation. MFFT is always measured following the procedure described in an ASTM report (D 2354), which was reproduced in our laboratory.

1.7 Perspectives

From the published data, it appears that there is still no acceptable method to incorporate polar monomers into polyethylene by catalytic way. Existing "knowhow", such as introducing a long aliphatic chain between the double bond and the polar functionality or introducing of sterical hindrance near the polar group to "mask" this polar functionality do not resolve the problem in general. In addition, early-transition metal-based catalysts are extremely sensitive to water and even in the case when the copolymerization of polar monomers is possible, these catalysts are unable to withstand the aqueous environment, necessary for polymer dispersions producing. Some late-transition metal-based catalysts often need an activator, such as MAO, which also makes them unuseful for the polymerization in water.

At the same time, it is of interest to produce ethylene-hexadecene and ethylene-norbornene latexes by the way of catalysis, using already known types of water-tolerant catalysts, such as Ni-based keto-ylides and Pd-based sulfonated arylphosphines. The latexes, once obtained, are expected to be good candidates for anticorrosion coating formulations.

The advantage of the catalytic route is that it may allow the control of the microstructure of the polymer, which can not be achieved by radical route. A study of the effect of Lewis base and the effect of bulky functional groups, attached to the catalyst may lead to controlled variations in polymer microstructure. So that, new modified catalysts would be interesting to apply for copolymerization of the olefins.

In general, the catalytic copolymerization of polar monomers is a very challenging problem. However, since Pd-based sulfonated arylphosphine catalysts are tolerant to polar functionalities, the monomers which are even more polar than methyl acrylate, such as N-vinylpyrrolidinone and N-isopropylacrylamide, may prove to copolymerize with ethylene.

Finally, catalyst with such water tolerance combined with the capability of copolymerization of ethylene with polar monomers, could lead to the formation of latexes of the ethylene copolymers with polar monomer (such as acrylate).

These are some of problems which will be tackled in the following thesis.

1.8 References

1. von Pechmann, H. *Ber. Dtsch. Chem. Ges.* **1898,** 31, 2640-2646.
2. Bamberger, E.; Tschirner, F. *Ber. Dtsch. Chem. Ges.* **1900,** 33, 955-959.
3. Friederich, M. E. P.; Marvel, C. S. *J. Am. Chem. Soc* **1930,** 52, 376-387.
4. Koch, H.; Ibing, G. *Brennst.-Chem.* **1935,** 16, 141-148.
5. Carothers, W. H.; Hill, J. W.; Kirby, J. E.; Jacobson, R. A. *J. Am. Chem. Soc.* **1930,** 52, 5279-5288.
6. Fawcett, E. W.; Gibson, R. O. *J. Chem. Soc.* **1934**, 368-395.
7. Fawcett, E. W.; Gibson, R. O.; Perrin, M. W.; Patton, E. G.; Williams, E. G. Brit. Patent 471,590, Sep 6., 1937.
8. Gavens, P. D.; Bottrill, M.; Kelland, J. W.; McMeeking, J.; in *Comprehensive Organometallic Chemistry,* Wilkinson, G.; Stone, F. G. A.; Abel, E. W., Pergamon Press: Oxford, 1982; Vol. 3, ch. 22.5.
9. Ziegler, T.; Holzkamp, E.; Breil, H.; Martin, H. *Angew. Chem.* **1955,** 67, 541-547.
10. Natta, G.; Pino, P.; Corradini, P.; Danusso, F.; Mantica, E.; Mazzanti, G.; Moraglio, G.; . *J. Am. Chem. Soc.* **1955,** 77, 1708-1710.
11. Gardner, K.; Parsons, I. W.; Haward, R. N. *J. Polym. Sci., Part A: Polym. Chem.* **1978,** 16, 1683-1696.
12. *Belgian Pat.* 743,315 to Solvay, 1969.
13. Hogan, J. P.; Banks, R. L. **1958,** US Patent 2825721, 1958.
14. McDaniel, M. P. *Adv. Catal.* **1985,** 33, 47-98.

15. Sinn, H.; Kaminsky, W.; . *Adv. Organomet. Chem.* **1980,** 18, 99-149.

16. Alt, H. G.; Koppl, A., *Chem. Rev.* **2000,** 100, 1205-1221.

17. Shellenberg, J.; Leder, H. J. *Adv. Polym. Tech.* **2006,** 25, 141-151.

18. McKnight, A. L.; Waymouth, R. M. *Chem. Rev.* **1998,** 98, 2587-2598.

19. High Density Polyethylene Resins, Stanford Research Institute, Andrea Borusso, 2008.

20. Boffa, L. S.; Novak, B. M. *Chem. Rev.* **2000,** 100, 1479-1494.

21. Aaltonen, P.; Fink, G.; Lofgren, B.; Seppala, J. *Macromolecules* **1996,** 29, 5255-5260.

22. Stehling, U. M.; Stein, K. M.; Kesti, M. R.; Waymouth, R. M. *Macromolecules* **1998,** 31, 2019-2027.

23. Hakala, K.; Lofgren, B.; Helaja, T. *Eur. Polym. J.* **1998,** 34, 1093-1097.

24. Aaltonen, P.; Lofgren, B. *Eur. Polym. J.* **1997,** 33, 1187-1190.

25. Matsumura, K.; Fukumoto, O. *J. Polym. Sci., Part A: Polym. Chem.* **1971,** 9, 471-483.

26. Manders, B.; Sciandrone, L.; Hauck, G.; Kristen, M. O. *Angew. Chem. Int. Ed.* **2001,** 40, 4006-4007.

27. Britovsek, G. J. P.; Gibson, V. C.; Waas, D. F. *Angew. Chem. Int. Ed.* **1999,** 38, 428-447.

28. Chauvin, Y. *Angew. Chem. Int. Ed.* **2006,** 45, 3741-3747.

29. Keim, W.; Appel, R.; Gruppe, S.; Knoch, F. *Angew. Chem. Int. Ed.* **1987,** 26, 1012-1013.

30. Muller, U.; Keim, W.; Kruger, C.; Betz, P. *Angew. Chem. Int. Ed.* **1989,** 28, 1011-1013.

31. Keim, W.; Kowaldt, F. H.; Goddard, R.; Kruger, C. *Angew. Chem. Int. Ed.* **1978,** 17, 466-467.

32. Peukert, M.; Keim, W. *Organometallics* **1983,** 2, 594-597.

33. Klabunde, U.; Mulhaupt, R.; Herskovitz, T.; Janowicz, A. H.; Calabrese, J.; Ittel, S. D. *J. Polym. Sci., Part A: Polym. Chem.* **1987,** 25, 1989-2003.

34. Klabunde, U.; Ittel, S. D. *J. Mol. Catal.* **1987,** 41, 123-134.

35. Ostoja-Starzewski, K. A.; Witte, J. *Angew. Chem. Int. Ed.* **1987,** 26, 63-64.

36. Ostoja-Starzewski, K. A.; White, J.; Reichert, K. H.; Vasiliou, G.; in *Transition Metals and Orhanometallics as Catalysts for Olefin polymerization*, Kaminsky, W.; Sinn, H., Springer-Verlag: Berlin, 1988.

37. Johnson, L. K.; Killian, C. M.; Brookhart, M. *J. Am. Chem. Soc* **1995,** 117, 6414-6415.

38. Wang, C.; Friedrich, S.; Younkin, T. R.; Li, R. T.; Grbbs, R. H.; Bansleben, D. A.; Day, M. W. *Organometallics* **1998,** 17, 3149-3151.

39. Younkin, T. R.; Connor, E. F.; Henderson, J. I.; Friedrich, S. K.; Grubbs, R. H.; Bansleben, D. A. *Science* **2000,** 287, 460-462.

40. Schleis, T.; Heinmann, J.; Spaniol, T. P.; Mulhaupt, R.; Okuda, J. *Inorg. Chem. Commun.* **1998,** 1, 431-434.

41. MacKenzie, P. B.; Moody, L. S.; Killian, C. M.; Panasik, J. A.; McDevitt, J. P. *WO Patent* 9840374 to Eastman, 1998.

42. Brookhart, M. S.; Johnson, L. K.; Killian, C. M.; Arthur, S. D.; Feldman, J.; McCord, E. F.; McLain, S. J.; Kreutzer, K. A.; Bennett, A. M. A.; Coughlin, E. B.; Ittel, S. D.; Parthasarathy, A.; Tempel, D. J. *WO Patent* 9623010 to DuPont, 1995.

43. Mecking, S.; Johnson, L. K.; Wang, L.; Brookhart, M. *J. Am. Chem. Soc.* **1998,** 120, 888-899.

44. Ziegler, T. *Chem. Rev.* **1991,** 91, 651-667.

45. Musaev, D. G.; Svensson, M.; Morokuma, K.; Stromberg, S.; Zetterberg, K.; Siegbahn, P. E. M. *Organometallics* **1997,** 16, 1933-1945.

46. Michalak, A.; Ziegler, T. *Organometallics* **2000,** 19, 1850-1858.

47. Guan, Z.; Cotts, P. M.; McCord, E. F.; McLain, S. J. *Science* **1999,** 283, 2059-2062.

48. Simon, L. C.; Soares, J. B. P.; de Souza, R. F. *J. AIChE* **2000,** 46, 1234-1240.

49. Tempel, D. J.; Johnson, L. K.; Huff, R. L.; White, P. S.; Brookhart, M. *J. Am. Chem. Soc.* **2000,** 122, 6686-6700.

50. Svejda, S. A.; Johnson, L. K.; Brookhart, M. *J. Am. Chem. Soc.* **1999,** 121, 10634-10635.

51. Ye, Z.; AlObaidi, F.; Zhu, S. *Macromol. Chem. Phys.* **2004,** 205, 897-906.

52. Gates, D. P.; Svejda, S. A.; Oate, E.; Killian, C. M.; Johnson, L. K.; White, P. S.; Brookhart, M. *Macromolecules* **2000,** 33, 2320-2334.

53. Deng, L.; Margl, P.; Ziegler, T. *J. Am. Chem. Soc.* **1997,** 119, 1094-1100.

54. Johnson, L. K.; Mecking, S.; Brookhart, M. *J. Am. Chem. Soc.* **1996,** 118, 267-268.

55. Ittel, S. D.; Johnson, L. K.; Brookhart, M. *Chem. Rev.* **2000,** 100, 1169-1203.

56. Kiesewetter, J.; Kaminsky, W. *Chem. Eur. J.;* **2003,** 9, 1750-1758.

57. Johnson, L. K.; Killian, C. M.; Arthur, S. D.; Feldman, J.; McCord, E. F.; McLain, S. J.; Kreutzer, K. A.; Bennett, M. A.; Coughlin, E. B.; Ittel, S. D.; Parthasarathy, A.; Tempel, D. J.; Brookhart, M. S. *Patent WO/1996/023010.*

58. McLain, S. J.; McCord, E. F.; Johnson, L. K.; Ittel, S. D.; Nelson, L. T. J.; Arthur, S. D.; Halfhill, M. J.; Teasley, M. F.; Tempel, D. J.; Killian, C. M.; Brookhart, M. S. *Polym. Prepr. (Am. Chem. Soc., Div. Polym. Chem.)* **1997,** 38, 133.

59. Britovsek, G. J. P.; Gibson, V. C.; Kimberley, B. S.; Maddox, P. J.; McTavish, S. J.; Solan, G. A.; White, A. J. P.; Williams, D. J. *Chem. Commun.* **1998**, 849-850.

60. Small, B. L.; Brookhart, M.; Bennett, A. M. A. *J. Am. Chem. Soc.* **1998,** 120, 4049-4050.

61. Britovsek, G. J. P.; Bruce, M.; Gibson, V. C.; Kimberley, B. S.; Maddox, P. J.; Mastroianni, S.; McTavish, S. J.; Redshaw, C.; Solan, G. A.; Stromberg, S.; White, A. J. P.; Williams, D. J. *J. Am. Chem. Soc.* **1999,** 121, 8728-8740.

62. Small, B. L.; Brookhart, M. *J. Am. Chem. Soc.* **1998,** 120, 7143-7144.

63. Britovsek, G. J. P.; Clentsmith, G. K. B.; Gibson, V. C.; Goodgame, D. M. L.; McTavish, S. J.; Pankhurst, Q. A. *Catal. Commun.* **2002,** 3, 207-211.

64. Bianchini, C.; Giambastiani, G.; Rios, I. G.; Mantovani, G.; A.;, M.; Segarra, A. M. *Coord. Chem. Rev.* **2006,** 250, 1391-1418.

65. Tsuji, S.; Swenson, D. C.; Jordan, R. F. *Organometallics* **1999,** 18, 4758-4764.

66. Desjardins, S. Y.; Kavel, K. J.; Jin, H.; Skelton, B. W.; White, A. H. *J. Organomet. Chem.* **1996,** 515, 233-243.

67. Laine, T. V.; Lappalainen, K.; Liimatta, J.; Aitola, E.; Lofgren, B.; Leskela, M. *Macromol. Rapid Commun.* **1999,** 20, 487-491.

68. Cooley, N. A.; Green, S. M.; Waas, D. F.; Heslop, K.; Orpen, A. G.; Pringle, P. G. *Organometallics* **2001,** 20, 4769-4771.

69. Rush, S.; Reinmuth, A.; Risse, W.; O'Brien, J.; Ferro, D. R.; Tritto, I. *J. Am. Chem. Soc.* **1996,** 118, 12230-12231.

70. Gibson, V. C.; Tomov, A. *Chem. Commun.* **2001**, 1964-1965.

71. Johnson, L.; Bennett, A.; Dobbs, K.; Hauptman, E.; Ionkin, A.; Ittel, S.; McCord, E.; McLain, S.; Radzewich, C.; Yin, Z.; Wang, L.; Wang, Y.; Brookhart, M. *Polym. Mater. Sci. Eng.* **2002,** 86, 319-320.

72. Luo, S.; Jordan, R. F. *J. Am. Chem. Soc.* **2006,** 126, 12072-12073.

73. Foley, S. R.; Stockland, R. A.; Shen, H.; Jordan, R. F. *J. Am. Chem. Soc.* **2003,** 125, 4350-4361.

74. Williams, B. S.; Leatherman, M. D.; White, P. S.; Brookhart, M. *J. Am. Chem. Soc.* **2005,** 127, 5132-5146.

75. Berkefeld, A.; Mecking, S. *Angew. Chem. Int. Ed.* **2008,** 47, 2538-2542.

76. Wu, F.; Foley, S. R.; Burns, C. T.; Jordan, R. F. *J. Am. Chem. Soc.* **2005,** 127, 1841-1853.

77. Groux, L. F.; Weiss, T.; Reddy, D. N.; Chase, P. A.; Piers, W. A.; Ziegler, T.; Parvez, M.; Benet-Buchholz, J. *J. Am. Chem. Soc.* **2005,** 127, 1854-1869.

78. Szabo, M. J.; Galea, N. M.; Michalak, A.; Yang, S.-Y.; Groux, L. F.; Piers, W. E.; Ziegler, T. *J. Am. Chem. Soc.* **2005,** 127, 14692-14703.

79. Michalak, A.; Ziegler, T. *Organometallics* **2001,** 20, 1521-1532.

80. Drent, E.; van Dijk, R.; van Ginkel, R.; van Oort, B.; Pugh, R. I. *Chem. Commun.* **2002**, 744-745.

81. Haras, A.; Anderson, G. D. W.; Michalak, A.; Rieger, B.; Ziegler, T. *Organometallics* **2006,** 25, 4491-4497.

82. Hearley, A. K.; Nowack, R. J.; Rieger, B. *Organometallics* **2005,** 24, 2755-2763.

83. Vela, J.; Lief, G. R.; Shen, Z.; Jordan, R. F. *Organometallics* **2007,** 26, 6624-6635.

84. Kochi, T.; Yoshimura, K.; Nozaki, K. *Dalton Trans.* **2006**, 25-27.

85. Guironnet, D.; Roesle, P.; Runzi, T.; Gottker-Schnettman, I.; Mecking, S. *J. Am. Chem. Soc.* **2009,** 131, 422-423.

86. Kochi, T.; Noda, S.; Yoshimura, K.; Nozaki, N. *J. Am. Chem. Soc.* **2007,** 129, 8948-8949.

87. Kochi, T.; Nakamura, A.; Ida, H.; Nozaki, K. *J. Am. Chem. Soc.* **2007,** 129, 7770-7771.

88. Liu, S.; Borkar, S.; Newsham, D.; Yennavar, H.; Sen, A. *Organometallics* **2007,** 26, 210-216.

89. Zhou, X.; Bontemps, S.; Jordan, R. F. *Organometallics* **2008,** 27, 4821-4824.

90. Luo, S.; Vela, J.; Lief, G. R.; Jordan, R. F. *J. Am. Chem. Soc.* **2007,** 129, 8946-8947.

91. Weng, W.; Shen, Z.; Jordan, R. F. *J. Am. Chem. Soc.* **2007,** 129, 15450-15451.

92. Newsham, D. K.; Borkar, S.; Sen, A.; Conner, D. M.; Goodall, B. L. *Organometallics* **2007,** 26, 3636-3638.

93. Antonietti, M.; Landfester, K. *Prog. Polym. Sci.* **2002,** 27, 689-757.

94. Candau, F.; Pabon, M.; Anquetil, J.-Y. *Colloids Surf., A,* **1999,** 153, 47-59.

95. Antonietti, M.; Basten, R.; Lohmann, S. *Macromol. Chem. Phys.* **1995,** 196, 441-466.

96. Ramirez, L. P.; Landfester, K. *Macromol. Chem. Phys.* **2003,** 204, 22-31.

97. Shorck, F. J.; Back, A. *J. Appl. Polym. Sci.* **2004,** 94, 2555-2557.

98. Landfester, K. *Macromol. Symp.* **2000,** 150, 171-178.

99. Ugelstad, J.; El-Aaser, M. S.; Vanderhoff, J. W. *J. Polym. Sci., Part C: Polym. Lett.* **1973,** 11, 503-513.

100. Wang, S.; Poehlein, G. W.; Schork, F. J. *J. Polym. Sci., Part B: Polym. Phys.* **1997,** 35, 595-603.

101. Bechthold, N.; Tiarks, F.; Willert, M.; Landfester, K.; Antonietti, M. *Macromol. Symp.* **2000,** 151, 549-555.

102. Landfester, K.; Bechthold, N.; Tiarks, F.; Willert, M.; Landfester, K.; Antonietti, M. *Macromol. Symp.* **2000,** 151, 549-555.

103. Asua, J. M. *Prog. Polym. Sci.* **2002,** 27, 1283-1346.

104. Davies, S. S.; Smith, A. in *Theory and practice of emulsion technoology,* Smith, A. L., Academic Press: New York, 1976; p 325.

105. Higuchi, W. I.; Misra, J. *J. Pharm. Sci.* **1962,** 51, 459-466.

106. Chern, C. S.; Chen, T. J. *Colloid Polym. Sci.* **1997,** 275, 546-554.

107. Ugelstad, J.; Mork, P. C.; Kaggerud, K. H.; Ellingsen, T.; Berge, A. *Adv. Colloid Interface Sci.* **1980,** 13, 101-140.

108. Reimers, J. L.; Schork, F. J. *J. Appl. Polym. Sci.* **1996,** 60, 251-262.

109. Chern, C. S.; Chen, T. J.; Liou, Y. C. *Polymer* **1998,** 39, 3767-3777.

110. www.hielscher.com/ultrasonics/diperse.htm (as it is 30 April).

111. For example, see www.microfluidicscorp.com (as it is 30 April).

112. Erdem, B.; Sudol, E. D.; Dimonie, V. L.; El-Aasser, M. S. *J. Polym. Sci., Part A: Polym. Chem.* **2000,** 38, 4419-4430.

113. Mecking, S.; Claverie, J. in *Late Transition Metal Polymerization Catalysis.*Rieger, B.; Baugh, L. S.; Kacker, S.; Striegler, S., Wiley-VCH: Weinheim, 2003; p 231-278.

114. Claverie, J. P.; Soula, R. *Prog. Polym. Sci.* **2003,** 28, 619-662.

115. Mecking, S.; Held, A.; Bauers, F. M. *Angew. Chem. Int. Ed.* **2002,** 41, 544-561.

116. Wang, L.; Lu, R. S.; Bau, R.; Flood, T. C. *J. Am. Chem. Soc.* **1993,** 115, 6999-7000.

117. Held, A.; Bauers, F. M.; Mecking, S. *Chem. Commun.* **2000**, 301-302.

118. Held, A.; Mecking, S. *Chem. Eur. J.* **2000,** 6, 4623-4629.

119. Bauers, F. M.; Chowdhry, M. M.; Mecking, S. *Macromolecules* **2003,** 36, 6711-6715.

120. Soula, R.; Novat, C.; Tomov, A.; Spitz, R.; Claverie, J.; Drujon, X.; Malinge, J.; Saudemont, T. *Macromolecules* **2001,** 34, 2022-2026.

121. Soula, R.; Saillard, B.; Spitz, R.; Claverie, J.; Llauro, M. F.; Monnet, C. *Macromolecules* **2002,** 35, 1513-1523.

122. Soula, R.; Boyer, J. P.; Llauro, M. F.; Tomov, A.; Spitz, R.; Claverie, J.; Drujon, X.; Malinge, J.; Saudemont, T. *Macromolecules* **2001,** 34, 2022-2026.

123. Mecking, S.; Monteil, V.; Huber, J.; Kolb, L.; Wehrmann, P. *Macromol. Symp.* **2006,** 236, 117-123.

124. DeKock, R. L.; Hristov, I. H.; Anderson, G. D. W.; Gottker-Schnetmann, I.; Mecking, S.; Ziegler, T. *Organometallics* **2005,** 24, 2679-2687.

125. Hristov, I. H.; DeKock, R. L.; Anderson, G. D. W.; Gottker-Schnetmann, I.; Mecking, S.; Ziegler, T. *Inorg. Chem.* **2005,** 44, 7806-7818.

126. Bauers, F. M.; Mecking, S. *Macromolecules* **2001,** 34, 1165-1171.

127. Bauers, F. M.; Mecking, S. *Angew. Chem. Int. Ed.* **2001,** 40, 3020-3022.

128. Zuideveld, M. A.; Wehrmann, P.; Rohr, C.; Mecking, S. *Angew. Chem. Int. Ed.* **2004,** 43, 869-873.

129. Kolb, L.; Monteil, V.; Thomann, R.; Mecking, S. *Angew. Chem. Int. Ed.* **2005,** 44, 429-432.

130. Monteil, V.; Wehrmann, P.; Mecking, S. *J. Am. Chem. Soc.* **2005,** 127, 14568-14569.

131. Wehrmann, P.; Zuideveld, M. A.; Thomann, R.; Mecking, S. *Macromolecules* **2006,** 39, 5995-6002.

132. Monteil, V.; Bastero, A.; Mecking, S. *Macromolecules* **2005,** 38, 5393-5399.

133. Eychenne, P.; Perez, E.; Rico, I.; Bon, M.; Lattes, A.; Moisand, A. *Colloid Polym. Sci.* **1993,** 271, 1049-1054.

134. Chemtob, A.; Gilbert, R. G. *Macromolecules* **2005,** 38, 6796-6805.

135. Lipian, J.; Mimna, R. A.; Fondran, J. C.; Yandulov, D.; Shick, R. A.; Goodall, B. L.; Rhodes, L. F.; Huffman, J. C. *Macromolecules* **2002,** 35, 8969-8977.

136. Drent, E.; Budzelaar, P. H. M. *Chem. Rev.* **1996,** 96, 663-682.

137. Held, A.; Kolb, L.; Zuidveld, M. A.; Thomann, R.; Mecking, S.; Schmid, M.; Pietruschka, R.; Lindner, E.; Khanfar, M.; Sunjuk, M. *Macromolecules* **2002,** 35, 3342-3347.

138. Huber, J.; Mecking, S. *Angew. Chem. Int. Ed.* **2006,** 45, 6314-6317.

139. Claverie, J.; Viala, S.; Maurel, V.; Novat, C. *Macromolecules* **2001,** 34, 382-388.

140. Mecking, S. *Colloid Polym. Sci.* **2007,** 285, 605-619.

141. Steward, P. A.; Hearn, J.; Wilkinson, M. C. *Adv. Colloid Interface Sci.* **2000,** 86, 195-267.

142. Talen, H. W.; Hover, P. F. *Deutsche Farben Z* **1959,** 13, 50-55.

143. ASTM O 2354-68, Standard Test Method for Minimum Film Formation Temperature of Emulsion Vehicles, American Society for Testing Materials, Philadelphia, PA, 1993.

144. Brodnyan, J. G.; Konen, T. *J. Appl. Polym. Sci.* **1964,** 8, 687-697.

145. Eckersley, S. T.; Rudin, A. *J. Appl. Polym. Sci.* **1993,** 48, 1369-1381.

146. Eckersley, S. T.; Rudin, A. *J. Coat. Technol.* **1990,** 62, 89-100.

147. Sperry, P. R.; Snyder, B. S.; O'Dowd, M. L.; Lesko, P. M. *Langmuir* **1994,** 10, 2619-2628.

Chapter 2

RESEARCH PAPER

Solvent and Aqueous-Borne Polyolefin Coatings Obtained by Catalytic Polymerization

K. M. Skupov, J. Hobbs, J. P. Claverie

NanoQAM Research Center, Québec Center for Functional Materials, Department of Chemistry, University of Quebec at Montreal, 2101 rue Jeanne-Mance, CP 8888, Montreal, Quebec, H3C 3P8, Canada

Progress in Organic Coatings 2009, 65, 314-321.

Received 21 July 2008; Revised form 9 December 2008; Accepted 9 January 2009; Available online 23 February 2009.

This paper is related to coatings applications of several polyolefin copolymers (poly(ethylene-*co*-hexadecene) and poly(ethylene-*co*-norbornene)). PE polymers were either dissolved in an organic solvent or as latexes. The copolymers were studied by EIS for anticorrosion properties. The latexes and the copolymers were characterized by DSC, DLS and NMR.

My contribution to this paper was ~ 85 % by synthesising of most of the copolymers and their characterization, as well as the formation of the films and their characterization by EIS. Jason Hobbs, an undergraduate student, prepared several of the copolymers.

2.1 Abstract

Copolymers of ethylene with various olefins such as hexadecene, undecenol and norbornene were prepared by emulsion and solution polymerization, using a nickel-based catalytic system. Aqueous-based coatings could be produced from hexadecene-containing copolymers, however these coatings exhibited poor adhesion properties. Adhesion was improved by introducing polar groups, as in the case of poly(undecenol-co-ethylene), but the resulting films were very tacky. Copolymers of ethylene and norbornene were prepared by palladium-catalyzed polymerization. Solvent-based coatings of ethylene–norbornene copolymers were obtained when incorporating norbornene into the polymer in more than 15 mol. %. Using EIS experiments, the resulting films were shown to exhibit promising applications as barrier coatings for anticorrosion.

2.2 Keywords

Polyolefin film; Anticorrosion coating; Catalytic polymerization; Miniemulsion polymerization.

2.3 Introduction

Although it is used in a growing number of applications, high-density polyethylene (PE) is scarcely present in coatings formulations[1,2]. However, one can envision that the use of PE in barrier coatings formulations would present obvious advantages because of its intrinsic stability, hydrophobicity and chemical inertness. The prospect of using PE in a

solvent borne formulation is limited because PE is insoluble in any organic solvent at room temperature. Aqueous latex-based coatings are becoming increasingly popular because of obvious environmental advantages[3]. Upon water evaporation, the latex particles dry up and eventually form a continuous film when the polymer from one particle interpenetrates into another particle. This film-formation mechanism implies that the polymer has a T_g close to room temperature, in order to permit chain diffusion[4]. Evidently, aqueous dispersions of high-density linear PE are not suitable for this process because chains of PE are crystallized[5] and the diffusion from one particle to another cannot take place.

The crystallinity of PE can be disrupted by inserting branches along the backbone[6-8] resulting in an disruption of the crystalline packing, and a concomitant increase of T_g since long chain poly α-olefins possess higher T_g comparatively to PE[6]. Thus, highly branched PEs are amorphous[7] with a T_g of approximately −70 to −50 °C. When small amounts of undecenoic acid and dimethyloctadiene are incorporated into such a polymer, the adhesion of the coating on a substrate is significantly improved[8].

This report presents our first attempts at preparing coating formulations which are either solvent or aqueous borne via the catalytic copolymerization of ethylene with hexadecene or norbornene. Although nothing is known about the properties of coatings derived from these copolymers, one expects they should be good candidates for the protection against corrosion[9]. Corrosion remains a fundamental problem in the preservation of various metallic structures and it is often moderated by the use of anticorrosion coatings.[10] An ideal organic coating for such a usage must possess several essential

properties such as environmental suitability, high dielectric strength, chemical resistance, weather resistance, resistance to dirt pick up, extended life time, ease of application and above all, low water permeability. Mathematically, the coefficient of permeability can be expressed as the product of diffusion coefficient and solubility.[11] For PE, reported values of permeability range from 0.015 to 0.074 (g mm)/(m^2 day cmHg) at 25 °C.[12] These values are in the low range for water permeabilities for common organic polymers, as expected from the very low solubility of water in PE. In PE, water diffuses by a Fickian mechanism through the amorphous fraction and by channeling through micropores. Therefore, coatings based on linear and crystalline high-density PE are expected to have very low permeability due to the combination of the low solubility of water in the coating and the minimal amount of amorphous phase through which water could channel.[11-13]

There exist several commercial materials that are loosely referred to polyolefin coatings. PE encasement is not a true coating per se, because it usually does not bond to the substrate, but it is a standard corrosion control method, especially for water pipes.[14] Typically, the pipes are wrapped in a 100 μm thick high-density PE film which is taped every two feet. Pipes can be truly coated by polyolefins by extruding the polyolefin at high temperature over the pipe.[15] This method, which is obviously reserved to OEM parts, is now commonly used for many underwater pipes and offshore equipment. In most cases, the polyolefin is applied as a thick barrier layer (top-coat).

"Wax Emulsions" are very low molecular weight low-density polyethylene polymers that have been dispersed in water or in a solvent via an emulsification process.

They are used as additives in varnishes and paints and for anticorrosion purposes.[16] This product is easily applicable (brush or spray), but its barrier properties are low because polyolefin waxes are highly branched and amorphous materials which have often been modified with reactive groups (maleates, etc.) during a reactive processing step.

Since 2001, our group[5,17] and the group of Mecking[18,19] have been interested in preparing novel materials based on PE, either in solution or in emulsion. This report presents our first attempts to use these materials as coatings and to assess their anticorrosion properties. In a first section, the formation of coatings from poly(ethylene-*co*-hexadecene) will be presented. Unfortunately, in our hands, these coatings appear to be of low value, because of their inherent tackiness and poor adhesion. In a second section, coatings prepared from poly(ethylene-*co*-norbornene) will also be presented. Preliminary measurements indicate that these coatings are promising candidates for the formation of novel barrier coatings with anticorrosion properties.

2.4 Experimental part

2.4.1 Materials

Ethyl-4,4,4-trifluoro-2-(triphenylphosphoranylidene)acetoacetate (keto-ylide 1) and nickel dicyclooctadiene $Ni(COD)_2$ were purchased from Aldrich. The synthesis of ligand A (2-[bis(2-methoxy-phenyl)phosphanyl]-4-methyl-benzenesulfonic acid, P(*o*-OMe–$C_6H_4)_2$(*o*-SO_3H–C_6H_3), was based on the procedure detailed in ref. 20. Water was ultrapure grade (18.2 MΩ). For degassing, water was boiled for 120 min and then sparged with Ar

for several hours. Norbornene (NBE, Aldrich) was purified by passing it at 50 °C over a bed of activated basic alumina and activated molecular sieves. All other chemicals were purchased from Aldrich, used without further purification, but were dried and degassed using standard Schlenk techniques. All manipulations were done using standard inert atmosphere procedures. Steel coupons (6″ × 12″ × 1/8″) were cold-rolled ANSI 1018 steel (UNS G10180) from the Metal Samples Company. The epoxy coating (MIL P2444) was kindly provided by the Office of Naval Research.

2.4.2. Typical miniemulsion copolymerization procedure

In a Schlenk flask, 9.2 mg (0.033 mmol) of $Ni(COD)_2$ and 7.4 mg (0.017 mmol) of keto-ylide 1 were mixed in 13 mL of toluene in a nitrogen filled dry box. The mixture was introduced into 100 ml of water containing 15 g/L of surfactant sodium dodecyl sulfate (SDS) and 15 g/L of hydrophobe hexadecene under stirring. The mixture was emulsified using a Branson sonifier 450 W for 4 min under magnetic stirring and under argon. Finally the resulting emulsion was cannula-transferred into a 300 mL stainless steel reactor equipped with mechanical stirrer and heated at 55 °C. Ethylene was introduced immediately at 300 psi (20 atm). Ethylene was continuously fed into the reactor at the set pressure. After 2 h, the reactor was degassed by slowly releasing ethylene, and the reaction medium was collected. The latex was filtered (if needed) to separate the floc (part of the polymer in coagulated form). Activity of the reaction was calculated from the pressure drop from the feed reservoir. Solid content was analyzed by gravimetry.

2.4.3 Typical solution polymerization

In a Schlenk tube, 2.1 mg of ligand A (5.57×10^{-3} mmol) and 2.0 mg of $Pd_2(dba)_3$ (2.18×10^{-3} mmol) were suspended in 90 mL of toluene. Separately, NBE (10 g) was dissolved in 10 mL of toluene. The catalyst solution and the NBE solutions were then introduced into the 300 mL Parr reactor, immediately pressurized with 100 psi ethylene, and heated to 100 °C. When this temperature was reached, ethylene was supplied continuously at 300 psi, and the conversion of ethylene was monitored on-line. After 90 min, the reaction was stopped, and the polymer collected by precipitation in 4 volumes of methanol, filtered and dried under vacuum.

2.4.4 Coating preparation

Aqueous-borne latexes such as ethylene–hexadecene coatings were prepared by applying the latex of copolymer (~3 g, based on the latex, approximately 600 mg based on the polymer) to the steel plate. Water was left to evaporate overnight, generating films of approximately 200 μm thickness, based on the amount of polymer deposited. Because of the low solid content and low viscosity of these latexes, there were no differences between films prepared using a draw-bar (Microm-II, Gardco) or film prepared by brush application. Solvent borne coatings such as ethylene–norbornene copolymers were prepared by applying a 10 wt. % solution of the polymer dissolved in xylene.

2.4.5 Latex characterization

Particle size distribution was assessed by transmission electron microscopy (TEM) and dynamic light scattering (DLS). TEM measurements were effected on a Leo 922 using uranyl acetate as negative contrast agent. Particle size measurements were carried out using a capillary hydrodynamic fractionation instrument, CHDF 2000 from Matec Applied Sciences and by dynamic light scattering using a Nanotrac S/N:U1730 or a Microtrac VSR S3000 instrument.

2.4.5.1 Analysis of polymer microstructure

NMR spectra were recorded in d4-*o*-dichlorobenzene (ODCB) at 115 °C using NMR Varian 400 MHz (Mercury) and 500 MHz (Inova). Polymers were first washed with water in order to remove most of the adsorbed surfactant and unreacted monomer (when present). When residual surfactant was observed by ^{1}H NMR, the integrals of the polymer peaks were corrected to account for the presence of residual surfactant buried under the resonances of the polymer.

2.4.5.2 Pure PE

NMR ^{1}H (ODCB): 0.83 (t, ^{3}J = 6 Hz, CH_3), 1.26 (m, CH_2 "PE"), 1.56 (m, CH), 1.96 (m, CH_2 allyl), 4.71 (s, CH_2=CR_2), 4.86 (d, ^{3}J = 10 Hz, H^1H^2C=CH– trans), 4.92 (d, ^{3}J = 17 Hz, H^1H^2C=CH– cis), 5.35 (m, –CH=CH–), 5.73 (m, CH_2=CH–CH_2–).

2.4.5.3 Poly(ethylene–hexadecene) (expt. 9)

NMR ^{1}H (ODCB): 0.82 (m, CH_3), 1.26 (m, CH_2 "PE"), 1.54 (m, CH), 1.96 (m, CH_2 allyl), 4.71 (s, CH_2=CR_2), 4.86 (d, ^3J = 10 Hz, H^1H^2C=CH– trans), 4.92 (d, ^3J = 17 Hz, H^1H^2C=CH– cis), 5.37 (m, –CH=CH–), 5.73 (m, CH_2=CH–CH_2–).

Molecular weight of a copolymer (M_n, g/mol) was assessed as $M_n = I_{total}(14/2)/[I(–CH=CH_2) + I(–CH=CH–)/2]$ where I is the integral of the corresponding peak. The percentage of hexadecene units incorporation (X_{hd}) was calculated as $X_{hd} = \{28(r - 1 - y)/[M_n - 197(r - 1 - y)]\} \times 100\%$ where r is the ratio of CH_3– groups to the number of double bonds, that is to say the average number of CH_3 groups in a chain: $r = [I(CH_3)/3]/[I(–CH=CH_2) + I(–CH=CH–)/2]$ and y is a fraction of the chains with internal double bond: $y = [I(–CH=CH–)]/[I(–CH=CH_2) + I(–CH=CH–)]$. The number of long branches per 1000 C was assessed as: $N = \{28(r - 1 - y)/[M_n - 197(r - 1 - y)]\} \times 1000/2$.

2.4.5.4 Poly(ethylene–norbornene)

NMR ^{1}H (ODCB): 0.6–1.8 (m, CH_3, CH_2 and $CH_{main\ chain}$), 1.8–2.4 (m, $CH_{bridgehead\ of\ NB}$), 5.00 (m, CH_2=CH–), 5.45 (m, –CH=CH–), 5.77 (m, CH_2=CH–CH_2–).

The percentage of norbornene units incorporation (X_{nb}) was assessed as $X_{nb} = \{2b/(a - 2b)\} \times 100\%$ where b is the intensity of protons of bridgehead CH unit and a is the intensity of protons of the other CH_x (x = 1 or 2) units.[21]

The molecular weights, relative to polystyrene standards, were determined on a Waters GPC equipped with a RI detector and a set of PolymerLabs Mixed C columns. Melting points and T_g were measured on a modulated DSC (Q100, TA Instruments), with DSC scanning rate as 5 °C/min and modulation ±1.5 °C every 60 s.

Minimum Film-Formation Temperature (MFFT) was determined using an application bar constructed according to ASTM method, D 2354-98. The two ends of the metal bar were kept at different constant temperatures which were adjusted in order to provide a linear temperature gradient rising from 10 to 90 °C on the metal bar. The bar was covered by a plastic cover and an adjusted air flux was passed in the space between the bar and plastic cover in order to facilitate water evaporation and film formation.

2.4.6 Electrochemical impedance spectroscopy (EIS)

The anticorrosion properties of the polyolefin films were evaluated by EIS, using a PCI4 750 potentiostat, before and after aging in a Q-Fog Cyclic Corrosion Chamber from Q-Lab. The analysis was conducted in a Gamry PTC1 Paint Test Cell (exposed sample area of 15 cm^2) with 50 mL of electrolyte (NaCl, 0.5 M) equipped with Ag/AgCl electrode as reference electrode, coating sample as working electrode and graphite electrode as counter electrode. AC voltage (sine wave) of 10 mV (rms) was applied on a cell. The measurements were carried out at frequency range from 100 kHz to 0.01 Hz.

2.5 Results and discussion

2.5.1 Copolymers of ethylene with α-olefins

A method of aqueous catalytic miniemulsion polymerization was used for the preparation of latexes of high-density PE which is linear and highly crystalline.[5,19] Even at temperatures as high as 90 °C, no film was formed when the latex was applied onto a steel coupon, because PE crystals are not melted at this temperature, and this prevents the interpenetration of a polymer chain from one dried latex particle to another. Films could be formed by either melting the dried polymer onto the substrate (T = 135 °C) or by solvent-casting from a solution of PE in dichlorobenzene at 130 °C. Both these methods are unpractical in many environments, and we have investigated the preparation of a polyolefinic formulation with a minimum film-forming temperature (MFFT) around room temperature.

For this purpose, we first considered the preparation of copolymers of ethylene with hexadecene (Figure 2.1). They were prepared in an emulsion process, using a nickel-based catalyst formed *in situ* as shown in Figure 2.1.[22] The catalyst is air sensitive but it is both water tolerant and active for the copolymerization of ethylene with α-olefins.

The resulting copolymer is a polyethylene, containing a number of C14 branches from hexadecene insertion. Importantly, the catalyst cannot homopolymerize hexadecene, but hexadecence can be incorporated in the ethylenic polymer. The resulting copolymer cannot be dissolved in organic solvents at ambient temperature, which makes the formation of a solvent-cast film impossible at room temperature.

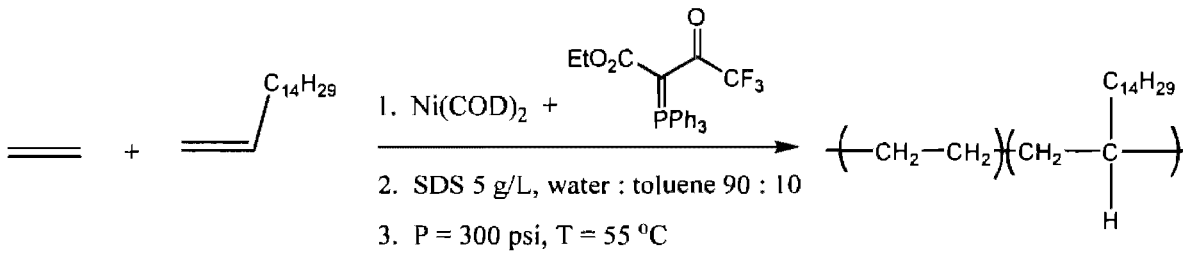

Figure 2.1: Preparation of poly(ethylene-*co*-hexadecene) in miniemulsion, using an *in situ* prepared nickel catalyst.

To our surprise, we found that it was possible to form films from aqueous-borne formulations at room temperature (Figure 2.2).

Several factors were found to influence the film-formation process, such as the solid content of the latex, the amount of hexadecene incorporated into the polymer and the presence of polar groups (*vide infra*). These latexes are prepared by a catalytic miniemulsion process whereby the catalyst, dissolved in a minimum of organic solvent is emulsified with surfactant (SDS) and a hydrophobe in water. The resulting 'miniemulsions' are protected from Ostwald ripening and exhibit droplet of approximately 250 nm in size.

Upon polymerization, each droplet is converted into a latex particle. Results for these miniemulsion experiments carried out in 100 mL of water and at an ethylene pressure of 300 psi (20 atm) are presented in Table 2.1.

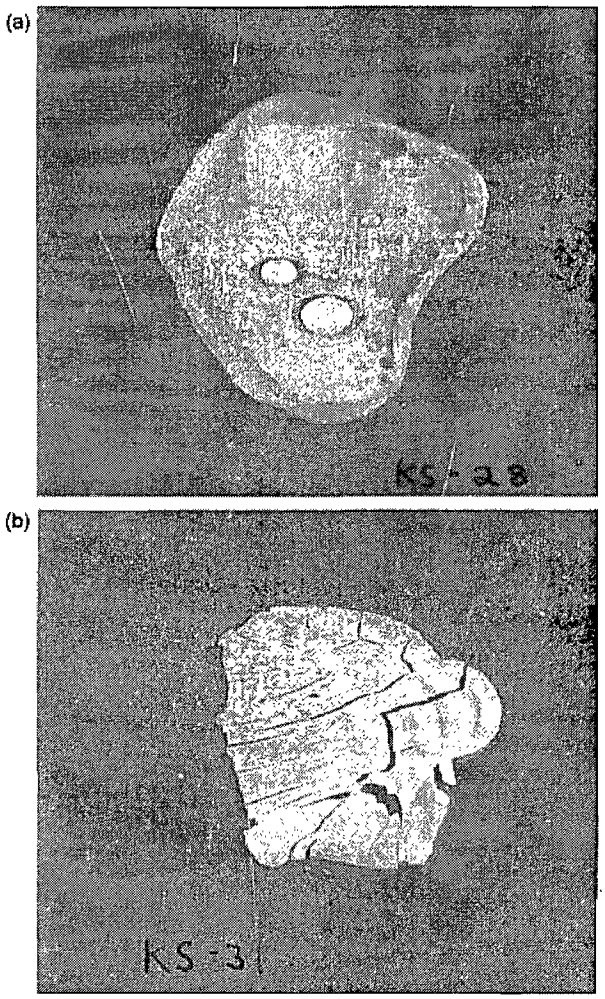

Figure 2.2: Poly(ethylene-*co*-hexadecene) latexes applied on a steel coupon (a: entry 10, b: entry 6 in Table 2.1). At low hexadecene content (b), the polymer crystallinity prevents the formation of a continuous film. Drops of water were deposited onto the coating (a) surface to illustrate the hydrophobicity of the coating. Brown spots: corrosion spots due to the presence of water during the film formation.

Table 2.1: Poly(ethylene-*co*-hexadecene) copolymers prepared by (mini)emulsion polymerization.

Entry	$Ni(COD)_2$ mg	Mol ratio Ni/L	Toluene, (mL)	SDS (g/L)	$C_{16}H_{32}$ (g/L)	T, (°C)	Activity max, ($kg_{PE}/g_{Ni}/h$)	particle size (nm)	SC[f] of latex, (%)
1	33	4/1	20	15	15	65	12	floc	21.4
2	11	4/1	10	15	15	65	5	floc	11.5
3	11	4/1	3	5	10	65	4.5	470	7.5
4[a]	4.6	2/1	13	20	20	55	21	1205	8.6
5[a]	9.2	2/1	13	15	15	55	11	floc	18.0
6[b]	9.2	2/1	13	15	15	55	9	98.1	26.7
7[b]	9.2	2/1	13	15	30	55	4	72.9	17.5
8[b]	9.2	2/1	13	15	45	55	4	295	13.9
9[b]	9.2	2/1	13	15	60	55	5	285	24.1
10[b]	9.2	2/1	13	15	75	55	6	95.2	20.7
11[b]	9.2	2/1	13	15	90	55	7	260	24.4
12[c]	9.2	2/1	13	15	15	60	0.5	145[d]	22.0
						80[e]	1.5		

[a] Significant flocculation was observed. [b] Increased power of sonication. [c] 10-undecen-1-ol in conc. 45 g/L was added. [d] Measured by CHDF. [e] After 3 h of reaction. [f] SC is solid content of the latex (%).

For these experiments, the peak activity does not change and the solid content remains around to 20 % when the latex is stable: the resulting copolymer contains less than 350 ppm of nickel black (metal).

In contrast to our past study[22] that focused mostly on latexes with low solids, it was necessary to prepare latexes with moderate to high solid contents and with a wide range of particle size distributions. Higher solid contents were required in order to favor the film-formation process. This was achieved by varying several parameters such as the amount of catalyst and solvent, the temperature of the reaction, the sonication power during the catalyst emulsification step, the concentration of surfactant and hexadecene (hydrophobe and comonomer) and the molar ratio of $Ni(COD)_2$/keto-ylide (the two components of the catalytic system). As seen from Table 2.1, an increase in sonication power (entries 6–12, Table 2.1) during the formation of the miniemulsion results in solid contents as high as 27 %, smaller particle sizes and a lower amount of coagulum, as confirmed by TEM (Figure 2.3). Partially flocculated latexes (entries 1–5; low sonication power) possess large aggregates making them unsuitable for smooth film formation.

Among stable latexes (entries 6–12; high sonication power, Figure 2.3) it was found that only polymers with hexadecene incorporation values higher than approximately 3.5 mol. % are capable of forming films at room temperature (Figure 2.2a and entry 10 in comparison to Figure 2.2b - entry 6).

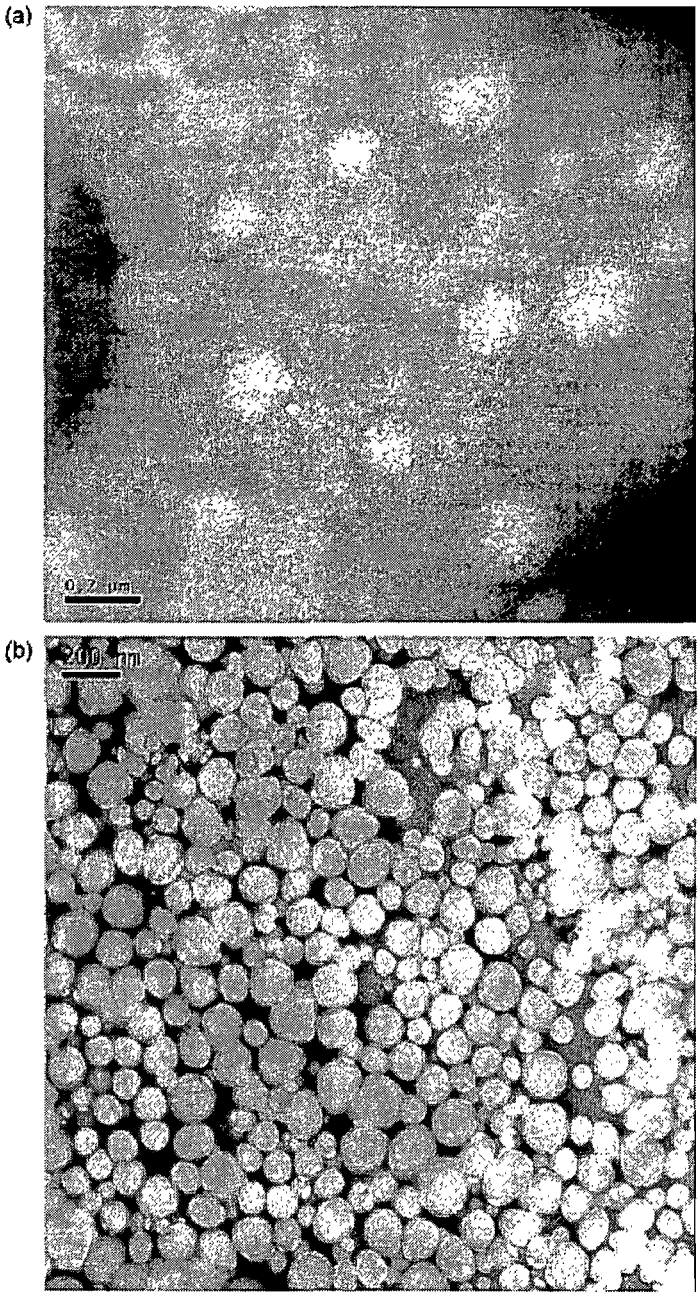

Figure 2.3: TEM micrograph of latexes of (a) poly(ethylene-*co*-hexadecene) (entry 9, Table 2.1) and (b) poly(ethylene-*co*-undecenol) (entry 12 (b), Table 2.1).

The coating from entry 7 displayed a few small cracks, which is consistent with a relatively high melting point and crystallinity (108.3 °C and 25.5 % versus 98.3 °C and 17.2 % in the case of expt. 10). At lower hexadecene incorporation (0.9–3.2 mol. %) the aqueous-borne films are extremely brittle with no adhesion to the surface (expts. 6, 8, 9, 11). Corresponding minimum film formation temperature (MFFT) values were found to be higher than 50 °C. Although the latexes did not contain floc just after synthesis, they slowly creamed after a few days. This can be explained by the higher crystallinity of these polymers, in accordance with literature data on instability of crystalline-PE latexes.[17,18]

The reactions were performed with a fixed amount of hexadecene which is introduced at the beginning of the reaction, whereas ethylene is continuously fed into the reactor. As a result, early during the polymerization, hexadecene is inserted, resulting in the formation of true copolymers, whereas later on during the reaction, mostly pure polyethylene is formed. Analysis of the microstructure by ^{13}C NMR indicates that the hexadecene units are always isolated along the chain, which is in agreement with the overall low incorporation ratio (Table 2.2). Thus, the polymer produced in these reactions is a mixture of branched and linear PE. This is confirmed by DSC which shows very broad melting transitions, indicative of the heterogeneity of the polymer. The DSC characteristics of these copolymers (Table 2.2) resemble those of ultra low-density PE: the melting transition extends from –50 °C to above 100 °C.

Table 2.2: Characterization of the poly(ethylene-*co*-hexadecene) copolymers.

entry	Como-nomer incorpor. (mol. %)[c]	Branch/ 1000 C	M_n (g/mol)[c]	T_m (°C)	ΔH_{melt} (J/g)	% Crystal-linity	Onset point (°C)	% PE melted below RT
100% cryst PE[a]	-	-	-	140	290	100	-	-
Pure PE[b]	-	~0	1400	116.4	131.2	45.2	50	0
6	2.7	13.5	900	115.2	112.0	38.6	-15	3.9
7	4.6	23.0	400	108.3	75.0	25.9	-25	10.3
8	0.9	4.5	2640	107.5	57.4	19.8	-45	14.6
9	3.2	16.0	2060	109.5	63.3	21.8	-30	11.4
10	3.5	17.5	950	98.3	50.6	17.4	-40	21.1
11	3.0	15.0	880	102.2	62.6	21.6	-50	18.5
12	n/d	n/d	480	100.9	69.3	23.9	-60	17.6

[a] Values from ref. 23. [b] Polymerization in toluene. [c] From NMR, assuming copolymers possess no short branches, which is the case for the homopolymerization of ethylene, n/d—not determined.

Accordingly, several thermal characteristics of these polymers values are consigned in Table 2.2: onset of the melting peak, top of melting peak (T_m), amount of crystallinity calculated using a standard $\Delta H_{melt} = 290$ J/g for pure PE,[23,24] and amount of PE melted below room temperature (25 °C). There is no precise correspondence between comonomer incorporation and capacity to form films (compare, for example, entry 7 for which the film has small cracks and 10, Figure 2.2a). Other factors, such as amount of crystallinity, melting transition temperature and amount of PE melted below room temperature are important. It is important to remember that the latex formed by this catalytic process is heterogeneous: it contains pure ethylene linear chains as well as hexadecene-rich branched chains. In the case of entry 10, the polymer is very heterogeneous, as shown by the very broad melting transition in DSC (the onset of the peak is at –40 °C, whereas the top of the peak is at 98 °C). Although the amount of incorporated hexadecene is not the highest, a small portion of the chains is highly branched, and is in the melt at room temperature. The fraction of such chains is sufficiently high to allow film formation. On the other hand, for the polymer from entry 9, which contains an equivalent amount of hexadecene, the melting transition is not as broad, and does not contain a large enough amount of melted chains at room temperature to allow for the formation of a continuous film. We infer that the melted fraction acts as glue between crystallites, insuring film cohesion.

Contrarily to our expectations, inserting hexadecene in the chain is not sufficient to break the crystallinity, and it does not produce an amorphous polymer, however, it yields crystallites with very low melting points. The films resulting from these polymers are never

totally transparent, even with little crystallinity. It could be argued that in the presence of this residual crystallinity, no complete coalescence occurs. Coalescence would only be complete if all crystallinity has disappeared, resulting in a polymer which would be liquid at room temperature.

The poly(ethylene-*co*-hexadecene) films are waxy and do not adhere very well to a metal substrate or to an epoxy substrate. Introduction of polar groups can improve adhesion and possibly facilitate polymer chains interpenetration in between polymer particles during film formation. For this purpose, 10-undecen-1-ol was chosen as a comonomer because it resembles hexadecene, both containing a terminal double bond and a long normal aliphatic chain. In particular, during the polymerization the "poisoning" effect[25,26] which is due to the presence of a polar functionality in a monomer is not predominant for the case of undecenol copolymerization because the hydroxyl functionality is far from the double bond and therefore from the coordination site of the catalyst. The miniemulsion procedure requires the presence of a hydrophobe to prevent the initial droplets from undergoing Ostwald ripening. Undecenol was found to be unable to provide this stabilization mechanism (not hydrophobic enough), therefore hexadecene was also used in the copolymerization. The resulting copolymers are supposed to be copolymers of ethylene, hexadecene and undecenol (Table 2.1, entry 12). Using ^{1}H NMR spectroscopy, it was found that undecenol is the only comonomer which is inserted under these conditions. This copolymer is able to form a film (MFFT less than room temperature) which adheres well to a metallic substrate (adhesion strength was not assessed quantitatively, but the film could

not be peeled off manually, unlike the poly(ethylene-*co*-hexadecene) copolymers. Visual inspection indicates that the film-formation process is satisfactory. However, these films were found to be very tacky, as expected for films where a significant portion of the polymer is in the melt. This prompted us to turn our attention toward another choice of comonomer.

2.5.2 Copolymers of ethylene with norbornene

Copolymers of ethylene with α-olefins are essentially crystalline. The crystallinity can be reduced by incorporation of hexadecene comonomer, but the estimated T_g of the amorphous phase is extremely low (~ −100 °C, close to the one of polyethylene). In order to address this problem, we have turned our attention toward the ethylene–norbornene copolymers. Poly(1,2-norbornene) has a T_g which is above 350 °C, temperature at which it decomposes. Thus, by adjusting its composition, it is virtually possible to tune the T_g of an ethylene–norbornene copolymer from −100 to 350 °C which corresponds to the approximate T_g of pure polyethylene and polynorbornene.[27]

Our first polymerization trials, using the aforementioned nickel-based catalyst, resulted in the formation of only a small amount of copolymer (~0.05 g) with a T_g = −15 °C (Figure 2.4). Thus, this catalyst has not been selected to prepare these copolymers.

The polymers were thus prepared using a Pd-based arylsulfonated phosphine catalyst (Figure 2.5).

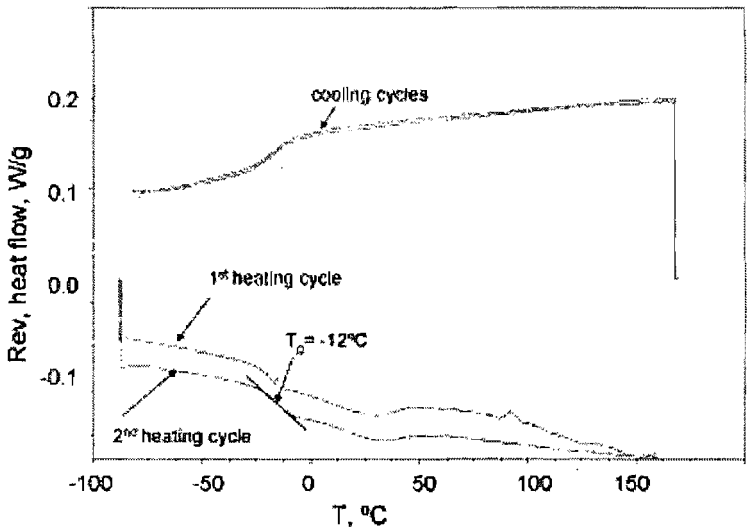

Figure 2.4: DSC of poly(ethylene-*co*-norbornene) obtained with a Ni-based catalyst.

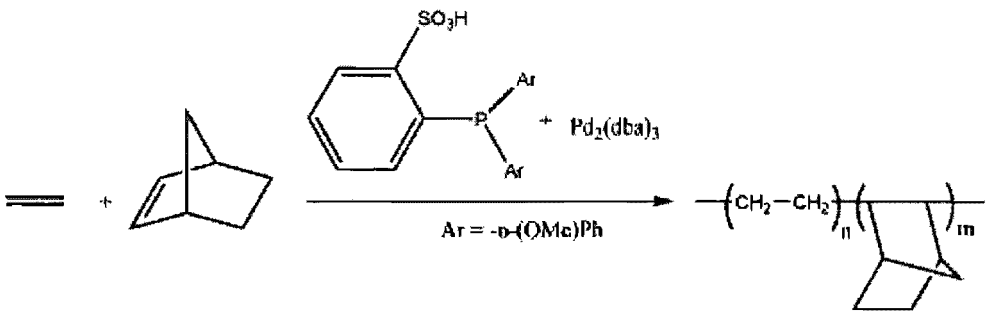

Figure 2.5: Copolymerization of ethylene and norbornene using a palladium arylsulfonate phosphine-based catalyst.

The synthesis of the polymers either in toluene solution or in an emulsion-based process has been described in a recent work.[28] A large range of copolymers was prepared, containing up to 50 mol. % of norbornene. Thus, the T_g of the copolymers could be varied up to 150 °C, which corresponds to the T_g of an alternated atactic ethylene–norbornene copolymer. When the amount of inserted norbornene is below 12 mol. %, the crystallinity of the polyethylene becomes predominant, and the polymer melts at temperatures higher than 90 °C.[29] Thus copolymers containing less than 12 mol% of norbornene are not suitable to form films (Table 2.3), whereas copolymers with higher percentage can be used to form films via a solvent-casting process (Figure 2.6).

2.5.3. Anticorrosion coatings based on polyolefins

Polyolefins are very hydrophobic and they should be able to prevent the diffusion of water to a metallic surface, and therefore act as a barrier coating. Barrier coatings are usually used as top-coats. Accordingly, two types of coatings were prepared: as a single layer coating applied directly onto steel, and as a top-coat applied on an epoxy primer. Two methods were used to prepare the coatings: the first one consists in applying a latex (aqueous-borne coating) and the second one consists in applying a polymer solution (5–10 wt. % in xylene, solvent borne coating). At room temperature, hexadecene-containing films can only be prepared via an aqueous-borne process. When applied directly on steel, the water from the latex is trapped under the coating, generating corrosion spots which are visible (Figure 2.2a).

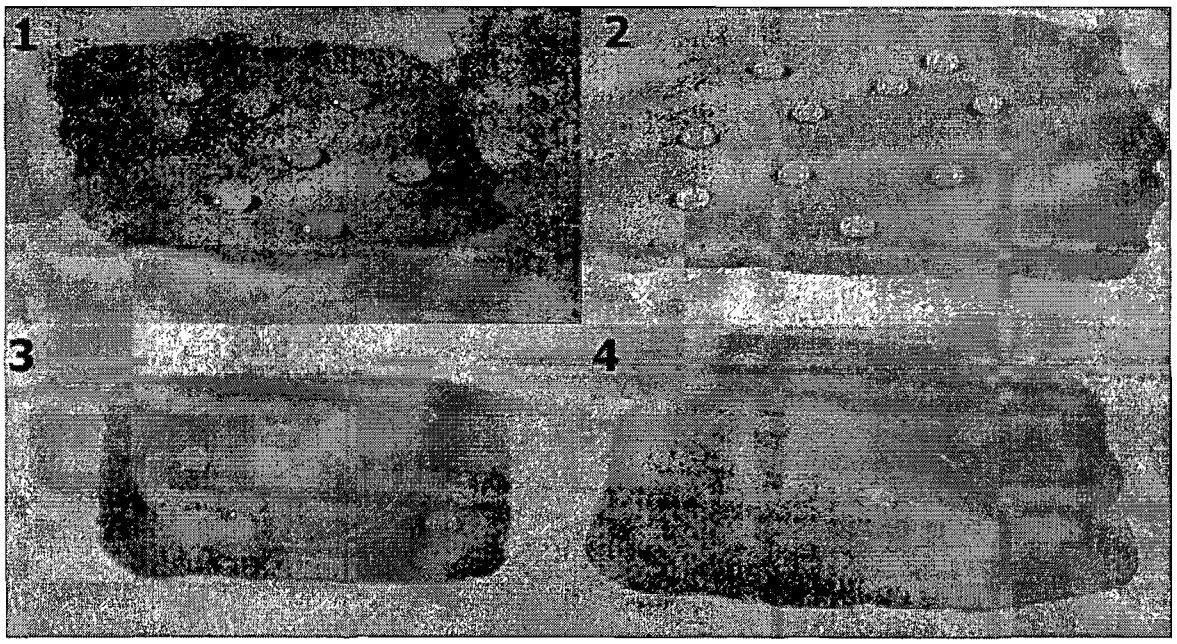

Figure 2.6: Coatings of poly(ethylene-*co*-norbornene) prepared by solvent-casting a xylene solution of the polymer onto steel coupons (1 – expt. 13; 2 – expt. 14; 3 – expt. 15; 4 – expt. 16 in Table 2.3). The circles correspond to the imprint of the corrosion cell used for the EIS experiment. Drops of water have been deposited onto the coatings to illustrate the hydrophobicity of the surface.

Table 2.3. Ethylene–norbornene copolymerization in solution in toluene (T = 95 °C, m (toluene) = 100 mL, m (phosphine) = 2.1 mg, m ($Pd_2(dba)_3$) = 2.0 mg).

Experiment	Conc. norbornene (g/L)	P_{Et} (psi)	norbornene (mol. %)	$m_{polymer}$ (g)	T_g (°C)	T_m (°C)	M_n (g/mol)	PDI[a]
13	50	300	38	0.33	78	-	31450	2.08
14	100	300	42	0.71	103	-	51230	1.89
15[a]	12	100	21	1.49	17	-	26040	1.76
16[a]	11	200	19	1.55	18	-	27030	1.75
17	10	300	11	2.58	15	98	n/m	n/m

n/m – not measured. [a] By GPC.

Therefore, two-layer coatings were evaluated, consisting of an epoxy primer applied on steel, and a poly(hexadecene-*co*-ethylene) on top of it. An epoxy coating was chosen because it is widely used as anticorrosion primer on steel.[30]

The EIS studies of these polyolefin compositions were carried out using 0.5 M solution of NaCl as electrolyte. Bode and Nyquist plots were recorded at frequencies ranging from 100 kHz to 0.01 Hz. The EIS measurements were corrected to 15 cm^2 area of solution-coating contact and reported as polarization resistance (R_p). Reasonable fits for Bode and Nyquist plots were found using two circuit models, one for an insulated coating (an uncompensated resistance in series with a polarization resistance and parallel capacitor) and one for a coating with water diffusion (see Figure 2.7). The model providing the best fit was retained for the analysis of the data.[31-33]

When the aqueous-borne PE-coating (entry 10 in Table 2.1) was applied on the epoxy primary coating, the value of polarization resistance (R_p) was unexpectedly low ($7.5 \cdot 10^6\ \Omega\ cm^2$). The data were suitable fitted by a diffusion model, indicating that these coatings do not exhibit acceptable barrier properties. Possibly, diffusion of water from the latex into the epoxy may have occurred during the water evaporation. Alternatively, the coating has started to detach from the epoxy surface because of its low adhesion. A marginally higher R_p ($2.4 \cdot 10^8\ \Omega\ cm^2$) was observed for the coating prepared in entry 12 with undecenol as comonomer, which exhibits improved adhesion.

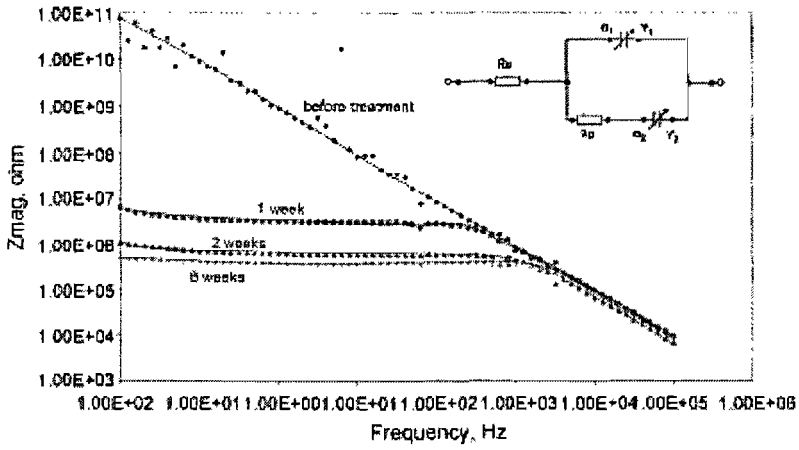

Figure 2.7: Bode plots for ethylene–norbornene coatings (entry 16 and Table 2.5) before and after treatment in cyclic corrosion chamber Q-Fog.

Therefore, we believe the presence of water during coating preparation steps makes the coating composition permeable to water and consequently decreases polarization resistance values, and this prompted us to investigate copolymers of ethylene and norbornene which can be used in solvent-based formulations.

The poly(ethylene-*co*-norbornene) coatings were applied directly onto the steel surface from a xylene solution. Polarization resistance of these coatings (Table 2.4) ranged from $3.5 \cdot 10^7$ to $1.5 \cdot 10^{12}\ \Omega\ cm^2$. These values are reasonable for a barrier coating, considering a conventionally accepted arbitrary value of $R_p \approx 106\ \Omega\ cm^2$ as the lower limit for an efficient anticorrosion coating.[34] These coatings were aged in an accelerated manner using a Q-Fog chamber (a salt box), and the EIS was measured after being aged for 1, 2 and 8 weeks (Figure 2.7, Table 2.4 and Table 2.5). After 1 week the coating from expt. 13 showed a value of $R_p = 6.0 \cdot 104\ \Omega\ cm^2$ and it had lost its anticorrosion properties, so that it was not further considered. The R_p values for the coatings from expts. 14 and 15 were respectively $7.7 \cdot 10^5$ and $1.6 \cdot 10^5\ \Omega\ cm^2$ which is quite close to the limit of the insulator region, and the coating of expt. 16 has R_p value as $4.5 \cdot 10^7\ \Omega\ cm^2$ which is in insulator region, but the decreased values mean that the pores open up and the coatings start to be permeable to water. On the 2nd week, the coatings from expts. 14 and 15 had a polarization resistance of respectively $1.3 \cdot 10^5$ and $3.4 \cdot 10^4\ \Omega\ cm^2$. These values are characteristic of a loss of anticorrosion characteristics. At the same time the coating from expt. 16 has a polarization resistance value of $8.7 \cdot 10^6\ \Omega\ cm^2$, which means that after 2 weeks of harsh treatment the coating is still not completely permeable to water.

Table 2.4: EIS R_p values for poly(ethylene-*co*-norbornene) coatings (entries 13–16) before and after treatment in acyclic corrosion chamber Q-Fog.

Time in Q-Fog	entry 13, R_p (Ω cm^2)	entry 14, R_p (Ω cm^2)	entry 15, R_p (Ω cm^2)	entry 16, R_p, (Ω cm^2)
before treatment	3.45×10^{7}	8.85×10^{8}	6.02×10^{8}	1.48×10^{12}
1 week	6.00×10^{4}	7.71×10^{5}	1.64×10^{5}	4.49×10^{7}
2 weeks	1.50×10^{5}	1.26×10^{5}	3.42×10^{4}	8.69×10^{6}
8 weeks	3.08×10^{3}	2.55×10^{5}	3.02×10^{4}	5.25×10^{6}

Table 2.5: EIS values for poly(ethylene-*co*-norbornene) coating (entry 16) before and after treatment in acyclic corrosion chamber Q-Fog. The values are obtained by fitting either a simple resistive coating model (polarization resistance in parallel with a capacitance and in series with an uncompensated resistance), or a model which takes into account the diffusion a water (see Figure 2.7).

time	Model							
	Resistive coating			Diffusion model				
	R_p (Ω cm^2)	Y (F s$^{\alpha-1}$)	α	$R_{p,}$ (Ω cm^2)	Y_1 (F s$^{\alpha-1}$)	α_1	Y_2 (F s$^{\alpha-1}$)	α_2
before treatment	1.48×10^{12}	1.80×10^{-10}	1.0					
1 week	5.04×10^{7}	1.78×10^{-10}	1.0					
2 weeks				8.69×10^{6}	2.36×10^{-10}	1.0	7.06×10^{-6}	0.41
8 weeks				5.25×10^{6}	1.80×10^{-10}	1.0	2.36×10^{-5}	0.54

At that point, all the EIS data could be effectively fitted by a diffusion circuit model (Figure 2.7 and Table 2.4 and Table 2.5). On the 8th week, the coatings from entries 13 to 15 had completely lost their insulator ability, but the coating from entry 16 shows R_p value of $5.2 \times 10^6\ \Omega\ cm^2$, indicating that the coating is still performing as a barrier coating, albeit less efficiently than before treatment. This is expected, as an 8-week aging treatment is considered as a treatment sufficiently long to discriminate between an acceptable and a non-acceptable coating. The EIS Bode and Nyqist plots for the coating from the polymer of entry 16 are shown in Figure 2.7, indicating that R_p is decreasing with treatment duration. Obviously the anticorrosion properties of these coatings are inferior to existing commercial products. However, it is important to remember that commercial products, which are the results of a long optimization process, are most often formulated and anticorrosion properties are not only conveyed by the resin, but also by the additives.

It is interesting to notice that anticorrosion properties are related to the amount of norbornene incorporated into the copolymer. As seen from Table 2.3, the coating with optimal anticorrosion properties is the amorphous polymer with the lowest norbornene incorporation (19 mol. %). Coatings with higher norbornene incorporations are amorphous, but probably are more permeable to water because of the lower content of ethylene units. On the other hand, if the amount of ethylene in the copolymer is larger than 85 mol. %, then the copolymer is crystalline (see entry 17), and it is not prone to form a coating.

2.6 Conclusions

Latexes of ethylene–hexadecene were obtained by catalytic emulsion polymerization with solid contents up to 27 wt. %. The latexes can be applied to several substrates (epoxy, steel) where they form films upon water evaporation, owing to the low crystallinity of the polymer. However, the films are very tacky and do not adhere well to the substrate at which they are deposited. These films perform poorly as anticorrosion barrier coatings, probably because of trapped water in the coating when the film is formed.

Ethylene–norbornene copolymers have been produced under the form of latexes and also dissolved into organic solvents. Solvent-borne coatings were prepared using these polymers. Interestingly, there is an emerging structure–property relationship between the composition of the copolymer and its capacity to prevent corrosion, as the film constituted of the amorphous polymer having the highest percentage of ethylene is the film having the best anticorrosion behavior. Additionally, this film is hydrophobic and is expected to have excellent UV and chemical stability, because it is only constituted of saturated hydrocarbons. Therefore, although far from a commercially acceptable solution in the present state, it is possible that it would be an interesting candidate for a binder component of anticorrosion barrier coating formulations.

2.7 Acknowledgements

This work was supported by the ONR (Grant N0000140410693), UQAM (PAFARC program) and by NanoQuébec (IMR program). We thank Dr. Farrel Martin for his generous assistance and training for the realization and interpretation of EIS experiments.

2.8 References

1. G.M. Harris, Mater. Protect. Perform. 12 (1973), 19–22
2. A.S. Bel'chikov, L.P. Vasil'eva, I.N. Popova, A.Kh. Spivak, Plast. Massy 4 (1976), 65–66.
3. E. Almeida, Ind. Eng. Chem. Res. 40 (2001), 15–20.
4. P.A. Steward, J. Hearna, M.C. Wilkinson, Adv. Colloid Interf. Sci. 86 (2000), 195–267.
5. R. Soula, C. Novat, A. Tomov, R. Spitz, J. Claverie, X. Drujon, J. Malinge, T. Saudemont, Macromolecules 34 (2001), 2022–2026.
6. H.A. Schneider, Polymer 46 (2005), 2230–2237.
7. D. Mäder, J. Heinemann, P. Walter, R. Mülhaupt, Macromolecules 33 (2000), 1254–1261.
8. J.M. Santos, M.R. Ribeiro, M.F. Portela, J.M. Bordado, Chem. Eng. Sci. 56 (2001), 4191–4196.
9. P.S. Chum, W.J. Kruper, M.J. Guest, Adv. Mater. 12 (2000), 1759–1767.
10. B.R. Johnson, Ind. Chem. (Lond.) 13 (1988), 427–432.

11. N.S. Sangaj, V.C. Malshe, Prog. Org. Coat. 50 (2004), 28–39.

12. C.H. Klute, P.J. Franklin, J. Polym. Sci. 32 (1958), 161–176.

13. S. Marais, Q.T. Nguyen, C. Devallencourt, M. Metayer, T.U. Nguyen, P. Schaetzel, J. Polym. Sci., Part B: Polym. Phys. 38 (2000), 1998–2008.

14. H. Miyamoto, Water Supply (1987), 5.

15. AWWA C105/A21.5-99, "ANSI Standard for Polyethylene Encasement for Ductile-Iron Pipe Systems", AWWA, Denver, CO (1999).

16. V. Otieno-Alego, G.A. Heath, D.L. Hallam, D.C. Creach, Proceedings—Corrosion and Prevention (1997), 1–8 paper 019.

17. R. Soula, J.P. Broyer, M.F. Llauro, A. Tomov, R. Spitz, J. Claverie, X. Drujon, J. Malinge, T. Saudemont, Macromolecules 34 (2001), 2438–2442.

18. F.M. Bauers, M.M. Chowdhry, S. Mecking, Macromolecules 36 (2003), 6711–6715 (and references within).

19. F.M. Bauers, R. Thomann, S. Mecking, J. Am. Chem. Soc. 125 (2003), 8838–8840.

20. E. Drent, R. van Dijk, R. van Ginkel, B. van Oort, R.I. Pugh, Chem. Commun. (2002), 964–965.

21. C.H. Bergstrom, B.R. Sperlich, J. Ruotoistenmaki, J.V. Seppala, J. Polym. Sci., Part A 36 (1998), 1633–1638.

22. R. Soula, B. Saillard, R. Spitz, J. Claverie, M.F. Llaurro, C. Monnet, Macromolecules 35, (2002), 1513–1523.

23. P.J. Flory and A. Vrij, J. Am. Chem. Soc. 85 (1963), 3548–3553.

24. M. Gopalan and L. Mandelkern, J. Phys. Chem. 71 (1967), 3833–3841.

25. L.S. Boffa and L.M. Novak, Chem. Rev. 100 (2000), 1479–1493.

26. S. Borkar, H. Yennawar, A. Sen, Organometallics 26 (2007), 4711–4714.

27. X. Mi, Z. Ma, L. Wang, Y. Ke Y. Hu, Macromol. Chem. Phys. 204 (2003), 868–876.

28. K.M. Skupov, P.R. Marella, J.L. Hobbs, L.H. McIntosh, B.L. Goodall, J.P. Claverie, Macromolecules 39 (2006), 4279–4281.

29. K. Thorshaug, R. Mendichi, L. Boggioni, I. Tritto, S. Trinkle, C. Friedrich, R. Mülhaupt, Macromolecules 35 (2002), 2903–2911.

30. For example M.Y. Shon, H.S. Kwon, Corrosion Science 49 (2007), 4259–4275.

31. D. Loveday, P. Peterson, B. Rodgers, J. Coat. Technol. Coat. Tech. 8 (2004), 46–52.

32. D. Loveday, P. Peterson, B. Rodgers, J. Coat. Technol. Coat. Tech. 10 (2004), 88–93.

33. D. Loveday, P. Peterson, B. Rodgers, J. Coat. Technol. Coat. Tech. 2 (2005), 23–27.

34. S.K. Singh, S.P. Tambe, V.S. Raja, D. Kumar, Prog. Org. Coat. 60 (2007), 186–193.

Chapter 3

RESEARCH PAPER (COMMUNICATION)

Catalytic Copolymerization of Ethylene and Norbornene in Emulsion

K. M. Skupov[a], P. R. Marella[a], J. L. Hobbs[a], L. H. McIntosh[b], B. L. Goodall[b], J. P. Claverie[a]

[a] Materials Science Program, University of New Hampshire, Durham, New Hampshire 03824.

[b] Emerging Technology Department, Rohm and Haas Company, 727 Norristown Road, PO Box 904, Spring House, Pennsylvania 19477.

Macromolecules 2006, 39 (13), 4279-4281.

Received May 15, 2006; Revised Manuscript Received May 21, 2006; Published online 1 June 2006.

The paper is devoted to the synthesis of poly(ethylene-*co*-norbornene) in organic solution and in aqueous emulsion. The polymerization in aqueous emulsion leads to the formation of the latexes. The copolymers and latexes were characterized by DSC, GPC, TEM, NMR and DLS. My contribution (75 % of the work presented here) includes the synthesis and characterization of most of the copolymers and latexes by DLS, DSC, TEM, NMR, GPC. J. Hobbs, an undergraduate student, contributed by preparing several of the copolymers under my guidance. P. Marella prepared the ligands, following the synthesis which was developed by the group of B. Goodall in Rohm and Haas. L. McIntosh and B. Goodall contributed to the research intellectually by giving us access to an efficient protocol for the ligand synthesis.

3.1 Introduction

The copolymerization of ethylene and norbornene (NBE) has attracted a lot of attention recently.[1] Unlike pure polyethylene, the copolymer is amorphous with a T_g potentially varying from −100 °C to more than 300 °C (corresponding to the T_g of pure PE and PNBE).[2] Clearly, latexes of such polymers would present unique properties, as conventional latexes are usually limited to T_g's up to 125 °C (T_g of PMMA). They would also be highly durable, UV and chemically resistant, and very hydrophobic. Such latexes could be prepared by an emulsion polymerization process which is a widely spread technology in polymer manufacturing.[3] Furthermore, the use of water as a suspending medium is an environmental advantage, and it can be safely used as a continuous phase or a solvent for carrying out very exothermic reactions such as polymerizations because of its very high heat capacity. Heterophase polymerizations (in water or any other medium) also benefit from the fact that even at high solids (up to 60 % polymer volume fraction in the liquid) the viscosity remains low or moderate. Finally, the polymer, in the form of a latex, is free-flowing; therefore, it is easily formulated and often does not require any further processing.

We[4] and the group of Mecking[5] have shown that it is possible to prepare latexes of polyethylene by the catalytic polymerization of ethylene. For that purpose, palladium- and nickel-based catalysts were used because of their reduced oxophilicity and their propensity to preferentially coordinate ethylene over water. Such catalysts are usually very hydrophobic, and both groups have shown that it is possible to emulsify the catalytic

solution using a miniemulsion process.[6] This miniemulsified catalyst can then be used as "initiator" in a conventional emulsion process.

In this preliminary report, we describe the preparation of latexes of ethylene and NBE, using a palladium-based catalyst.

3.2 Experimental Section

3.2.1 General

Ligand **A**, P(*o*-OMe-C_6H_4)$_2$(*o*-SO_3H-C_6H_4), was prepared according to the procedure detailed in ref 7. All manipulations were done under argon using standard Schlenk techniques. Water was ultrapure grade (18.2 MΩ) and degassed by boiling for 120 min, followed by sparging with Ar for several hours. NBE was purified by passing it at 50 °C over a bed of activated basic alumina and activated molecular sieves. Sodium dodecyl sulfate (SDS) was recrystallized from methanol. All other chemicals were used without further purification. The molecular weights, relative to polystyrene standards, were determined on a Waters GPC equipped with a RI detector and a set of PolymerLabs Mixed C columns. Particle sizes were measured on a light-scattering Microtrac VSR S3000. Melting points and T_g were measured on a modulated DSC (Q100, TA Instruments). Transmission electron microscopy (TEM) measurements were effected on a Tecnai12 (V = 80 kV, W filament) using uranyl acetate as negative contrast agent.

3.2.2 Typical Solution Polymerization

In a Schlenk tube, 2.24 mg of ligand **A** (5.57×10^{-3} mmol) and 2.0 mg of $Pd_2(dba)_3$ (2.18×10^{-3} mmol) were suspended in 90 mL of toluene. NBE (10 g) was dissolved in 10 mL of toluene. The catalyst solution and the NBE solutions were then introduced into the 300 mL Parr reactor, immediately pressurized with 100 psi ethylene, and heated at 100 °C. When the temperature was reached, the reactor was continuously fed with ethylene at 300 psi, and the conversion of ethylene was monitored on line. After 90 min, the reaction was stopped, and the polymer collected by precipitation in 4 volumes of methanol.

3.2.3 Typical Emulsion Polymerization

In a Schlenk tube, 65.5 mg of ligand **A** (163×10^{-3} mmol) and 59 mg of $Pd_2(dba)_3$ (64×10^{-3} mmol) were dissolved in 20 mL of dichloromethane containing 3.0 g of hexadecane. This solution was introduced in a separate container containing 150 mL of a 20 g/L SDS aqueous solution. The mixture was sonicated using a 600 W Branson sonicator for 4 min and then introduced to the pressure reactor. The reactor was then loaded with NBE and pressurized with ethylene (300 psi). After 1 h (100 °C, 1000 rpm), the reaction was stopped, and a free-flowing white latex was collected from the reactor.

3.3 Results and Discussion

Drent *et al.* first reported that the catalytic system we are using can copolymerize ethylene with acrylates[8] and carbon monoxide with ethylene[7] in a nonalternating fashion.

The phosphine sulfonate is thought to undergo oxidative addition on the palladium(0) complex ($Pd_2(dba)_3$) to generate the active species.[9,10] Well-defined neutral alkyl phosphine sulfonate Pd(II) species have recently been described and used for the nonalternating copolymerization of ethylene and CO in the presence of fluorinated boranes.[9] Since this latter species cannot be used in an aqueous environment, we opted for the borane-free catalytic system constituted of a ligand and a source of Pd(0).

In a typical E-NBE run (Figure 3.1), the catalytic activity, as measured from the uptake of ethylene, increases for the first 20 min and then decreases to virtually zero activity after several hours. In Table 3.1, we report the maximum turnover frequency (TOF, in h^{-1}).

As expected, solution copolymerization of ethylene and NBE in toluene occurs at a slower rate than the homopolymerization of ethylene (entry 1 vs 2 in Table 3.1). NBE incorporation increases as ethylene pressure decreases and NBE concentration increases, reflecting the expected higher reactivity of ethylene vs NBE. As a prerequisite to copolymerizing ethylene and NBE in emulsion, it was necessary to assess the solubility of both monomers and of the catalyst in water. Both catalyst components are completely insoluble in water. Our attempts to prepare stable latexes by introducing the catalytic powder in the aqueous dispersion of monomers and surfactant resulted in the formation of polymer microparticles (average diameter ~44 μm) akin to those formed in a suspension polymerization of ethylene in an alkane diluent.

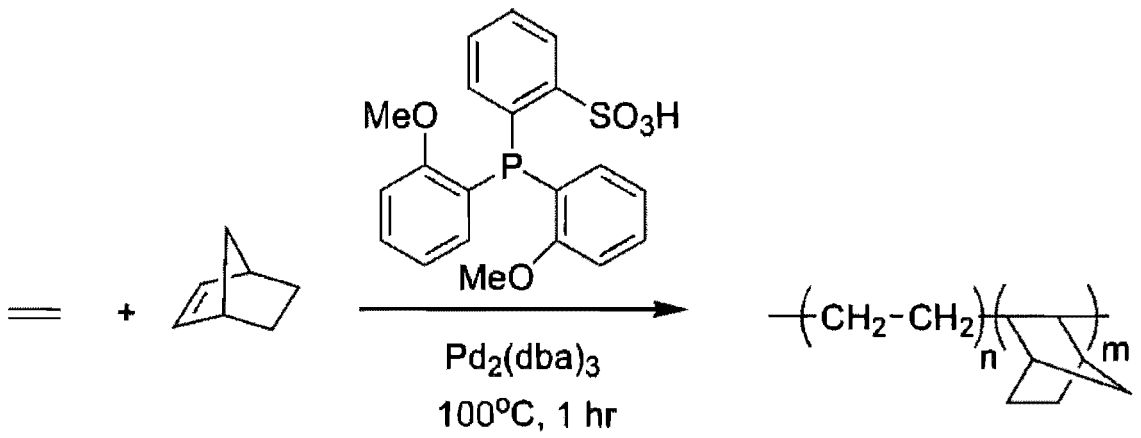

Figure 3.1: Palladium-catalyzed copolymerization of ethylene and NBE (dba = dibenzilideneacetone).

Table 3.1: Experimental Conditions for the Copolymerization of Ethylene and NBE.

entry	[Pd] (μmole/L)	[NBE] (g/L)	P (psi)	process[a]	TOF max (h^{-1})	conv(NBE) (%)
1	24	0	300	S	52000	-
2	24	10	300	S	3000	27
3	23	57	60	S	nd[b]	6
4	24	50	300	S	nd	36
5	24	100	300	S	nd	43
6	25	11	200	S	nd	35
7	25	10	100	S	530	36
8	644	20	300	E	nd	38
9	638	40	300	E	416	51
10	645	100	300	E	nd	42
11	640	50	300	E	326	81
12	644	100	100	E	nd	93
13	1047	50	60	E	nd	32

[a] S stands for solution process, E for emulsion process. [b] nd: not determined (< 300 h^{-1}).

Consequently, the catalyst was dissolved in a minimum of organic solvent (either dichloromethane or toluene) containing hexadecane, and the organic solution was then miniemulsified in an aqueous surfactant solution by sonicating. The resulting miniemulsion has a droplet size, as measured by light scattering, of around 150 nm, and it is stable for several hours. The solubility of NBE in water (0.13 g/L at 25 °C)[11] is comparable to the solubility of styrene in water (0.18 g/L). Thus, as in the case of a styrene radical polymerization, it was possible to introduce NBE in the reaction medium where it forms large droplets stabilized by surfactant. These droplets are significantly larger than the miniemulsion droplets containing the catalyst: as with a conventional emulsion polymerization, they serve as monomer reservoirs, and no polymerization occurs in those, as shown by the absence of large particles in the final latex (Table 3.2 and Figure 3.2). At 300 psi and 100 °C, the solubility of ethylene in water has been reported to be ~1 g/L.[12] Because of its small size (large diffusion coefficient) and high water solubility compared to those of most acrylic and styrenic monomers, transport of ethylene through the aqueous phase occurs readily. Therefore, as in a conventional emulsion polymerization, the diffusion of these monomers through the aqueous phase is not expected to control the rate of polymerization. However, the transport of ethylene at the interface gas water can be rate-limiting: in our hands, activity of the emulsion polymerization strongly depends on the design of the reactor, type of stirring blade used during the polymerization, and of course stirring rate.

Table 3.2: Characteristics of the Copolymers.[a]

entry	polym wt. (g)	SC[b] (%)	d_p[c] (nm)	M_n (g/mol)	PDI[d]	% NBE[e]	T_g[i] (°C)	T_m[i] (°C)	% cryst[j]
1	1.4	na[f]	na	ncs[g]	ncs	0		127	58
2	2.6	na	na	ncs	ncs	12	15	98	5
3	0.5	na	na	48000	2.0	1.8	113		
4	0.9	na	na	32000	2.1	36	78		
5	0.7	na	na	51000	1.9	43	103		
6	1.5	na	na	26000	1.8	35	17		
7	1.6	na	na	27000	1.8	36	18	110	nd
8	na	5.2	418	9000	2.0	38	-11	90	1.5
9	na	5.7	198	4500	2.2	30	7	98	2.5
10	na	floc[h]	365[h]	1900	3.0	13	0	92	4
11	na	9.3	213	4100	2.8	44	139	88	1
12	na	5.1	765	3900	3.0	44	171	97	2.5
13	na	3.6	226	nd	nd	44	140	88	4.5

[a] For the polymers prepared via a solution process, the weight of polymer is reported, whereas the solid content of the latex is reported for the polymers prepared by emulsion polymerization. [b] Solid content. [c] Particle diameter. [d] Polydispersity index. [e] Molar percentage of NBE in the copolymer. [f] Does not apply. [g] Not completely soluble

[h] Flocculated after several hours. [i] Determined in modulated DSC (heating/cooling rate) 5 °C/min, modulation (1.5 °C / 60 s). Values are reported for the first heating pass. [j] Percentage of crystallinity for the polymer in the native state (first heating), based on the ΔH_f of the orthorhombic PE crystal (290 J/g).

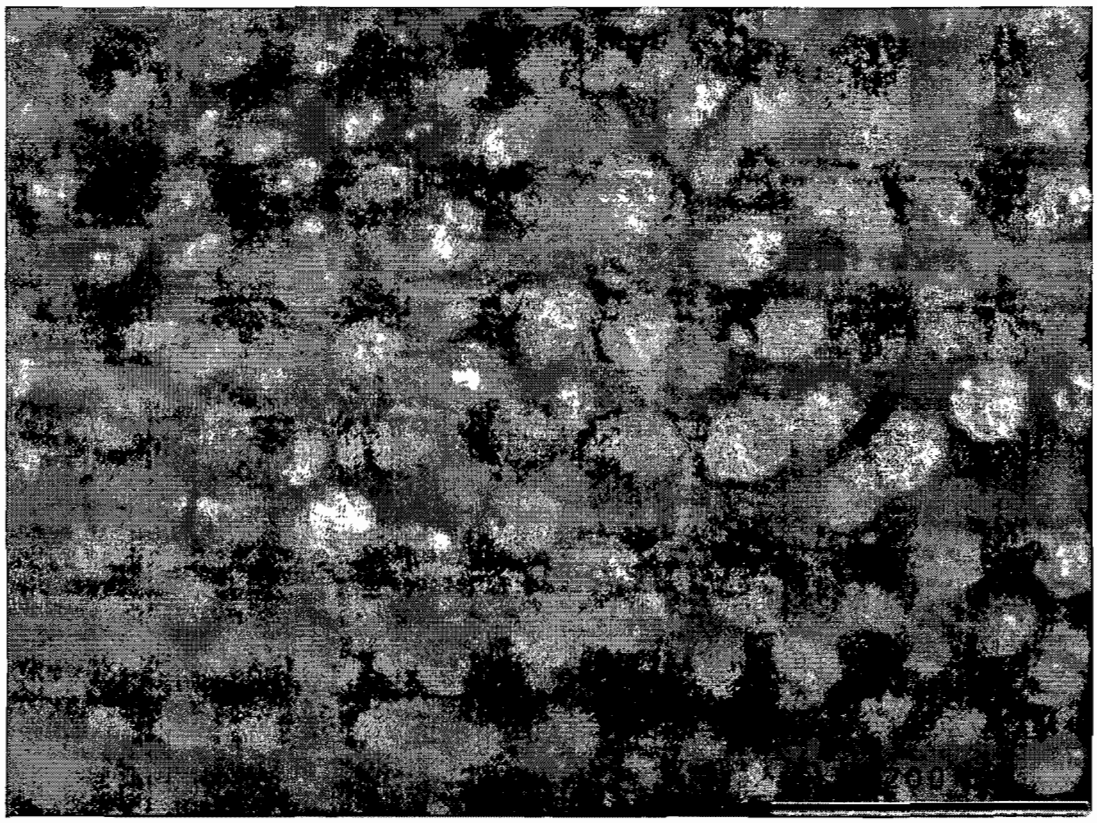

Figure 3.2: TEM cliché of a PE-*co*-PNBE latex (entry 13, Table 3.1).

The polymerization process can be viewed as a hybrid between an emulsion polymerization (monomer and initiator introduced directly to the continuous phase) and a miniemulsion polymerization (monomer and eventually initiator are emulsified in droplets which can be viewed as individual isolated nanoreactors). In our case, the role of the catalytic miniemulsion is unclear: it probably serves as a medium to transport the catalyst. In comparison to a conventional emulsion polymerization, relatively high stir rates (around 1000 rpm) were used, which can promote the fusion and fission of the miniemulsion droplets and therefore diffusion of the catalyst from initial droplets to growing polymer particles.[13] While keeping in mind that physical limitations occur in this type of emulsion polymerization (at least for ethylene), a few observations can be made on the polymerization kinetics: first, the catalytic activity is significantly lower in an emulsion process compared to solution conditions. DeKock *et al.* have reported that water hydrolyzes the metal–alkyl bond of cationic palladium diimine and nickel salicylaldiminate polymerization catalysts.[14] We have found that for the catalytic system A + $Pd_2(dba)_3$ water also acts as a strong poison of the catalyst: the rate of homopolymerization of ethylene in THF decreases when small amounts of water are introduced. For example, under otherwise similar conditions, the TOF is 177 000 h^{-1} in dry THF, 117 000 h^{-1} in THF containing 0.1 % of water, 7 900 h^{-1} in THF containing 1 % water, and nonmeasurable in THF containing 10 % water. The molecular weights of the E-NBE copolymers are also significantly lower when water is present (Table 3.2). It may be explained by possibile effect of water which may lead to chain transfer or deactivate the catalyst (via hydrolysis of the metal–carbon

bond). It is also interesting to note that NBE conversions are in general higher for emulsion than for solution polymerizations (Table 3.1). NBE conversions were calculated from the knowledge of the weight of collected polymer and the copolymer composition, as assessed by ^{1}H NMR.[15] For example, for entries 2 and 3 (solution polymerization), the NBE conversions are 27 % and 6 %, respectively, whereas for entries 11 and 12 (emulsion polymerization), the NBE conversions are 81 % and 93 % (Table 3.1). Higher NBE conversions may be attributed to the compartmentalization effect that occurs in emulsion polymerization: the reaction can be viewed as a bulk (solventless) polymerization occurring in a series of nanoreactors dispersed in water. High local concentration of NBE in each nanoreactor, and possibly slow diffusion of ethylene at the interface gas water, globally favors NBE incorporation. However, this tendency may not to be the same when very different catalyst concentrations and reaction times are applied. The incorporation may also depend on catalyst concentration and reaction time.

The emulsion copolymers are very heterogeneous in composition. They contain a NBE-rich fraction (> 20 mol. %) which is readily soluble in chloroform at room temperature and another fraction which is rich in ethylene and hardly soluble at room temperature. This compositional heterogeneity translates into a very complex behavior in modulated DSC. At the first heating cycle, the reversible heat capacity curve presents one or several broad T_g transitions and one melting point (on the total heat flow curve), whereas at the second heating a single T_g is usually present. The melting point corresponds to the ethylene-rich fraction which is crystalline, and the high T_g corresponds to the NBE-rich

fraction. When the dried latex is analyzed by DSC, both fractions are phase-separated, but when heated past T_g and then cooled, these two fractions become miscible. On the other hand, the copolymer produced in a solvent is not phase separated when dried. The complex DSC pattern observed for the latex is a signature of the morphological features of the latex nanoparticle which is predominantly developed during the emulsion polymerization process.[16] The exact nature of the morphology of PE-*co*-NBE latex particles is currently under scrutiny.

Using ^{13}C NMR analysis,[17] the polymers were found to contain both *meso* and *racemic* NEN sequences (usually in a ratio *m*:*r* = 1:2), as expected in the absence of stereocontrol. No NN diads or NNN triads were observed, which is consistent with the observation that this catalyst does not homopolymerize NBE under these conditions. Polymers having a high NBE content (entries 5 and 12 in Table 3.1) are nearly perfectly alternated ethylene NBE copolymers, which are similar to those produced by constrained geometry catalysts such as $Me_2Si(Me_4Cp)(N^tBu)TiCl_2$.[18] The T_g of these alternated copolymers are ~140 °C (depending on tacticity).[1c]

The resulting latex of this emulsion polymerization is almost devoid of floc and colloidally stable for weeks. Transmission electron microscopy (Figure 3.2) indicates that the nanoparticles are spherical in shape, with a broad size distribution (typically comprised between 50 and 600 nm). Interestingly, we found that some of these latexes can form continuous films upon drying. We envision this could permit the preparation of very hydrophobic, durable, and UV and chemically resistant aqueous-based coatings.

3.4 Conclusion

Using palladium-based catalysts, ethylene and NBE were copolymerized in emulsion. By this route, latexes which are either rich in ethylene or rich in NBE (up to 50 mol. %, corresponding to an alternating copolymer) can be obtained, allowing one to vary the T_g over a large range of temperatures.

3.5 Acknowledgements

This work was supported by the NSF GOALI grant 0354825 and ONR grant N0000140410693. We thank Dr. Pypaert (Yale University) for technical help with the TEM.

3.6 References and notes

1. (a) Kiesewetter, J.; Kaminsky, W. *Chem. Eur. J.* **2003**, 9, 1750. (b) Makovetskii, K. L.; Bykov, V. I.; Bagdasar'yan, A. K.; Finkel'shtein, E. S.; Bondarenko, G. N.; Butenko, T. A. *Vysokomol. Soedin.* **2005**, 47, 197. (c) Benedikt, G. M.; Elce, E.; Goodall, B. L.; Kalamarides, H. A.; McIntosh, L. H.; Rhodes, L. F.; Selvy, K. T.; Andes, C.; Oyler, K.; Sen, A. *Macromolecules* **2002**, 35, 8978. (d) Tritto, I.; Boggioni, L.; Jansen, J. C.; Thorshaug, K.; Sacchi, M. C.; Ferro, D. R. *Macromolecules* **2002**, 35, 616.

2. Goodall, B. L. In *Late Transition Metal Polymerization Catalysis*; Rieger, B., Saunders Baugh, L., Kacker, S., Striegler, S., Eds.; Wiley VCH: Weinheim, **2003**; p 101.

3. Fitch, R. M. *Polymer Colloids: A Comprehensive Introduction*; Academic Press: San Diego, CA, **1997**.

4. (a) Soula, R.; Saillard, B.; Spitz, R.; Claverie, J. P.; Llaurro, M. F.; Monnet, C. *Macromolecules* **2002**, 35, 1513. (b) Soula, R.; Novat, C.; Tomov, A.; Spitz, R.; Claverie, J. P.; Drujon, X.; Malinge, J.; Saudemont, T. *Macromolecules* **2001**, 34, 2022.

5. Bauers, F. M.; Mecking, S. *Macromolecules* **2001**, 34, 1165. Mecking, S.; Held, A.; Bauers, F. M. *Angew. Chem., Int. Ed.* **2002**, 41, 544. Bauers, F. M.; Chowdry, M. M.; Mecking, S. *Macromolecules* **2003**, 36, 6711. Bauers, F. M.; Thomann, R.; Mecking, S. *J. Am. Chem. Soc.* **2003**, 125, 8840

6. See for example ref 4a. For a review on radical miniemulsion polymerization, see for example: Tang, P. L.; Sudol, E. D.; Adams, H. E.; Silebi, C. A.; Aaser, M. S. E. In *Polymer Latexes: Preparation, Characterization, and Applications*; Daniels, E. D. S., El Aasser, M., Eds.; ACS Symposium Series 492; American Chemical Society: Washington, DC, **1992**; p 72.

7. Drent, E.; van Dijk, R.; Van Ginkel, R.; Van Oort, B.; Pugh, R. I. *Chem. Commun.* **2002**, 964.

8. Drent, E.; van Dijk, R.; Van Ginkel, R.; Van Oort, B.; Pugh, R. I. *Chem. Commun.* **2002**, 744.

9. Hearley, A. K.; Nowack, R. J.; Rieger, B. *Organometallics* **2005**, 24, 2755.

10. Kochi, T.; Yoshimura, K.; Nozaki, K. *Dalton Trans.* **2006**, 25.

11. Howard, P. H.; Meylan, W. M. In *Handbook of Physical Properties of Organic Chemicals*; Lewis Publishers: Boca Raton, FL, **1997**.

12. Bradbury, E. J.; McNulty, D.; Savage, R. L.; McSweeney, E. E. *Ind. Eng. Chem.* **1951**, 44, 211.

13. Landfester, K.; Bechtold, N.; Tiarks, F.; Antonietti, M. *Macromolecules* **1999**, 32, 5222.

14. DeKock, R. L.; Hristov, I. H.; Anderson, G. D. W.; Gottker-Schnetmann, I.; Mecking, S.; Ziegler, T. *Organometallics* **2005**, 24, 2679. Hristov, I. A.; DeKock, R. L.; Anderson, G. D. W.; Gottker-Schnetmann, I.; Mecking, S.; Ziegler, T. *Inorg. Chem.* **2005**, 22, 7806.

15. Bergstrom, C. H.; Sperlich, B. R.; Ruotoistenmaki, J.; Seppala, J. V. *J. Polym. Sci., Part A* **1998**, 36, 1633.

16. Stubbs, J. M.; Sundberg, D. C. *J. Polym. Sci., Part B* **2005**, 43, 2790.

17. Tritto, I.; Marestin, C.; Boggioni, L.; Sacchi, M. C.; Brintzinger, H. H.; Ferro, D. *Macromolecules* **2001**, 34, 5770. Tritto, I.; Marestin, C.; Boggioni, L.; Zetta, L.; Provasoli, A.; Ferro, D. *Macromolecules* **2000**, 33, 8931.

18. Ruchatz, D.; Fink, G. Macromolecules 1998, 31, 4674. McKnight, A. L.; Waymouth, R. M. *Macromolecules* **1999**, 32, 2816.

Chapter 4

RESEARCH PAPER (COMMUNICATION)

Palladium Aryl Sulfonate Phosphine Catalysts for the Copolymerization of Acrylates with Ethene

K. M. Skupov[a], P. R. Marella[a], M. Simard[b], G. P. A. Yap[c], N. Allen[d], D. Conner[d], B. L. Goodall[d], J. P. Claverie[a]

[a] Department of Chemistry, UQAM, CP8888, Montreal, QC, Canada

[b] Laboratory of X-ray Diffraction, University of Montreal, QC, Canada

[c] Department of Chemistry and Biochemistry, University of Delaware, Newark, DE, 19716, USA.

[d] Rohm and Haas Company, 727 Norristown Road, Spring House, PA, 19477, USA.

Macromolecular Rapid Communications, 2007, 28, 2033 – 2038.

Received 19 May 2007; Revised 16 July 2007; Accepted 17 July 2007; Published online 3 September 2007

This paper is devoted to the synthesis of well-defined Pd-based sulfonated arylphosphine catalysts with different Lewis bases such as pyridine and N,N,N',N'-tetramethylethylenediamine. When N,N,N',N'-tetramethylethylenediamine was used, a binuclear catalyst was formed. The catalyst showed higher activity than in-situ catalysts, at the same time the different Lewis bases did not affect the activity. Using these catalysts, the copolymers of ethylene with norbornene and acrylates were obtained in organic solution. The X-ray structures of the catalyst coordinated to pyridine and the one coordinated to N,N,N',N'-tetramethylethylenediamine were obtained. The copolymers were characterized by DSC, GPC and NMR.

My contribution to this paper is ~75 % being the synthesis of copolymers and catalysts, their characterization by NMR, DSC and GPC. Pooja Marella, a M.Sc. student at UNH, repeated the synthesis of the catalysts several times. She obtained crystals of the mononuclear catalyst, I obtained crystals of the binuclear catalyst. M. Simard and G. P. A. Yap are the crystallographers who solved the structures. N. Allen, D. Conner and B. Goodall contributed intellectually to the paper by giving us access to an efficient protocol for $PdMe_2$(TMEDA) synthesis and an initial synthetic route for the mononuclear catalyst.

4.1 Abstract

The reaction of 2-[bis(2-methoxy-phenyl)phosphanyl]-4-methyl-benzenesulfonic acid (**a**) and 2-[bis(2',6'-dimethoxybiphenyl-2-yl)phosphanyl]benzenesulfonic acid (**b**) with dimethyl(N,N,N',N'-tetramethylethylenediamine)-palladium(II) ($PdMe_2$(TMEDA)) leads to the formation of TMEDA bridged palladium based polymerization catalysts (**1a** and **1b**). Upon reaction with pyridine, two mononuclear catalysts are formed (**2a** and **2b**). These catalysts are capable of homopolymerizing ethylene and also copolymerizing ethylene with acrylates or with norbornenes. With ligand **b**, high molecular weight polymers are formed in high yields, but higher comonomer incorporations are obtained with ligand **a**.

4.2 Introduction

The evolution of olefin polymerization catalysis since Ziegler's discovery in 1953 has involved a prolific coupling of polymer science with organometallic chemistry. However, there are still no commercially viable catalysts for the controlled copolymerization of simple olefins with polar functional monomers. Currently, commercial processes for the copolymerization of ethylene with polar monomers such as methyl acrylate (MA) or other acrylates employ free radical processes, which require extreme pressures and afford little or no control over polymer architecture (tacticity or crystallinity, blockiness, molecular weight and distribution thereof) and thus limit the range of material performance available. A need exists for new molecular catalysts capable of polymerizing

polar monomers with a controlled microstructure and for copolymerizing the same monomers with olefins (e.g., ethylene, propylene) under mild reaction conditions.[1]

A significant advance was reported by Brookhart *et al.*[2] who discovered that cationic palladium diimines can copolymerize ethylene and acrylates to afford branched copolymers where the acrylate is placed in a terminal position, via a chain-walking mechanism. True main chain insertion was reported for the first time in 2002 by Drent et al.[3] who described the use of a Pd based catalytic system containing a chelating phosphine sulfonate aryl ligand to generate linear copolymers that included the incorporation of acrylate monomers. This seminal report is a proof of the concept that acrylates can be truly copolymerized with ethylene, even though yields, molecular weights and molar incorporations were limited. Also in 2002, the Dupont group[4] reported that linear copolymers of ethylene and acrylates could be prepared by increasing the ethylene pressure to 1 000 psi and by adding large excesses (200 – 300 ×) of the Lewis acid tris(pentafluorophenyl)borane to nickel catalysts bearing hindered diimine ligands ("Brookhart catalysts"). The high pressures required and large excess of Lewis acid used to overcome the «polymer backbiting» problem (backbiting refers to the process in which the carbonyl function of the last inserted acrylate unit chelates the catalyst center and thereby inhibits further monomer coordination and insertion) are reminiscent of conditions used in a work more than 30 years old,[5] in which 2 mol. % of acrylic acid was incorporated into isotactic polypropylene by protecting the acid with a readily available Lewis acid, diethylaluminum chloride. Clearly, there is an important need to develop novel catalytic

structures that are capable tolerating a greater range of functionalities without compromising catalytic activity and to give control over the molecular weight distribution.

Here, we describe well-defined palladium catalysts based on phosphine sulfonate aryl ligands which are capable of incorporating acrylates such as methyl acrylate (MA). Related catalyst structures have been reported recently: a neutral phosphine sulfonate Pd alkyl was recently described by Rieger et al. for the copolymerization of ethylene (E) and CO.[6] Related anionic complexes were also recently reported to copolymerize E and acrylates.[7] In both cases, these catalysts were based on the bis-o-methoxyphenylphosphinobenzene-2-sulfonic acid ligand, which was the original ligand chosen by Drent.[3] In the original report by Drent, and in our work, this ligand yielded polymers of medium to low molecular weight (*vide infra*). In order to address this issue, we present here a significantly bulkier analog, which permits the preparation of high molecular weight polymers with elevated catalytic activities. Interestingly, this novel catalyst is not only capable copolymerizing ethylene with acrylate, but also ethylene with norbornene, thus opening the door to a myriad of novel functional materials.

4.3 Experimental Part

Ligand **a** (2-[bis(2-methoxy-phenyl)phosphanyl]-4-methyl-benzenesulfonic acid, P(o-OMe-C_6H_4)$_2$(-3-Me-6-SO_3H-C_6H_3)), was prepared according to the procedure detailed in ref. 3, but by replacing benzene sulfonic acid by toluene sulfonic acid. A simpler procedure can also be found in ref. 8. Ligand **b** (2-[bis(2',6'-dimethoxy-biphenyl-2-

yl)phosphanyl]benzenesulfonic acid, P[*o*-(2',6'-$(OMe)_2C_6H_3$)-C_6H_4]$_2$(o-SO_3H-C_6H_4)) was prepared according to ref. 8. Dimethyl(N,N,N',N'-tetramethylethylenediamine)-palladium(II) ($PdMe_2$(TMEDA)) was prepared according to ref. 9. All manipulations were done under argon using standard Schlenk techniques. Solvents were purified by distillation over CaH_2 and degassed using three freeze pump thaw cycles, except for diethyl ether (Et_2O), which was purchased in the anhydrous grade and degassed as mentioned above. Solvents were kept over activated molecular sieves. All acrylic monomers were purified by sparging them with argon, and passing them over a bed of inhibitor remover resin (Aldrich), then spiked with tert-butyl catechol (0.25 % wt:wt).

Molecular weight distributions were measured on a Waters Alliance GPC/V 2000 instrument equipped with two Styragel HT6E and one Styragel HT2 column, and a RI detector. The samples were eluted at a flow rate of 1 mL min^{-1} at 135 °C in 1,2,4-trichlorobenzene and stabilized with 2,6-di-tert-butyl-4-methylphenol, BHT (2 g L^{-1}).

4.3.1 Preparation of 1a,

[MePdP(-3-Me-6-SO_3-C_6H_3)(o-OMePh)$_2$]$_2$($NMe_2CH_2CH_2NMe_2$)

0.063 g (0.25 mmol) of $PdMe_2$(TMEDA) and 0.104 g (0.25 mmol) of ligand a were dissolved in 10 mL of dry tetrahydrofuran (THF) under an inert atmosphere and stirred for 1 h. The white precipitate was collected, washed with ether (3 × 5 mL) and dried. This complex was difficult to characterize because of its low solubility in conventional organic solvents. The yield was 0.106 g (0.089 mol, 36 %).

^{1}H NMR ($CDCl_3$): δ = 8.01 (dd, 4 H, $^3J_1$ = 3 Hz, $^3J_2$ = 5 Hz), 7.49 (t, 8 H, ^3J = 7 Hz), 7.01-6.88 (m, 10 H), 3.62 (s, 12 H, OMe), 3.58 (s, 2 H, $Me_2NCH_aH'_aCH_aH_a'NMe_2$), 3.38 (s, 2 H, $Me_2NCH_aH'_aCH_aH'_aNMe_2$), 2.62 (s, 12 H, $(CH_3)_2N$), 2.22 (s, 6 H, CH_3), 0.03 (d, 6 H, $^2J_{HP}$ = 2 Hz, $PdCH_3$).

^{31}P NMR ($CDCl_3$): δ = 3.25 (s, 2 P).

4.3.2. Preparation of 2a, MePd(pyridine)P(-3-Me-6-SO_3-C_6H_3)(o-OMe-Ph)$_2$

0.247 g (1 mmol) of $PdMe_2$(TMEDA) and 0.406 g of **a** (1 mmol) were dissolved in 25 mL of dry THF under an inert atmosphere and stirred for 30 min. Pyridine (0.386 g, 5 mmol) was then added and stirred for another 30 min. During the stirring, white precipitation occurred. After adding 25 mL of Et_2O, the precipitate was collected, washed with Et_2O and dried under a vacuum overnight. The yield was 0.535 g (89%).

^{1}H (CD_2Cl_2): δ = 8.75 (d, ^3J = 5 Hz, 2 H, *ortho*-H $_{pyridine}$), 7.96 (dd, ^3J = 5 Hz, ^3J = 8 Hz, 1H, -C(SO_3)- C**H**-), 7.86 (t, ^3J = 8 Hz, 1 H, *para*-H $_{pyridine}$), 7.60 (m, 2 H, C(OMe)-CP=C**H**-CH), 7.5 (tdd, ^3J = 8 Hz, ^4J = 2 Hz, $^4J_{HP}$ = 2 Hz, C(OMe)-CP=CH-C**H**), 7 (dd, 2 H, ^3J = 8 Hz, ^3J = 6.2 Hz, 2 H, *meta*-H $_{pyridine}$), 7.26 (d, ^3J = 8 Hz, 1 H, CMe=C**H**-CH-C(SO_3)), 7.08 (d, $^3J_{PH}$ = 11 Hz, 1 H, -CP=C**H**-CMe-), 7.1-6.9 (m, 4 H, *meta*-**H** + *para*-**H** in *o*-(OMe)C_4H_6P), 3.68 (s, 6 H, OMe), 2.26 (s, 3 H, ArCH_3), 0.24 (d, $^3J_{PH}$ = 2.79 Hz, 3 H, Pd-Me).

^{13}C (CD_2Cl_2): δ = 160.7 (**C**-Me), 150.4 (N-**C**=C), 146.0 (**C**Me, $^3J_{CP}$ = 15 Hz), 138.6 (PC=**C**H in *o*-OMe-C_6H_4-P, $^2J_{CP}$ = 7 Hz), 137.9 (*ipso*-**C** in *o*-OMe-C_6H_4-P, $^1J_{CP}$ = 57 Hz),

137.5 (CSO_3), 135.1 (*para*-$C_{pyridine}$), 132.2 (CP-CH=**C**H in *o*-OMe-C_6H_4-P), 130.7 (-**C**H-C(SO_3)=C(P)), 127.6 (-CMe=**C**H-CH-C(SO_3)), 126.5 (-CP=**C**H-CMe-), 125.0 (*meta*-$C_{pyridine}$), 120.5 (-CP=C(OMe)-**C**H-, $^3J_{CP}$ = 20 Hz), 116.5 (-**C**(P)-C(SO_3)-, $^1J_{CP}$ = 56 Hz), 111.5 (*para*-**C** in o-OMe-C_6H_4-P), 55.4 (OCH_3), 21.02 (Ar**C**H_3), 0.1 (**C**H_3-Pd)

^{31}P NMR (CD_2Cl_2): δ = 20.3 (s, 1 P).

IR (ATR mode, CH_2Cl_2): 3 200, 2 985, 1 485, 1 260, 1 185, 1 108, 1 007, 895 cm^{-1}.

4.3.3. Preparation of 1b,

[MePdP[o-(2',6'-$(OMe)_2C_6H_3$)-C_6H_4]$_2$(o-SO_3-C_6H_4)]$_2$($NMe_2CH_2CH_2NMe_2$)

0.143 g (0.57 mmol) of Pd(TMEDA) and 0.347 g (0.57 mmol) 2-[Bis(2-{2,6-dimethoxy-phenyl}phenyl)phosphanyl]-benzenesulfonic acid (**b**) were dissolved in 5 mL of anhydrous THF under inert atmosphere and stirred for 2 h. The color of reaction mixture became gray. Then, 20 mL of anhydrous Et_2O were added and the mixture was cooled in a -20 °C freezer for 2 h. The precipitate was collected, washed with ether and dried under a vacuum overnight. The yield was 0.344 g (83%). The crystals for X-Ray studies were prepared by slow evaporation of catalyst solution in $CHCl_3$.

^{1}H NMR ($CDCl_3$): δ = 7.9 (m, 6 H, Ar), 7.4 (t, ^{3}J = 7 Hz, 4 H, Ar), 7.3 (t, ^{3}J = 8 Hz, 4 H, Ar), 7.1 (m, 10 H, Ar), 6.7 (m, 4 H, Ar), 6.3 (t, ^{3}J = 9 Hz, 8 H, Ar), 3.5 (s, 6 H, OCH_3), 3.1 (s, 10 H, OCH_3 + NCH_2), 2.2 (s, 12 H, NCH_3), 0.1 (s, 6 H, $PdCH_3$).

^{13}C NMR ($CDCl_3$): δ = 155.3, 148.3, 147.8, 145.9, 145.7, 138.6, 138.5, 135.7, 135.0, 134.2, 133.2, 132.2, 132.1, 130.4, 129.8, 127.5, 127.3, 126.8, 125.6, 125.5, 125.4, 124.9, 124.3, 123.9, 123.8, 122.5, 121.9, 116.7, 101.3, 101.0 ,63.7, 53.1, 52.9, 1.2.

^{31}P NMR ($CDCl_3$): δ = 10.2 (s, 2 P).

4.3.4 Preparation of 2b,

MePd(pyridine)P[o-(2',6'-$(OMe)_2C_6H_3$)-C_6H_4]$_2$(o-SO_3-C_6H_4)

0.325 g (1.28 mmol) of $PdMe_2$(TMEDA) and 0.790 g (1.28 mmol) of 2-[bis(2-{2,6-dimethoxyphenyl}phenyl)-phosphanyl]benzenesulfonic acid (ligand b) were dissolved in 40 mL of anhydrous THF under an inert atmosphere and stirred for 30 min. Then, 0.507 g (6.43 mmol) of pyridine was added and stirred for another 40 min. A white precipitate formed, to which 40 mL of Et_2O was added. The mixture was cooled in a -20 °C freezer for 2 h. The precipitate was collected, washed with Et_2O and dried under a vacuum overnight. The yield was 0.76 g (73 %). The CIF file (X-ray structure) was deposited in the CCDC as structure 654080. The crystals for X-Ray studies were prepared by slow evaporation of catalyst solution in $CHCl_3$.

^{1}H ($CDCl_3$): δ = 8.55 (d, ^{3}J = 5 Hz, 2 H, *ortho*-$H_{pyridine}$) 7.85 (dd, 1 H, $H_{aryl\ sulfonate}$), 7.8-7.7 (m, 3H, 1 $H_{aryl\ sulfonate}$ + 2 H in 2',6'-$(OMe)_2C_6H_3$), 7.6 (t, ^{3}J = 8 Hz, 1 H, *para*-$H_{pyridine}$), 7.43 (t, ^{3}J = 7 Hz, 2H, 2 H in 2',6'-$(OMe)_2C_6H_3$), 7.37-7.29 (m, 4 H, *meta*-H $_{pyridine}$ + 2 H in 2',6'-$(OMe)_2C_6H_3$), 7.13 (m, 3 H, 1 $H_{aryl\ sulfonate}$ + 2 $H_{arylphosphine}$), 6.95 (m, 3H, 1 $H_{aryl\ sulfonate}$ + 2 $H_{arylphosphine}$), 6.39 (d, ^{3}J = 8 Hz, 2 H, $H_{arylphosphine}$), 6.20 (d, ^{3}J = 10 Hz,

2H, $H_{arylphosphine}$), 3.62 (s, 6H, OCH_3), 3.36 (s, 6 H, OCH_3), 0.230 (d, $^3J_{HP}$ = 2 Hz, 3 H, Pd-CH_3)

^{13}C ($CDCl_3$): δ = 157.3, 150.7, 149.9, 148.6 (d, J_{CP} = 15.1 Hz), 141.2 (d, J_{CP} = 11 Hz), 137.74, 136.3 (m), 135.0 (d, J_{CP} = 7 Hz), 133.9, 133.4, 129.8, 129.7, 129.3, 129.0, 128.6 (d, J_{CP} = 44 Hz), 128.3 (d, J_{CP} = 52 Hz), 127.0, 125.0, 118.7, 103.5 (d, J_{CP} = 6 Hz), 55.4, 55.3, 55.0, 54.9, 3.6, 1.3.

^{31}P NMR ($CDCl_3$): δ = 16.9 (s, 1 P).

4.3.5 Polymerizations

Depending upon the volume of solvent and the reaction pressure, polymerizations were carried out either in a stainless steel reactor (450 mL, Parr) or in an Andrews Glass Labcrest glass pressure reaction bottle (150 mL). Catalyst, toluene and comonomer were added to a Schlenk flask in a nitrogen filled glove box. The reactor, which was first dried and kept under nitrogen, was loaded with the toluene solution by cannula transfer from the Schlenk flask under nitrogen. The reactor was then sealed, pressurized with ethylene, stirred and heated. The polymerizations were performed at constant pressure, and the rate of ethylene consumption was monitored by the decrease of the ethylene pressure in the feed reactor. The polymers were obtained by precipitated in methanol, collected by centrifugation, washed with methanol and dried in a vacuum. Copolymers containing more than a few molar percent of comonomers were nearly totally soluble in $CDCl_3$. However, we found that the analysis of the copolymers in $CDCl_3$ nearly always resulted in an

overestimation of the molar incorporation of the comonomer because ethylene rich chains are not totally soluble in this medium. Despite its impracticality, all the ^{1}H NMR results were obtained in *o*-dichlorobenzene-d4 at 115 °C, thus ensuring that all polymer chains were accounted for.

4.4 Results and discussion

The Pd(II) neutral complexes **1a** and **1b** were prepared by the facile one pot reaction of the corresponding zwitterionic ligand (**a** or **b**)[8] with $PdMe_2$(TMEDA) (Figure 4.1). The TMEDA bridged dimer (**1a** or **1b**) could be isolated and purified, but if pyridine was added at the end of the reaction, the dimer was dissociated to afford catalyst **2a** or **2b** in yields ranging from 55 % to 85 %. The structure of all the catalysts was confirmed by ^{1}H and ^{13}C NMR spectroscopy. Elemental analysis was not performed since the catalyst contains small amounts of solvent. X-ray structures were obtained for catalyst **1b** (Figure 4.2) and **2b** (Figure 4.3), indicating that these species adopt a rare square pyramidal structure[10] with a weakly interacting oxygen in the apex of a pyramid (Pd-O6 = 2.824 Å for **1b**, Pd-O7 = 3.196 Å for **2b**). Rieger *et al.*[7] found that a neutral Pd(II) complex containing ligand a adopted a similar conformation, with apical Pd-O = 3.35 Å. This oxygen is well positioned to act as an incoming ligand in a substitution reaction, and could favor the displacement of a coordinated Lewis base. This observation is significant for the copolymerization of ethylene and acrylates.

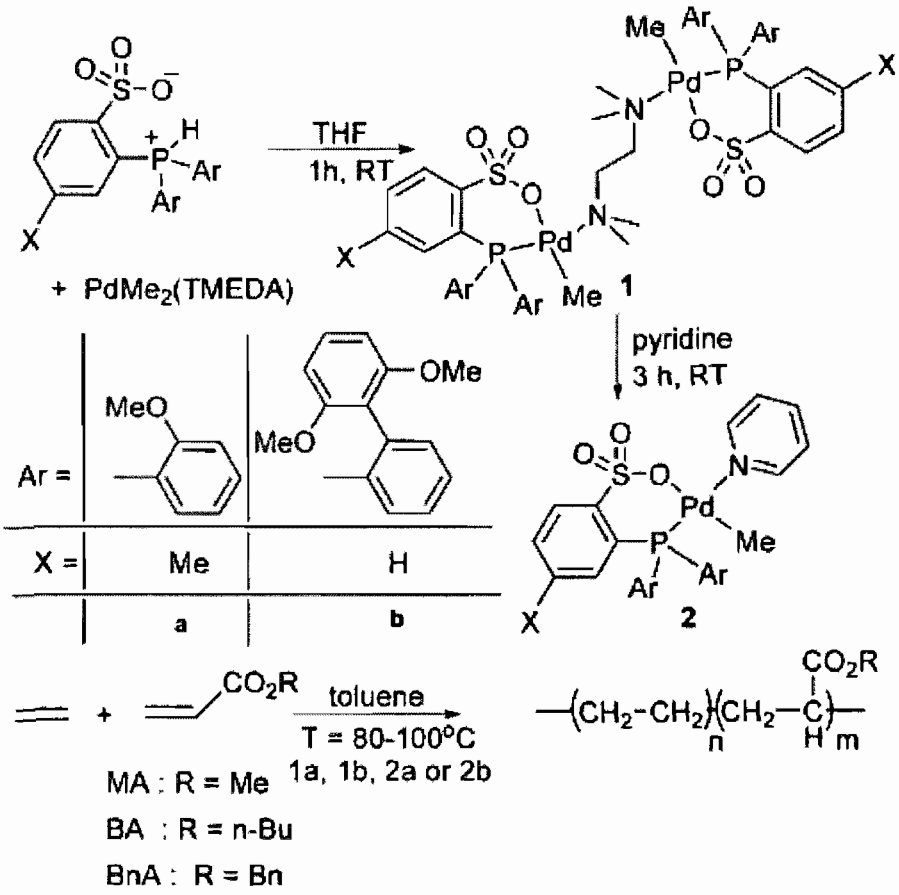

Figure 4.1: Structure of the palladium catalysts.

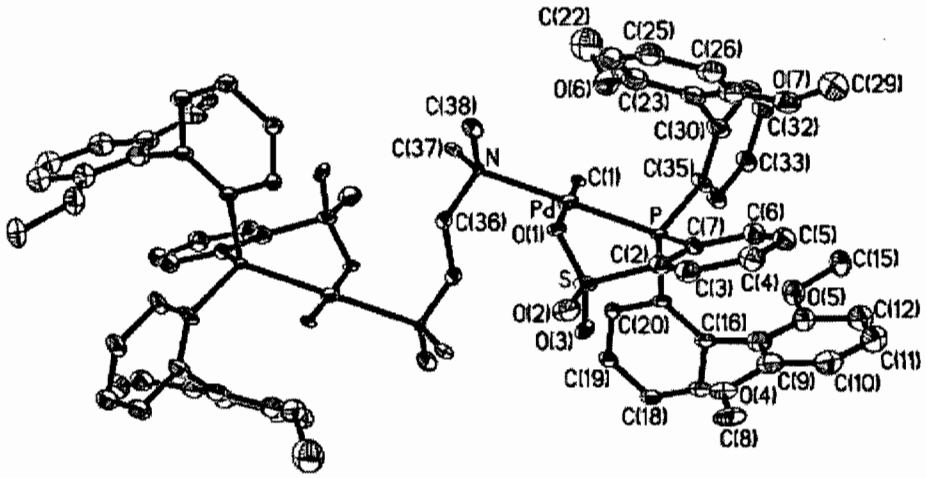

Figure 4.2: Molecular diagram with numbering scheme for the catalyst structure **1b** with 30 % probability ellipsoids and H atoms omitted for clarity. Selected bond distances (Å) and angles of complex **1b**: O(1)-Pd = 2.207(17), C(1)-Pd = 2.12 (2), P-Pd = 2.238(6), N-Pd = 2.228(13), O(1)-S = 1.407(16), C(1)-Pd-P = 85.1(6), C(1)-Pd-O(1) = 178.3(7), O1-Pd-N = 84.9(6), N-Pd-P = 179.5 (5), O(1)-Pd-P = 94.6(4).

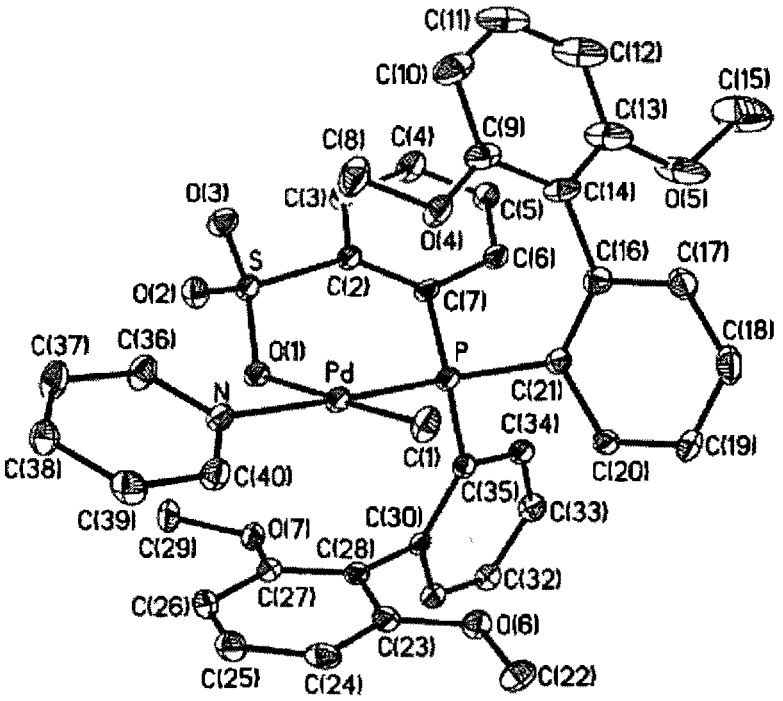

Figure 4.3: Molecular diagram with numbering scheme for the catalyst structure **2b** with 30 % probability ellipsoids and H atoms omitted for clarity. Selected bond distances (Å) and angles of complex **2b**: O(1)-Pd = 2.158(3), C(1)-Pd = 2.022(5), P-Pd = 2.2313(15), N-Pd = 2.131(4), O(1)-S = 1.483(3), C(1)-Pd-N = 95.3(7), C(1)-Pd-N = 89.47(18), C(1)-Pd-P = 92.74(15), C(1)-Pd-O(1) = 177.77(16), N-Pd-O1 = 92.74(15), N-Pd-P = 177.39(11), O(1)-Pd-P = 85.04(10).

Indeed, with palladium diimines, the formation of a CO-bonded chelate after the 2,1-insertion of an acrylate blocks the polymerization until a chain-walking mechanism increases the size of the palladacycle, thus rendering the chelate less thermodynamically favorable. As a result, the acrylate group always ends up in a terminal position in the copolymer.[2] With catalysts **1** and **2**, the formation of the CO-bonded chelate after an acrylate insertion may be broken by the transient coordination of the apical methoxy ligand via a reaction which, at first glance, is energetically neutral, both in terms of enthalpy (breaking a Pd-O and forming a Pd-O) and in terms of entropy. Could the apical methoxy ligand promote the dissociation of bound acrylate? The catalyst formed upon reaction of 2-diphenylphosphanyl benzenesulfonic acid with $PdMe_2$(TMEDA) generated a structure which was found to be inactive in our hands for the polymerization of ethylene. Bearing in mind that this scenario remains unproven, we assessed the activity of this family of catalyst (Table 4.1) as well as their ability to copolymerize ethene with other acrylates.

Catalysts **1b** and **2b** are more active than catalysts **1a** and **2a** and generate polymers with higher molecular weights, as shown in Table 4.1 (compare experiments 2 to 1, 4 to 3, 7 to 5, 9 to 8, 11 to 10 and 18 to 16). The number average molecular weight of the polymers prepared with ligand a was around 10 000 g mol^{-1}, which also corresponds to the molecular weight of the polymers prepared by Drent *et al.*,[3] using ligand **a** and $Pd(dba)_2$ or $Pd(OAc)_2$. By contrast, ligand **b** generates polymers with molecular weights of 100 000 g $\cdot$ mol^{-1} and above. Such a result is not unexpected, as it has been shown by Brookhart *et al.*[11] that the presence of a bulky ligand leads to a decrease of the rate of chain transfer by

preventing coordination of incoming ethylene in the axial position. The use of a bulky ligand can also prevent the formation of an inactive bis-chelate,[12] but this reaction manifold should only be prominent when preparing the catalyst *in situ* from the ligand and a suitable Pd source. In fact, active catalysts could be formed by the reaction of ligand a or b with $Pd_2(dba)_3$ or $PdMe_2(TMEDA)$. The polymers formed with these systems had microstructures similar to those formed with the corresponding well-defined catalysts, but activities were usually slightly lower (TOF of 236 000 h^{-1} for a reaction catalyzed by **b** + $Pd_2(dba)_3$ with conditions similar to entry 7). This behavior may stem from the formation of a bis-chelate and also from the lack of solubility of **a** or **b** in toluene (since they are zwitterionic). Other factors such as the low thermal stability of $PdMe_2(TMEDA)$ may also be invoked to explain these results. The *in situ* catalytic systems were not further investigated because these well defined catalysts are extremely easy to prepare, they are soluble in a variety of organic solvents and they are more active.

In Table 4.1, the activities were calculated over 1 h of reaction time. However, when the temperature was maintained at 85 °C, the polymerization could be sustained for 12 h, yielding no less than 40 g of polyethylene starting from less than 1 mg of catalyst. Using THF as the polymerization 'solvent', the polymerization rates were decreased (by approximately one order of magnitude), but we found that the reactions could be sustained at 85 °C (using **1b** or **2b**) for more than 16 h, thus exemplifying the exceptional stability of these catalysts. Comparing bimetallic catalyst (**1**) to its monometallic counterpart (**2**), **1** seemed slightly more active, in good agreement with the fact that pyridine is a strong

Table 4.1: Polymerization data.

	Como-nomer	cata-lyst	P	T	Catalyst	Monomer[a]	% incor-poration[b]	TOF	M_n	PDI
			psi	°C	$\mu mol \cdot L^{-1}$	$mol \cdot L^{-1}$		h^{-1}	$g \cdot mol^{-1}$	
1	none	1a	300	85	56	0		8200	25200	3.1
2	none	1b	300	85	5	0		48000	156000	4.0
3	none	2a	300	85	56	0		4100	18200	2.8
4	none	2b	300	85	5	0		37000	227000	3.9
5	none	1b	300	100	56	0		726000	135000	3.0
6	none	2a	300	100	5	0		14200	14500	2.9
7	none	2b	300	100	5	0		567000	189000	2.2
8	MA	1a	100	85	110	1.5	6.0	680	8900	5.2
9	MA	1b	100	85	12	1.5	2.5	2400	31500	3.0
10	MA	2a	100	85	110	1.5	8.0	300	9300	2.7
11	MA	2b	100	85	12	1.5	3.0	2600	41200	2.5
12	MA	2a	300	85	110	1.5	6.0	760	4300	2.5
13	MA	2a	100	100	110	1.5	9.4	<100	6200	1.6
14	BA	2b	100	85	12	1.5	2.8	1400	nm[e]	nm[e]
15	BnA	2b	100	85	12	1.5	3.5	3500	nm[e]	nm[e]
16	NBE	2a	60	80	85	0.5	43.0	<100	48000[d]	1.8
17	NBE	2a	300	100	85	0.15	8.9	800	58000[d]	1.9
18	NBE	2b	60	80	33	0.5	11.6	6500	131000[d]	2.1
19	NBE	2b	300	100	33	0.15	2.0	185000	nm[e]	nm

[a)]Initial concentration in toluene; [b)]Molar percent of incorporation determined by ^1H NMR;

[c)] In this chapter TOF = number of moles of monomer polymerized per moles of Pd metal

and per hour; [d]Measured in $CHCl_3$ GPC at room temperature, calibrated with PS standards; [e]nm: not measured.

inhibitor of the catalytic activity, 5 equivalents relative to the catalyst concentration being sufficient to completely shut down the polymerization. TMEDA was also found to inhibit the polymerization, but larger concentrations (50 equivalents for **2a**) were needed to stop the polymerization. For both catalyst **2a** and **2b**, bound pyridine was not displaced by ethylene, TMEDA and MA under spectroscopic conditions, as shown in ^1H NMR by monitoring the doublet at 8.75 ppm (respectively 8.55 ppm) corresponding to protons of the bound pyridine in **2a** (respectively **2b**), whereas a doublet at 8.60 ppm corresponds to free pyridine. Interestingly, at room temperature, the exchange between free and bound pyridine was rapid relative to the NMR timescale for catalyst **2a**, but slow for catalyst **2b**.

As expected, the addition of MA resulted in a reduction of the catalytic activity. Incorporation of the comonomer was favored by higher comonomer concentrations and lower ethene pressure (Table 4.1, entry 12 vs. 10). Thus, a compromise must be found between acceptable activity and incorporation. Slightly higher incorporations are obtained at higher temperatures (entry 13 vs. 10), which is likely to be because of the lower solubility of ethylene in toluene at higher temperature.

The (homo)polyethylene generated with these catalysts was found to be virtually devoid of branches, pointing out the absence of the chain-walking mechanism. Similarly, the copolymers of MA and ethene were found to be linear with main chain incorporation of

MA, in agreement with reported data by Drent.[3] Importantly, the presence of a radical polymerization mechanism could be ruled out because the polymer formed by radical copolymerization of ethylene and MA initiated by AIBN under similar conditions (toluene, T = 85 °C, P = 300 psi) did not show characteristic -CH_2-CH_2-CH(COOR)-CH_2-CH_2- signals in ^{1}H NMR measurements. Furthermore, all monomers were inhibited with a radical trap, and did not spontaneously polymerize under our reaction conditions.

While catalysts based on ligand **b** allowed the production of polymers of high molecular weight with high activities, the incorporation of comonomers was also significantly lower. We assume that this is due to the bulk of the ligand which prevents the approach of the larger comonomer. Nonetheless, these catalysts are not only able to incorporate MA, but also several other acrylic comonomers such as n-butyl acrylate (BA) and benzyl acrylate (BnA) (Table 4.1, experiment 14 and 15). Interestingly, norbornene (NBE) can also be copolymerized with the same family of catalysts (Figure 4.4). The copolymerization of ethylene and NBE does result in only a small decrease of activity (compare entry 19 to 7), yielding copolymers which can be quite rich in comonomer. The analysis of these copolymers by ^{13}C and ^{1}H NMR indicated that two norbornene units were never adjacent, which is consistent with the observation that NBE does not homopolymerize with these catalysts.

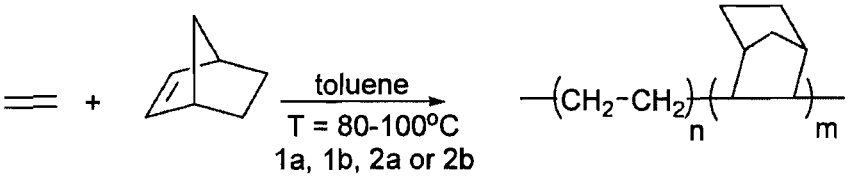

Figure 4.4: Copolymerization with NBE.

4.5 Conclusion

Neutral late transition metal catalysts based on aryl phosphine sulfonates were shown to be useful in preparing a number of functional groups containing high molecular weight ethylene copolymers under mild laboratory conditions. Significantly, these catalysts were easily prepared in a one-step reaction, crystallographic structures were obtained. High TOFs were observed for catalyst **1b** and **2b**, demonstrating the tolerance of these catalysts for both acrylates and norbornenes.

4.6 Acknowledgements

This work was supported by the NSF GOALI program and NSERC.

4.7 Keywords

Copolymerization, metal-organic catalysts/organometallic catalysts, polyethylene (PE), polyolefins, transition metal chemistry.

4.8 Supporting information (Appendix A)

Supporting information for this article is available on the WWW under http://www.wiley-vch.de/contents/jc_2263/2007/marc200700370_s.pdf or from the author.

4.9 References

1. L. S. Boffa, B. M. Novak, *Chem. Rev.* **2000**, 100, 1479.
2. L. K. Johnson, S. Mecking, M. Brookhart, *J. Am. Chem. Soc.* **1996**, 118, 267.
3. E. Drent, R. v. Dijk, R. v. Ginkel, B. v. Oort, R. I. Pugh, *Chem. Commun.* **2002**, 744.
4. L. Johnson, A. Bennett, K. Dobbs, E. Hauptman, A. Ionkin, S. Ittel, E. McCord, S. McLain, C. Radzewich, Z. Yin, L. Wang, Y. Wang, M. Brookhart, *Polym. Mater. Sci. Eng.* **2002**, 86, 319.
5. K. Matsumura, O. Fukumoto, *J. Polym. Sci., Part A: Polym. Chem.* **1971**, 9, 471.
6. A. K. Hearley, R. J. Nowak, B. Rieger, *Organometallics* **2005**, 24, 2755.
7. T. Kochi, K. Yoshimura, K. Nozaki, *Dalton Trans.* **2006**, 25.
8. EP 176254572A2 (2007), Rohm and Haas, invs. : N. T. Allen, T. C. Kirk, B. L. Goodall, *Chem. Abstr.* ***2007***, 249480.
9. W. de Graaf, J. Boersma, W. J. J. Smeets, A. L. Spek, G. Van Koten, *Organometallics*, **1989**, 8 , 2907.
10. M. J. Green, G. J. P. Britovsek, K. J. Cavell, B. W. Skelton, A. H. White, *Chem. Commun.* **1996**, 1563.
11. L. K. Johnson, C. M. Killian, M. Brookhart, *J. Am. Chem. Soc.* **1995**, 117, 6414.
12. E. F. Connor, T. R. Younkin, K. I. Henderson, A. W. Waltmann, R. H. Grubbs, *Chem. Commun.* **2003**, 2273.

Chapter 5

RESEARCH PAPER (COMMUNICATION)

Linear Polyethylene with Tunable Surface Properties by Catalytic Copolymerization of Ethylene with N-Vinyl-2-pyrrolidinone and N-Isopropylacrylamide

K. M. Skupov, L. Piche, J. P. Claverie

NanoQAM Research Center, Department of Chemistry and Biochemistry, University of Quebec at Montreal, 2101 rue Jeanne-Mance, CP 8888, Montreal, Quebec H3C 3P8, Canada

Macromolecules, 2008, 41 (7), 2309–2310.

Received 31 January 2008; Revised 4 March 2008; Published online 13 March 2008.

This paper ivestigates the synthesis of ethylene copolymers extremely polar comonomers, such as N-vinyl-2-pyrrolidinone and N-isopropylacrylamide. The catalytic reactions done using Pd-based sulfonated arylphosphine catalyst. The characterization of the copolymers was performed by DSC, NMR, IR and water contact angle measurements.

My contribution to this paper represents ~ 90 % of the total work related to the copolymer synthesis and characterization. L. Piché, a M.Sc. student at UQAM, prepared several batches of catalyst for this work, following the procedure described in the previous chapter.

5.1 Introduction

One of the reasons for the ubiquity of high-density polyethylene (PE) is that its physical properties can be drastically altered by careful manipulation of its microstructure and particularly by controlling the length and distribution of alkyl branches along the chain. Instead of alkyl chains, it would be desirable to introduce low amounts of polar groups via postfunctionalization or copolymerization[1] because they are expected to greatly impart toughness, flexibility, crack resistance, gas permeability, miscibility, adhesion, and paintability of PE. Apart from CO, only a small number of polar monomers such as alkyl acrylates,[2a,b] vinyl ethers,[3] and acrylonitrile[4] have been successfully copolymerized with ethylene (E) by a catalytic process. In a seminal work, Brookhart *et al.* found that cationic palladium α-diimine complexes can insert a molecule of acrylate predominantly in the terminal position of a branched copolymer.[5] In 2002, Drent *et al.* achieved main-chain acrylate incorporation using Pd-based aryl sulfonated phosphines as *in situ* catalysts under mild conditions.[2a] This catalyst[2b,c] has the unique capacity to incorporate polar monomers that have never been copolymerized before, albeit with low incorporations: 5 mol. % for vinyl ether,[3] 9 mol. % for acrylonitrile (half of it in a terminal position),[4] and less than 1 mol. % for vinyl fluoride.[6] The copolymerization of E with a small amount of a truly polar comonomer (i.e., hydrophilic and even water-soluble) would yield novel materials whereby the polar groups would significantly change the surface properties of PE, allowing it to be painted for example.

Copolymers of E with low amounts of polar monomers such as N-isopropylacrylamide (NIPAM)[7] and N-vinylpyrrolidinone (NVP)[8] can be prepared by free-radical chemistry under high pressure (1 300 – 2 400 atm). The resulting copolymers are highly branched, resulting in a drastic loss of crystallinity: polymers containing more than 2–3 % NVP are amorphous waxes.[8] Clearly, radical copolymerization of E with these polar monomers does not afford control over the architecture of the polymer. In an elegant work, Wagener et al. investigated the properties of linear copolymers of E and several polar monomers obtained by either ROMP or ADMET.[9] However, to our knowledge, linear copolymers of E with NIPAM and NVP have never been reported.

5.2. Results and discussion

We have probed the feasibility of the direct copolymerization of E with NVP or NIPAM using Pd-based well-defined catalyst 1, which shows activity in copolymerization of E with acrylates,[2,12] norbornene,[10-12] vinyl ethers,[3] and acrylonitrile[4] (Figure 5.1). Higher temperature (experiments 6 and 8) generates lower yields due to rapid catalyst decomposition. For all cases, the incorporation is low, but it was observed exclusively in the main chain, as demonstrated by ^{1}H NMR and ^{13}C NMR (see Supporting Information, Appendix B). In average, the resulting copolymers contain 1–3 polar groups per chain. At 95 °C (Table 5.1) catalyst **1** is able to incorporate NIPAM and NVP, albeit a decrease of the molecular weight of the resulting copolymer and a significant lowering of the activity comparatively with ethylene homopolymerization were observed.

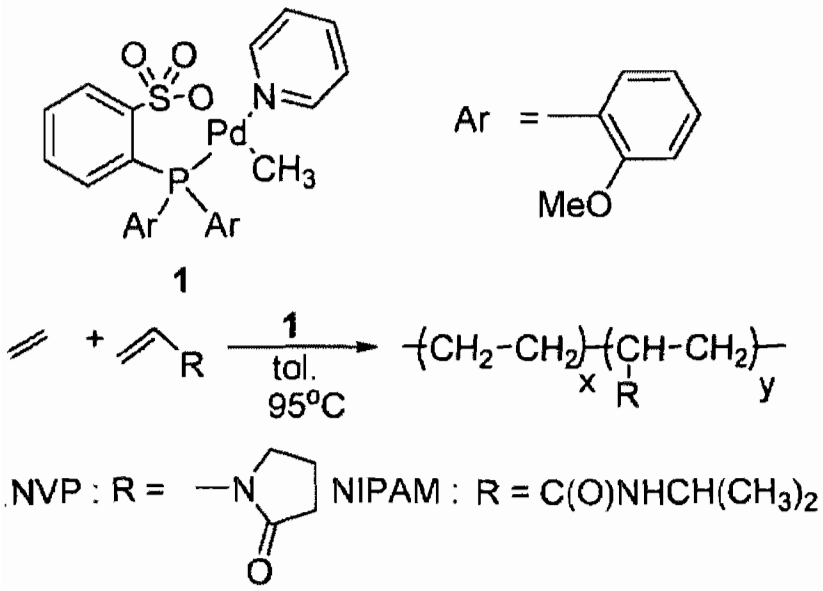

Figure 5.1: Copolymerization reaction.

Table 5.1: Copolymerization of ethylene with NVP and NIPAM in toluene at 95 °C.

expt	monomer	catalyst, mg/L	pressure, psi	TON, mol_{pol}/(mol_{Pd} h)	mon incorp. mol. %	time of reaction, h	T_m, °C	crystallinity, %[c]	M_n, g/mol[d]	contact angle, x/y,[b]	mass of polymer, g
1	none	25	300	62900	0	2	129.3	72.4	>5000	121.9/118.5	29.3
2	NVP	164	350	1930	<0.1	3	128.0	70.5	~5000	109.8/111.7	9.7
3	NVP	165	400	1200	0.3	3	127.7	68.1	3770	109.1/108.0	5.2
4	NVP	150	300	64	1.2	72	119.8	48.8	3410	105.7/103.5	6.5
5	NVP	194	350	27	2.0	50	115.1	43.4	4190	101.3/95.2	2.0
6[a]	NVP	75	150	34	2.6	3.5	107.5	35.8	3021	nd	0.081
7	NIPAM	150	420	193	3.4	6	111.7	35.0	1230	112.3/107.2	1.6
8[a]	NIPAM	100	200	23	4.1	4	nd	nd	1290	109.7/100.9	0.080

[a] $T_{reaction}$ = 115 °C; [b] before and after vapor treatment; [c] $\Delta H_{100\%\ cryst\ PE\ melt}$ = 294 J/g; [d] determined by NMR; nd: not determined

These copolymers are essentially linear (~1 br / 1000 C by ^{13}C NMR), except when the reaction is carried out at high temperature (115 °C, 5 Me branches / 1000 C for entry 6). All the polymer chains contain one insaturation, which is consistent with the expected chain transfer mechanism via β-hydride abstraction; however, a high proportion of those are internal, probably due to isomerization by either **1** or a decomposition product of **1**. Indeed, heating **1** in the presence of 250 equiv. of 1-octene at 95 °C generates only trace amounts of dimers and trimers and mostly 2-octene and 3-octene. Interestingly, β-hydride abstraction only occurs after an E insertion, and no terminal NVP or NIPAM unit was observed. For acrylate polymerization catalyzed by **1**, β-hydride abstraction can occur after an acrylate insertion, but most acrylates are inserted in the main chain.[2] With Brookhart catalyst, the acrylate ends up in a terminal position via a chain-walking mechanism, unless extreme pressures and an excess of Lewis acid cocatalyst are used.[6]

The introduction of polar units in low amounts along the PE chains results in a lowering of the melting point (T_m, Table 5.1). The T_m of the linear copolymers containing polar groups obtained by late transition metal catalysis (LTM) varies linearly with the number of polar groups ($r^2 > 0.99$, solid line in Figure 5.1), irrespectively of the nature of the polar group, as shown by the fact that both the T_m of ethylene–methyl acrylate (E–MA) copolymers prepared with **1**,[12] and those of E–NVP polymers are aligned on the same line. This is a legacy of the randomness of these copolymers, which obeys a Flory exclusion model whereby T_m is a colligative property (independent of the nature of the branch).[9] Significantly, the T_m of the linear polymers is 10 – 20 °C above the T_m of the branched ones prepared by free radical polymerization.

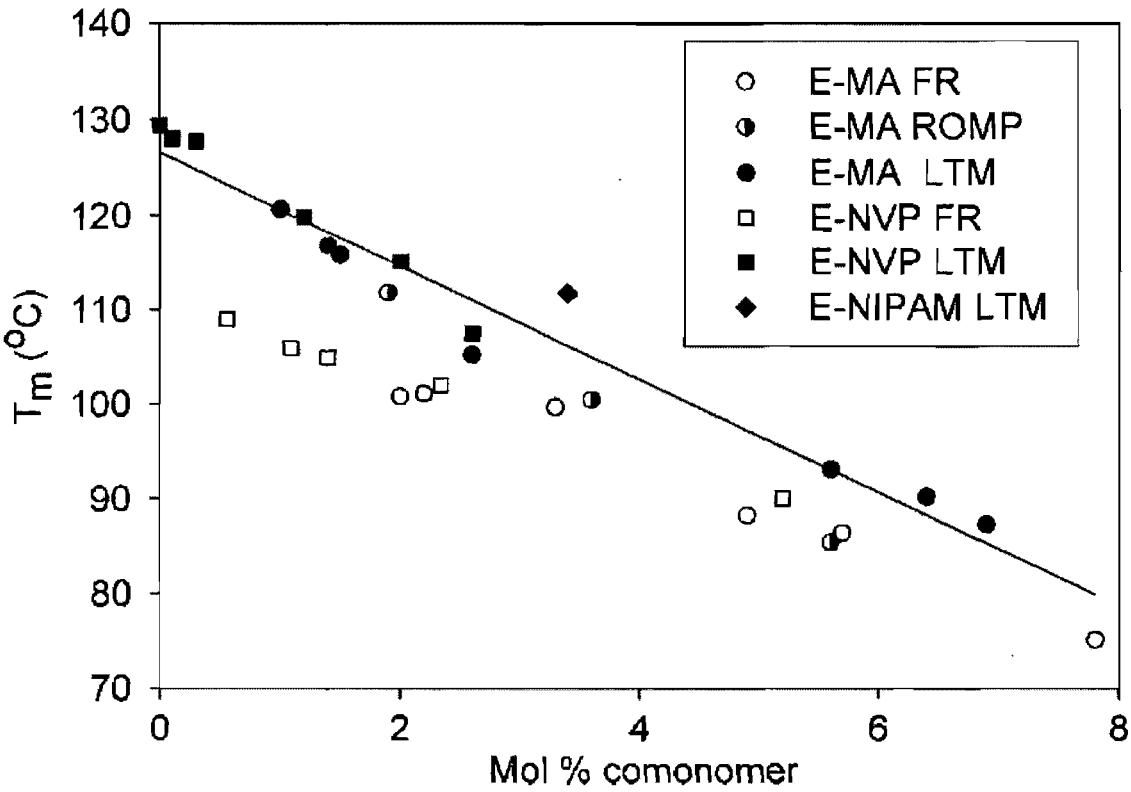

Figure 5.2: Comparison of linear (LTM, late transition metal catalyzed and ROMP) and branched (FR, free radical) copolymers vs mol. % of comonomer (LTM E-MA: prepared by our group,[12] LTM E-NVP: Table 5.1, LTM E-NIPAM: Table 5.1, E-MA ROMP: prepared in ref.[9], E-MA FR: commercial samples,[9] E-NVP FR: prepared in ref[8]).

The E–NIPAM copolymer exhibits a T_m (111.7 °C) slightly above the predicted value (106.2 °C) for a copolymer with this level of incorporation. This deviation, which is small enough to be considered a statistical fluctuation, may also be explained by the fact that the crystal is reinforced by the presence of H-bonds, as shown by a characteristic N–H stretching band at 3299 cm^{-1}. H-bonds were also found in a 2.1 mol. % NIPAM containing PE obtained by radical means.[7]

Thermal properties are consistent with the fact that these copolymers are essentially PE-like: crystalline and with melting points close to 120 °C. However, the presence of a small amount of highly polar functionalities is sufficient to drastically alter their surface properties. Solvent-borne films were prepared by applying a solution of polymer in refluxing chlorobenzene on a glass substrate. Once dried, the water contact angle (CA) of these polymer films was evaluated (Table 5.1) and found to decrease with monomer incorporation. It is well-established that CA is dependent not only on the PE microstructure but also on the roughness of the surface and therefore on its preparation method.[14] For example, for pure PE, literature CA values vary from 90° to 170°.[15,16] In our case, for pure PE, a CA of 121° was found, which is consistent with the high values of CAs obtained for solvent-cast films. The introduction of a small amount of polar groups is sufficient to reduce the CA by as much as 22°. Aging the films with a hot atmosphere saturated with water provokes the segregation of the most polar groups at the interface polymer–air, resulting in a CAs as low as 95°, which is now close to the CA of water on polystyrene (92°),[17] a paintable polymer. This significant drop in CA is also comparable to the typical

reduction of CA generated by corona discharge[18] on a solvent-cleaned PE. This plasma treatment is widely used in industry to improve bondability, wettability, and paintability of PE by the introduction of surface oxygen or nitrogen-containing groups.

5.3 Conclusion

To conclude, linear copolymers of E and NVP or NIPAM were prepared and shown to combine the main characteristics of HDPE with a significantly higher surface energy. We envision that such an approach could enable PE to be painted in the future without specific surface treatment. Importantly, the synthesis of catalysts which allow higher comonomer incorporations is currently under scrutiny. These catalysts would permit the preparation of novel amphiphilic copolymers based on E, NVP, and NIPAM and of easily functionalized PE.

5.4 Acknowledgements

This work was supported by NSERC (discovery grant) and NSF (Goali grant 0354825).

5.5 Supporting information (Appendix B)

Experimental part of the polymerization reactions and polymer characterization (NMR, DSC, IR data). This material is available free of charge via Internet at http://pubs.acs.org.

5.6 References and notes

1. Boffa, L. S.; Novak, B. M. *Chem. Rev.* **2000**, 100, 1479-1493.
2. (a) Drent, E.; van Dijk, R.; van Ginkel, R.; van Oort, B.; Pugh, R. I. *Chem. Commun.* **2002**, 744-745. (b) Kochi, T.; Yoshimura, K.; Nozaki, K. *Dalton Trans.* **2006**, 25-27. (c) Hearley, A. K.; Nowack, R. J.; Rieger, B. *Organometallics*, **2005**, 24, 2755-2763.
3. Luo, S.; Vela, J.; Lief, G .R.; Jordan, R. F. *J. Am. Chem. Soc.* **2007**, 129, 8946-8947.
4. Kochi, T.; Noda, S.; Yoshimura, K.; Nozaki, K. *J. Am. Chem. Soc.* **2007**, 129, 8948-8949.
5. (a) Johnson, L. K.; Mecking, S.; Brookhart, M. *J. Am. Chem. Soc.* **1996,** 118, 267-268. (b) Mecking, S.; Johnson, L. K.; Wang, L.; Brookhart, M. *J. Am. Chem. Soc.* **1998**, 10, 888-899 (c) Johnson, L.; Bennett, A.; Dobbs, K.; Hauptman, E.; Ionkin, A.; Ittel, S.; McCord, E.; McLain, S.; Radzewich, C.; Yin, Z.; Wang, L.; Wang, Y.; Brookhart, M. *Polym. Mater. Sci. Eng.* **2002**, 86, 319-320.
6. Weng, W.; Shen, Z.; Jordan, R. F. *J. Am. Chem. Soc.* **2007**, 129, 15450-15451
7. Mortimer, G. A. *J. Appl. Polym. Sci.* **1974**, 18, 2847-2854
8. Clampitt, B. H.; Hughes, R. H. *Anal. Chem.* **1968**, 40, 449-451
9. Lehman, S. E.; Wagener, K. B.; Baugh, L. S.; Rucker, S. P.; Schulz, D. N.; Varma-Nair, M.; Berluche, E. *Macromolecules* **2007**, 40, 2643-2656.
10. Liu, S.; Borkar, S.; Newsham, D.; Yennawar, H.; Sen, A. *Organometallics* **2007**, 26, 210-216.

11. Skupov, K. M.; Marella, P. R.; Hobbs, J. L.; McIntosh, L. H.; Goodall, B. L.; Claverie, J. P. *Macromolecules* **2006**, 39, 4279-4281.

12. Skupov, K. M.; Marella, P. R.; Simard, M.; Yap, G. P. A.; Allen, N.; Conner, D.; Goodall, B. L.; Claverie, J. P. *Macromol. Rapid Commun.* **2007**, 28, 2033-2038.

13. Brandrup, J.; Immergut, E. H. *Polymer Handbook*; Wiley: New York, **1999**.

14. A solvent-borne process was chosen over a melt process for the sake of commodity.

15. Adamson, A. W.; Gast, A. P. In *Physical Chemistry of Surfaces*; Wiley: New York, **1997**; p 365.

16. Lu, X.; Zhang, C.; Han, Y. *Macromol. Rapid Commun.* **2004**, 25, 1606-1610.

17. Qian, H.; Zhang, Y. X.; Huang, S. M.; Lin, Z. Y. *Appl. Surf. Sci.* **2007**, 253, 4659-4667.

18. Xiao, G. *J. Colloid Interface Sci.* **1995**, 171, 200-204.

Chapter 6.

RESEARCH PAPER

Kinetic and mechanistic aspects of ethylene and acrylates catalytic copolymerization in solution and in emulsion

K. M. Skupov,[a] J. Hobbs,[a] P. Marella,[a] D. Conner,[b] S. Golisz,[b] B. L. Goodall,[b]

J. P. Claverie[a]

[a] NanoQAM Research Center, Quebec Center for Functional Materials, Department of Chemistry, University of Quebec at Montreal, 2101 rue Jeanne-Mance, CP8888, Montreal, Quebec H3C 3P8, Canada.

[b] Emerging Technology Department, Rohm and Haas Company, 727 Norristown Road, Spring House, PA, 19477, USA.

Macromolecules, ASAP, doi:10.1021/ma901210u.

Received: 5 June 2009; Revised: 13 August 2009; Accepted: 14 August 2009; Published online: 24 August 2009.

This paper is devoted to the synthesis of the ethylene copolymers with acrylates prepared in solution and in aqueous emulsion using Pd-based sulfonated arylphosphine catalysts. In the case of emulsion polymerization, latexes were obtained and characterized by NMR, DLS, TEM, GPC, DSC. The polymerization kinetics and the coordination of pyridine and of acrylate on the catalyst were determined by LT NMR.

My contribution to this work is ~60 % of the total work and includes copolymers and latexes syntheses and their characterizations. J. Hobbs, an undergraduate student at UNH, performed several of the solution polymerization experiments, used for kinetics analysis. P. Marella, a M.Sc. student at UNH, did most of the low temperature NMR experiments with J. Claverie. D. Conner, S. Golisz and B. Goodall are our collaborators at Rohm and Haas and contributed to the research intellectually.

6.1 Abstract

Ethylene was copolymerized with acrylates in solution and in emulsion using sulfonated arylphosphine Pd-based catalysts. The copolymerization of C_2H_4 and methyl acrylate in toluene was slowed by the σ-coordination of the acrylate on Pd. The substitution of pyridine by itself was shown to proceed via an associative mechanism with activation parameters $\Delta H^{\ddagger}$ = 16.8 kJ/mol and $\Delta S^{\ddagger}$ = -98 J mol^{-1} K^{-1} whereas the activation parameters for the substitution of pyridine by methyl acrylate were found to be $\Delta H^{\ddagger}$ = 18.1 kJ/mol and $\Delta S^{\ddagger}$ = - 87 J mol^{-1} K^{-1}. Using these Pd-based catalysts in an emulsion polymerization process, latexes of copolymers of ethylene with various acrylates having particle diameters ~200 nm were obtained for the first time. Their solid contents did not exceed 5 % because of the low activity of the catalyst resulting from the coordination of water and from the slow decomposition of the active site by water.

6.2. Introduction

Numerous aqueous-borne coatings are designed around a polymeric base which is prepared by radical polymerization in emulsion.[1,2] For many applications, aqueous-borne coatings, despite their environmental friendliness, have not supplanted solvent-borne coatings because of the high hydrophilicity of the intrinsic constituents of the polymer (acrylates, vinyl acetate, etc.). The preparation of hydrophobic and durable aqueous-base

coatings would be highly desirable. We[3-8] and Mecking[9-14] have separately reported the possibility of polymerizing ethylene (E) in emulsion via a catalytic pathway. Latexes of high density polyethylene (HDPE) were prepared, but such products which are essentially crystalline, could not form films when the latex was applied on a substrate. This turned our interest to the preparation of less crystalline E-rich copolymers by the polymerization in emulsion. These copolymers are expected to have lower melting points (T_m) and higher glass transition temperatures (T_g) than PE.[15] For example, we recently demonstrated that it is possible to prepare coatings having moderate anti-corrosion properties using copolymers of norbornene and ethylene.[15, 16] We also have shown that the catalytic copolymerization of ethylene with polar comonomers such as N-vinyl pyrrolidone and N-isopropyl acrylamide yields materials which are wettable by water.[17] Based on these past results, it is expected that the latexes prepared from ethylene copolymers with acrylic monomers would combine the best of two worlds: the exceptional durability, hydrophobicity and imperviousness to environmental damage of polyolefins to the myriad of benefits of polyacrylates such as high UV stability, adhesive properties, polarity to list just a few. For the first time, we report the preparation of such material using the catalytic copolymerization of E and acrylates such as methyl acrylate (MA), *n*-butyl acrylate (BA), benzyl acrylate (BnA) and 2-phenoxyethyl acrylate (PEA) in emulsion.

The catalytic copolymerization of ethylene (E) and acrylates has only been recently explored. Brookhart *et al.* discovered that cationic palladium diimines copolymerize ethylene and acrylates to afford branched copolymers.[18] The acrylate is placed in an end-

chain position through a chain walking reaction. Based on this mechanism, Popeney *et al.*[19] reported that it is possible to prepare copolymers with high levels of acrylate incorporation using cyclophane-based Pd(II) N,N-α-diimine complexes where the axial binding sites are shielded. Drent *et al.*[20] recently disclosed that an ill-defined catalytic system containing a phosphine sulfonate and a palladium complex (tris(dibenzylideneacetone)dipalladium(0), ($Pd_2(dba)_3$) or palladium (II) acetate, ($Pd(OAc)_2$)) permits the copolymerization of ethylene and acrylates where the acrylates are incorporated in a main chain position. Well-defined palladium catalysts containing a phosphine aryl sulfonate ligand were then disclosed by Hearley *et al.*,[21], Goodall *et al.*,[22, 23] Kochi *et al.*,[24, 25] Liu *et al.*,[26] Skupov *et al.*,[27] Luo *et al.*,[28] Borkar *et al*[29] and Vela *et al.*[30] Among those reports, acrylate copolymerization with ethylene was only mentioned by Goodall,[22, 23] Skupov,[27] and Kochi,[24] During the elaboration of this paper, it was recently reported that using a palladium aryl sulfonate catalyst ligated by DMSO instead of pyridine, it was possible to attain very high acrylate incorporations with the possibility of acrylate homopolymerizing.[31]

6.3 Experimental Section

6.3.1 Materials

All manipulations were done under argon using standard Schlenk techniques. Ligands **1a** (2-[bis(2-methoxy-phenyl)phosphanyl]-4-methyl-benzenesulfonic acid and **1b** (2-[bis(2-methoxy-phenyl)phosphanyl]-benzenesulfonic acid were prepared according to

published procedure.[22,32] Catalysts **2a** and **2b** were prepared and characterized according to literature.[27] Solvents were purified by distillation over CaH_2 and degassed using three freeze pump thaw cycles and kept over activated molecular sieves. Water was ultrapure grade (18.2 MΩ), and degassed by boiling for 120 minutes, followed by sparging with Ar for several hours. All acrylic monomers were purified by sparging them with argon, and passing it over a bed of inhibitor remover resin (Aldrich). They were then spiked with *tert*-butylcatechol (0.25 % wt:wt). Sodium dodecylsulfate (SDS) was recrystallized from methanol.

6.3.2 Polymerization procedures

Depending on the volume of solvent and the reaction pressure, polymerizations were carried out in a stainless steel reactor (450 mL, Parr) for pressures comprised between 80 to 400 psi or in Andrews Glass Labcrest glass pressure reaction bottle (150 mL) for pressures comprised between 15 to 100 psi.

6.3.2.1 Typical polymerization in organic solution

In a Schlenk flask, 6.6 mg ($16.4 \cdot 10^{-6}$ mol) of ligand **1b** and 6.0 mg ($6.56 \cdot 10^{-6}$ mol) of tris(dibenzylideneacetone)dipalladium ($Pd_2(dba)_3$), were dissolved in 100 mL of toluene containing 1 g of methyl acrylate and 1 mg of 2,6-di-*tert*-butyl-4-methylphenol, BHT. This solution was then introduced to the stainless steel reactor which was immediately pressurized with 100 psi ethylene, and heated at 100 °C. When this

temperature was reached, the reactor was continuously fed with ethylene at 300 psi and the activities were calculated from the rate of ethylene consumption, which was monitored by the decrease of the ethylene pressure in the feed tank. The pressure in the feed tank was digitally recorded (1 point every 0.1 s) and the loss of pressure in the feed tank was converted into the number of moles of ethylene consumed over time. The TOF was calculated as the time derivative of this number divided by the number of moles of catalyst. After one hour, the reactor was cooled down to room temperature and slowly depressurized. The polymers were precipitated in four volumes of methanol, collected by centrifugation or filtered, washed with methanol and dried under vacuum.

6.3.2.2 Typical polymerization in emulsion

Catalyst **2a** (35 mg) was dissolved in 2.5 mL of dichloromethane containing 0.5 g of hexadecane and 2 mg of BHT in a Schlenk flask. This solution was added by cannula transfer to 50 mL of an aqueous solution of sodium dodecyl sulfate, SDS, (concentration 15 g/L) containing 2 mg of 4-hydroxy-2,2,6,6-tetramethylpiperidin-1-oxyl (hydroxyTEMPO). The mixture was sonicated using a 600 W Branson sonicator for 4 min and then introduced into pressure reactor. The reactor was then loaded with 2 g of methyl acrylate, and pressurized with ethylene. Activities (TOF) were recorded in the same manner as for solution experiments. After several hours (100 °C, 1000 rpm), the reaction was stopped, and a free-flowing white latex was collected from the reactor.

6.3.3 Characterization

The molecular weight distributions were determined by gel permeation chromatography (GPC) using a Viscotek HT GPC equipped with triple detection operating at 160 °C. The eluent was 1,2,4-trichlorobenzene, and separation was performed on three PolymerLabs Mixed B(-LS) columns. The dn/dc of pure linear polyethylene was found to be 0.106 mL/g at this temperature. The dn/dc of several copolymers were also determined. A linear extrapolation between the dn/dc of the copolymer and the weight % composition in acrylate was then performed, leading to the determination of an extrapolated dn/dc of poly(methyl acrylate) (0.2179 mL/g). The dn/dc of any copolymer was then calculated as the weighted-average of the dn/dc of pure PE and dn/dc of pure poly(methyl acrylate). Particle sizes were measured by quasi-elastic light scattering (QELS) on a light-scattering Microtrac VSR S3000. Transmission electron microscopy (TEM) measurements were effected on a Tecnai12 (V = 80 kV or 120 kV, W filament) using uranyl acetate as negative contrast agent and a Morada 13MPX digital camera. Samples were first ultrafiltered for serum exchange and then lightly sonicated before applying on the TEM grid. All the NMR spectra were recorded on Varian 400 MHz (Mercury) and 500 MHz (Inova). NMR spectra of the polymers were recorded in d4-*o*-dichlorobenzene (ODCB) at 115 °C.

6.3.4 Variable temperature NMR experiments

These studies were performed by recording ^{1}H NMR and ^{13}C NMR spectra of catalyst **2b** in dichloromethane-d2 (c = 0.104 mol/L) with various amounts of pyridine and

monomers at temperatures ranging from -90 to -60 °C. Once the spectra were recorded, they were analyzed using the Mexico program by Bain for the exchange processes.[33] Pyridine was set as a AA'BB'C system.[34] The Mexico program uses the linewidth and chemical shifts of bound and free pyridine in the absence of exchange. The linewidth of free pyridine in the absence of exchange (i.e. the absence of catalyst) was measured at -90 °C. The same linewidth was used for pyridine bound to the catalyst. The variation of the chemical shifts of pyridine with temperature was also taken into account by recording the spectrum of pyridine and of the catalyst alone at temperatures ranging from -90 °C to -50 °C. The results generated by the Mexico program were visually checked using WinDNMR software by Reich, which offers the capability to superimpose an experimental spectrum and an exchange simulated spectrum.[35]

6.4 Results and discussion

6.4.1 Copolymerization of C_2H_4 and methyl acrylate, MA in toluene

Drent reported that it is possible to copolymerize C_2H_4 with MA using *in situ* formed diarylphosphinobenzene-2-sulfonic acid **1b** and $Pd_2(dba)_3$ or $Pd(OAc)_2$.[20] We later reported the synthesis of the corresponding neutral catalyst for the copolymerization of C_2H_4 and acrylates by reaction of diarylphosphinobenzene-2-sulfonic acid with $PdMe_2$(tmeda) in the presence of pyridine (**2a** and **2b**, Figure 6.1).[27]

Drent reported that it is possible to copolymerize C_2H_4 with MA using *in situ* formed diarylphosphinobenzene-2-sulfonic acid **1b** and $Pd_2(dba)_3$ or $Pd(OAc)_2$.[20] We later

reported the synthesis of the corresponding neutral catalyst for the copolymerization of C_2H_4 and acrylates by reaction of diarylphosphinobenzene-2-sulfonic acid with $PdMe_2(tmeda)$ in the presence of pyridine (**2a** and **2b**, Figure 6.1).[27] These catalysts are active for the copolymerization of various acrylates with C_2H_4.

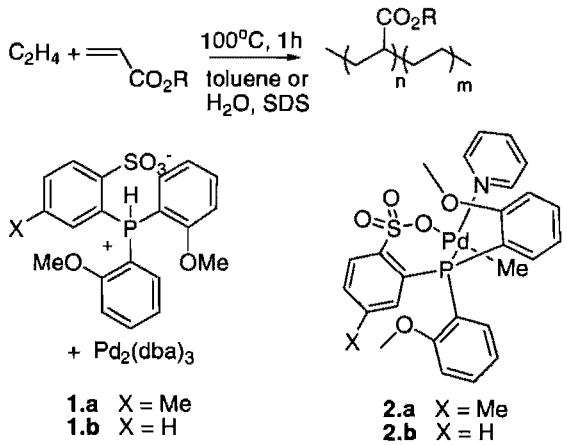

Figure 6.1: Catalytic copolymerization scheme of ethylene with acrylate and the catalysts used.

These catalysts are active for the copolymerization of various acrylates with C_2H_4. The instantaneous activities or turnover frequencies (TOF) in moles of C_2H_4 per mole of palladium and per hour reported in this paper correspond to the rate at which ethylene is consumed from a feed tank. The TOF values reported in Table 6.1 are the maximum activity values once the reactor has reached its set-point temperature and the complete dissolution of ethylene. In our experimental setup, heating and dissolution occurs within 15 minutes. The kinetics curves were measured (Figure 6.2) after this initial 15 minutes delay is passed. These values are reproducible (less than 10 % deviation between repeat experiments) as long as the same reactor and the same experimental parameters (stirring, stirrer design, cooling loop design, temperature of the cooling liquid, etc...) are used. When the catalytic activity is low, such as in the case of emulsion reactions, the exact TOF values can be difficut to measure. Turnover numbers (TON) for C_2H_4 and MA, are also reported in this paper. In this chapter the TON values correspond to the total mole amount of C_2H_4 (or of MA) inserted per mole of catalyst divided by the reaction time. This number, calculated from the copolymer yield and composition, is accurate even for low activity reactions, but is influenced both by the rate of monomer insertion and the rate at which the catalyst is deactivated. Hence, this TON value should not be used to extract kinetic information. The TON values can be close to TOF values in some cases because a part of copolymer is formed in the time when the exact measurement of TOF values is very difficult due to the reactor heating and ethylene dissolution process.

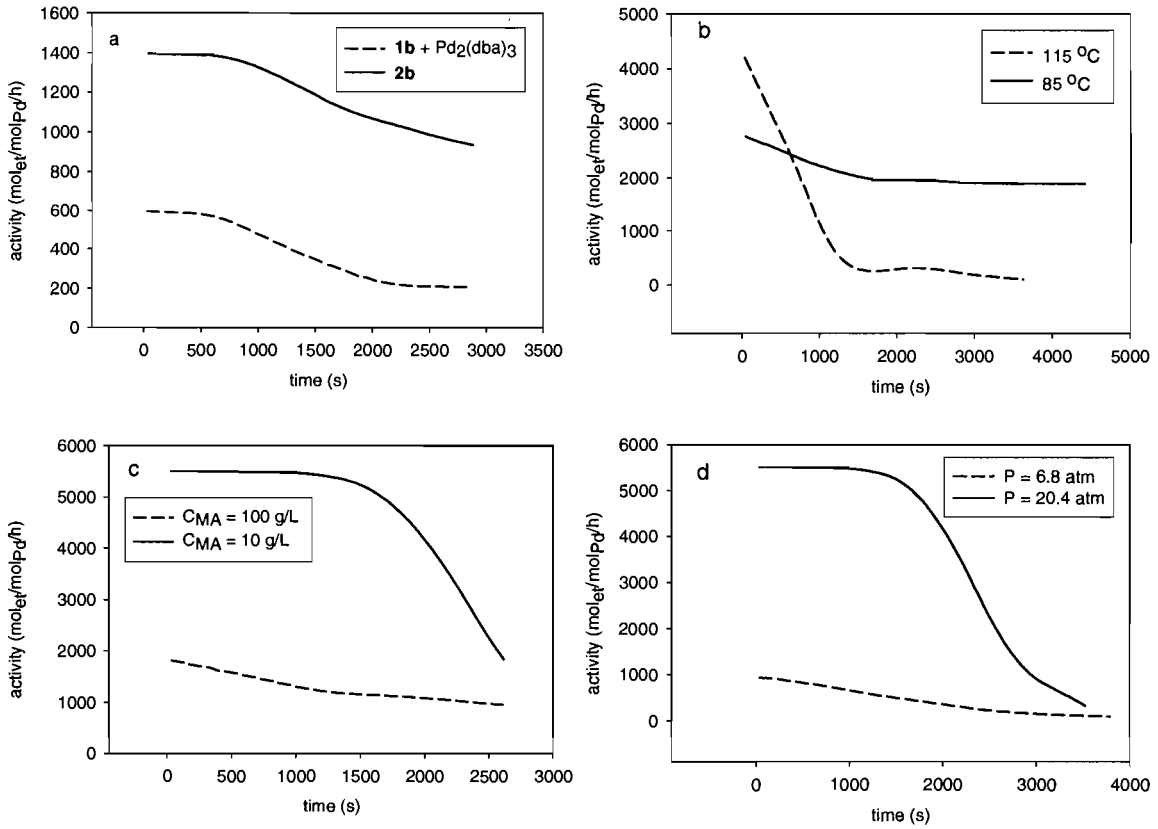

Figure 6.2: The influence of reactions parameters on the activity of the catalyst: a) influence of the nature of the catalyst: **1a** + $Pd_2(dba)_3$ (dashed line, expt. 1S) vs **2b** (solid line, expt. 2S) ([Pd] = 110 μmol/L, [MA] = 100 g/L, T = 100 °C, $P(C_2H_4)$ = 300 psi) b) influence of temperature: T = 115 °C (dashed line, expt. 5S) vs T =85 °C (solid line, expt. 6S) ([**2b**] = 110 μmol/L, $P(C_2H_4)$ = 300 psi, [MA] = 10 g/L) c) influence of MA concentration: [MA] = 100 g/L (dashed line, expt. 2S) vs [MA] = 10 g/L (solid line, expt. 7S) ([**2b**] = 110 μmol/L, T = 100 °C, $P(C_2H_4)$ = 100 psi). d) influence of ethylene pressure: $P(C_2H_4)$ = 100 psi (dashed line, exp. 8S) vs $P(C_2H_4)$ = 300 psi (solid line, expt. 7S) ([**2b**] = 110 μmol/L, T = 100 °C, [MA] = 10 g/L).

Only experiments with temperature control (exotherm less than 5 °C) are reported here. Consequently, experiments where large amounts of catalyst were used, which in our hands lead to higher acrylate incorporation, were not included in this study.

In the case of homopolymerization of C_2H_4, the activities of the *in situ* and well-defined systems are comparable.[27] However, for the copolymerization of C_2H_4 with MA, the activity of the *in situ* system is two to three times lower than for the well-defined catalyst (Figure 6.2 a, Table 1, experiments 1S and 2S), seemingly indicating that a lower number of sites are active for the *in situ* system. Comonomer incorporations are similar for copolymerizations ran with both systems. Ligand **1b**, based on a benzene sulfonic acid backbone, is similar in terms of catalytic activity, molecular weight and comonomer incorporation to ligand **1a** based on *p*-toluene sulfonic acid (Table 6.1, comparing experiments 3S and 4S). In our hands, it was slightly easier to dehydrate benzene sulfonic acid than toluene sulfonic acid, allowing the synthesis of **1b** to proceed with a higher yield than for **1a**.[22] The use of either structure **a** (toluene sulfonic) or **b** (benzene sulfonic) does not offer any significant advantage or difference, and both catalysts will be used interchangeably in the rest of the discussion.

The copolymerization can be performed at temperatures ranging from 85 °C to 110 °C. As expected (Figure 6.2 b), the catalytic system has a shorter life time (less than one hour) and a higher maximum activity (TOF) at 110 °C than at 85 °C. This TOF value is likely underestimated because a significant portion of the catalyst is most likely deactivated before the temperature reaches 110 °C. At 85 °C, the polymerization can be sustained for

several hours, but with a low activity. An acceptable compromise is around 100 °C, at which both, activity and productivity are maximized. As expected, the molecular weights of the copolymer decrease with increasing reaction temperature (compare experiments 5S, 6S and 7S). For all copolymers, the main chain incorporation of the acrylate has been demonstrated by ^{1}H NMR analysis: for every methyne C**H**-CO(OMe) proton, four methylene protons -C**H$_2$**-CHCO(OMe)-C**H$_2$**- are observed in two separate peaks corresponding to the two diastereotopic positions. Polymers are also linear (as demonstrated by Mark-Houwink plots in GPC and by NMR). Polymer for which the chain-ends could be detected by ^{1}H NMR were terminated by the usual β-hydride elimination process, occurring either after an ethylene (> 75 %) or after a 2,1-acrylate insertion (< 25 %). The activity depends on the concentration of both comonomers (Figure 6.1c and 6.1d), indicating that the polymerization kinetics is not zero-order with respect to monomer concentration (see below).

The kinetics of homopolymerization of ethylene can be seen as an equilibrium between coordination and dissociation of C_2H_4 on the active site and insertion of C_2H_4 in the Pd alkyl bond (Figure 6.3).

In order to determine k_2, k_{-1} and k_1, the following approach was adopted. First, analytical expressions for the concentration of pyridine and for TOF were determined (see Supporting Information, Appendix C).

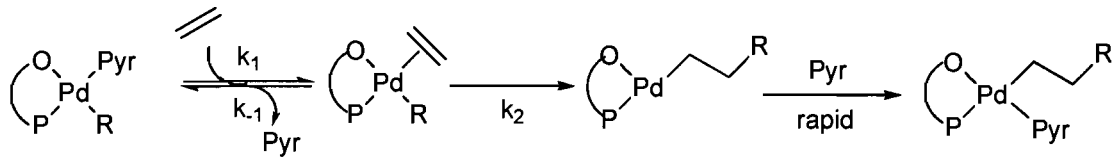

Figure 6.3. Kinetic scheme for C_2H_4 homopolymerization.

Table 6.1: Copolymerization of C_2H_4 with various acrylates (MA : methyl acrylate, BA : n-butyl acrylate, BnA : benzyl acrylate, PEA : 2-phenoxy ethyl acrylate).

Expt[a]	T (°C)	Cat	Mono-mer	[mono-mer] (g/L)	P (psi)	Pol. wt (g)	SC[b] (%)	dp[c] (nm)	M_n[d] (g/mol)	%A[e]	TOF (h^{-1})	TON (C_2H_4), h^{-1}	TON (A), h^{-1}
1S	100	**1b**	MA	100	300	0.6			5400	6.9	600	735	110
2S	100	**2b**	MA	100	300	1.4			9800	6.3	1800	1605	320
3S	100	**1b**	MA	50	200	0.4			nd	6.4	<500	540	75
4S	100	**1a**	MA	50	200	0.35			nd	5.6	<500	350	40
5S	115	**2b**	MA	10	300	3.0			5900	1.1	4050	4715	105
6S	85	**2b**	MA	10	300	2.5			21000	0.6	2650	3180	40
7S	100	**2b**	MA	10	300	4.0			5800	0.8	5300	6380	100
8S	100	**2b**	MA	10	100	0.65			8900	2.6	900	960	50
9S	100	**1a**	MA	10	100	0.85			9500	2.6	870	1030	55
10S	100	**1a**	MA	10	200	1.0			11600	1.5	720	1580	50
11S	100	**1a**	MA	10	300	2.35			13400	1.0	3400	3730	75
12S	100	**2b**	MA	40	60	0.10			nd	9.6	42	55	11
13S	100	**1b**[f]	MA	25	60	0.13			nd	6.8	200	48	4
14S	100	**1b**[f]	MA	25	100	0.40			2200	6.6	526	146	11
15S	100	**1b**[f]	BA	35	60	0.04			nd	6.3	54	13	1
1E[g]	100	**1b**	MA	40	60		floc	floc	nd	nd	nd	nd	nd
2E[g]	100	**2a**	MA	200	90		floc	floc	nd	nd	nd	nd	nd
3E	100	**2b**	MA	40	50		4.5	185	5400	2.7	nd	420	8
4E	100	**2b**	MA	40	50		5.0	135	15000	2.8	nd	36	0.7
5E	100	**2a**	MA	140	85		0.9	678	5000	1.2	nd	13	0.1
6E	100	**2b**	MA	40	65		1.9	197	4500	1.0	nd	136	0.9
7E	100	**2b**	BnA	60	60		3.6	209	nd	9.7	nd	154	25
8E	100	**2b**	BA	60	300		2.2	108	nd	3.4	nd	519	27
9E	100	**2b**	PEA	100	70		1.8	170	nd	8.1	nd	110	14

For the ligands **1a** and **1b**, $Pd_2(dba)_3$ was used as source of Pd. [a] S – polymerization in toluene, E – polymerization in emulsion, [b] solid content of the latex determined by gravimetry [c] particle diameter by DLS, [d] determined by GPC (not suitable when the weight of polymer is less than 0.4 g) [e] molar incorporation of acrylate determined by ^{1}H NMR, [f] $PdMe_2$(tmeda) was used as a source of Pd, [g] no hexadecane and no sonication were used for this expt.

In order to determine k_2, k_{-1} and k_1, the following approach was adopted. First, analytical expressions for the concentration of pyridine and for TOF were determined (see supplementary materials). Initial guesses for k_2, k_1 and k_{-1} were chosen, allowing us to calculate TOF which could be compared to experimentally measured TOF. Using a non linear optimization procedure, the values of k_2, k_1 and k_{-1} giving the least error between calculated and experimental error were found to be 102 s^{-1}, 5 L mol^{-1} s^{-1} and 10^8 L mol^{-1} s^{-1}. Although there is a good agreement between measured and calculated TOF values (Table 6.2 and Figure 6.4), the accuracy is probably low due to the limited number of experiments. Notwithstanding the exact values of these rate constants, it is possible to draw several conclusions based on the order of magnitude of these constants. First, the pyridine coordination equilibrium is very much in favor of the pyridine bound form ($K = k_1/k_{-1} \sim 10^{-7}$). Secondly, the activity is maximum when all the palladium are bound to C_2H_4, that is to say when the rate of polymerization is $k_2 [Pd]_0$, and therefore when the turnover frequency is $TOF_{max} = k_2$. The ratio of the measured activity TOF to the maximum activity, TOF_{max}, is the proportion of Pd atoms that are coordinated to C_2H_4. At a pressure of 300 psi, only 3 % of the catalyst is bonded to C_2H_4, and 97 % bonded to pyridine at a given time (Table 6.2). Although the conditions are very different (catalyst concentration higher and C_2H_4 pressure lower in the NMR tube) it will be seen below that C_2H_4 bound Pd species are not observed spectroscopically, also indicative of an unfavorable pyridine substitution by C_2H_4.

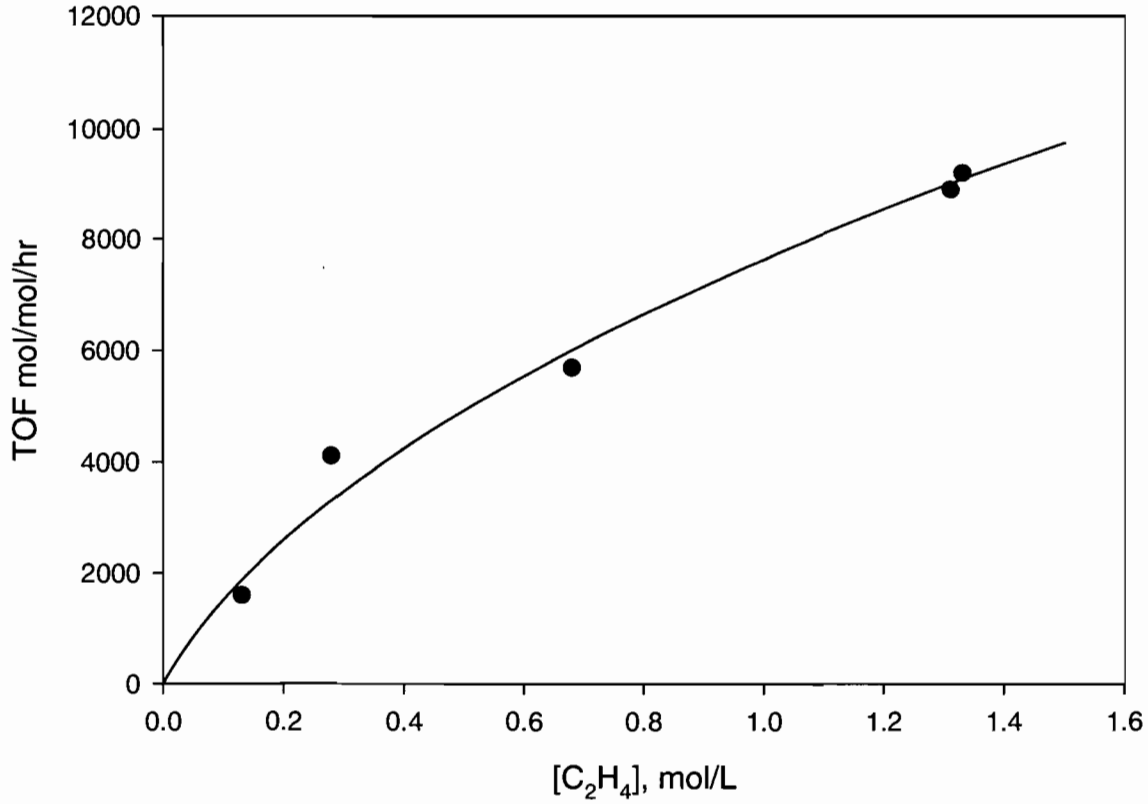

Figure 6.4: Activity vs. C_2H_4 concentration for C_2H_4 homopolymerization by catalyst **2b** (see experimental conditions in Table 6.2). The plain-line curve is a fit of the activity TOF vs concentration of ethylene using $k_2 = TOF_{max} = 102\ s^{-1}$, $k_1 = 5\ L\ mol^{-1}\ s^{-1}$ and $k_{-1} = 10^8\ L\ mol^{-1}\ s^{-1}$ (details on the fit given in Supporting Information (Appendix C)).

Table 6.2: Influence of the C_2H_4 pressure for C_2H_4 homopolymerization wih catalyst **2b**. All reactions were performed with a catalyst concentration of 76 μmol/L in 50 mL toluene at 85 °C (reactor size : 100 mL).

Pressure C_2H_4 (psi)	$[C_2H_4]^a$ (mol L^{-1})	TOF (mol mol^{-1} h^{-1})	% pyridine bound[b]	% C_2H_4 bound[b]	R_1[c] (mol L^{-1} s^{-1})	R_2[d] (mol L^{-1} s^{-1})
47	0.13	1600	99.5	0.5	$5.4\ 10^{-5}$	$3.9\ 10^{-5}$
90	0.28	4100	99	1	$1.2\ 10^{-4}$	$7.0\ 10^{-5}$
200	0.68	5700	98	2	$2.8\ 10^{-4}$	$1.3\ 10^{-4}$
257	1.31	8900	97	3	$5.4\ 10^{-4}$	$1.9\ 10^{-4}$
287	1.33	9200	97	3	$5.4\ 10^{-4}$	$1.9\ 10^{-4}$

[a]Concentration of C_2H_4 in saturated toluene calculated using Peng-Robinson thermodynamic state equations for toluene and ethylene (data not shown). [b]Calculated from the ratio of TOF to TOF_{max} , using the calculated value of k_2 = 102 s^{-1} for TOF_{max} (= 368,000 mol mol^{-1} h^{-1}). [c]Calculated rate of the reaction of ethylene coordination (forward rate) [d]Calculated rate of the insertion reaction. The concentrations of Pd bound to ethylene and palladium bound to pyridine were calculated using equations developed in the Supporting Information (Appendix C).

Last, under polymerization conditions, the reaction of ethylene coordination ($R_1 = k_1 [C_2H_4] [Pd\text{-}pyr]$, Table 6.2) goes approximately at the same rate than the insertion reaction ($R_2 = k_2 [Pd\text{-}C_2H_4]$). Contrarily to our initial belief, the insertion step is not preceded by a fast preequilibrium of ethylene coordination: both reactions go at comparable rates.

In the case of C_2H_4 and MA copolymerization, the kinetic scheme includes two pyridine displacement reactions (one by MA, the other one by C_2H_4), and four possible propagation steps (insertion of MA or insertion of C_2H_4 in a growing chain which has C_2H_4 or a MA as the last inserted monomer). Moreover, the oxygen lone pair of the carbonyl group of the acrylate could coordinate the catalyst: in this case, MA would not only be a monomer, but it would also be a catalyst inhibitor. Consequently, all copolymerizations are characterized by a significant decrease in activity; however, Guironnet *et al.*[31] have concluded that this decrease was due rather to a slow insertion of monomer in [(P^O)Pd{CH(COOMe)CH_2R}(monomer)]. Based on the pioneering work of Brookhart *et al.* on cationic palladium diimines,[36] Drent *et al.*[20] have inferred that the decrease of activity was due to the formation of a stable chelate after acrylate insertion.

To clarify which phenomenon is responsible for the loss of catalytic activity in C_2H_4 and MA copolymerizations, polymerizations were performed in the presence of a non-polymerizable ester analog to MA such as ethyl acetate and methyl propionate (Table 6.3). Compared to polymerizations done in toluene, the use of an ester as solvent results in lower

Table 6.3: Influence of various additives on C_2H_4 homopolymerization by **2** and **3**.

Solvent	temperature (°C)	$P(C_2H_4)$ (psi)	[catalyst] µmol/L	TOF (mol mol^{-1} h^{-1})
		Catalyst **3**		
toluene	100	300	5	570 10^3
toluene + 5 ml EtOAc	100	300	5	86 10^3
THF	85	300	5	16.7 10^3
THF + 0.2 mL water	85	300	5	14.8 10^3
THF + 1 mL water	85	300	5	13.8 10^3
THF + 5 mL water	85	300	5	10.5 10^3
THF + 10 mL water	85	300	5	9.1 10^3
		Catalyst **2b**		
EtOAc	100	300	51	740
methyl propionate	100	300	51	530
toluene[a]	100	380	104	8900
toluene + 6 mL EtOAc[a]	100	380	104	6800

[a] Copolymerization with MA (10 g/L)activities. This indicates that esters coordinate to the catalyst.

This was confirmed for catalyst **3**[27] (Figure 6.5), which has a high activity but it only inserts small amounts of acrylates (Table 6.3). The addition of 5 % ethyl acetate to the solvent results in a 7-fold decrease in catalytic activity, clearly indicating that esters inhibit the catalyst (the solubility of the catalyst and of ethylene are not expected to be drastically changed by the addition of 5 % of ethyl acetate). The 'poisoning' effect of ethyl acetate was also noticeable during the copolymerization of acrylates (Table 6.3): the copolymerization rate is decreased by 30 % when ethyl acetate at a concentration of 35 g/L is present.

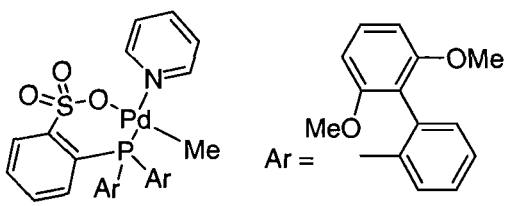

3

Figure 6.5: Structure of catalyst **3**.

Before determining the rate of pyridine substitution by an acrylate (or more generally by an ester), a simpler reaction of pyridine exchange was studied (Figure 6.6).

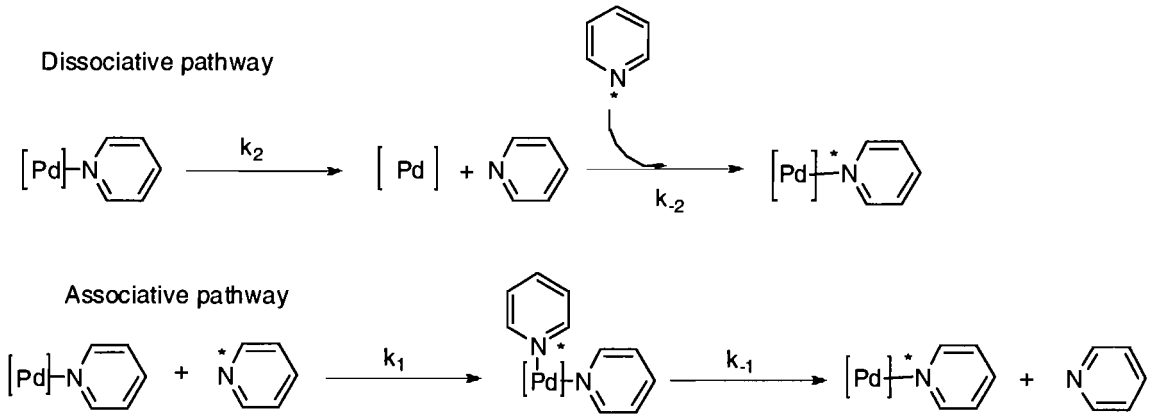

Figure 6.6: Possible mechanisms for pyridine exchange.

The exchange kinetics of pyridine in either bound or free states of the catalyst were studied in dichloromethane by both ^{1}H and ^{13}C NMR lineshape analysis over a wide range of temperatures.[37] At room temperature, a sample of catalyst **2b** containing 3 % free pyridine, exhibited two separate set of resonances for the pyridine protons in ^{1}H NMR at room temperature (Figure 6.7 a). This is in contrast to a single time-averaged resonance that was observed when 10 % free pyridine was is added (Figure 6.7 b). The resonance of each time-averaged peak, in either a slow-exchange regime or fast-exchange regime can be fitted by a Lorentzian curve and whose shape depends on a parameter τ defined as the lifetime of pyridine interaction (Figure 6.8).

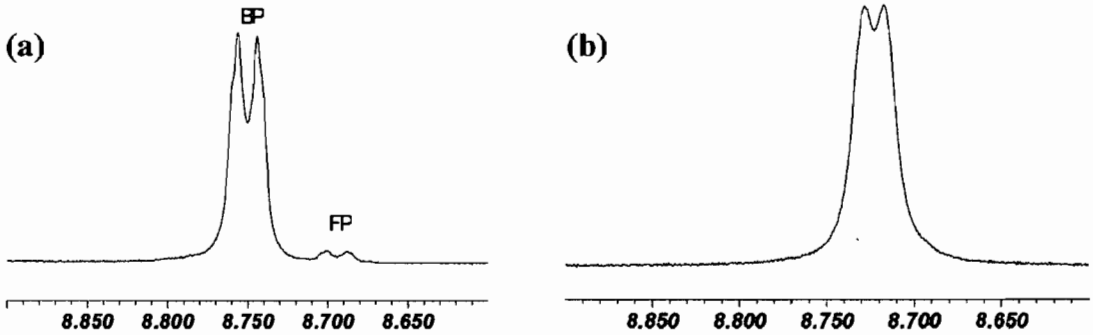

Figure 6.7: Resonance of the proton α to nitrogen in pyridine for catalyst **2a** in CD_2Cl_2 at room temperature. BP : bound pyridine, FP : free pyridine. a. Slow exchange regime (catalyst **2a** + 3 % pyridine). b. Fast exchange regime (catalyst **2a** + 10 % pyridine).

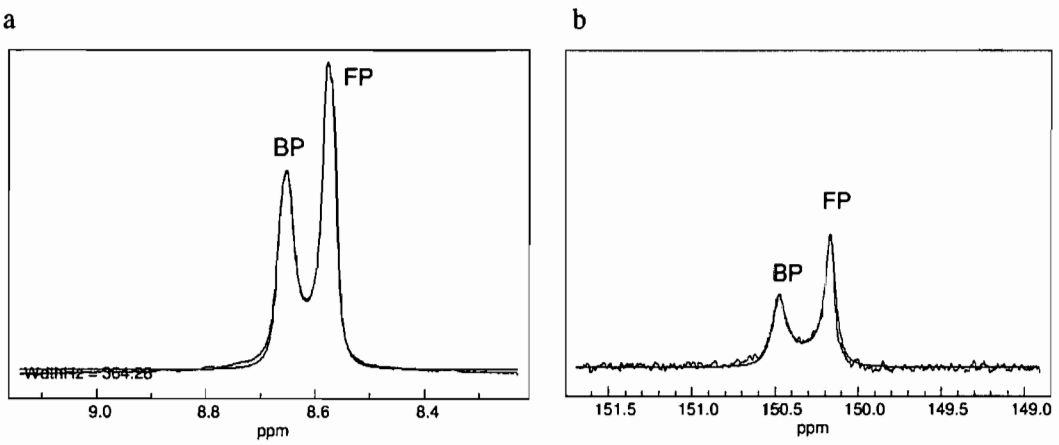

Figure 6.8: Overlay of the calculated and experimental ^{1}H NMR (a, left) and ^{13}C NMR spectra (b, right) for catalyst **2a** (0.079 mol/L) and added pyridine (0.104 mol/L) in CD_2Cl_2 at -90 °C.

This lifetime is defined mathematically as $\tau_A\tau_B/(\tau_A+\tau_B)$ where τ_A and τ_B are respectively the lifetime of pyridine in the bound and free state.[38] The measurements were done at various temperatures and at three different measured concentrations of pyridine. The resonance of the C**H**=N proton was analyzed both by ^{13}C and ^{1}H NMR, providing two values of τ that were averaged (Table 6.4).

For Scheme 6.6, the lifetime τ is given by:[37-39]

$$\frac{1}{\tau[pyridine]_{total}} = k_1 + k_2 \frac{1}{[pyridine]_{free}} \qquad (6.1)$$

Hence, a plot of $1/(\tau[\text{pyridine}]_{total})$ vs $1/[\text{pyridine}]_{free}$ should yield a straight line of slope k_2 (dissociative mechanism rate constant) and intercept k_1 (associative mechanism rate constant).

Figure 6.9 clearly indicates that at temperatures ranging from -90 to -60 °C, the dissociative contribution (slope) is negligible and pyridine exchange occurs exclusively by an associative pathway. Higher temperatures cannot be probed with this technique because the fast exchange limit is reached, except when low concentrations of FP are used (see Figure 6.7a). An Eyring plot (Figure 6.10) indicates that the activation parameters for the associative exchange are $\Delta H^{\ddagger}$ = 16.8 kJ/mol and $\Delta S^{\ddagger}$ = - 98 J mol^{-1} K^{-1}, the negative value for the activation entropy being expected for an associative process.

Table 6.4: $1/\tau$ for catalyst **2a** in CD_2Cl_2 at temperatures ranging from -60 °C to -90 °C (BP : bound pyridine, FP : free pyridine). Above -60 °C, coalescence occurred and the width of the peak is principally influenced by experiment-dependent parameters ($1/T_2^*$) and not by the exchange process.

Temperature = -60 °C		
$1/\tau$ (s^{-1})	[BP] (mol/L)	[FP] (mol/L)
321	0.079	0.105
266	0.024	0.086
285	0.079	0.052
197	0.073	0.034
Temperature = -70 °C		
$1/\tau$ (s^{-1})	[BP] (mol/L)	[FP] (mol/L)
195	0.079	0.105
124	0.024	0.086
178	0.079	0.052
123	0.073	0.034
Temperature = -80 °C		
$1/\tau$ (s^{-1})	[BP] (mol/L)	[FP] (mol/L)
112	0.079	0.105
74	0.024	0.086
106	0.079	0.052
74	0.073	0.034
Temperature = -90 °C		
$1/\tau$ (s^{-1})	[BP] (mol/L)	[FP] (mol/L)
61	0.079	0.105
42	0.024	0.086
59	0.079	0.052
42	0.073	0.034

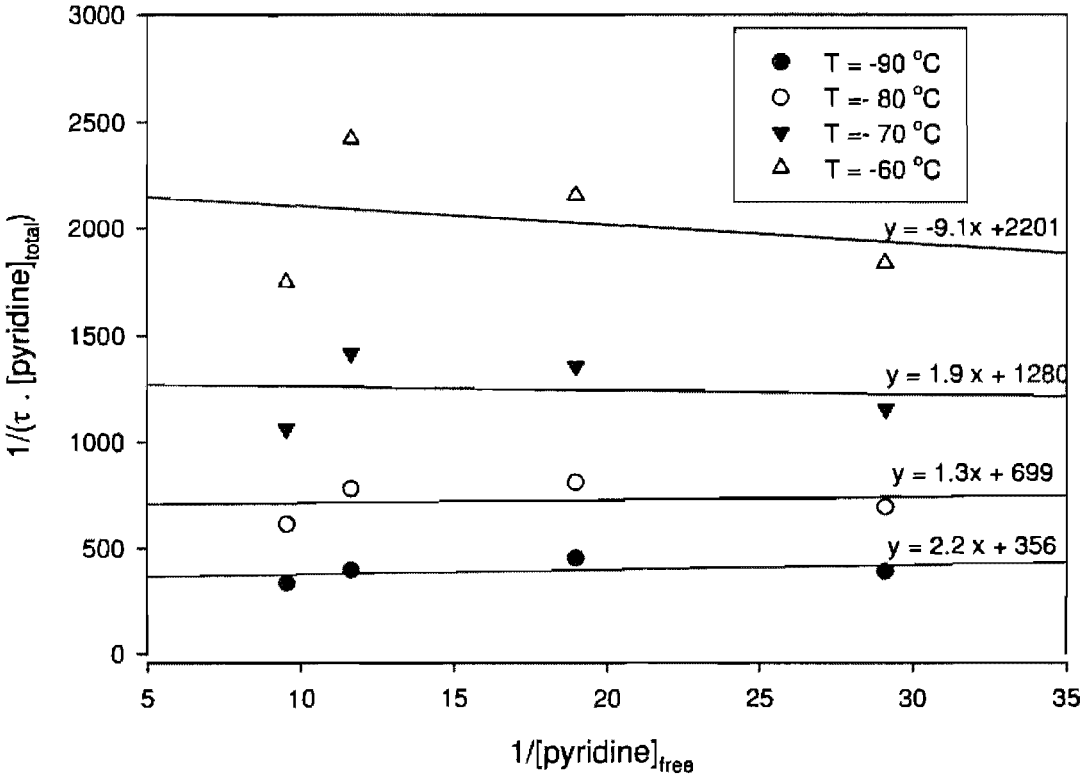

Figure 6.9: $1/(\tau\ [\text{pyridine}]_{total})$ vs $1/[\text{pyridine}]$ for catalyst **2a** in CD_2Cl_2.

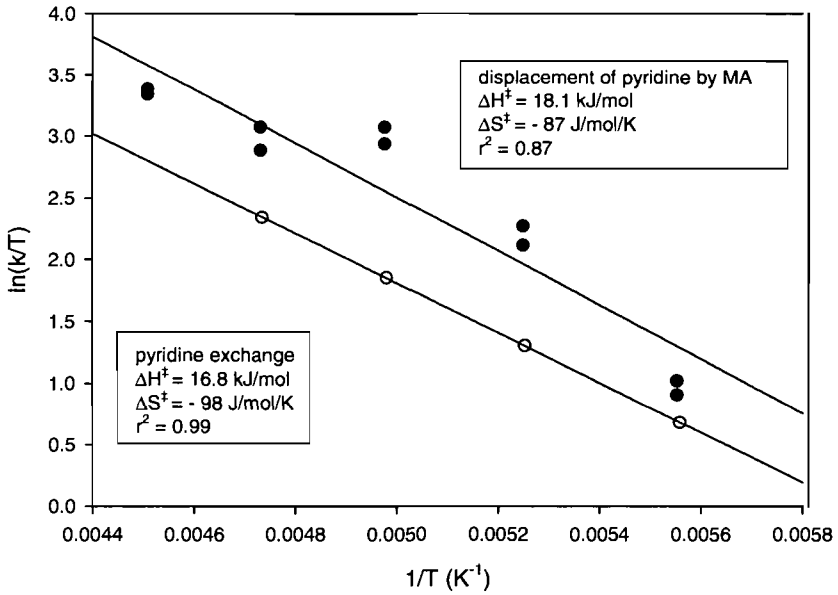

Figure 6.10: Eyring plots for the substitution of pyridine by pyridine and by MA via an associative mechanism.

We now turn our attention toward the displacement of pyridine either by an acrylate or by C_2H_4. Based on the fact that pyridine exchange occurs by an associative mechanism, we assume that the substitution of pyridine by MA or by C_2H_4 also occurs via an associative route (Figure 6.11). This substitution reaction occurs on a time scale that can be probed by NMR. As shown in Figure 6.12, the resonances of the pyridine protons coalesce in the presence of MA or ethylene. It is important to state that neither acrylate nor ethylene-bound complexes are observed spectroscopically, indicating that pyridine is a strong donor. However, the presence of either MA or ethylene decreases the lifetime of pyridine in the bound state, τ, as observed by NMR.

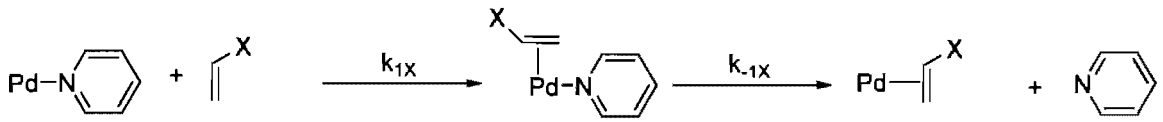

Figure 6.11: Substitution of pyridine by ethylene (X = H) or an acrylate (X = COOR).

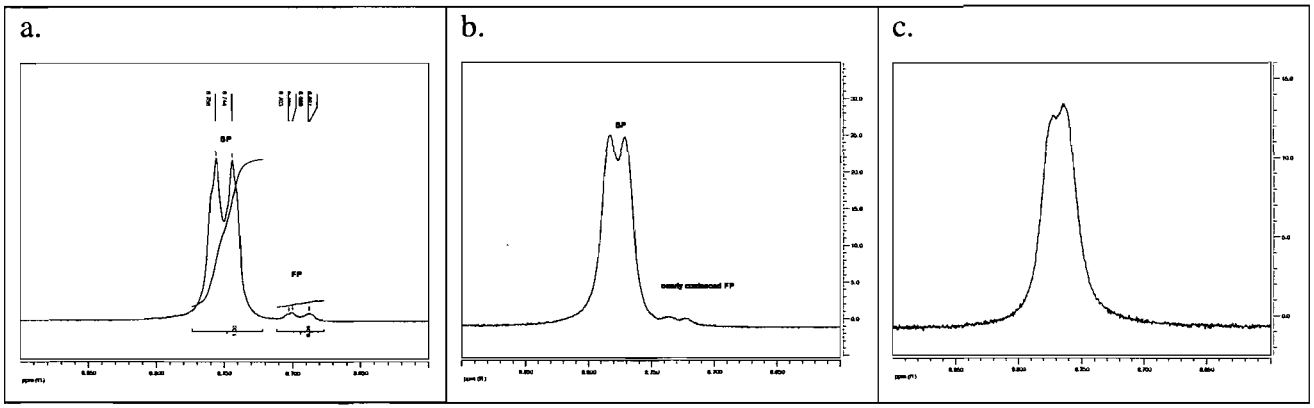

Figure 6.12: Resonance of the proton α to nitrogen in pyridine for catalyst **2a** in CD_2Cl_2 at room temperature. BP : bound pyridine, FP : free pyridine. a. catalyst **2a** with 3 % of FP. b. catalyst **2a** with 3 % of FP and 5 equivalents of ethylene and c. catalyst **2a** with 3 % of FP and one equivalent of MA.

This lifetime is given by :

$$\frac{1}{\tau} = k_1 [pyridine]_{total} + k_{1X} [X]_{total} \qquad (6.2)$$

Using both ^1H and ^{13}C NMR lineshape analysis, τ was measured at several temperatures (Table 6.5). The values of k_1 were calculated from the activation parameters obtained above (Figure 6.10). From equation (6.2), the kinetic rate constant for ligand displacement, k_{1x}, can thus be obtained. However, for the case of susbstitution of pyridine by C_2H_4, the C_2H_4 concentration dissolved in the sample changes considerably with temperature, and no reliable values could be obtained for k_{1E}. For the associative substitution of pyridine by MA, it was found that the activation parameters are $\Delta H^{\ddagger}$ = 18.1 kJ/mol and $\Delta S^{\ddagger}$ = - 87 J mol^{-1} K^{-1} (Figure 6.10 and Table 6.5).

Importantly, using this technique, it is not possible to assess whether the activation parameters measured for acrylate coordination correspond to coordination via a π-bond (involving the C=C) or via a σ-bond (involving the O lone pair). Interestingly, the activation parameters for pyridine or MA coordination on the catalyst are significantly smaller than the literature values reported for olefin complexation on other late transition metal polymerization catalysts. For example, the activation enthalpies of complexation of C_2H_4 on salicylaldiminato nickel or cationic palladium diimines complexes have been calculated to be in the range of 50 to 80 kJ/mol.[40, 41] However, to our knowledge, these energies have been calculated by removing the phosphine ligand to produce a coordinately unsaturated site followed by coordination of ethylene. Therefore, a dissociative process has been implicitly assumed by the authors, whereas in our case an associative pathway is taking place. For our catalysts, the low enthalpy of activation is balanced by the very negative activation entropy consistent with an associative process.

Table 6.5: $1/\tau$ for catalyst **2a** in CD_2Cl_2 at temperatures ranging from -50 °C to -90 °C, obtained by line shape analysis of ^1H and ^{13}C spectra.

T (°C)	$1/\tau$ (Hz) (^1H NMR)	$1/\tau$ (Hz) (^{13}C NMR)	k_1[a] (L mol^{-1} s^{-1})	k_{1A} (L mol^{-1} s^{-1}) (^1H NMR)	k_{1A} (L mol^{-1} s^{-1}) (^{13}C NMR)
-90	32	30	358	445	498
-80	85	95	700	1840	1570
-70	210	189	1281	3780	4340
-60	253	224	2213	3780	4560
-50	369	380	3641	6530	6230

[a] calculated from the activation parameters of Figure 6.10.

To conclude this section, it is clear that the displacement of pyridine by C_2H_4 or acrylate is a key step in our polymerizations. Removal of pyridine would have for effect to transfer the limiting step toward olefin insertion for ethylene polymerization. This was achieved by Guironnet *et al.*[31] with the preparation of a DMSO-ligated sulfonated aryl phosphine palladium complex and by Vela *et al.*[30] have shown that pyridine can be captured with tris(pentafluorophenyl) borane, generating a catalyst which is more active for polymerization of ethylene. However, even when pyridine is removed or absent, the possibility of poisoning the catalyst by σ-coordination of the acrylate cannot be discarded.

6.4.2 Emulsion copolymerization of C_2H_4 and acrylates

Catalyst **2a** and **2b** have been shown to promote the emulsion copolymerization of C_2H_4 with styrene[29] and with norbornene.[15] The results of MA-E copolymerization in organic solution encouraged us to probe an emulsion polymerization process with the aim of latex formation. In our hands, the copolymerization of E and an acrylate by the system $Pd_2(dba)_3$ / **1a** or **1b** (Expt 1E, Table 6.1) generates polymer particles with large sizes (>>1μm), unlike an emulsion polymerization which yields nanoparticles. Therefore all emulsion polymerizations were performed with the well-defined catalysts **2a** and **2b**. When **2a** or **2b**, dissolved in a small amount of organic solvent, is added to water and surfactant, the polymerization reaction results in the formation of millimeter size polymer particles (expt. 2E, Table 6.1). However, the final product of the reaction is a latex when the initial organic solution containing **2a** or **2b** is miniemulsified, that is to say when o/w nanosize

droplets are formed upon sonication of an emulsion containing the organic solution, hexadecane, water and surfactant. Attempts to bypass this emulsification procedure results either in the formation of polymers which are not dispersed, or in the absence of polymerization (probably because of the poor accessibility of the catalyst in the medium). The miniemulsion droplets have a diameter around 150 nm as measured by dynamic light scattering. They remain stable for several hours. The role of hexadecane is to prevent Ostwald ripening (disappearance of the smallest droplets and swelling of the largest ones, until the mixture is totally phase separated).[42] The size and stability of this miniemulsion depends on several factors, such as the amount of surfactant and sonication time and power. These parameters are currently under scrutiny in our laboratory. When a miniemulsion is stable, it appears as a homogeneous white medium by optical microscopy (Figure 6.13a). This is consistent with the fact that the miniemulsion consists of droplets that are smaller than the optical resolution (approx 1 μm). Then, an acrylate can eventually be added to the aqueous phase. If saturation is reached ($c > 50$ g/L for methyl acrylate, $c < 10$ g/L for all other acrylates), large droplets containing the excess acrylate are formed (Figure 6.13b, size $>> 1$ μm). These droplets are significantly larger than the miniemulsion droplets and they serve as monomer reservoirs during the reaction. No polymer is formed in these large droplets, as shown by the absence of large particles in the final latex (Figure 6.13c). The amount of organic solvent (dichloromethane) in these polymerizations is small (typically 7 mL per 100 mL of water).

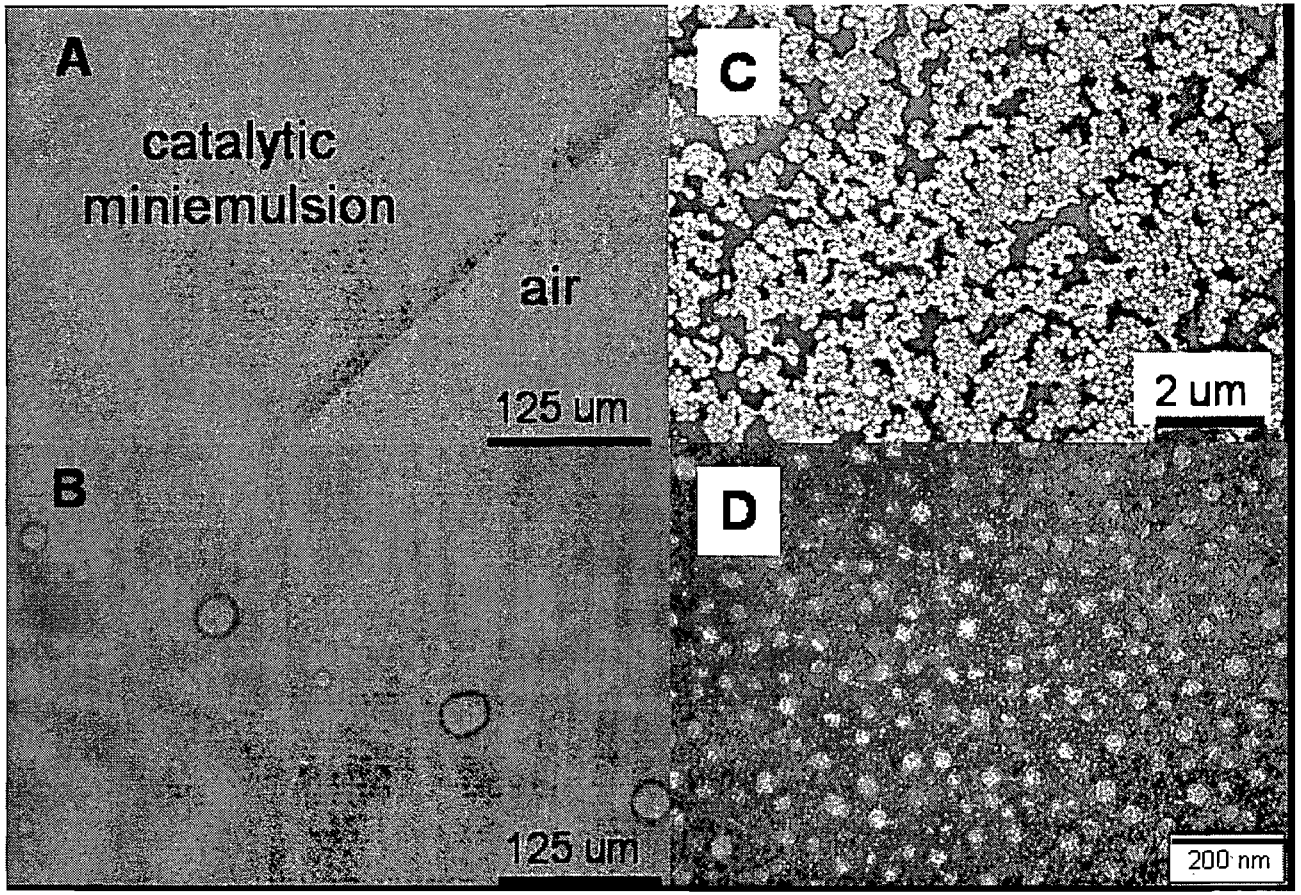

Figure 6.13: a. Optical microscopy picture of a catalyst miniemulsion (37 mg of **2** dissolved in 3 mL of CH_2Cl_2 and 0.3 mL of hexadecane dispersed in 100 mL of an SDS aqueous solution, c = 20 g/L). The size of the o/w droplets is below optical diffraction limit, resulting in a homogenous liquid. b. After adding MA (c = 100 g/L) to the catalytic miniemulsion, MA droplets of several microns are formed. C.

transmission electronic microscopy (TEM) picture of the poly(ethylene-co-acrylate) nanoparticles formed by polymerization of miniemulsion b (entry 4E in Table 6.1). d. TEM picture of the smaller particles (d = 25 nm +/- 7 nm). These particles appear as faint white spots in Figure 6.13c.

Initially, the organic solvent is located in the miniemulsion droplets (size around 150 nm). The reactions are performed at 100 °C and it is unclear what is the proportion of dichloromethane remaining in the liquid phase. During the degassing step, we believe that most of the dichloromethane is stripped, yielding a latex virtually free of volatile organic compounds.

With a stable catalytic miniemulsion in hand, the emulsion polymerization can be triggered upon heating in the presence of C_2H_4. At 100 psi and 100 °C, the solubility of C_2H_4 in water has been reported to be approximately 0.35 g/L, a high enough value to expect its diffusion through the aqueous phase not to be rate limiting. [43] However, transport of C_2H_4 at the gas-water interface can be rate-limiting: in our hands, activity of the emulsion polymerization strongly depends on the design of the reactor and type of stirring blade used during the polymerization and of course stirring rate. In all cases, the polymerization occurs significantly slower than for polymerization run in organic medium (*vide infra*).

The latexes resulting from these polymerizations are formed of particles having a bimodal diameter distribution centered on 120 nm and 25 nm, as confirmed by TEM (Fig.8 C, D) and dynamic light scattering. These suspensions are colloidally stable and are constituted of mostly spherical particles, which contrasts with the elongated particles observed for HDPE latexes.[4, 12] This difference can be explained by the low crystallinity of the poly(ethylene-co-acrylate) copolymers. The presence of a population of smaller polymer particles (diameter ~ 25 nm) is a consequence of the high amount of surfactant used in our formulations. Based on the data of Bechthold *et al.*,[44] the amount of surfactant (SDS) necessary to stabilize droplets of diameter 125 nm is 0.0461 $g_{SDS}/g_{dispersed\ phase}$,

whereas an amount of 0.13 $g_{SDS}/g_{dispersed\ phase}$ was used in our case. The excess surfactant forms micelles (initial diameter ~ 5 nm) which contain catalyst, and which are later converted into polymer particles. Therefore, in parallel to the miniemulsion polymerization process, a 'microemulsion' polymerization process whereby micelles are nucleated and polymerized is occurring in our reactions.[45]

Interestingly, unlike copolymerizations performed in solutions, latexes made with acrylates such as butyl acrylate, phenoxyethyl acrylate, benzyl acrylate (BA, PEA, BnA) have higher acrylate incorporations than those made with MA (expts 7E-9E in Table 6.1). In the emulsion process, the locus of the polymerization is the growing polymer particle. However, a significant portion of MA is located in the aqueous phase (solubility > 50 g/L) and also in the gas phase at 100 °C, resulting in the formation of polymers with low MA incorporation. By contrast, comonomer incorporations are higher for other acrylates because the polymerization occurs in a polymer particle which only contains polymer, acrylate, C_2H_4 and a trace of organic solvent (at the polymerization pressure and temperature, most of the dichloromethane is in the gas phase). Such experimental conditions would be equivalent to a solution reaction performed in neat monomer.

Spontaneous radical polymerization of the acrylate was only prevented when two radical inhibitors, an organosoluble one (BHT) and a water soluble one (hydroxyTEMPO) were used. The use of BHT alone was not sufficient to prevent formation of poly(methyl acrylate) via a radical mechanism, which is consistent with the presence of a high concentration of MA in water.

As observed for polymerizations performed in organic solvent, the highest acrylate incorporations in emulsion are reached when the reactions are performed at low ethylene pressure, 50 psi (expts 3E and 4E). The molecular weights of the emulsion polymers are comparable to those obtained in solution if one does not take into account in the GPC chromatogram a very low molecular weight population which was attributed to surfactant and hexadecane.

All the emulsion polymerizations are significantly slower than the solvent ones, resulting in latexes which have low solid contents. Several literature reports have focused on the decrease of activity in the presence of water. DeKock *et al.* has reported that water promotes the decomposition of the active site via a Wacker-type reaction (attack of OH on ethylene)[46] and protonolysis of the metal-alkyl bond (in the absence of ethylene) was also observed for N,O-chelated salicylaldiminate Ni-based complexes (Grubbs catalysts).[47] In our case, the hydrolytic stability of the catalyst was assessed by heating **2a** at 100 °C for several hours in the presence of water (Figure 6.14) : no hydrolysis of the Pd-Me bound was observed.

Based on the finding that acrylate can coordinate the catalyst in a σ-fashion (*vide supra*), we have surmised that water may also coordinate the catalyst (Figure 6.15). Precise determination of kinetic parameters in the presence of water for catalysts **2a** and **2b** proved to be difficult because measurements of low activities are not precise with our experimental setup.

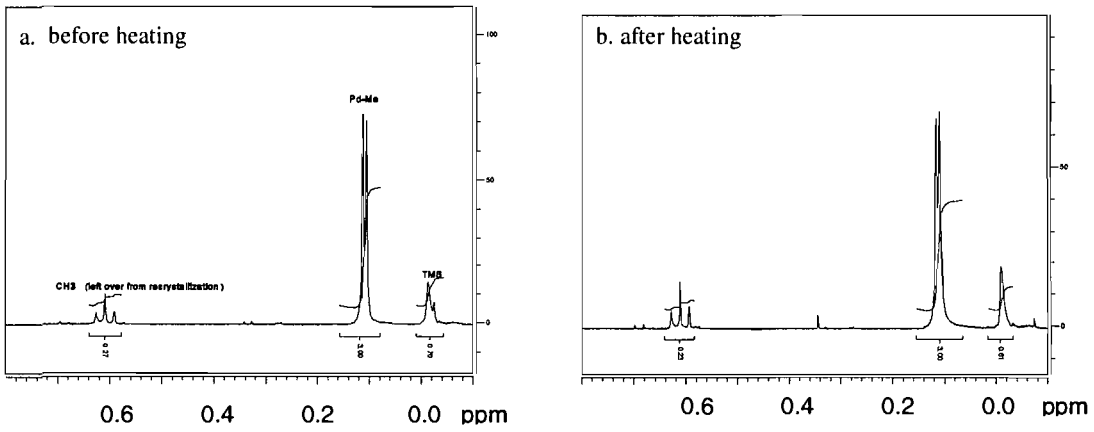

Figure 6.14: ^{1}H NMR ($C_2Cl_4D_2$) of **2a** (Pd-CH_3 region) after being heated at 100 °C for 2 hours in the presence of D_2O (30 mg of **2a** in 1.5 mL of $C_2Cl_4D_2$ and 0.2 mL of D_2O). The insert (Pd-Me region) shows that the methyl group is not degraded under these conditions. No CH_4 (product of hydrolysis of Pd-Me with water, at 0.3 ppm) could be observed.

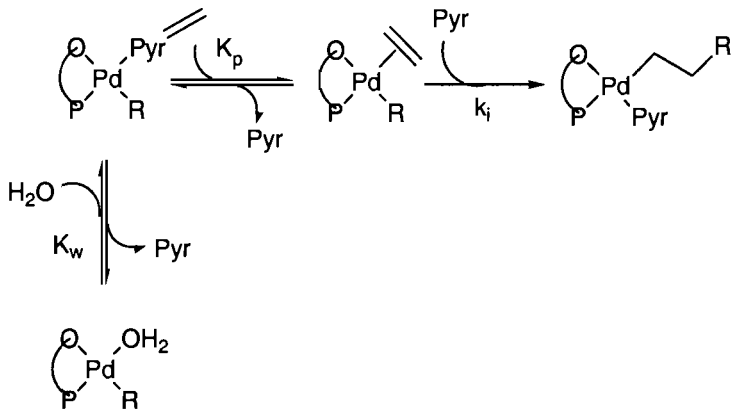

Figure 6.15: Reversible inhibition of the catalyst by water.

Therefore, the very active catalyst **3** (Figure 6.5) was used for this study. Polymerizations of C_2H_4 were performed in THF containing various concentrations of water, THF being used instead of toluene because it is miscible with water (Table 6.3). Interestingly, the catalytic activity decreases with increasing concentrations of water (Figure 6.16), in agreement with the fact that water may coordinate the catalyst. As expected for a competitive inhibitor, there is an inverse relationship between the catalytic activity (TOF) and the concentration of water (Figure 6.17). For the polymerizations run in anhydrous THF or low concentrations of water, no decrease of the activity over time is observed, which indicates that the catalyst is long-lived under these conditions. When the concentration of water in the system is sufficiently high, a decrease of the activity is observed with time (Figure 6.16) as some of the active sites have been deactivated by the presence of water. For a water concentration of 3.9 mol/L, the activity after one hour is 60 % of its initial value, indicating that only 40% of the active sites have been decomposed by water. Therefore, one can assume that all the active sites are active in the first minutes of the reaction, as the effect of the decomposition reaction is only important for longer times. Therefore, the decrease of activity in aqueous medium is due to the combination of two factors: coordination of water on Pd and specific water-induced decomposition of the active site. The fact that decomposition was not observed spectroscopically (Figure 6.14) is not contradictory with the water-induced decomposition of the catalyst during the reaction: as shown by Mecking *et al.*,[46] Wacker-type reactions (involving the participation of C_2H_4) are a likely culprit for the decomposition of the catalyst. For catalyst **3**, the decomposition reaction becomes noticeable only after prolonged reaction times, whereas coordination of water is reducing the activity in a constant manner throughout the reaction duration.

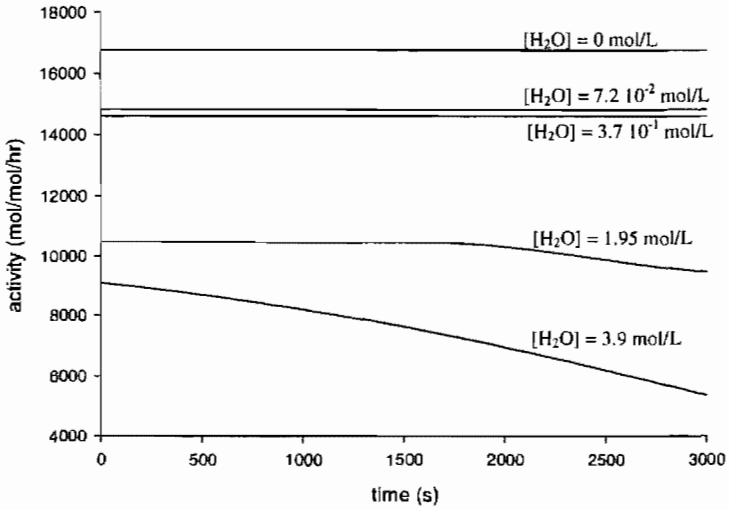

Figure 6.16: Catalytic activity (TOF) for the homopolymerization of ethylene by **3** in THF containing various amounts of water (T = 85 °C, [**3**] = 5.2 μmol/L, P = 300 psi).

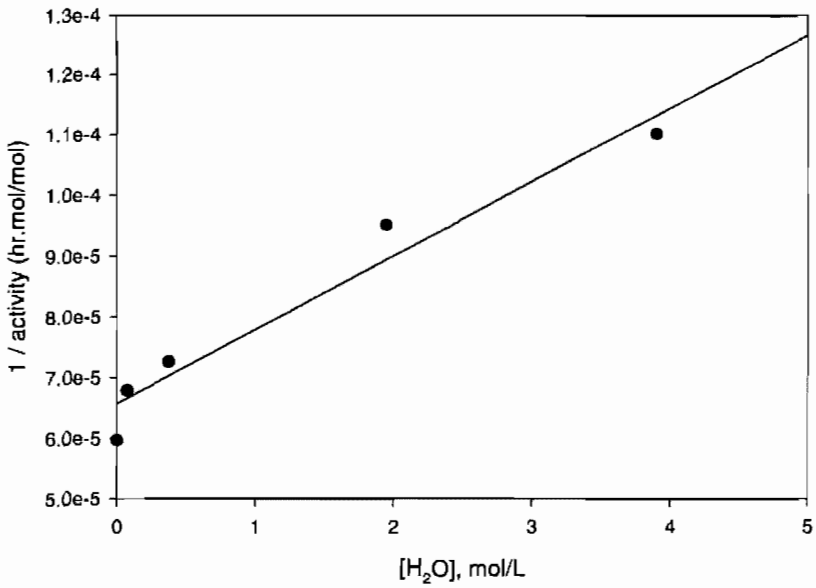

Figure 6.17: Inverse of the initial activity vs water concentration in THF (experiments of Figure 6.16, T = 85 °C, [**3**] = 5.2 μmol/L, P = 300 psi).

Both of these factors are expected to be at play for polymerization in emulsion with catalysts **2a** and **2b**, however, their precise magnitude is unknown at this time.

6.5 Conclusions

We report for the first time the preparation of latexes of poly(ethylene-co-acrylate) made by catalytic emulsion polymerization. These latexes are colloidally stable and are expected to present interesting properties that will be explored in the future. However, their preparation is hampered by the low activity of these catalysts in an aqueous environment. This low activity originates from the combination of three factors. First pyridine is strongly bound to the catalyst: at a pressure of 300 psi in toluene less than 5 % of the catalyst is bound to C_2H_4 (Table 6.2). This quantity is expected to further decrease in an aqueous environment because at the same pressure, the solubility of ethylene is lower. Second, when an acrylate is present, it coordinates both in a π- and a σ-fashion. Therefore, an acrylate is not only a monomer but also an inhibitor of the catalyst. Consequently, high acrylate incorporations are achieved only to the detriment of the catalytic activity. Last, water also acts as a poison, both by coordination to Pd and by irreversible deactivation of the Pd alkyl, as already shown for other complexes by DeKock *et al.*[46, 47] The precise contribution of each of these factors to the deactivation of the catalyst in our systems is not known at this time, and it is probably highly dependent on the reaction conditions.

Another important feature of this work is the discovery that the ligand substitution occurs via an associative pathway. Retrospectively, an associative mechanism for ligand

susbstitution has already been extensively demonstrated for simple coordination complexes.[48] Unlike cationic palladium diimines for which the associative mechanism has been found to play a pivotal role in the regulation of molecular weight, the associative nature of the ligand substitution reaction has often been overlooked for neutral Ni and Pd polymerization catalysts. As a corollary, for the determination of complexation energies, either experimentally or by DFT studies, both associative and dissociative mechanisms should be probed. In the future we intend to measure such complexation energies for complexes having sterically hindered axial faces (such as **3**), in order to assess whether the substitution still occurs by an associative mechanism, or whether a dissociative route is followed.

6.6 Aknowledgements

This work was supported by the U.S. DoC (NIST, Advanced Technology Program, Cooperative Agreement 70NANB4H3014), the NSF (Goali Grant 0354825), NSERC Discovery Program, and the Canadian Foundation for Innovation. We thank Mr. Daigle for technical help.

6.7 Supporting Information (Appendix C)

Derivation of the analytical expression for TOF and details on the determination of k_1, k_2, and k_{-1}. This material is available free of charge via Internet at http://pubs.acs.org/.

6.8 References

1. Fitch, R. M., *Polymer Colloids: A Comprehensive Introduction.* Academic Press: San Diego, 1997.
2. Lowell, P. A.; El-Aasser, M. S., *Emulsion Polymerization and Emulsion Polymers.* John Wiley: Chichester, 1997.
3. Soula, R.; Broyer, J. P.; Llauro, M. F.; Tomov, A.; Spitz, R.; Claverie, J.; Drujon, X.; Malinge, J.; Saudemont, T. *Macromolecules* **2001,** *34*, (8), 2438-2442.
4. Soula, R.; Novat, C.; Tomov, A.; Spitz, R.; Claverie, J.; Drujon, X.; Malinge, J.; Saudemont, T. *Macromolecules* **2001,** *34*, (7), 2022-2026.
5. Soula, R.; Saillard, B.; Spitz, R.; Claverie, J.; Llaurro, M. F.; Monnet, C. *Macromolecules* **2002,** *35*, (5), 1513-1523.
6. Claverie, J. P.; Soula, R. *Prog. Polym. Sci.* **2003,** *28*, (4), 619-662.
7. Mecking, S.; Claverie, J. P., Transition metal-catalyzed polymerization in aqueous systems. In *Late Transition Metal Polymerization Catalysis*, Rieger, B.; Baugh, L. S.; Kacker, S.; Striegler, S., Eds. Wiley-VCH: Weinheim, 2003; pp 231-278.
8. Soula, R.; Claverie, J.; Spitz, R.; Guyot, A. *Surfactant Science Series* **2003,** *115*, 77-92.
9. Bauers, F. M.; Mecking, S. *Macromolecules* **2001**, *34*, (5), 1165-1171.
10. Mecking, S.; Held, A.; Bauers, F. M. *Angew. Chem. Int. Ed.* **2002,** *41*, (4), 544-561.
11. Bauers, F. M.; Chowdhry, M. M.; Mecking, S. *Macromolecules* **2003,** *36*, (18), 6711-6715.

12. Bauers, F. M.; Thomann, R.; Mecking, S. *J. Am. Chem. Soc.* **2003,** *125*, (29), 8838-8840.

13. Kolb, L.; Monteil, V.; Thomann, R.; Mecking, S. *Angew. Chem. Int. Ed.* **2005**, *44*, (3), 429-432.

14. Mecking, S. *Colloid Polym. Sci.* **2007**, *285*, (6), 605-619.

15. Skupov, K. M.; Marella, P. R.; Hobbs, J. L.; McIntosh, L. H.; Goodall, B. L.; Claverie, J. P. *Macromolecules* **2006,** *39*, (13), 4279-4281.

16. Skupov, K. M.; Hobbs, J.; Claverie, J. P. *Prog. Org. Coat.* **2009,** *65*, (3), 314-321.

17. Skupov, K. M.; Piche, L.; Claverie, J. P. *Macromolecules* **2008,** *41*, (7), 2309-2310.

18. Johnson, L. K.; Mecking, S.; Brookhart, M. *J. Am. Chem. Soc.* **1996,** *118*, (1), 267-268.

19. Popeney, C. S.; Camacho, D. H.; Guan, Z. *J. Am. Chem. Soc.* **2007,** *129*, (33), 10062-10063.

20. Drent, E.; van Dijk, R.; van Ginkel, R.; van Oort, B.; Pugh, R. I. *Chem. Commun.* **2002**, (7), 744-745.

21. Hearley, A. K.; Nowack, R. J.; Rieger, B. *Organometallics* **2005,** *24*, (11), 2755-2763.

22. Allen, N. T.; Goodall, B. L.; McIntosh, L. H. Substantially Linear Polymers and Methods of Making and Using Same. US 2007/049712 A1, 17 July 2006.

23. Goodall, B. L.; Allen, N. T.; Conner, D. M.; Kirk, T. C.; McIntosh, L. H., III; Shen, H. *Polym. Prepr. (Am. Chem. Soc., Div. Polym. Chem.)* **2007,** *48*, (1), 202.

24. Kochi, T.; Yoshimura, K.; Nozaki, K. *Dalton Trans.* **2005**, (1), 25-27.

25. Kochi, T.; Noda, S.; Yoshimura, K.; Nozaki, K. *J. Am. Chem. Soc.* **2007,** *129*, (29), 8948-8949.

26. Liu, S.; Borkar, S.; Newsham, D.; Yennawar, H.; Sen, A. *Organometallics* **2007,** *26*, (1), 210-216.

27. Skupov, K. M.; Marella, P. R.; Simard, M.; Yap, G. P. A.; Allen, N.; Conner, D.; Goodall, B. L.; Claverie, J. P. *Macromol. Rapid Commun.* **2007,** *28*, (20), 2033-2038.

28. Luo, S.; Vela, J.; Lief, G. R.; Jordan, R. F. *J. Am. Chem. Soc* **2007,** *129*, (29), 8946-8947.

29. Borkar, S.; Newsham, D. K.; Sen, A. *Organometallics* **2008,** *27*, (14), 3331-3334.

30. Vela, J.; Lief, G. R.; Shen, Z.; Jordan, R. F. *Organometallics* **2007,** *26*, (26), 6624-6635.

31. Guironnet, D.; Roesle, P.; Ruenzi, T.; Gottker-Schnetmann, I.; Mecking, S. *J. Am. Chem. Soc.* **2009,** *131*, (2), 422-423.

32. De Graaf, W.; Boersma, J.; Smeets, W. J. J.; Spek, A. L.; Van Koten, G. *Organometallics* **1989,** *8*, (12), 2907-2917.

33. Bain, A. D.; Duns, G. J. *Can. J. Chem.* **1996,** *74*, 819-824.

34. Castellano, S.; Sun, C.; Kostelnik, R. *J. Chem. Phys.* **1967,** *46*, (1), 327-330.

35. Reich, H. J.; Goldenberg, W. S.; Gudmundsson, B. O.; Sanders, A. W.; Kulicke, K. J.; Simon, K.; Guzei, I. A. *J. Am. Chem. Soc* **2001,** *123*, (33), 8067-8079.

36. Mecking, S.; Johnson, L. K.; Wang, L.; Brookhart, M. *J. Am. Chem. Soc.* **1998,** *120*, (5), 888-899.

37. Shamsipur, M.; Karkhaneeib, E.; Afkhamib, A. *Polyhedron* **1998,** *17*, (21), 3809-3815.

38. Cahen, Y. M.; Dye, J. L.; Popov, A. I. *J. Phys. Chem.* **1975,** *73*, (13), 1292-1295.

39. Pons, M.; Millet, O. *Prog. Nucl. Magn. Reson. Spectrosc.* **2001,** *38*, 267-324.

40. Michalak, A.; Ziegler, T. *Organometallics* **2003,** *22*, (10), 2069-2079.

41. Michalak, A.; Ziegler, T. *Organometallics* **2000,** *19*, (10), 1850-1858.

42. Landfester, K.; Bechthold, N.; Tiarks, F.; Antonietti, M. *Macromolecules* **1999,** *32*, (16), 5222-5228.

43. Bradbury, E. J.; McNulty, D.; Savage, R. L.; McSweeney, E. E. *Ind. Eng. Chem.* **1952,** *44*, (1), 211-212.

44. Bechthold, N.; Tiarks, F.; Willert, M.; Landfester, K.; Antonietti, M. *Macromol. Symp.* **2000,** *151*, (1), 549-555.

45. Monteil, V.; Wehrmann, P.; Mecking, S. *J. Am. Chem. Soc* **2005,** *127*, (42), 14568-14569.

46. DeKock, R. L.; Hristov, I. H.; Anderson, G. D. W.; Gottker-Schnetmann, I.; Mecking, S.; Ziegler, T. *Organometallics* **2005,** *24*, (11), 2679-2687.

47. Hristov, I. H.; DeKock, R. L.; Anderson, G. D. W.; Gottker-Schnetmann, I.; Mecking, S.; Ziegler, T. *Inorg. Chem.* **2005,** *44*, (22), 7806-7818.

48. Atwood, J. D., *Inorganic and Organometallic Reaction Mechanisms, 2nd Edition.* Wiley VCH: New York, 1997.

Chapter 7.

General Discussion and Conclusions

7.1 Solution and emulsion copolymerization of ethylene with non-polar olefins

Our results, obtained from the catalytic copolymerization of ethylene with non-polar α-olefins demonstrated that hexadecene and undecenol incorporation is possible into polyethylene, leading tocopolymers with various levels of incorporation. Catalytic miniemulsion polymerization, proceeds at relatively low temperature (55-65 ^{o}C) and pressure (300 psi) in aqueous medium. The *in situ* catalyst, generated from $Ni(COD)_2$ and keto-ylide $EtOC(O)C(PPh_3)C(O)CF_3$ was used for copolymerization because its tolerance to polar media. The miniemulsion was prepared by mixing a small amount of a catalyst solution in an organic solvent (toluene) with surfactant SDS and hexadecane as a hydrophobe in an aqueous medium.

7.1.1 Organic solvent in the latex

We were unable to form stable miniemulsions and stable latexes in the absence of organic solvents. The smallest amount of organic solvent used was ~10 wt. % of the final product. This is an important limitation of this emulsion process. For the copolymerization of ethylene with acrylates, dichloromethane could be used as a solvent instead of toluene or benzene. Dichloromethane is readily removed from the formed latex, but it cannot be used for nickel phosphino enolates catalyzed copolymerizations. Unfortunately, this catalyst readily decomposes in the presence of halogenated solvents. Polyolefin latexes with zero volatile organic compounds (VOC) have never been prepared. Several ways to remediate

this problem were investigated in this thesis, but none were satisfactory. First, it may be possible to use an organic solvent which is also polymerizable (for example styrene or phenoxyethyl acrylate). However, at the current time (*vide infra*), the catalysts available cannot copolymerize these comonomers and ethylene in emulsion satisfactorily. Second, it could be possible to use water-soluble catalysts. We have prepared a palladium aryl sulfonate complexed by the water soluble phosphine TPPTS. In our hands, this catalyst has very low activity (or no activity). This finding corroborates those of Mecking on polymerization with water-soluble salicylaldiminato Ni(II) – methyl complexes catalysts.[1] Mecking also investigated the preparation of polyethylene latexes without any organic solvent by using a microemulsion polymerization technique. However, a careful analysis of his results indicates that the amount of surfactant in the final product (by weight) is approximately of the same order as that of the polymer. Clearly, the microemulsion route can only be seen as a proof of concept, and not a real solution to the problem of the presence of organic solvent. Several routes could be investigated in the future to lower the VOC content in a polyolefin latex. One of the practical limitations encountered is the limited solubility of the catalyst. It would be desirable to prepare a catalyst with a high solubility in organic medium (for example soluble in hexadecene). For this purpose, the introduction of branched aliphatic substitutents on the phosphine could be quite effective.

7.1.2 Colloidal aspects pertaining to the latex

In order to obtain a stable miniemulsion, sonication was applied. The role and power of this sonication step is pivotal. Sonication is necessary to decrease the droplet size where each droplet, stabilized with SDS, is prevented from growing by collision with other droplets. We observed that 'poorly' sonicated miniemulsions (i.e. low power or too short times) do not lead to the formation of latexes. Possibly, large droplets (> 1 μm) remain in the system when the sonication step is not properly carried out. Each droplet, large or small, behaves as a polymerization minireactor. We infer that when the droplet is too large, the polymerization results in local overheating, and possibly decomposition of the catalyst. This phenomenon does not occur for small droplets which can readily exchange heat with water. At the current time, the reaction does not offer any control over final polymer particle size and particle numbers. Several experiments were attempted where the polymerization was run for a long time (24 hours rather than the usual 2 hours), however, only coagulated latex was collected in this case. At this moment it is not clear if this coagulation is due to a high solid content or to destabilization by intense shearing in the polymerization reactor. A study of the particle size and number in relation with reaction parameters would be needed, but this study has so far been impeded by the somewhat limited reproducibility of the emulsification step.

7.1.3. Characterization of the latexes

Despite the hurdles mentioned above, latexes with particle size < 1 μm were produced as confirmed by DLS, CHDF and TEM. The solid content of the latexes reached 27 %, with a range of comonomer incorporation of 1 – 5 mol. % and M_n values were 500 – 3000 g/mol. The analysis of these novel latexes proved to be problematic at times.

In CHDF, a UV detector is used when the product has no chromophore in water. In TEM, these nanoparticles exhibit a very low contrast, and only negative staining proved to be efficient for observing these objects. However, negative staining is well-known to lead to artifacts of all sorts. For example, residual comonomers in low concentration can leave 'white" imprints in TEM which can be viewed as particles. Thus, latexes must be dialyzed with ultra-filtration in order to give reproducible results.

On the TEM images, the latex particles of poly(E-co-HD) show a spherical form and smooth shape. These findings differ from particles of pure polyethylene latex, prepared under similar conditions, which possess irregular shape due to the high crystallinity of the homopolymer. The crystallinity of the copolymers is decreased by the incorporation of hexadecene as confirmed by modulated DSC. Also, DSC proved to be a difficult technique to use. It is usual to measure crystallinity by integrating the area of the melting transition of PE, and comparing it with the enthalpy of melting of 100 % crystallinity HDPE. However, the copolymer of poly(E-co-HD) has a melting point which spans from -40 °C up to 120 °C. For peaks that large, it is difficult to draw a realistic baseline, both because only few data are collected below -40 °C, and also because the baseline is not horizontal

(due to the contribution of C_p to the baseline). On top of this very broad melting peak, several other phenomena can be observed (such as melting of residual amounts of hexadecene around). The presence of a very large melting transition can be explained by the composition drift which is inherent with the polymerization process: at first, the medium (miniemulsion droplets) is very rich in comonomer, resulting in chains rich in hexadecene, whereas it becomes poorer and poorer as the polymerization progresses. The comonomer-rich chains, which can be viewed as highly branched polyethylene, crystallize at low temperature (even below room-temperature!). However, even for highly branched copolymers (containing in average 3.5 % hexadecene, therefore 17.5 branches every 1000 C), the crystallinity content is 17 %, and the melting point (calculated at the top of the peak exotherm) is 98 °C, but the onset of melting is around -40 °C. The Flory copolymer crystallization model[2] allows one to calculate the volume fraction of amorphous and crystalline units for a given melting point:

$$\frac{1}{T_m} - \frac{1}{T_m^o} = -\frac{R}{\Delta H_m} \ln N \qquad (7.1)$$

where T_m^o is the melting point of pure polyethylene, ΔH_m is the enthalpy of crystallization of homopolymer crystals, N is the fraction of crystallizable units.

In our case, the value T_m^o was chosen at 116 °C which corresponds to the melting point of a linear PE of very low molecular weight. In addition, one can assume that each time a tertiary C atom (branching point) is present due to hexadecene incorporation, 4 CH_2 on each side of the tertiary C do not crystallize. The value of 4 CH_2 has been chosen arbitrarily. Therefore, each time a branching point is present, a total of 13 carbons are non-

crystallizable and excluded from the crystal. The number of branches per 1000 C is thus given by 1000 (1-N)/13. This simple model allows one to calculate the correspondence between melting point and number of branches per 1000 C (Table 7.1).

On the thermogram (Figure 7.1), it is clear that the melt transition can be viewed as the summation of numerous individual melting points, each corresponding to a polymer with a different branching density. Even if this model is overly simplistic, it gives a very good idea of the complex (and polydisperse) nature of the objects that are formed with these catalysts.

7.1.4 Applications of the polyolefin latexes: formation of films

One of the applications of the olefin copolymers is their usage as anticorrosion coatings. Due to its hydrophobic nature, polyethylene is expected to act as a good electrical insulator and as a barrier coating to prevent water diffusion. Solvent-borne and aqueous-borne coatings can be produced by solvent evaporation from polymer solution or by water evaporation from latexes. Polyethylene is not soluble at room temperature in any organic solvent, which rules out the 'solvent coating' route. Polyethylene is also very crystalline; thus formation of films from aqueous-borne coatings is impossible. Another factor is that for water borne coatings, the polymer T_g should be close to room temperature for effective film formation (T_g of PE is ~ -120 ^{o}C).

Table 7.1: Fraction of CH units at different melting points.

T_m	$1/T_m$	ln N	N	fraction of CH
10	0.0035	-0.94	0.39	0.047
20	0.0034	-0.82	0.44	0.043
30	0.0033	-0.71	0.49	0.039
40	0.0032	-0.61	0.54	0.035
50	0.0031	-0.51	0.60	0.031
60	0.0030	-0.42	0.66	0.026
70	0.0029	-0.34	0.71	0.022
80	0.0028	-0.26	0.77	0.017
90	0.0028	-0.18	0.84	0.013
100	0.0027	-0.11	0.90	0.0078
110	0.0026	-0.039	0.96	0.0030
120	0.0025	0	1	0

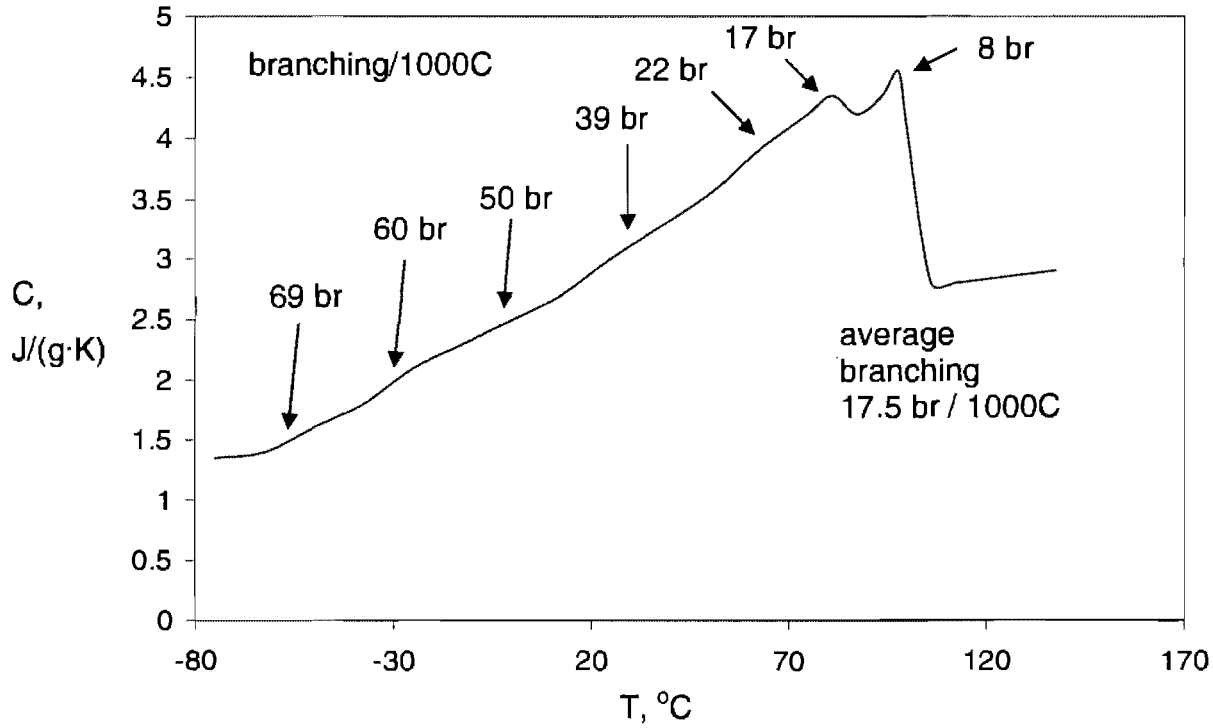

Figure 7.1: mDSC thermogram for a copolymer E-HD (experiment 10 in Chapter 2). The arrows above the thermogram point to the theoretical melting point of a PE having the indicated number of branches per 1000 C.

The incorporation of different comonomers may decrease the crystallinity and increase T_g, rendering possible the formation of aqueous-borne coatings. It would allow also to increase the polymer solubility in organic solvent at room temperature, making a film formation easier among the use of solvent-borne coatings. Our results show that ethylene-norbornene copolymers can form coatings and these coatings possess anticorrosion properties when they contain > 15 mol. % of norbornene. Lower amounts of norbornene are not sufficient to break the PE crystallinity. Higher amounts of norbornene result in polymers that are less 'PE' like, and therefore probably slightly more permeable to water. Thus, the optimum composition has been found to be around 19 mol. %. At this composition, the polymer still possesses the advantages and barrier properties of polyethylene, and the main role of the norbornene units is to break the crystallinity and increase the T_g to room temperature.

These results are still preliminary, and further work is needed to lead to the formulation of an exploitable coating. These engineering facets are far beyond the scope of my thesis. Several interesting issues could be investigated. Fillers are nearly always incorporated to the coating to improve its anticorrosion properties. It would be interesting to see whether nanoparticles of highly crystalline polyethylene embedded in the amorphous copolymer could act as a filler. Adhesion is also a key-point which has not been investigated in depth. It is clear that adhesion is promoted by the presence of polar functionalities in the copolymer, hence justifying the need to copolymerize ethylene with polar monomers.

Although our study is in fact a proof of concept that anticorrosion films can be prepared from polyolefins, it is important to present the broader impacts of this research. Each year, in average, 4.2 % of the gross national product of a country is spent to remediate corrosion issues (http://www.corrosioncost.com/information/otherstudies/index.htm).[3] For example, in Montreal, bridges and steel structures need to be often repainted at considerable cost. Repainting involves sand-blasting the spent coating and reapplying a fresh series of layers, usually constituted of epoxy or polyurethane coatings. These coatings are expensive, are not environmentally friendly and their lifetime is limited. Maybe, such coatings could be replaced by polyolefins.

7.2 Copolymerization of olefins with polar olefins

7.2.1 Limitations of the keto-ylide Ni catalysts

The catalyst produced from Ni-complex and keto-ylide was able to copolymerize ethylene with α-olefins, such as hexadecene and undecenol, in aqueous medium. However, in the copolymerization of ethylene with the bulkier norbornene, only a few milligrams of a very sticky copolymer were obtained. The catalyst was also found to be inactive for the copolymerization of acrylates. In fact, $Ni(COD)_2$ was found to decompose in the presence of methyl acrylate, probably by displacement of COD, followed by precipitation of Ni(0). Using the combinatorial series of reactors of Rohm and Haas, we have investigated whether it would be possible to start the polymerization with ethylene only in order to form the nickel phosphinoenolate, followed by a late addition of acrylate (once the active catalyst is

formed). However the introduction of acrylate always resulted in a complete halt of the polymerization. Clearly, the nickel based catalyst which was used in the group until 2004 is not suitable for the copolymerization of ethylene with acrylates.

7.2.2 Pd-based sulfonated aryl phosphine P,O-chelated catalysts

Following the report of Drent, a Pd-based sulfonated aryl phosphine P,O-chelated catalyst was chosen for its tolerance to water and high activity (for a palladium catalyst) in ethylene polymerization. The catalysts studied in this work are show in Figure 7.2. When this work was started, the only contribution on this catalyst was a short communication by Drent. Now more than 15 papers have since appeared on these catalysts (see Introduction chapter). This family of palladium sulfonated aryl phosphine catalysts has revolutionized the domain of ethylene copolymers. Extensive studies on reactivity of acrylonitrile with Pd-based olefin polymerization catalysts were performed. Such points as high σ-coordinating ability of the nitrogen atom of CN-group and low reactivity of α-CN substituted palladium species were found.[4-6] The copolymerization of acrylonitrile and ethylene was investigated by us at the time it was disclosed by the first time by Nozaki.[7] However, we were unable to incorporate acrylonitrile because the ethylene pressures required for the copolymerization are not accessible with our polymerization setup (they are higher than the delivery pressure of commercial ethylene tanks).

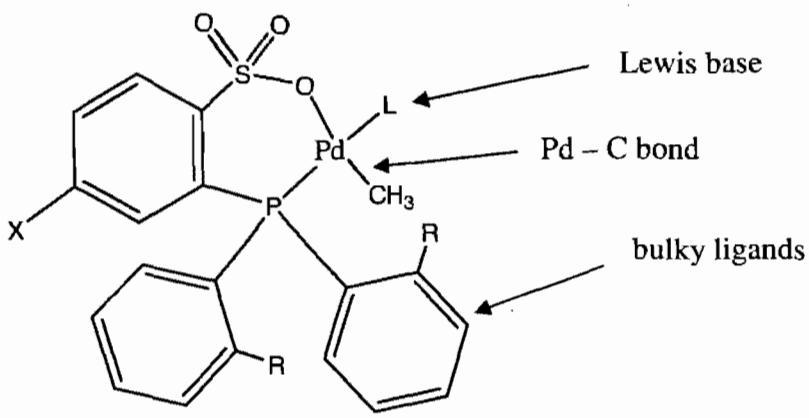

1. R = OMe, X = H, L = py

2. R = OMe, X = Me, L = py

3. R = OMe, X = Me, L = ½ tmeda; (dimer)

4. R = $C_6H_4(o\text{-}OMe)_2$, X = H, L = py

5. R = $C_6H_4(o\text{-}OMe)_2$, X = H, L = ½ tmeda; (dimer)

Figure 7.2: Pd-based catalysts.

7.2.3 Toward a more active catalyst

The initial phosphine system reported by Drent leads to moderately active catalysts able to generate polymers of low to medium molecular weight. This is obviously a strong limitation. For example, copolymers of AN and E prepared by Nozaki were contaminated by as much as 0.5 % Pd. This situation is far from unique, and copolymers of E and MA (resp. VF) with highest incorporation reported by Mecking (resp. Jordan) contain 0.5 (resp. 21) % of Pd. The latexes of poly(E-co-MA) prepared in this work also contained 0.5 % Pd. Therefore, it is necessary to find catalysts that are more active and which lead to polymers of higher molecular weight. This can be achieved by changing the steric and electronic environment of the ligand.

It has been demonstrated that low activity in the copolymerization of ethylene with acrylate is the result of a combination of pyridine poisoning, acrylate coordination in a σ-fashion and in addition, coordination of water to the catalyst. Pyridine poisoning has been addressed both by Nozaki (using lutidine) and by Mecking (using DMSO). The Mecking procedure for DMSO-coordinated catalyst is cumbersome, as it necessitates the elimination of DMSO under vacuum. The possibility of removing pyridine with a Lewis acid has also been explored by Jordan and Sen. None of these strategies address the two other factors which contribute to loss of activity (i.e. acrylate and water coordination). It is clear that other ligand structures need to be investigated. This was done in our group by probing catalysts based on sulfonated Schiff bases (work of a summer student), however, these catalysts did not exhibit any catalytic activity. Several other sulfonated aryl phosphine Pd

catalysts are currently synthesized in the group, so as to unravel a series of structure-property relationships. A useful tool in the determination of such relationships is in the use of computer modeling. Until 2007, my project relied on the participation of the Rohm and Haas modeler, Dr. Susan Fitzwater. Several DFT calculations were performed on ligand binding energy, presence or absence of chelate formation with an acrylate, etc... In 2007, it was discovered that pyridine exchange occurs via an associative pathway. This implied that all calculations based on dissociative routes had to be revised. Another student in the group is currently taking over this part of the project. Another tool which could prove to be invaluable for the discovery of a more active catalyst would be in the use of FTIR spectroscopy. Acrylates and carbonyl compounds are choice models for this technique because of the strong C=O stretching bond. Preliminary investigations (Figure 7.3; the term Pd(111) and Pd(111)dimer are used correspondingly for structures 4 and 5 on Figure 7.2) clearly show a displacement of the C=O wavenumber, but not in the expected direction. Usually, binding of the C=O bond to a metal is accompanied by a weakening of the bond. For example, in ref.[8] the authors report wavelength decrease when metal is coordinated with carbonyl oxygen (from 1730 to 1710 cm^{-1}). Whereas the opposite was observed in our case. A possible explanation is that the binding of the C=C bond is observed, which results in loss of conjugation in the α,β-unsaturated ester, and therefore an increase in the wavenumber of the C=O stretch. However, the coordination of the C=C has never been detected by NMR.

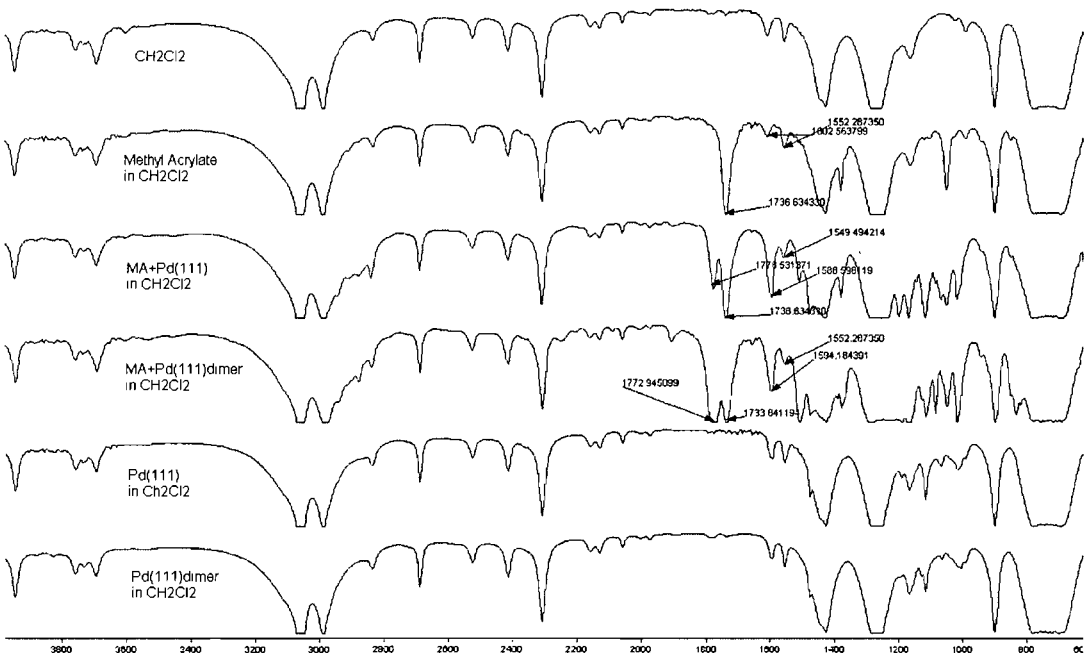

Figure 7.3: Catalyst studies by FTIR (ATR mode). Catalyst concentration: ~100 mg in 500 μL of solvent. Acrylate concentration : ~10 mg in 500 μL of solvent.

It was found that bulky groups in the catalyst lead to a polymer with higher molecular weight, due to the prevention of chain transfer reaction. However, when chain transfer is limited by virtue of steric hindrance, incorporation of comonomers, which are always bulkier than ethylene, becomes more difficult. Therefore, there is a tradeoff between comonomer incorporation and polymer molecular weight. For example, coplolymers with high norbornene incorporation can only be obtained with an aryl sulfonated phosphine bearing the OMe-phenyl groups. Such copolymers of ethylene and norbornene, which contain ~45 mol. % of norbornene were found to be nearly perfect alternating copolymers, according to ^{13}C NMR studies. Furthermore, NN diads were never observed, which is indicative that the bulk of norbornene is limiting the incorporation.

Well-defined catalysts are preferable for the copolymerization because the catalytic complex is already formed and it can be assumed that a higher number of Pd atoms participate in the polymerization reaction in this case. Five catalysts were studied in this process (Figure 7.2) with the structure difference in bulky groups and Lewis base. No significant difference in activity and comonomer incorporation was observed when pyridine or N,N,N',N'-tetramethylethylenediamine were used as Lewis bases.

7.3 Amphiphilic properties of the copolymers and further perspectives

Copolymers of ethylene with polar monomers, such as acrylates, N-vinyl pyrrolidinone or N-isopropylacrylamide may possess amphiphilic properties due to polar and assumingly hydrophilic functionalities. At the same time, the copolymers obtained by

catalytic polymerization are much less branched compared with the copolymers obtained by radical route. Therefore, the copolymers are expected to combine the properties of crystalline polyethylene andamphiphilic properties. This combination may finally result in "wettable polyethylene". Due to amphiphilic properties of the copolymer, in principle, nanoparticles could be formed with hydrophobic core (CH_2) and hyrdrophilic polar functionalities in the shell. Here, only preliminary studies of this topic are discussed.

The E-MA copolymers were soluble in chloroform if the mol. % of acrylate was > ~ 12 mol. % . Otherwise, the copolymer was only partially soluble in chloroform, and only the soluble part may be exploitable in the studies for amphiphilic properties. When the copolymer of 8 mol.% was investigated, only the fraction soluble in chloroform was considered.

At first, a general approach for the formation of nanoparticles consisted in THF addition to chloroform solution of the copolymer which was insoluble in pure THF. By this method, particles were expected to be formed and by changing the solvent to water, leading to amphiphilic structures constituted of a core of CH_2 units and an external layer of $COOCH_3$ groups should be obtained. The ester group could subsequently be hydrolyzed to provide for electrostatic stability.

When THF was slowly added to a chloroform solution, of the 8 mol. % of MA copolymer a turbidity change was registered by UV spectroscopy, which may have indicated particle formation. Concomitantly, ^1H NMR spectroscopy was used to monitor solutions of polymer in chloroform-THF mixtures. The relative decrease of an CH_2 peak

intensity served as an indication of $(CH_2)_n$ core formation. However, only a very low change in the integral of CH_2 peak vs CO_2Me peak was observed (~5 – 10 % when 40 mol. % of THF was added), leading to the conclusion that the increase in turbidity was mostly due to polymer precipitation rather than particle formation. A similar work was performed for a copolymer of poly(ethylene-co-*tert*-butylacrylate), leading to a similar conclusion.

We therefore decided to perform the hydrolysis of the ester group prior to self-assembly. In order to hydrolyze the polymer, trifluoroacetic acid can be used when reaction was carried out in refluxing chlorobenzene (to solubilize the polymer). For the hydrolysis of the methyl ester groups, another method was chosen (Figure 7.4). The copolymer of E with MA having as much as 12 mol.% of MA was already completely soluble in chloroform and in THF.

The reaction was carried out in chloroform with iodotrimethylsilane.

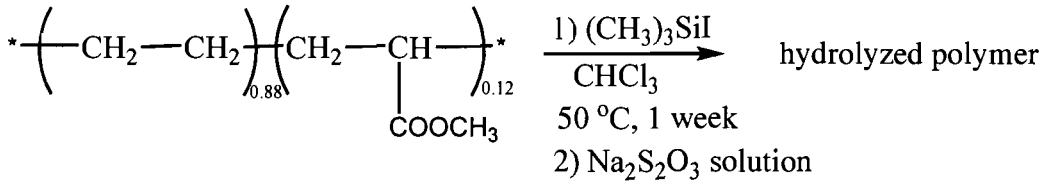

Figure 7.4: Hydrolysis of poly(ethylene-co-methyl acrylate).

The reaction was carried out for ~ 1 week and all the acrylate groups were hydrolyzed. A $Na_2S_2O_3$ aqueous solution was added in order to reduce I_2, then the polymer was solubilized in THF, the sulfur formed, was removed by centrifugation and the polymer

was precipitated in acidic water, filtered and dried. Typical yields of the reactions were 60-70 %. The reaction was carried out for a shorter period, the ester groups were not hydrolyzed completely.

For hydrolyzed copolymers with less than 8 mol. % incorporation of acrylic acid, it was impossible to find a suitable solvent to perform this reaction. Finally, calculations of the solubility parameters for poly(ethylene-co-acrylic acid) with 6.5 mol. % of AA were performed. The parameters δ_d, and δ_h were calculated and the graph of δ_h vs δ_v was plotted. ($\delta_v = [\delta_d + \delta_p]^{0.5}$). Due to to the high crystallinity of this copolymer, only swellability was achieved using the solvents mentioned as red in Figure 7.5. For higher contents of AA, such as 10-12 mol. %, the copolymer is totally soluble in THF which would allow to perform self-assembly of this copolymer using THF-water mixtures.

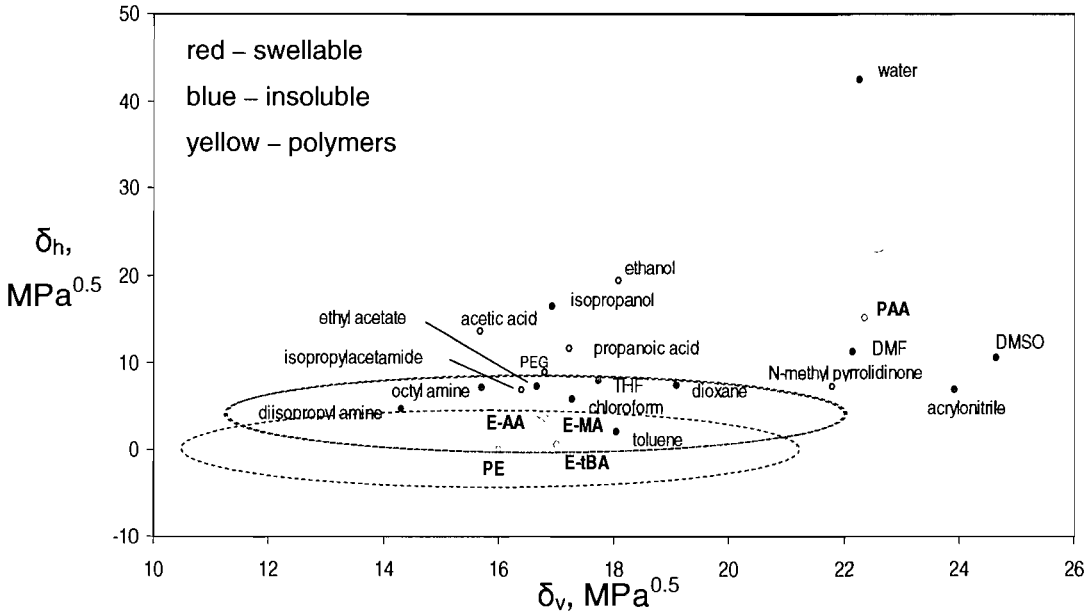

Figure 7.5: Plot of solubility parameters for different solvents.

7.4. Conclusions

In this study, copolymers of ethylene with non-polar monomers (hexadecene, norbornene) and polar monomers (methyl acrylate, N-vinyl pyrrolidinone, N-isopropyl acrylamide) were prepared. The reactions were carried out in organic solution and in aqueous emulsion. Several of these polymers had never been prepared before, and were characterized by NMR and DSC. The products of emulsion polymerizations lead to the formation of polymer nanoparticles suspended in water (latexes). These dispersions were characterized by DLS and TEM. We found that these latexes can be used for the formation of aqueous-borne coatings. However, these coatings were found not to be as efficient as solvent borne coatings for imparting anticorrosion properties. For example, solvent-borne coatings of ethylene-norbornene copolymers were examined by EIS and they were shown to exhibit anticorrosion properties for several weeks under harsh treatment in a salt box (Q-Fog).

Ni-based keto-ylide catalysts were tolerant to water and allowed to copolymerize ethylene with hexadecene in water. Only olefins where the functionality was remote enough could be copolymerized with this nickel based system. For all other systems we developed a Pd-based sulfonated arylphosphine catalyst family. These catalysts are very versatile, allowing to copolymerize ethylene with norbornenes, acrylates, acrylamides and N-vinyl pyrrolidinone. Thus, we were able to copolymerize ethylene and acrylates in emulsion, albeit with low activity. It is clear that further improvement of the catalyst, in

particular concerning incorporation levels, activity and molecular weight distribution, will be necessary in order to prepare novel and innovative latexes.

7.5 References

1. I. Gottker-Schnetmann, B. Korthals, S. Mecking, *J. Am. Chem. Soc.*, **2006**, 128, 7708-7709.

2. E. P. Otocka, T. K. Kwei, *Macromolecules*, **1968**, 1, 401-405.

3. http://www.corrosioncost.com/information/otherstudies/index.htm as it is 8 June 2009.

4. F. Wu, S. R. Foley, C. T. Burns, R. F. Jordan, *J. Am. Chem. Soc.*, **2005**, 127, 1841-1853.

5. F. Wu, R. F. Jordan, *Organometallics*, **2006**, 25, 5631-5637.

6. L. F. Groux, T. Weiss, D. N. Reddy, P. A. Chase, W. E. Piers, T. Ziegler, M. Parvez, J. Benet-Buchholz, *J. Am. Chem. Soc.*, **2005**, 127, 1854-1869.

7. T. Kochi, S. Noda, K. Yoshimura, K. Nozaki, *J. Am. Chem Soc.*, **2007**, 129, 8948-8949.

8. P. Kapoor, A Pathak, R. Kapoor, P. Venugopalan, M. Corbella, M. Rodriguez, J. Robles, A. Llobet, *Inorg. Chem.*, **2002**, 41, 6153-6160.

Appendix A

Supplementary Information

Palladium Aryl Sulfonate Phosphine Catalysts for the Copolymezation of Acrylates with Ethene

K. M. Skupov, P. R. Marella, M. Simard, G. P. A. Yap, N. Allen, D. Conner, B. L. Goodall, J. P. Claverie

Macromolecular Rapid Communications, 2007, 28, 2033 – 2038.

A.1 Spectroscopic characterization of catalyst 2a

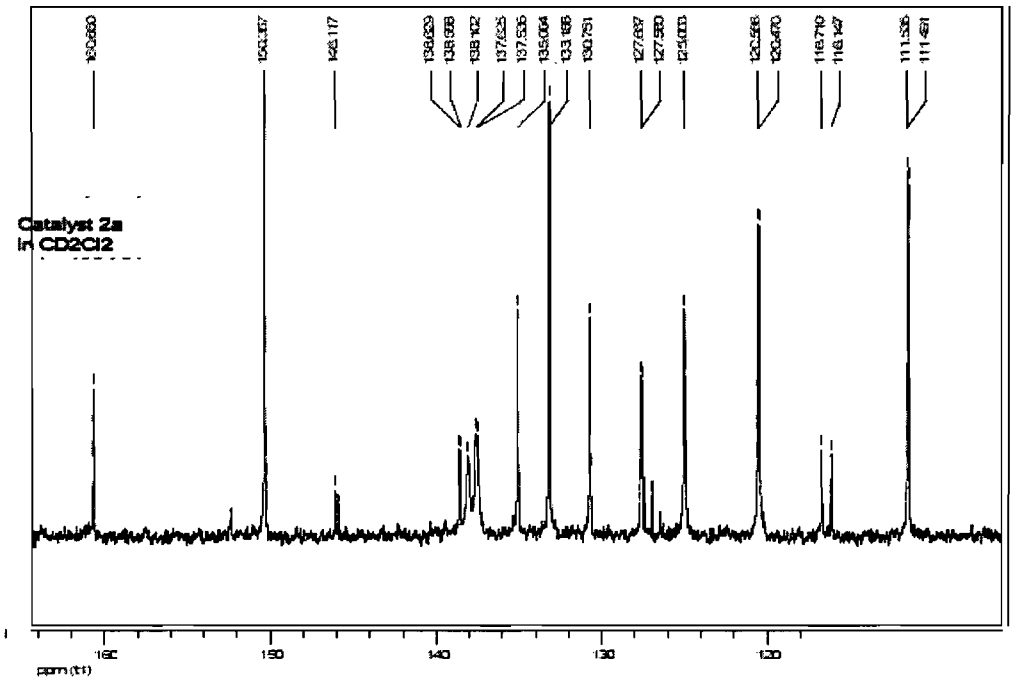

Figure A.1: Spectroscopic characterization of catalyst **2a** (^{13}C NMR, low field).

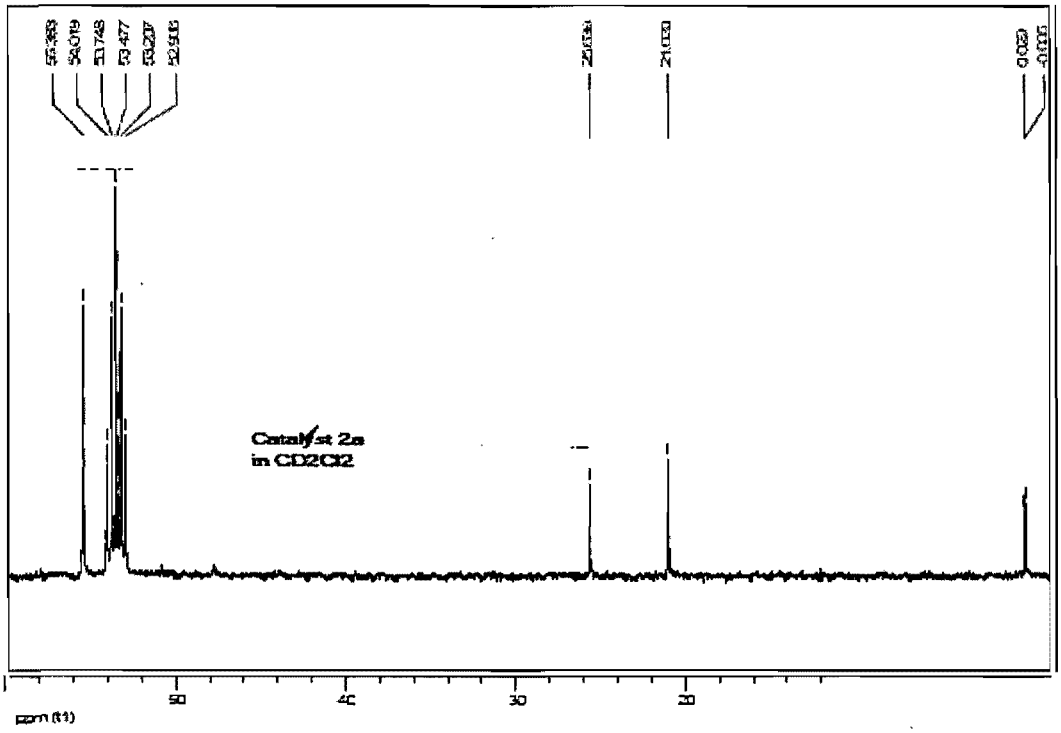

Figure A.2: Spectroscopic characterization of catalyst 2a (^{13}C NMR, high field).

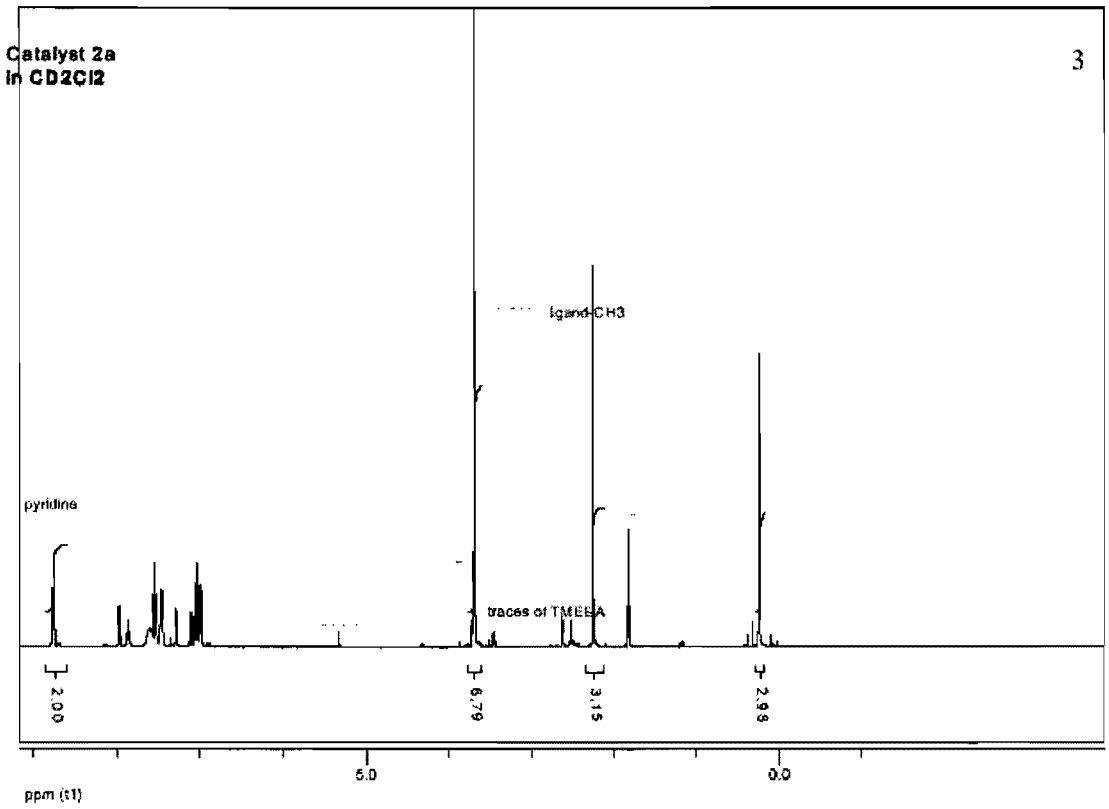

Figure A.3: Spectroscopic characterization of catalyst 2a (^{1}H NMR).

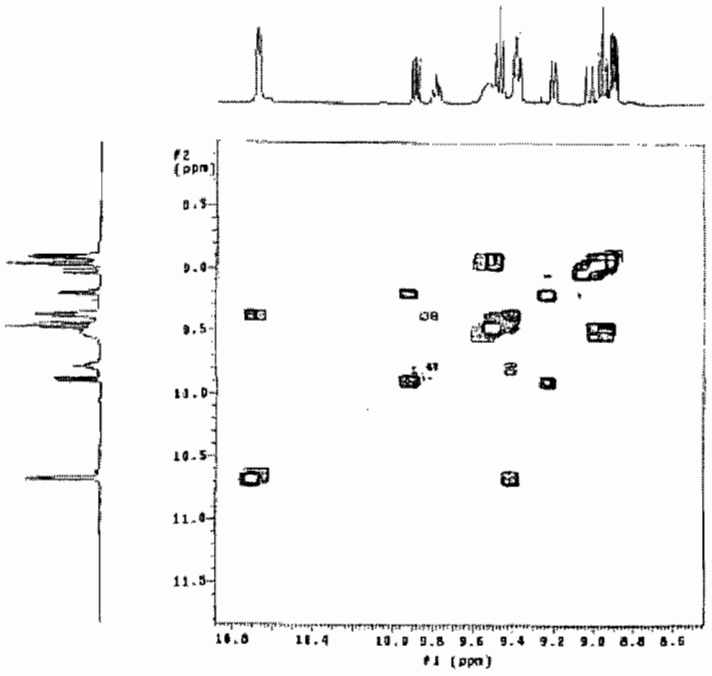

Figure A.4: Spectroscopic characterization of catalyst **2a** (NMR, COSY).

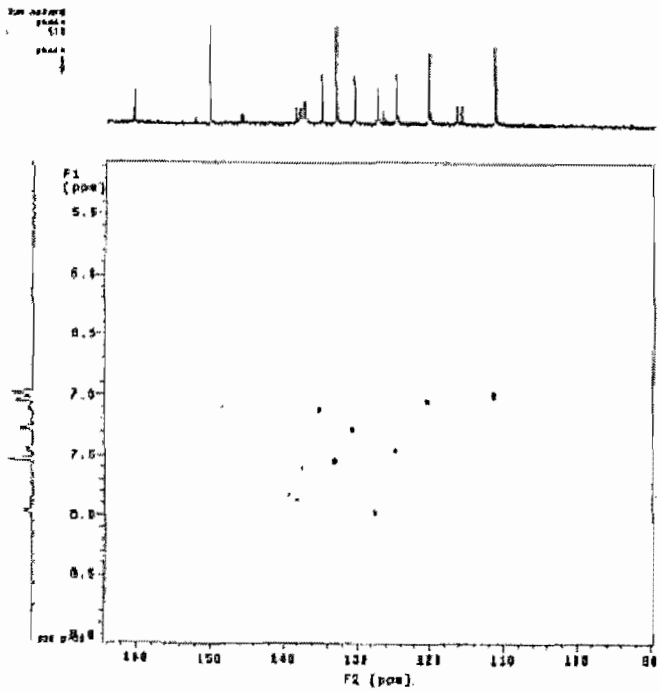

Figure A.5: Spectroscopic characterization of catalyst **2a** (NMR, HETCOR).

A.2 NMR of the copolymers MA-ethylene

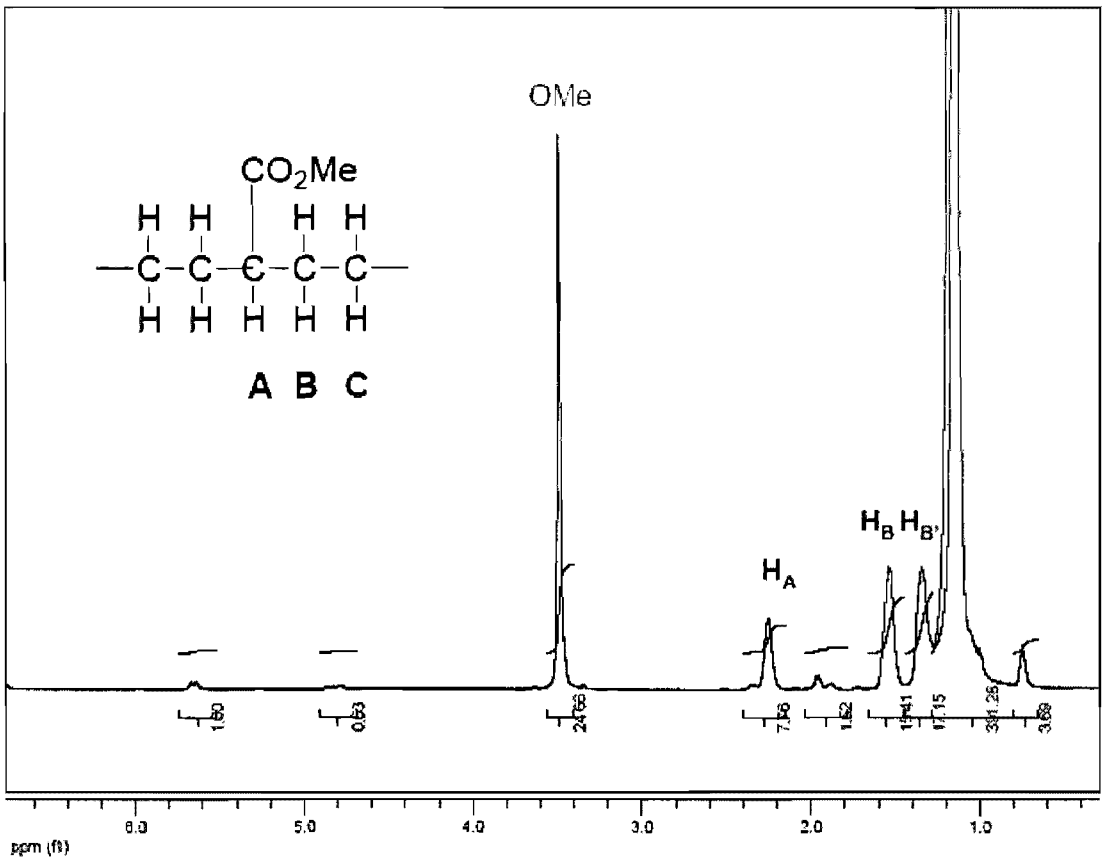

Figure A.6: Typical NMR of the copolymer MA-ethylene.

NB: The assignments of the ^{1}H NMR differ slightly from the one proposed by Drent *et al.* in E. Drent, R. van Dijk, R. van Ginkel, B. van Oort and R.I. Pugh *Chem Commun.*, **2002,** 744. B and B' are the two diastereotopic protons in b-position of the $CHCO_2Me$ group.

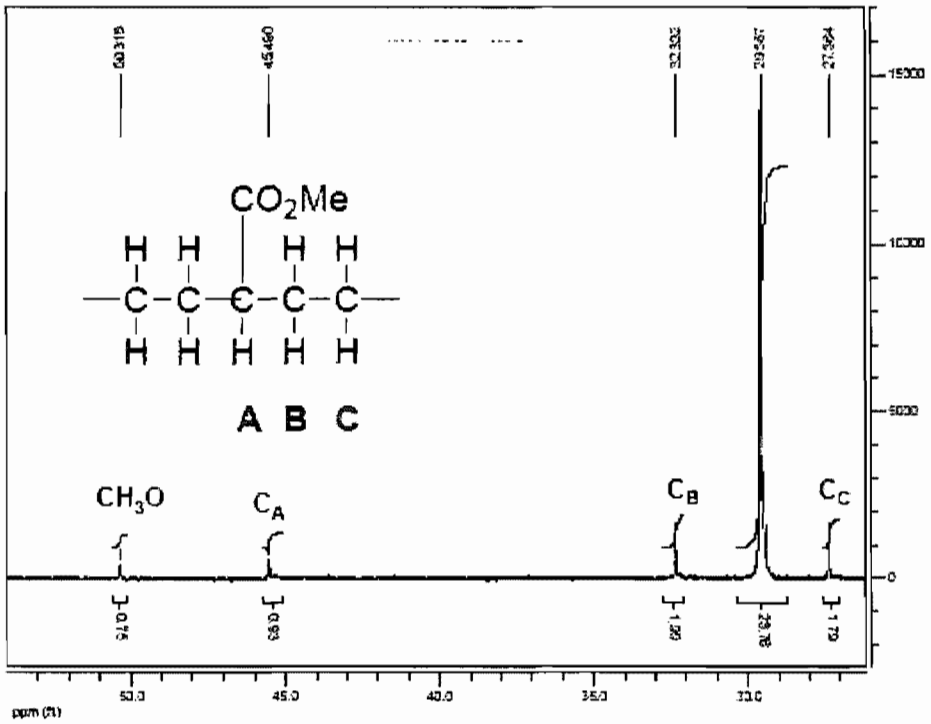

Figure A.7: ^{13}C NMR assignements of the copolymer (E-MA).

C13 assignement of the copolymer (in agreement with E. Drent, R. van Dijk, R. van Ginkel, B. van Oort and R.I. Pugh *Chem Commun.*, **2002**, 744).

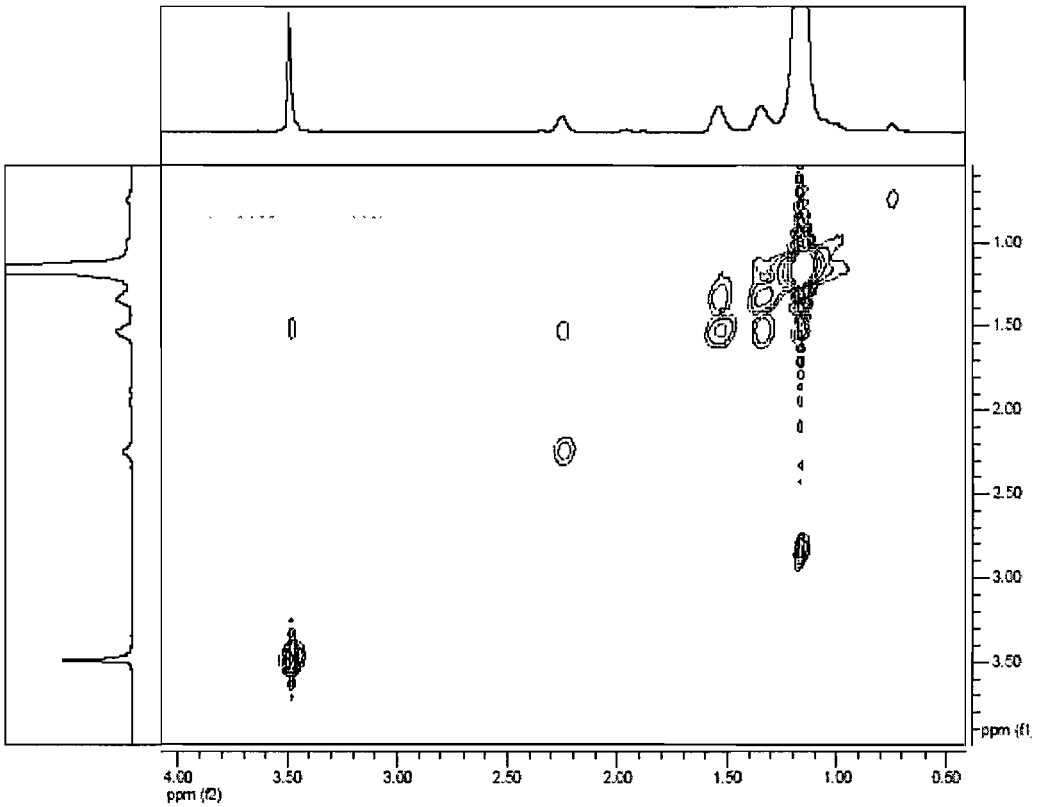

Figure A.8: COSY for the MA-E copolymer.

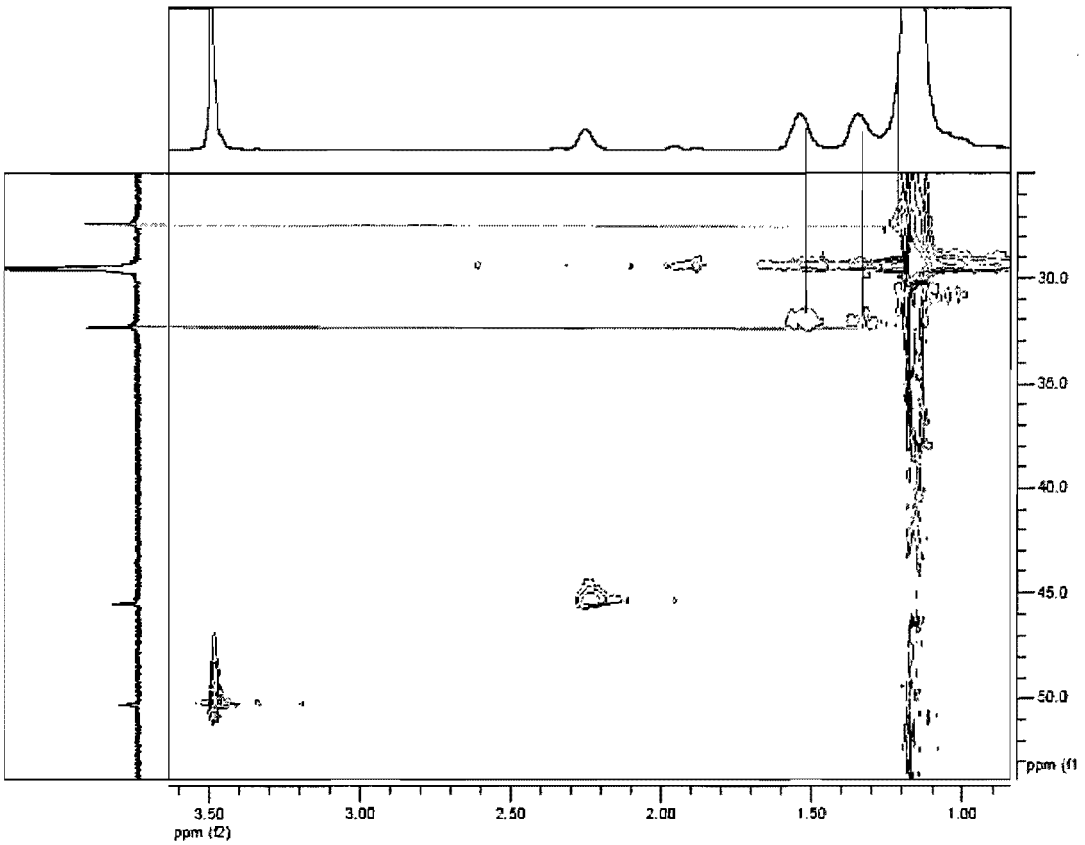

Figure A.9: HMQC of E-MA in ODCB at 100 °C.

The HMQC clearly indicates that the B and B' protons are attached to the same carbon, and the C protons are masked by the main ethylene resonance.

A.3 NMR of the copolymers NBE-ethylene

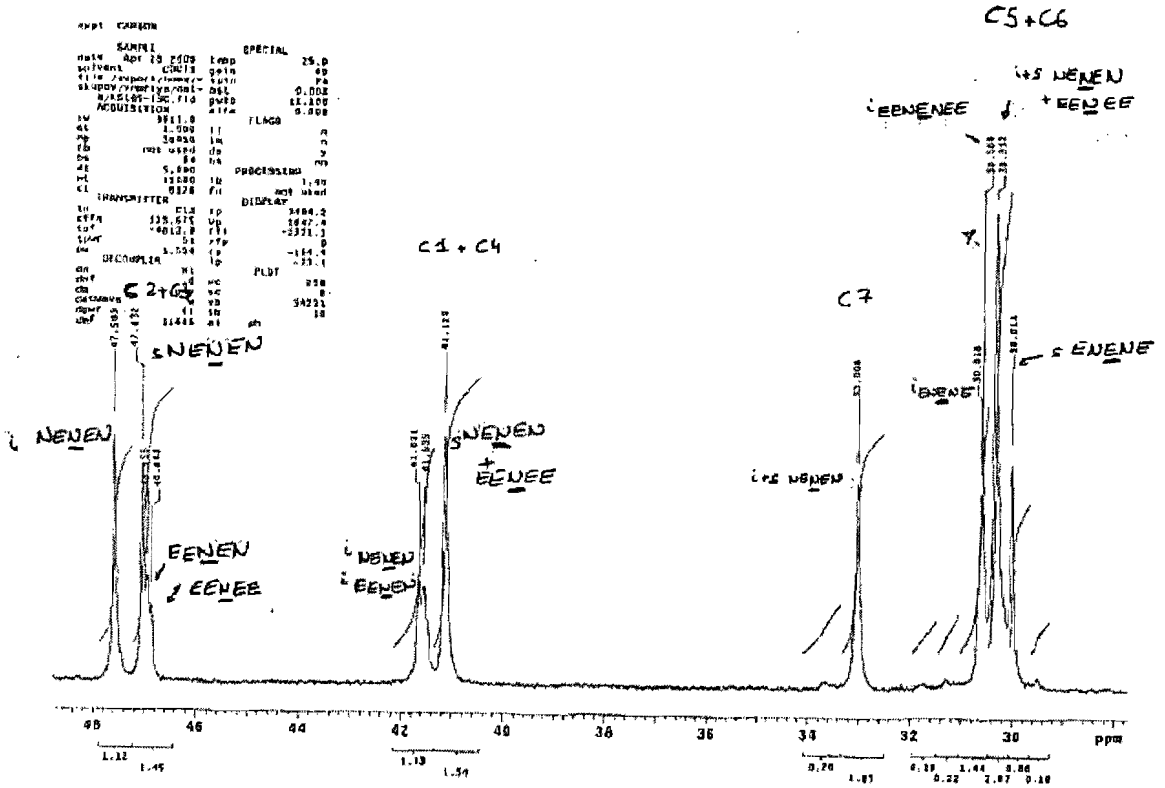

Figure A.10: ^{13}C NMR of the copolymer NBE-ethylene.

Calculations of % norbornene were conducted using formula from ref. Christer H. Bergstrom, Brend R. Sperlich, Juhana Ruotoistenmaki, Jukka V. Seppala, *J.Polym. Sci. Part A: Polym. Chem.*, 36, **1998**, 1633-1638.

Assignements for the ^{13}C NMR were taken from Tritto, I.; Marestin, C., Boggioni, L.; Sacchi, M. C.; Brintzinger, H. H.; Ferro, D. *Macromolecules* **2001**, 34, 5770. Tritto, I.;

Marestin, C.; Boggioni, L.; Zetta, L.; Provasoli, A.; Ferro, D. *Macromolecules* **2000**, 33, 8931.

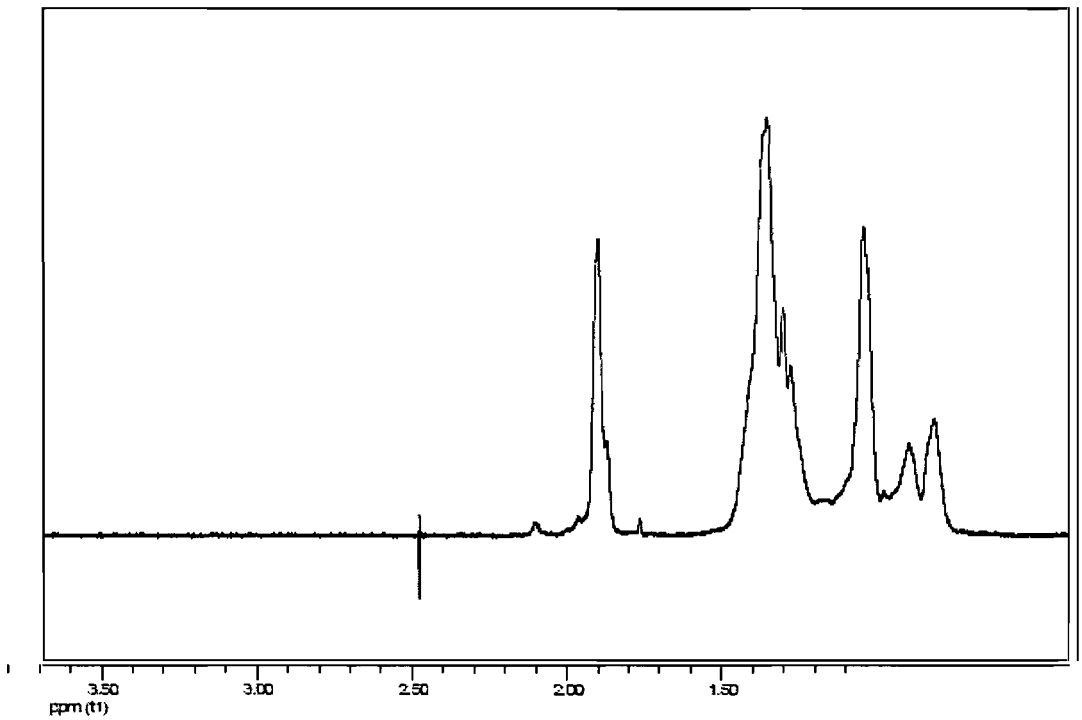

Figure A.11: ^{1}H NMR of E-NB copolymer.

A.4 X-Ray structure for catalyst 1b

Despite several attempts to grow better crystals, compound 1b consistently yielded small, multiple, weakly diffracting crystals and the results reported represent our best effort. The space group was identified unambiguously from the systematic absences in the diffraction data. The structure obtained is consistent with non-crystallographic characterization. This catalyst was difficult to crystallize and it cocrystallized with at least one solvent molecule (probably THF). The final data have been corrected for the solvent contribution included in the structure, using the SQUEEZE option of the PLATON program (see Spek, A. L.; *J. Appl. Cryst.,* 36 (2003) 7-13.)

Table A.1: Crystal data and structure refinement for $C_{76}H_{82}N_2O_{14}P_2Pd_2S_2$.

Identification code	CLAVR1
Empirical formula	C76 H82 N2 O14 P2 Pd2 S2
Formula weight	1586.30
Temperature	100(2)K
Wavelength	1.54178 Å
Crystal system	Monoclinic
Space group	$P2_1/c$
Unit cell dimensions	a = 12.177(2) Å $\alpha = 90^\circ$ b = 11.390(2) Å $\beta = 94.603(9)^\circ$ c = 26.221(5) Å $\gamma = 90^\circ$

Volume	3625.0(11)Å^3
Z	2
Density (calculated)	1.453 g/cm^3
Absorption coefficient	5.495 mm^{-1}
F(000)	1636
Crystal size	0.15 x 0.15 x 0.04 mm
Theta range for data collection	3.38 to 56.37°
Index ranges	$-13 \leq h \leq 13$, $-12 \leq k \leq 11$, $-27 \leq \ell \leq 27$
Reflections collected	54990
Independent reflections	4647 [R_{int} = 0.158]
Absorption correction	Semi-empirical from equivalents
Max. and min. transmission	0.8500 and 0.5300

Refinement method	Full-matrix least-squares on F^2
Data / restraints / parameters	4647 / 576 / 385
Goodness-of-fit on F^2	2.297
Final R indices [I>2sigma(I)]	R1 = 0.2277, wR_2 = 0.5645
R indices (all data)	R1 = 0.2553, wR_2 = 0.5719
Largest diff. peak and hole	2.963 and -1.717 e/Å^3

Table A.2: Atomic coordinates (x 10^4) and equivalent isotropic displacement parameters ($Å^2$ x 10^3) for $C_{76}H_{82}N_2O_{14}P_2Pd_2S_2$. U_{eq} is defined as one third of the trace of the orthogonalized U_{ij} tensor.

	x	y	z	U_{eq}
Pd	838(2)	3057(2)	4362(1)	91(1)
P	2416(4)	2407(5)	4081(3)	62(2)
S	1629(5)	5055(6)	3693(3)	86(2)
O(1)	641(11)	4507(13)	3804(7)	78(4)
O(2)	1451(19)	6160(20)	3394(10)	134(8)
O(3)	2470(12)	5172(17)	4134(7)	93(6)
O(4)	4939(19)	4410(20)	3708(9)	124(7)
O(5)	5510(20)	600(30)	4282(11)	152(8)
O(6)	-300(20)	1100(30)	3920(12)	149(8)
O(7)	1790(20)	320(20)	2672(11)	142(8)
N	-732(10)	3717(14)	4637(6)	37(3)
C(1)	1062(18)	1699(16)	4912(9)	58(6)
C(2)	2228(16)	4066(16)	3311(7)	88(6)
C(3)	2323(18)	4469(15)	2816(8)	105(7)
C(4)	2819(19)	3770(20)	2466(6)	116(8)
C(5)	3221(19)	2667(19)	2611(7)	104(7)
C(6)	3127(17)	2263(14)	3105(8)	97(7)
C(7)	2630(16)	2963(16)	3456(6)	70(6)
C(8)	4940(40)	5310(40)	3295(16)	157(15)
C(9)	5230(20)	3400(20)	3538(12)	133(7)
C(10)	5710(30)	3070(30)	3097(10)	151(9)
C(11)	6150(30)	1950(30)	3058(10)	159(9)
C(12)	6120(30)	1170(20)	3462(13)	154(9)
C(13)	5640(20)	1500(20)	3904(10)	136(7)
C(14)	5190(20)	2610(30)	3942(9)	122(7)
C(15)	5800(40)	-570(40)	4128(18)	162(15)
C(16)	4725(12)	2850(16)	4415(6)	88(6)
C(17)	5522(9)	3240(17)	4786(7)	94(7)
C(18)	5219(12)	3607(17)	5260(6)	91(6)
C(19)	4117(13)	3584(16)	5364(6)	80(6)
C(20)	3320(9)	3194(15)	4994(7)	78(6)
C(21)	3623(11)	2827(15)	4519(6)	75(6)
C(22)	-930(60)	400(70)	4180(20)	230(20)
C(23)	-150(30)	1210(30)	3511(8)	138(8)
C(24)	-900(20)	1840(20)	3188(12)	137(9)
C(25)	-710(20)	1990(20)	2677(11)	139(9)
C(26)	230(20)	1520(30)	2489(9)	135(8)
C(27)	976(19)	900(20)	2811(12)	137(7)
C(28)	790(20)	740(20)	3322(11)	122(7)
C(29)	1870(40)	310(40)	2101(14)	143(14)
C(30)	1783(16)	227(16)	3658(7)	112(6)
C(31)	1814(17)	-992(16)	3648(7)	117(7)
C(32)	2505(18)	-1599(11)	4004(8)	101(7)
C(33)	3166(17)	-987(15)	4371(7)	103(7)
C(34)	3135(16)	233(15)	4381(7)	103(7)
C(35)	2444(17)	840(11)	4025(8)	92(6)
C(36)	-523(19)	4860(20)	4814(9)	69(6)
C(37)	-1140(20)	3170(30)	5097(12)	98(9)
C(38)	-1540(30)	3780(40)	4193(11)	116(11)

Table A.3: Hydrogen coordinates (x 10^4) and isotropic displacement parameters ($Å^2$ x 10^3) for $C_{76}H_{82}N_2O_{14}P_2Pd_2S_2$.

	x	y	z	U_{eq}
H(1A)	1388	2026	5236	87
H(1B)	1554	1100	4789	87
H(1C)	348	1344	4966	87
H(3)	2048	5223	2717	127
H(4)	2884	4046	2128	139
H(5)	3561	2189	2371	125
H(6)	3402	1510	3204	116
H(8A)	5437	5952	3406	236
H(8B)	4191	5619	3223	236
H(8C)	5187	4950	2985	236
H(10)	5728	3609	2821	181
H(11)	6482	1730	2757	190
H(12)	6428	404	3436	185
H(15A)	5613	-1134	4388	242
H(15B)	6598	-602	4091	242
H(15C)	5400	-759	3800	242
H(17)	6275	3256	4715	113
H(18)	5764	3874	5513	110
H(19)	3910	3835	5688	97
H(20)	2567	3178	5065	93
H(22A)	-1318	864	4420	339
H(22B)	-480	-199	4360	339
H(22C)	-1478	13	3934	339
H(24)	-1546	2159	3317	165
H(25)	-1225	2421	2457	167
H(26)	357	1629	2139	162
H(29A)	1426	-345	1950	214
H(29B)	2635	211	2025	214
H(29C)	1580	1051	1955	214
H(31)	1362	-1411	3398	141
H(32)	2526	-2433	3997	122
H(33)	3638	-1402	4614	124
H(34)	3587	652	4631	124
H(36A)	-1176	5115	4987	83
H(36B)	-486	5366	4509	83
H(37A)	-1805	3576	5185	147
H(37B)	-568	3235	5383	147
H(37C)	-1301	2342	5028	147
H(38A)	-2178	4242	4281	173
H(38B)	-1780	2987	4092	173
H(38C)	-1204	4158	3907	173

Table A.4: Anisotropic parameters ($Å^2$ x 10^3) for $C_{76}H_{82}N_2O_{14}P_2Pd_2S_2$. The anisotropic displacement factor exponent takes the form: $-2\,p^2\,[\,h^2\,a^{*2}\,U_{11} + ... + 2\,h\,k\,a^*\,b^*\,U_{12}\,]$

	U11	U22	U33	U23	U13	U12
Pd	50(1)	51(1)	171(3)	-5(1)	-4(1)	-6(1)
P	25(3)	26(3)	131(6)	-8(3)	-7(3)	-1(2)
S	65(4)	39(4)	149(6)	5(4)	-20(4)	-5(3)
O(1)	29(7)	31(8)	171(12)	-4(8)	-13(8)	-1(6)
O(2)	89(14)	84(15)	220(20)	17(15)	-16(14)	0(12)
O(3)	34(8)	84(13)	160(15)	-6(12)	2(9)	14(8)
O(4)	115(13)	109(14)	145(14)	5(13)	-11(11)	-53(12)
O(5)	125(14)	127(16)	202(17)	-35(14)	-1(14)	38(14)
O(6)	132(15)	133(16)	184(18)	-1(16)	14(15)	-13(13)
O(7)	105(14)	117(15)	192(16)	-24(14)	-57(13)	3(12)
N	14(5)	40(7)	57(7)	-3(6)	9(5)	3(5)
C(1)	56(13)	15(10)	103(17)	-9(10)	7(12)	-12(9)
C(2)	83(12)	79(13)	98(13)	0(11)	-16(11)	-4(11)
C(3)	102(14)	98(14)	114(14)	1(13)	-8(13)	-3(13)
C(4)	117(15)	105(15)	124(15)	2(13)	-5(13)	5(13)
C(5)	106(14)	92(14)	113(14)	-9(13)	-2(13)	3(13)
C(6)	100(13)	86(13)	103(13)	-2(12)	1(12)	0(12)
C(7)	70(8)	62(8)	78(9)	-14(7)	-6(7)	1(7)
C(8)	160(30)	120(30)	190(30)	30(20)	20(20)	-90(20)
C(9)	110(13)	124(14)	163(14)	-3(13)	2(12)	-37(13)
C(10)	135(16)	139(17)	179(17)	-3(16)	18(14)	-30(15)
C(11)	135(16)	153(18)	189(17)	-9(16)	17(15)	-11(16)
C(12)	132(16)	143(17)	188(17)	-19(15)	11(15)	-4(15)
C(13)	114(13)	119(14)	175(15)	-24(13)	13(13)	8(13)
C(14)	100(12)	102(12)	159(13)	-9(12)	-12(12)	-14(12)
C(15)	140(30)	110(30)	240(30)	-30(30)	30(20)	50(20)
C(16)	61(10)	57(11)	141(13)	-9(10)	-16(10)	-15(9)
C(17)	69(12)	60(12)	148(15)	3(12)	-24(12)	-8(10)
C(18)	73(12)	60(12)	138(15)	-3(12)	-12(12)	-13(11)
C(19)	59(11)	51(11)	128(14)	-7(11)	-15(11)	6(10)
C(20)	49(10)	50(11)	133(14)	-14(11)	-2(10)	13(9)
C(21)	44(10)	45(11)	131(14)	-7(11)	-14(10)	-7(9)
C(22)	230(40)	190(40)	260(40)	20(30)	-10(30)	20(30)
C(23)	129(13)	112(14)	168(16)	-17(14)	-9(14)	-16(12)
C(24)	122(15)	113(15)	172(17)	-31(15)	-17(15)	-3(14)
C(25)	120(16)	115(16)	177(17)	-22(15)	-20(15)	-15(14)
C(26)	114(15)	110(15)	176(16)	-11(14)	-25(14)	-20(14)
C(27)	114(13)	107(14)	182(14)	-17(13)	-32(13)	-17(12)
C(28)	116(13)	85(12)	160(13)	-22(12)	-13(12)	-26(11)
C(29)	150(30)	140(30)	130(20)	10(20)	-30(20)	20(20)
C(30)	128(13)	54(11)	152(13)	-15(11)	1(11)	-17(11)
C(31)	128(14)	75(12)	147(14)	-8(12)	-1(12)	-20(12)
C(32)	106(10)	79(9)	117(10)	-2(8)	-3(8)	-7(8)
C(33)	111(13)	52(11)	144(14)	-8(11)	-5(12)	15(11)
C(34)	120(14)	39(11)	149(15)	-12(11)	1(12)	20(11)
C(35)	118(14)	25(10)	131(14)	-11(10)	-6(12)	-1(11)
C(36)	52(8)	74(9)	79(9)	-9(7)	-1(7)	9(7)
C(37)	81(17)	61(17)	150(20)	-52(16)	11(17)	-23(14)
C(38)	100(20)	140(30)	97(19)	-70(19)	-6(17)	-10(20)

Table A.5: Bond lengths [Å] and angles [°] for $C_{76}H_{82}N_2O_{14}P_2Pd_2S_2$.

Pd-C(1)	2.12(2)	C(1)-PD-N	95.3(7)
Pd-O(1)	2.207(17)	O(1)-PD-N	84.9(6)
Pd-N	2.228(13)	C(1)-PD-P	85.1(6)
Pd-P	2.238(6)	O(1)-PD-P	94.6(4)
P-C(35)	1.791(14)	N-PD-P	179.5(5)
P-C(7)	1.798(16)	C(35)-P-C(7)	105.7(9)
P-C(21)	1.854(13)	C(35)-P-C(21)	106.8(9)
S-O(1)	1.407(16)	C(7)-P-C(21)	108.0(9)
S-O(3)	1.487(19)	C(35)-P-PD	112.3(7)
S-O(2)	1.50(3)	C(7)-P-PD	112.0(7)
S-C(2)	1.710(16)	C(21)-P-PD	111.7(6)
O(4)-C(9)	1.29(3)	O(1)-S-O(3)	115.20(11)
O(4)-C(8)	1.49(4)	O(1)-S-O(2)	113.10(12)
O(5)-C(15)	1.44(4)	O(3)-S-O(2)	113.20(13)
O(5)-C(13)	1.44(4)	O(1)-S-C(2)	103.9(1)
O(6)-C(23)	1.11(3)	O(3)-S-C(2)	102.5(1)
O(6)-C(22)	1.33(6)	O(2)-S-C(2)	107.50(13)
O(7)-C(27)	1.27(3)	S-O(1)-PD	114.8(9)
O(7)-C(29)	1.51(4)	C(9)-O(4)-C(8)	110(3)
N-C(36)	1.40(3)	C(15)-O(5)-C(13)	115(3)
N-C(38)	1.47(3)	C(23)-O(6)-C(22)	135(5)
N-C(37)	1.47(3)	C(27)-O(7)-C(29)	113(3)
C(2)-C(3)	1.39	C(36)-N-C(38)	108(2)
C(2)-C(7)	1.39	C(36)-N-C(37)	100.70(17)
C(3)-C(4)	1.39	C(38)-N-C(37)	115(2)
C(4)-C(5)	1.39	C(36)-N-PD	106.50(12)
C(5)-C(6)	1.39	C(38)-N-PD	107.40(14)
C(6)-C(7)	1.39	C(37)-N-PD	118.30(15)
C(9)-C(10)	1.39	C(3)-C(2)-C(7)	120
C(9)-C(14)	1.39	C(3)-C(2)-S	113.60(12)
C(10)-C(11)	1.39	C(7)-C(2)-S	126.40(12)
C(11)-C(12)	1.39	C(4)-C(3)-C(2)	120
C(12)-C(13)	1.39	C(3)-C(4)-C(5)	120
C(13)-C(14)	1.39	C(4)-C(5)-C(6)	120
C(14)-C(16)	1.43(3)	C(7)-C(6)-C(5)	120
C(16)-C(17)	1.39	C(6)-C(7)-C(2)	120
C(16)-C(21)	1.39	C(6)-C(7)-P	120.30(11)
C(17)-C(18)	1.39	C(2)-C(7)-P	119.60(11)
C(18)-C(19)	1.39	O(4)-C(9)-C(10)	132(2)
C(19)-C(20)	1.39	O(4)-C(9)-C(14)	107(3)
C(20)-C(21)	1.39	C(10)-C(9)-C(14)	120
C(23)-C(24)	1.39	C(11)-C(10)-C(9)	120
C(23)-C(28)	1.39	C(10)-C(11)-C(12)	120
C(24)-C(25)	1.39	C(13)-C(12)-C(11)	120
C(25)-C(26)	1.39	C(12)-C(13)-C(14)	120
C(26)-C(27)	1.39	C(12)-C(13)-O(5)	117(2)
C(27)-C(28)	1.39	C(14)-C(13)-O(5)	122(2)
C(28)-C(30)	1.56(3)	C(13)-C(14)-C(9)	120
C(30)-C(31)	1.39	C(13)-C(14)-C(16)	115(2)
C(30)-C(35)	1.39	C(9)-C(14)-C(16)	125(2)
C(31)-C(32)	1.39	C(17)-C(16)-C(21)	120
C(32)-C(33)	1.39	C(17)-C(16)-C(14)	111.10(15)
C(33)-C(34)	1.39	C(21)-C(16)-C(14)	128.60(15)
C(34)-C(35)	1.39	C(16)-C(17)-C(18)	120
C(35)-C(36)#1	1.58(5)	C(19)-C(18)-C(17)	120
		C(18)-C(19)-C(20)	120
C(1)-PD-O(1)	178.3(7)	C(19)-C(20)-C(21)	120

C(20)-C(21)-C(16)	120	C(23)-C(28)-C(30)	125(2)
C(20)-C(21)-P	112.2(1)	C(31)-C(30)-C(35)	120
C(16)-C(21)-P	127.8(1)	C(31)-C(30)-C(28)	112.70(16)
O(6)-C(23)-C(24)	120(3)	C(35)-C(30)-C(28)	125.80(16)
O(6)-C(23)-C(28)	120(3)	C(32)-C(31)-C(30)	120
C(24)-C(23)-C(28)	120	C(31)-C(32)-C(33)	120
C(23)-C(24)-C(25)	120	C(34)-C(33)-C(32)	120
C(24)-C(25)-C(26)	120	C(35)-C(34)-C(33)	120
C(27)-C(26)-C(25)	120	C(34)-C(35)-C(30)	120
O(7)-C(27)-C(26)	126(3)	C(34)-C(35)-P	117.00(11)
O(7)-C(27)-C(28)	114(3)	C(30)-C(35)-P	122.90(11)
C(26)-C(27)-C(28)	120	N-C(36)-C(36)#1	121(3)
C(27)-C(28)-C(23)	120		
C(27)-C(28)-C(30)	114(2)		

Symmetry transformations used to generate equivalent atoms:

#1 -x,-y+1,-z+1.

Table A.6: Torsion angles [°] for $C_{76}H_{82}N_2O_{14}P_2Pd_2S_2$.

C(1)-PD-P-C(35)	45.9(1)
O(1)-PD-P-C(35)	-135.8(9)
N-PD-P-C(35)	-142(100)
C(1)-PD-P-C(7)	164.7(9)
O(1)-PD-P-C(7)	-17.1(8)
N-PD-P-C(7)	-24(63)
C(1)-PD-P-C(21)	-74.1(9)
O(1)-PD-P-C(21)	104.2(8)
N-PD-P-C(21)	98(63)
O(3)-S-O(1)-PD	-36.60(14)
O(2)-S-O(1)-PD	-169.10(13)
C(2)-S-O(1)-PD	74.60(12)
C(1)-PD-O(1)-S	45(24)
N-PD-O(1)-S	143.30(11)
P-PD-O(1)-S	-36.7(1)
C(1)-PD-N-C(36)	116.00(15)
O(1)-PD-N-C(36)	-62.30(14)
P-PD-N-C(36)	-56(64)
C(1)-PD-N-C(38)	-128.50(19)
O(1)-PD-N-C(38)	53.20(19)
P-PD-N-C(38)	60(64)
C(1)-PD-N-C(37)	3.70(16)
O(1)-PD-N-C(37)	-174.50(15)
P-PD-N-C(37)	-168(100)
O(1)-S-C(2)-C(3)	115.20(12)
O(3)-S-C(2)-C(3)	-124.50(12)
O(2)-S-C(2)-C(3)	-4.90(15)
O(1)-S-C(2)-C(7)	-66.50(16)
O(3)-S-C(2)-C(7)	53.80(16)
O(2)-S-C(2)-C(7)	173.30(14)
C(7)-C(2)-C(3)-C(4)	0
S-C(2)-C(3)-C(4)	178.40(15)
C(2)-C(3)-C(4)-C(5)	0
C(3)-C(4)-C(5)-C(6)	0
C(4)-C(5)-C(6)-C(7)	0
C(5)-C(6)-C(7)-C(2)	0
C(5)-C(6)-C(7)-P	175.50(14)
C(3)-C(2)-C(7)-C(6)	0
S-C(2)-C(7)-C(6)	-178.20(17)
C(3)-C(2)-C(7)-P	-175.60(14)
S-C(2)-C(7)-P	6.30(17)
C(35)-P-C(7)-C(6)	-21.50(13)
C(21)-P-C(7)-C(6)	92.50(12)
PD-P-C(7)-C(6)	-144.1(9)
C(35)-P-C(7)-C(2)	154.10(12)
C(21)-P-C(7)-C(2)	-91.90(12)
PD-P-C(7)-C(2)	31.50(12)
C(8)-O(4)-C(9)-C(10)	14(4)
C(8)-O(4)-C(9)-C(14)	-179(2)
O(4)-C(9)-C(10)-C(11)	166(3)
C(14)-C(9)-C(10)-C(11)	0
C(9)-C(10)-C(11)-C(12)	0
C(10)-C(11)-C(12)-C(13)	0
C(11)-C(12)-C(13)-C(14)	0
C(11)-C(12)-C(13)-O(5)	172(3)
C(15)-O(5)-C(13)-C(12)	-6(4)
C(15)-O(5)-C(13)-C(14)	167(3)
C(12)-C(13)-C(14)-C(9)	0
O(5)-C(13)-C(14)-C(9)	-172(3)
C(12)-C(13)-C(14)-C(16)	-180(2)
O(5)-C(13)-C(14)-C(16)	8(3)

O(4)-C(9)-C(14)-C(13)	-169(3)
C(10)-C(9)-C(14)-C(13)	0
O(4)-C(9)-C(14)-C(16)	11(2)
C(10)-C(9)-C(14)-C(16)	180(3)
C(13)-C(14)-C(16)-C(17)	85.50(17)
C(9)-C(14)-C(16)-C(17)	-94.30(19)
C(13)-C(14)-C(16)-C(21)	-100(2)
C(9)-C(14)-C(16)-C(21)	80(2)
C(21)-C(16)-C(17)-C(18)	0
C(14)-C(16)-C(17)-C(18)	174.90(19)
C(16)-C(17)-C(18)-C(19)	0
C(17)-C(18)-C(19)-C(20)	0
C(18)-C(19)-C(20)-C(21)	0
C(19)-C(20)-C(21)-C(16)	0
C(19)-C(20)-C(21)-P	-177.60(12)
C(17)-C(16)-C(21)-C(20)	0
C(14)-C(16)-C(21)-C(20)	-174(2)
C(17)-C(16)-C(21)-P	177.20(15)
C(14)-C(16)-C(21)-P	3(2)
C(35)-P-C(21)-C(20)	-107.90(11)
C(7)-P-C(21)-C(20)	138.8(1)
PD-P-C(21)-C(20)	15.2(1)
C(35)-P-C(21)-C(16)	74.70(14)
C(7)-P-C(21)-C(16)	-38.60(13)
PD-P-C(21)-C(16)	-162.1(9)
C(22)-O(6)-C(23)-C(24)	79(7)
C(22)-O(6)-C(23)-C(28)	-102(6)
O(6)-C(23)-C(24)-C(25)	179(3)
C(28)-C(23)-C(24)-C(25)	0
C(23)-C(24)-C(25)-C(26)	0
C(24)-C(25)-C(26)-C(27)	0
C(29)-O(7)-C(27)-C(26)	-3(4)
C(29)-O(7)-C(27)-C(28)	169(2)
C(25)-C(26)-C(27)-O(7)	172(3)
C(25)-C(26)-C(27)-C(28)	0
O(7)-C(27)-C(28)-C(23)	-173(3)
C(26)-C(27)-C(28)-C(23)	0
O(7)-C(27)-C(28)-C(30)	18(2)
C(26)-C(27)-C(28)-C(30)	-169(2)
O(6)-C(23)-C(28)-C(27)	-179(3)
C(24)-C(23)-C(28)-C(27)	0
O(6)-C(23)-C(28)-C(30)	-11(3)
C(24)-C(23)-C(28)-C(30)	168(2)
C(27)-C(28)-C(30)-C(31)	-86.10(16)
C(23)-C(28)-C(30)-C(31)	105.00(18)
C(27)-C(28)-C(30)-C(35)	108.10(19)
C(23)-C(28)-C(30)-C(35)	-61(3)
C(35)-C(30)-C(31)-C(32)	0
C(28)-C(30)-C(31)-C(32)	-167(2)
C(30)-C(31)-C(32)-C(33)	0
C(31)-C(32)-C(33)-C(34)	0
C(32)-C(33)-C(34)-C(35)	0
C(33)-C(34)-C(35)-C(30)	0
C(33)-C(34)-C(35)-P	177.60(15)
C(31)-C(30)-C(35)-C(34)	0
C(28)-C(30)-C(35)-C(34)	165(2)
C(31)-C(30)-C(35)-P	-177.50(16)
C(28)-C(30)-C(35)-P	-13(2)
C(7)-P-C(35)-C(34)	129.10(12)
C(21)-P-C(35)-C(34)	14.30(14)
PD-P-C(35)-C(34)	-108.5(1)

C(7)-P-C(35)-C(30)	-53.30(14)
C(21)-P-C(35)-C(30)	-168.10(12)
PD-P-C(35)-C(30)	69.10(13)
C(38)-N-C(36)-C(36)#1	-163(3)
C(37)-N-C(36)-C(36)#1	76(3)
PD-N-C(36)-C(36)#1	-48(3)

Symmetry transformations used to generate equivalent atoms:

#1 -x,-y+1,-z+1

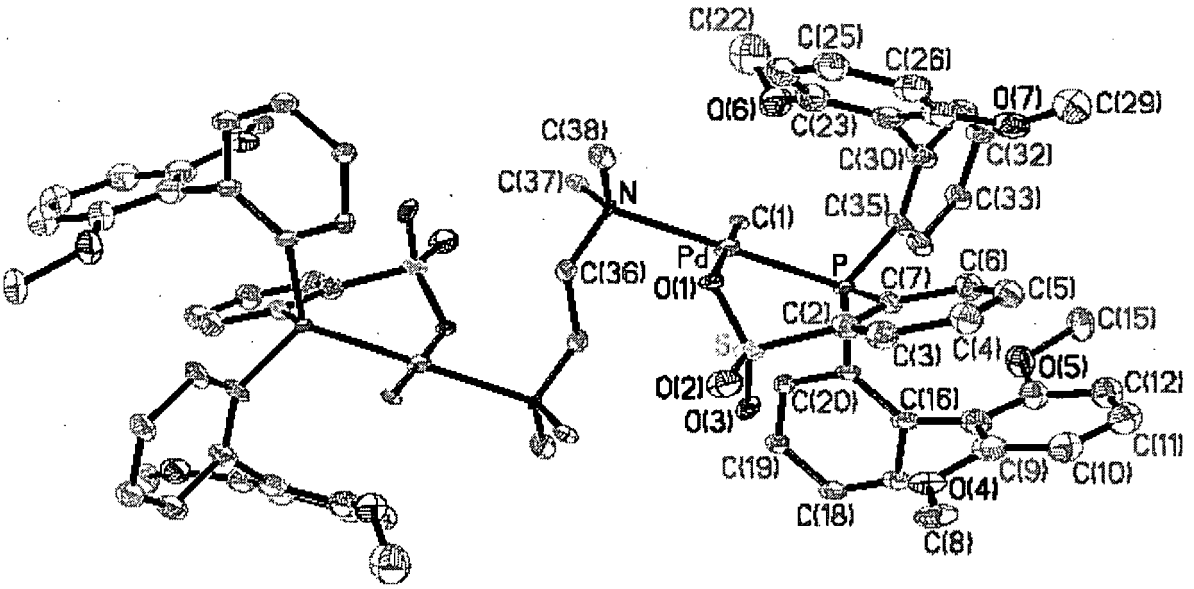

Figure A.12: ORTEP view of the $C_{76}H_{82}N_2O_{14}P_2Pd_2S_2$ compound with the numbering scheme adopted. Ellipsoids drawn at 30% probability level. Hydrogen atoms are represented by sphere of arbitrary size.

REFERENCES

Bruker (1997). SHELXTL (1997). Release 5.10; The Complete Software Package for Single Crystal Structure Determination. Bruker AXS Inc., Madison, USA.

Bruker (2006). SAINT Release 7.34A. Integration Software for Single Crystal Data. Bruker AXS Inc., Madison, USA.

Bruker (2006). APEX2 Release 2.1-0; Bruker Molecular Analysis Research Tool, Bruker AXS Inc., Madison, USA.

Sheldrick, G. M. (1996). SADABS, Bruker Area Detector Absorption Corrections. Bruker AXS Inc., Madison, USA.

Sheldrick, G. M. (2004). SADABS, Bruker Area Detector Absorption Corrections. Bruker AXS Inc., Madison, USA.

Sheldrick, G. M. (1997a). SHELXS97. Program for Crystal Structure solution. University of Gıottingen, Germany.

Sheldrick, G. M. (1997b). SHELXL97. Program for crystal structure refinement. University of Gıottingen, Germany.

Spek, A. L. (2000). PLATON, 2000 version; Molecular Geometry Program, University of Utrecht, Utrecht, Holland.

A.5 X-Ray structure for catalyst 2b

Single crystal X-ray diffraction studies. Crystal data and structure refinement details are shown in Table 1. A crystal was selected and mounted on a glass fiber with viscous oil and cooled to the data collection temperature. Diffraction data were collected on a Bruker-AXS APEX CCD diffractometer. The data-set was treated with SADABS absorption corrections. Unit-cell parameters were determined by sampling three different sections of the Ewald sphere. No symmetry higher than triclinic was observed in the diffraction data and the structural solution in the centrosymmetric space group option, P-1, yielded chemically reasonable and computationally stable results of refinement. Two molecules of cocrystallized THF solvent were located in the asymmetric unit. All non hydrogen atoms were refined with anisotropic displacement parameters. All hydrogen atoms were treated as

idealized contributions. Structure factors are contained in SHELXTL 6.12 program library (G. Sheldrick, 2001; Siemens XRD, Madison, WI). The supplementary crystallographic data for this paper have been deposited under reference numbers CCDC 654080. These data can be obtained free of charge via www.ccdc.cam.ac.uk/conts/retrieving.html; or from the Cambridge Crystallographic Data Centre, 12, Union Road, Cambridge, CB2 1EZ, UK; fax: +44 1223 336033; or deposit@ccdc.cam.ac.uk

Table A.7: Crystal data and structure refinement for 2b.

Identification code	clav001
Empirical formula	C48 H54 N O9 P Pd S
Formula weight	958.35
Temperature	120(2) K
Wavelength	0.71073 Å
Crystal system	Triclinic
Space group	P-1
Unit cell dimensions	a = 9.502(5) Å α = 101.53(3)° b = 13.999(4)Å β = 93.23(2)° c = 17.344(5) Å γ = 107.15(3)°

Volume	2143.6(14)Å^3
Z	2
Density (calculated)	1.485 g/cm^3
Absorption coefficient	5.495 mm^{-1}
F(000)	976
Crystal size	0.22 x 0.12 x 0.08 mm
Theta range for data collection	1.74 to 28.32°
Index ranges	$-12 \leq h \leq 12$, $-18 \leq k \leq 18$, $-23 \leq \ell \leq 21$
Reflections collected	7063
Independent reflections	9722 [R_{int} = 0.158]
Absorption correction	Semi-empirical from equivalents
Max. and min. transmission	0.9552 and 0.8833
Refinement method	Full-matrix least-squares on F^2
Data / restraints / parameters	9722 / 0 / 555
Goodness-of-fit on F^2	1.021
Final R indices [I>2sigma(I)]	R1 = 0.0656, wR2 = 0.1557
R indices (all data)	R1 = 0.0951, wR2 = 0.1776
Largest diff. peak and hole	0.821 and -0.829 e.A^-3

Table A.8: Atomic coordinates (x 10^4) and equivalent isotropic displacement parameters ($Å^2$ x 10^3) for 2b. U(eq) is defined as one third of the trace of the orthogonalized U_{ij} tensor.

	x	y	z	U(eq)
Pd	2387(1)	1927(1)	3035(1)	26(1)
P	590(1)	2352(1)	2441(1)	24(1)
S	686(1)	2518(1)	4503(1)	26(1)
N	4074(4)	1546(3)	3654(2)	25(1)
O(1)	920(4)	1656(3)	3929(2)	28(1)
O(2)	-338(4)	2133(3)	5033(2)	35(1)
O(3)	2068(4)	3266(3)	4887(2)	33(1)
O(4)	3584(4)	4340(3)	3137(2)	40(1)
O(5)	403(6)	5518(3)	1717(4)	83(2)
O(6)	915(4)	-14(3)	975(2)	31(1)
O(7)	-1174(4)	-428(3)	3286(2)	34(1)
C(1)	3705(6)	2201(4)	2177(3)	35(1)
C(2)	-218(5)	3172(4)	3948(3)	28(1)
C(3)	-890(6)	3794(4)	4426(3)	39(1)
C(4)	-1618(7)	4372(5)	4101(3)	47(2)
C(5)	-1693(7)	4322(4)	3299(3)	40(1)
C(6)	-1008(6)	3719(4)	2828(3)	32(1)
C(7)	-246(5)	3134(4)	3139(3)	26(1)
C(8)	4570(7)	4462(5)	3826(3)	52(2)
C(9)	2839(7)	5038(4)	3153(3)	41(1)
C(10)	2937(7)	5835(5)	3808(4)	52(2)
C(11)	2176(8)	6516(5)	3753(5)	66(2)
C(12)	1334(8)	6441(5)	3060(5)	69(2)
C(13)	1240(7)	5648(5)	2415(5)	58(2)
C(14)	1954(6)	4919(4)	2449(3)	40(1)
C(15)	7(10)	6360(6)	1551(6)	98(3)
C(16)	1814(6)	4086(4)	1728(3)	33(1)
C(17)	2378(7)	4413(4)	1064(3)	46(2)
C(18)	2246(7)	3751(5)	343(3)	45(2)
C(19)	1541(6)	2719(4)	265(3)	37(1)
C(20)	987(6)	2366(4)	906(3)	29(1)
C(21)	1112(5)	3029(4)	1650(3)	25(1)
C(22)	1917(6)	-168(4)	411(3)	35(1)
C(23)	1065(6)	-303(4)	1672(3)	28(1)
C(24)	2149(6)	-713(4)	1895(3)	36(1)
C(25)	2144(6)	-989(4)	2620(3)	39(1)
C(26)	1090(6)	-891(4)	3110(3)	36(1)
C(27)	-7(6)	-497(4)	2879(3)	29(1)
C(28)	7(5)	-157(4)	2181(3)	26(1)
C(29)	-1094(8)	-553(5)	4082(3)	46(2)
C(30)	-1200(5)	222(4)	1910(3)	23(1)
C(31)	-2544(6)	-523(4)	1578(3)	29(1)
C(32)	-3728(6)	-276(4)	1273(3)	31(1)
C(33)	-3570(6)	742(4)	1286(3)	34(1)
C(34)	-2278(5)	1498(4)	1626(3)	29(1)
C(35)	-1063(5)	1263(4)	1956(3)	24(1)
C(36)	4117(6)	1693(4)	4441(3)	34(1)
C(37)	5136(6)	1445(5)	4901(3)	38(1)
C(38)	6159(6)	1051(4)	4545(3)	35(1)
C(39)	6127(6)	902(4)	3734(3)	35(1)

C(40)	5071(6)	1150(4)	3316(3)	31(1)
O(8)	5389(8)	2709(5)	227(4)	111(2)
C(41)	6727(10)	2519(9)	-122(4)	102(4)
C(42)	7977(8)	3796(6)	369(4)	61(2)
C(43)	7147(12)	4113(10)	915(10)	208(10)
C(44)	5914(13)	3724(7)	815(8)	124(5)
O(9)	5809(9)	6493(5)	1567(4)	114(3)
C(45)	6201(10)	6041(5)	2209(4)	66(2)
C(46)	6657(12)	6977(6)	2891(4)	86(3)
C(47)	5564(12)	7520(6)	2700(6)	103(4)
C(48)	5117(8)	7169(5)	1836(5)	63(2)

Table A.9: Bond lengths [Å] and angles [°] for 2b.

Pd-C(1)	2.022(5)
Pd-N	2.131(4)
Pd-O(1)	2.158(3)
Pd-P	2.2313(15)
P-C(21)	1.829(5)
P-C(7)	1.840(5)
P-C(35)	1.852(5)
S-O(2)	1.438(4)
S-O(3)	1.441(4)
S-O(1)	1.483(3)
S-C(2)	1.796(5)
N-C(36)	1.336(6)
N-C(40)	1.338(6)
O(4)-C(9)	1.363(7)
O(4)-C(8)	1.425(6)
O(5)-C(13)	1.359(9)
O(5)-C(15)	1.414(8)
O(6)-C(23)	1.363(6)
O(6)-C(22)	1.432(5)
O(7)-C(27)	1.364(6)
O(7)-C(29)	1.427(6)
C(2)-C(7)	1.392(6)
C(2)-C(3)	1.397(7)
C(3)-C(4)	1.386(7)
C(4)-C(5)	1.376(8)
C(5)-C(6)	1.383(7)
C(6)-C(7)	1.404(6)
C(9)-C(14)	1.396(8)
C(9)-C(10)	1.401(8)
C(10)-C(11)	1.369(10)
C(11)-C(12)	1.375(11)
C(12)-C(13)	1.387(9)
C(13)-C(14)	1.390(8)
C(14)-C(16)	1.500(7)
C(16)-C(17)	1.399(8)
C(16)-C(21)	1.407(7)
C(17)-C(18)	1.374(8)
C(18)-C(19)	1.377(8)
C(19)-C(20)	1.374(7)
C(20)-C(21)	1.408(6)
C(23)-C(24)	1.391(7)
C(23)-C(28)	1.407(7)
C(24)-C(25)	1.386(8)
C(25)-C(26)	1.371(8)
C(26)-C(27)	1.391(7)
C(27)-C(28)	1.386(7)
C(28)-C(30)	1.488(6)
C(30)-C(31)	1.394(7)
C(30)-C(35)	1.409(6)
C(31)-C(32)	1.379(7)
C(32)-C(33)	1.383(7)
C(33)-C(34)	1.371(7)
C(34)-C(35)	1.411(6)
C(36)-C(37)	1.384(7)
C(37)-C(38)	1.371(7)
C(38)-C(39)	1.377(7)
C(39)-C(40)	1.370(7)

O(8)-C(44)	1.501(11)
O(8)-C(41)	1.508(10)
C(41)-C(42)	1.832(13)
C(42)-C(43)	1.355(11)
C(43)-C(44)	1.124(13)
O(9)-C(48)	1.331(10)
O(9)-C(45)	1.466(9)
C(45)-C(46)	1.513(9)
C(46)-C(47)	1.514(13)
C(47)-C(48)	1.475(13)

C(1)-Pd-N	89.47(18)
C(1)-Pd-O(1)	177.77(16)
N-Pd-O(1)	92.74(14)
C(1)-Pd-P	92.74(15)
N-Pd-P	177.39(11)
O(1)-Pd-P	85.04(10)
C(21)-P-C(7)	106.9(2)
C(21)-P-C(35)	103.0(2)
C(7)-P-C(35)	101.3(2)
C(21)-P-Pd	115.81(15)
C(7)-P-Pd	112.99(16)
C(35)-P-Pd	115.26(15)
O(2)-S-O(3)	115.0(2)
O(2)-S-O(1)	110.4(2)
O(3)-S-O(1)	112.0(2)
O(2)-S-C(2)	105.6(2)
O(3)-S-C(2)	106.0(2)
O(1)-S-C(2)	107.2(2)
C(36)-N-C(40)	117.4(4)
C(36)-N-Pd	117.3(3)
C(40)-N-Pd	125.3(3)
S-O(1)-Pd	121.4(2)
C(9)-O(4)-C(8)	117.1(5)
C(13)-O(5)-C(15)	118.8(6)
C(23)-O(6)-C(22)	118.2(4)
C(27)-O(7)-C(29)	117.4(4)
C(7)-C(2)-C(3)	120.7(4)
C(7)-C(2)-S	126.7(4)
C(3)-C(2)-S	112.6(4)
C(4)-C(3)-C(2)	120.6(5)
C(5)-C(4)-C(3)	119.5(5)
C(4)-C(5)-C(6)	119.9(5)
C(5)-C(6)-C(7)	122.0(5)
C(2)-C(7)-C(6)	117.2(4)
C(2)-C(7)-P	125.3(4)
C(6)-C(7)-P	117.4(4)
O(4)-C(9)-C(14)	114.9(5)
O(4)-C(9)-C(10)	124.5(6)
C(14)-C(9)-C(10)	120.7(6)
C(11)-C(10)-C(9)	119.8(7)
C(10)-C(11)-C(12)	121.0(6)
C(11)-C(12)-C(13)	118.9(7)
O(5)-C(13)-C(12)	121.9(6)
O(5)-C(13)-C(14)	115.8(6)
C(12)-C(13)-C(14)	122.2(7)
C(9)-C(14)-C(13)	117.4(5)
C(9)-C(14)-C(16)	123.1(5)
C(13)-C(14)-C(16)	119.5(5)
C(17)-C(16)-C(21)	117.9(5)
C(17)-C(16)-C(14)	115.8(5)
C(21)-C(16)-C(14)	126.2(5)

C(18)-C(17)-C(16)	122.9(5)
C(17)-C(18)-C(19)	119.1(5)
C(20)-C(19)-C(18)	119.8(5)
C(19)-C(20)-C(21)	122.1(5)
C(16)-C(21)-C(20)	118.2(5)
C(16)-C(21)-P	127.7(4)
C(20)-C(21)-P	113.3(4)
O(6)-C(23)-C(24)	125.1(5)
O(6)-C(23)-C(28)	114.5(4)
C(24)-C(23)-C(28)	120.3(5)
C(25)-C(24)-C(23)	118.6(5)
C(26)-C(25)-C(24)	122.1(5)
C(25)-C(26)-C(27)	119.2(5)
O(7)-C(27)-C(28)	114.7(4)
O(7)-C(27)-C(26)	124.7(5)
C(28)-C(27)-C(26)	120.5(5)
C(27)-C(28)-C(23)	119.1(4)
C(27)-C(28)-C(30)	120.9(4)
C(23)-C(28)-C(30)	119.4(4)
C(31)-C(30)-C(35)	118.9(4)
C(31)-C(30)-C(28)	116.3(4)
C(35)-C(30)-C(28)	124.8(4)
C(32)-C(31)-C(30)	122.0(5)
C(31)-C(32)-C(33)	119.0(5)
C(34)-C(33)-C(32)	120.5(5)
C(33)-C(34)-C(35)	121.3(5)
C(30)-C(35)-C(34)	118.1(4)
C(30)-C(35)-P	124.5(3)
C(34)-C(35)-P	117.4(4)
N-C(36)-C(37)	122.4(5)
C(38)-C(37)-C(36)	119.4(5)
C(37)-C(38)-C(39)	118.6(5)
C(40)-C(39)-C(38)	118.7(5)
N-C(40)-C(39)	123.6(5)
C(44)-O(8)-C(41)	107.6(8)
O(8)-C(41)-C(42)	93.8(6)
C(43)-C(42)-C(41)	101.2(7)
C(44)-C(43)-C(42)	118.2(13)
C(43)-C(44)-O(8)	115.7(12)
C(48)-O(9)-C(45)	110.1(7)
O(9)-C(45)-C(46)	100.2(6)
C(45)-C(46)-C(47)	101.2(8)
C(48)-C(47)-C(46)	105.7(6)
O(9)-C(48)-C(47)	107.1(7)

Table A.10: Anisotropic displacement parameters ($Å^2$ x 10^3) for 2b. The anisotropic displacement factor exponent takes the form: $-2\,p^2\,[\,h^2\,a^{*2}\,U_{11} + ... + 2\,h\,k\,a^*\,b^*\,U_{12}\,]$

	U11	U22	U33	U23	U13	U12
Pd	30(1)	32(1)	20(1)	0(1)	-1(1)	19(1)
P	29(1)	26(1)	19(1)	0(1)	-2(1)	17(1)
S	28(1)	32(1)	21(1)	3(1)	1(1)	16(1)
N	24(2)	30(2)	22(2)	2(2)	-1(2)	14(2)
O(1)	32(2)	28(2)	26(2)	0(1)	1(1)	18(2)
O(2)	37(2)	42(2)	35(2)	13(2)	11(2)	23(2)
O(3)	31(2)	35(2)	32(2)	0(2)	-3(2)	14(2)
O(4)	44(2)	42(2)	25(2)	3(2)	-10(2)	5(2)
O(5)	76(4)	32(2)	121(5)	-12(3)	-55(3)	21(2)
O(6)	30(2)	36(2)	30(2)	6(2)	8(2)	17(2)
O(7)	48(2)	39(2)	22(2)	8(2)	5(2)	23(2)
C(1)	33(3)	55(3)	25(3)	7(2)	3(2)	28(3)
C(2)	32(3)	31(3)	23(2)	0(2)	-2(2)	20(2)
C(3)	52(3)	53(3)	23(3)	1(2)	3(2)	37(3)
C(4)	62(4)	62(4)	31(3)	-3(3)	1(3)	50(3)
C(5)	55(4)	44(3)	32(3)	6(2)	0(3)	37(3)
C(6)	42(3)	32(3)	24(2)	0(2)	-2(2)	21(2)
C(7)	32(3)	27(2)	20(2)	-4(2)	-2(2)	18(2)
C(8)	45(4)	61(4)	34(3)	14(3)	-12(3)	-4(3)
C(9)	41(3)	31(3)	40(3)	-4(2)	5(3)	2(2)
C(10)	47(4)	47(4)	38(3)	-5(3)	7(3)	-11(3)
C(11)	60(5)	31(3)	88(6)	-15(3)	27(4)	0(3)
C(12)	44(4)	36(4)	109(7)	-14(4)	6(4)	6(3)
C(13)	44(4)	33(3)	85(5)	-10(3)	-9(3)	13(3)
C(14)	34(3)	31(3)	41(3)	-8(2)	-7(2)	4(2)
C(15)	85(6)	55(5)	151(9)	-8(5)	-32(6)	45(5)
C(16)	34(3)	30(3)	31(3)	2(2)	-10(2)	11(2)
C(17)	55(4)	27(3)	41(3)	11(2)	-22(3)	-5(3)
C(18)	50(4)	45(3)	34(3)	21(3)	-8(3)	3(3)
C(19)	48(3)	43(3)	20(2)	5(2)	-2(2)	15(3)
C(20)	34(3)	26(2)	28(3)	4(2)	-2(2)	15(2)
C(21)	26(2)	28(2)	22(2)	2(2)	-5(2)	15(2)
C(22)	29(3)	45(3)	31(3)	0(2)	10(2)	17(2)
C(23)	31(3)	26(2)	29(3)	5(2)	2(2)	14(2)
C(24)	33(3)	28(3)	45(3)	-2(2)	0(2)	18(2)
C(25)	38(3)	35(3)	45(3)	3(2)	-12(3)	20(3)
C(26)	48(3)	33(3)	31(3)	7(2)	-6(2)	19(3)
C(27)	40(3)	26(2)	22(2)	1(2)	-2(2)	13(2)
C(28)	29(2)	25(2)	24(2)	0(2)	-3(2)	14(2)
C(29)	71(4)	50(4)	25(3)	16(3)	4(3)	29(3)
C(30)	29(2)	29(2)	14(2)	1(2)	1(2)	18(2)
C(31)	35(3)	30(3)	24(2)	5(2)	5(2)	13(2)
C(32)	28(3)	35(3)	28(3)	5(2)	3(2)	10(2)
C(33)	29(3)	41(3)	34(3)	4(2)	-3(2)	19(2)
C(34)	32(3)	32(3)	27(2)	3(2)	1(2)	19(2)
C(35)	27(2)	30(2)	20(2)	5(2)	4(2)	15(2)
C(36)	32(3)	50(3)	25(3)	5(2)	1(2)	23(3)
C(37)	35(3)	56(4)	28(3)	9(2)	-2(2)	22(3)
C(38)	30(3)	40(3)	36(3)	8(2)	-8(2)	15(2)
C(39)	28(3)	37(3)	44(3)	7(2)	3(2)	19(2)

C(40)	33(3)	39(3)	25(2)	5(2)	4(2)	19(2)
O(8)	119(6)	86(5)	119(6)	3(4)	13(5)	34(4)
C(41)	117(7)	205(11)	37(4)	22(5)	6(4)	132(8)
C(42)	54(4)	69(5)	56(4)	0(4)	-2(3)	23(4)
C(43)	67(7)	148(11)	289(19)	-138(12)	80(10)	-31(7)
C(44)	113(9)	62(6)	156(11)	-13(6)	-63(8)	4(6)
O(9)	152(7)	85(5)	74(4)	25(4)	-6(4)	-13(5)
C(45)	98(6)	38(4)	54(4)	6(3)	19(4)	11(4)
C(46)	154(9)	44(4)	44(4)	7(3)	0(5)	11(5)
C(47)	142(9)	55(5)	144(9)	49(6)	112(8)	43(6)
C(48)	47(4)	32(3)	99(6)	22(4)	-12(4)	-4(3)

Table A.11: Hydrogen coordinates (x 10^4) and isotropic displacement parameters ($Å^2$ x 10^3) for 2b.

	x	y	z	U(eq)
H(1A)	4746	2466	2411	52
H(1B)	3463	2708	1923	52
H(1C)	3544	1561	1779	52
H(3A)	-847	3821	4979	47
H(4A)	-2062	4801	4430	56
H(5A)	-2214	4700	3069	48
H(6A)	-1054	3701	2276	38
H(8A)	5092	3949	3728	77
H(8B)	4003	4368	4275	77
H(8C)	5293	5152	3948	77
H(10A)	3529	5903	4288	62
H(11A)	2232	7048	4201	79
H(12A)	824	6924	3023	83
H(15A)	-257	6247	978	147
H(15B)	848	6990	1735	147
H(15C)	-845	6428	1825	147
H(17A)	2874	5123	1114	55
H(18A)	2636	4003	-96	53
H(19A)	1437	2252	-230	45
H(20A)	505	1652	845	34
H(22A)	1640	25	-75	52
H(22B)	1868	-893	286	52
H(22C)	2931	258	635	52
H(24A)	2877	-803	1559	43
H(25A)	2896	-1255	2781	47
H(26A)	1108	-1090	3603	44
H(29A)	-1957	-437	4321	68
H(29B)	-183	-57	4389	68
H(29C)	-1087	-1251	4084	68
H(31A)	-2647	-1224	1560	35
H(32A)	-4639	-797	1057	37
H(33A)	-4364	918	1057	40
H(34A)	-2198	2194	1640	35
H(36A)	3424	1978	4694	41
H(37A)	5126	1547	5459	45
H(38A)	6876	884	4851	42
H(39A)	6823	633	3469	42
H(40A)	5045	1035	2756	37
H(41A)	6623	2399	-707	123
H(41B)	7001	1958	51	123
H(42A)	8912	3758	624	74
H(42B)	8209	4252	-7	74
H(43A)	7525	4034	1434	249
H(43B)	7324	4856	957	249
H(44A)	5432	4192	635	149
H(44B)	5573	3619	1330	149
H(45A)	7031	5762	2100	79
H(45B)	5340	5496	2307	79
H(46A)	7694	7404	2893	103
H(46B)	6542	6784	3408	103
H(47A)	4691	7337	2990	123

H(47B)	6036	8274	2849	123
H(48A)	4028	6843	1722	75
H(48B)	5405	7757	1578	75

Table A.12: Torsion angles [°] for 2b.

C(1)-Pd-P-C(21)	-14.2(2)
N-Pd-P-C(21)	134(3)
O(1)-Pd-P-C(21)	165.65(19)
C(1)-Pd-P-C(7)	-138.0(2)
N-Pd-P-C(7)	10(3)
O(1)-Pd-P-C(7)	41.8(2)
C(1)-Pd-P-C(35)	106.2(2)
N-Pd-P-C(35)	-106(3)
O(1)-Pd-P-C(35)	-74.00(19)
C(1)-Pd-N-C(36)	152.6(4)
O(1)-Pd-N-C(36)	-27.1(4)
P-Pd-N-C(36)	5(3)
C(1)-Pd-N-C(40)	-29.1(4)
O(1)-Pd-N-C(40)	151.2(4)
P-Pd-N-C(40)	-177(2)
O(2)-S-O(1)-Pd	179.9(2)
O(3)-S-O(1)-Pd	-50.6(3)
C(2)-S-O(1)-Pd	65.3(3)
C(1)-Pd-O(1)-S	-69(5)
N-Pd-O(1)-S	104.8(2)
P-Pd-O(1)-S	-73.8(2)
O(2)-S-C(2)-C(7)	-138.0(5)
O(3)-S-C(2)-C(7)	99.6(5)
O(1)-S-C(2)-C(7)	-20.2(5)
O(2)-S-C(2)-C(3)	44.4(5)
O(3)-S-C(2)-C(3)	-78.0(5)
O(1)-S-C(2)-C(3)	162.2(4)
C(7)-C(2)-C(3)-C(4)	1.0(9)
S-C(2)-C(3)-C(4)	178.8(5)
C(2)-C(3)-C(4)-C(5)	0.8(10)
C(3)-C(4)-C(5)-C(6)	-1.8(10)
C(4)-C(5)-C(6)-C(7)	1.1(9)
C(3)-C(2)-C(7)-C(6)	-1.8(8)
S-C(2)-C(7)-C(6)	-179.2(4)
C(3)-C(2)-C(7)-P	180.0(4)
S-C(2)-C(7)-P	2.5(7)
C(5)-C(6)-C(7)-C(2)	0.7(8)
C(5)-C(6)-C(7)-P	179.1(5)
C(21)-P-C(7)-C(2)	-150.9(4)
C(35)-P-C(7)-C(2)	101.6(5)
Pd-P-C(7)-C(2)	-22.3(5)
C(21)-P-C(7)-C(6)	30.9(5)
C(35)-P-C(7)-C(6)	-76.7(4)
Pd-P-C(7)-C(6)	159.4(4)
C(8)-O(4)-C(9)-C(14)	176.5(5)
C(8)-O(4)-C(9)-C(10)	-2.6(8)
O(4)-C(9)-C(10)-C(11)	178.0(6)
C(14)-C(9)-C(10)-C(11)	-1.1(9)
C(9)-C(10)-C(11)-C(12)	-1.1(10)
C(10)-C(11)-C(12)-C(13)	1.2(11)
C(15)-O(5)-C(13)-C(12)	20.3(12)
C(15)-O(5)-C(13)-C(14)	-161.7(7)

C(11)-C(12)-C(13)-O(5)	178.7(7)
C(11)-C(12)-C(13)-C(14)	0.8(11)
O(4)-C(9)-C(14)-C(13)	-176.1(5)
C(10)-C(9)-C(14)-C(13)	3.0(9)
O(4)-C(9)-C(14)-C(16)	0.4(8)
C(10)-C(9)-C(14)-C(16)	179.6(5)
O(5)-C(13)-C(14)-C(9)	179.1(6)
C(12)-C(13)-C(14)-C(9)	-2.9(10)
O(5)-C(13)-C(14)-C(16)	2.4(9)
C(12)-C(13)-C(14)-C(16)	-179.6(6)
C(9)-C(14)-C(16)-C(17)	-114.5(6)
C(13)-C(14)-C(16)-C(17)	62.0(8)
C(9)-C(14)-C(16)-C(21)	68.8(8)
C(13)-C(14)-C(16)-C(21)	-114.7(7)
C(21)-C(16)-C(17)-C(18)	1.5(9)
C(14)-C(16)-C(17)-C(18)	-175.5(6)
C(16)-C(17)-C(18)-C(19)	-0.6(9)
C(17)-C(18)-C(19)-C(20)	-0.2(9)
C(18)-C(19)-C(20)-C(21)	0.1(8)
C(17)-C(16)-C(21)-C(20)	-1.5(7)
C(14)-C(16)-C(21)-C(20)	175.1(5)
C(17)-C(16)-C(21)-P	167.4(4)
C(14)-C(16)-C(21)-P	-16.0(8)
C(19)-C(20)-C(21)-C(16)	0.7(7)
C(19)-C(20)-C(21)-P	-169.7(4)
C(7)-P-C(21)-C(16)	43.7(5)
C(35)-P-C(21)-C(16)	150.0(4)
Pd-P-C(21)-C(16)	-83.2(5)
C(7)-P-C(21)-C(20)	-147.0(4)
C(35)-P-C(21)-C(20)	-40.7(4)
Pd-P-C(21)-C(20)	86.1(4)
C(22)-O(6)-C(23)-C(24)	1.9(7)
C(22)-O(6)-C(23)-C(28)	-178.0(4)
O(6)-C(23)-C(24)-C(25)	-178.8(5)
C(28)-C(23)-C(24)-C(25)	1.1(7)
C(23)-C(24)-C(25)-C(26)	1.5(8)
C(24)-C(25)-C(26)-C(27)	-0.4(8)
C(29)-O(7)-C(27)-C(28)	-166.9(4)
C(29)-O(7)-C(27)-C(26)	14.5(7)
C(25)-C(26)-C(27)-O(7)	175.2(5)
C(25)-C(26)-C(27)-C(28)	-3.3(8)
O(7)-C(27)-C(28)-C(23)	-172.8(4)
C(26)-C(27)-C(28)-C(23)	5.8(7)
O(7)-C(27)-C(28)-C(30)	-1.4(7)
C(26)-C(27)-C(28)-C(30)	177.2(4)
O(6)-C(23)-C(28)-C(27)	175.2(4)
C(24)-C(23)-C(28)-C(27)	-4.7(7)
O(6)-C(23)-C(28)-C(30)	3.7(6)
C(24)-C(23)-C(28)-C(30)	-176.2(5)
C(27)-C(28)-C(30)-C(31)	-76.1(6)
C(23)-C(28)-C(30)-C(31)	95.3(6)
C(27)-C(28)-C(30)-C(35)	105.0(6)
C(23)-C(28)-C(30)-C(35)	-83.7(6)
C(35)-C(30)-C(31)-C(32)	1.8(7)
C(28)-C(30)-C(31)-C(32)	-177.2(4)
C(30)-C(31)-C(32)-C(33)	1.1(7)
C(31)-C(32)-C(33)-C(34)	-2.7(8)
C(32)-C(33)-C(34)-C(35)	1.4(8)
C(31)-C(30)-C(35)-C(34)	-3.0(7)
C(28)-C(30)-C(35)-C(34)	175.9(4)
C(31)-C(30)-C(35)-P	175.5(3)
C(28)-C(30)-C(35)-P	-5.6(7)

C(33)-C(34)-C(35)-C(30)	1.5(7)
C(33)-C(34)-C(35)-P	-177.2(4)
C(21)-P-C(35)-C(30)	123.7(4)
C(7)-P-C(35)-C(30)	-125.7(4)
Pd-P-C(35)-C(30)	-3.4(4)
C(21)-P-C(35)-C(34)	-57.7(4)
C(7)-P-C(35)-C(34)	52.8(4)
Pd-P-C(35)-C(34)	175.1(3)
C(40)-N-C(36)-C(37)	-0.4(8)
Pd-N-C(36)-C(37)	178.0(4)
N-C(36)-C(37)-C(38)	1.2(9)
C(36)-C(37)-C(38)-C(39)	-0.8(9)
C(37)-C(38)-C(39)-C(40)	-0.2(8)
C(36)-N-C(40)-C(39)	-0.7(8)
Pd-N-C(40)-C(39)	-179.0(4)
C(38)-C(39)-C(40)-N	1.0(8)
C(44)-O(8)-C(41)-C(42)	-6.9(8)
O(8)-C(41)-C(42)-C(43)	14.4(11)
C(41)-C(42)-C(43)-C(44)	-20(2)
C(42)-C(43)-C(44)-O(8)	17(3)
C(41)-O(8)-C(44)-C(43)	-3.7(19)
C(48)-O(9)-C(45)-C(46)	-38.9(9)
O(9)-C(45)-C(46)-C(47)	36.4(8)
C(45)-C(46)-C(47)-C(48)	-24.6(8)
C(45)-O(9)-C(48)-C(47)	23.6(9)
C(46)-C(47)-C(48)-O(9)	1.8(9)

Appendix B

Supplementary Information

Linear Polyethylene with Tunable Surface Properties by Catalytic Copolymerization of Ethylene with N-Vinyl-2-pyrrolidinone and N-Isopropylacrylamide

K. M. Skupov, L. Piche, J. P. Claverie

Macromolecules, 2008, 41 (7), 2309–2310

B.1 Experimental techniques

B.1.1 Materials

All the monomers except ethylene were spiked with the radical inhibitor BHT (2,6-di-tert-butyl-4-methyl-phenol, 2 mg/g) to exclude the possibility of monomer radical homopolymerization. Under the reaction conditions described below, no polymerization was observed in the absence of catalyst. All chemicals were purified using standard Schlenk procedures and handled under inert atmosphere. Catalyst 1 was prepared according to reference 11 in Chapter 5.

B.1.2 Standard polymerization

Catalyst 1 (30 mg, 0.05 mmol) and N-vinyl-2-pyrrolidinone (20 g, 0.18 mol) were dissolved in 150 mL of toluene in a dry box. Depending on the amount of catalyst, the solution may contain small amounts of undissolved catalyst. The mixture was introduced through a wide-bore cannula into a 400 mL stainless steel reactor. Ethylene was introduced at 300 psi and the mixture was heated at 95 °C under stirring (1000 rpm). After 3 hours the reactor was slowly degassed. The polymer was precipitated from methanol. The unreacted monomer was removed by Soxhlet extraction with methanol except when the amount of polymer collected from the reactor was less than 100 mg. In this case, the polymer was purified by intensive washing with water and methanol over a fritted glass filter. The polymer was then dried in vacuo.

B.1.3 Polymer characterization.

Melting points of the polymers were found by DSC using Perkin Elmer DSC7 (heating rate 5 °C/min). The reported T_m is the maximum of the melting transition in the second heating cycle. Relative crystallinity was calculated from enthalpies of melting for copolymers and pure PE by dividing the enthalpy of melting by the theoretical value of 294 J/g which corresponds to the heat of melting of a 100 % crystalline PE (reference 12). NMR spectra were recorded in d^4-*o*-dichlorobenzene at 115 °C and 85 °C (for the polymers which were soluble at this temperature) using NMR Varian 300 MHz and 600 MHz. Quantitative ^{13}C NMR were obtained by accumulation of more than 5000 scans, using an inverse 5 mm probe (pulse angle 22°, recycling delay 10 s, ungated decoupling).

Assignments were based on ref. Soula, R.; Saillard, B.; Spitz, R.; Claverie, J.; Llaurro, M. F.; Monnet, C., *Macromolecules*, **2002**, 35, 1513-1523. IR spectra were recorded using pellets of KBr on FTIR Nicolet 4700, Thermo Instruments Inc. Water contact angle was measured with a sessile drop using VCA-Optima Surface Analysis System with drop volume 0.5 μm and at least 3-7 measurements for each sample before and after water vapor treatment.

Solvent-cast films were prepared by solubilization of the polymers in refluxing chlorobenzene (1-5 g/L) and application to glass slide. The solvent was evaporated in a fume hood for 30 minutes, and a second layer of the polymer solution was then applied in order to make the film thicker. For the water vapor treatment, the films were put into contact with water vapor for 2 h in a confined vessel containing water at 95 °C. The films were then dried in a vacuum oven for 16 h.

Table B.1: Additional polymerization data.

expt.	monomer	$m_{mon.}$, g	catalyst, 1 mg	toluene solvent, ml	pressure, psi	time, h	T_m, °C	contact angle (°)	incorporation, mol%	$m_{pol.}$ g
1	none	0	5	200	300	2	129.3	121.9	-	29.3
2	NVP	20	36	200	350	3	128.0	109.8	~0	9.7
3	NVP	40	31	150	400	3	127.7	109.1	0.3	5.2
4	NVP	105	30	100	300	72	119.8	105.7	1.2	6.5
5	NVP	157	33	20	350	50	115.1	101.3	2.0	2.0
6	NVP	52	15	150	150	3.5	107.5	nd	2.6	0.081
7	NIPAM	17	30	200	420	6	111.7	112.3	3.2	1.6
8	NIPAM	25	20	150	200	4	nd	109.7	4.1	0.080

B.2 Spectroscopy characterization of polymers

(for assignments see NMR spectra section below).

B.2.1 NMR assignments

P(E-co-NIPAM) (expt. 7)

^{1}H NMR (ODCB): δ = 5.72 (m, CH_2=C<u>H</u>-), 5.34 (m, -C<u>H</u>=C<u>H</u>-), 5.01 (m, C<u>H</u>$_2$=CH-), 4.04 (m, C<u>H</u>$(CH_3)_2$), 1.91 (m, -CH_2-C<u>H</u>-CH_2-), 1.62 (m, -C<u>H</u>$^1H^2$-CH-C<u>H</u>$^1H^2$-), 1.26 (m, CH_2 "PE"), 1.04 (m, -CH(C<u>H</u>$_3)_2$), 0.83 (m, terminal CH_3).

^{13}C NMR (ODCB): δ = 174.0 (C=O), 48.0 (NCH), 41.0 (-CH_2<u>C</u>HCH_2-), 33.3 (CH_2 (A)), 29.8 (CH_2, ("PE")), 27.7 (CH_2(B)), 22.7 (CH_3).

IR (KBr): 3299, 2917, 2949, 1696, 1684, 1701, 1640, 1546, 1473, 1365, 1248, 1173, 1130, 908, 730 cm^{-1}.

P(E-co-NVP) (expt. 5)

^{1}H NMR (ODCB); δ = 5.73 (m, CH_2=C<u>H</u>-), 5.35 (m, -C<u>H</u>=C<u>H</u>-), 4.89 (m, C<u>H</u>$_2$=CH-), 4.09 (m, CHN), 3.03 (m, CH_2(a)), 2.18 (m, CH_2 (c)), 1.96 (m, =CH-CH_2-), 1,74 (m, CH_2, (b)), 1.36 (m, CH_2 (A)), 1.26 (CH_2 ("PE")), 0.96 (m, CH_3 (branch)), 0.83 (m, CH_3, (chain end)).

^{13}C NMR (ODCB): δ = 173.5 (C=O), 138.9 (CH_2=C<u>H</u>-), 131.7 (CH_3-CH=<u>C</u>H-), 130-125 (ODCB and -<u>C</u>H=<u>C</u>H-), 124.3 (CH_3-<u>C</u>H=CH_2-), 51.0 (N<u>C</u>H), 41.8 (CH_2 (a)), 37.3 (CH_2 (β)), 33.7 (-<u>C</u>H_2-CH=CH_2), 32.9 (CH (α)), 32.7 (CH_2 (A)), 32.6 (-<u>C</u>H_2-CH=CH-), 31.9 (CH_2, S3), 31.3 (CH_2 (c)), 30.1 (CH_2 (δ)), 29.8 (CH_2, ("PE", b_1, b_3)), 29.6 (CH_2 (a_3)), 29.5 (CH_2 (C)), 29.4 (CH_2 (S4)), 29.3 (CH_2 (b_3)), 29.2 (CH_2 (a_2)), 29.0 (CH_2 (a_1)), 27.2

(CH_2 (γ)), 26.5 (CH_2 (B)), 22.6 (CH_2 (S2)), 19.7 (*CH3 branch), 18.6 (CH_2 (b)), 17.5 ($\underline{C}H_3$-CH=CH-), 13.9 (CH_3 (S1)).

IR (KBr): 2919, 2849, 1969, 1473, 1421, 1283, 730, 719 cm^{-1}.

B.2.2 DSC curves

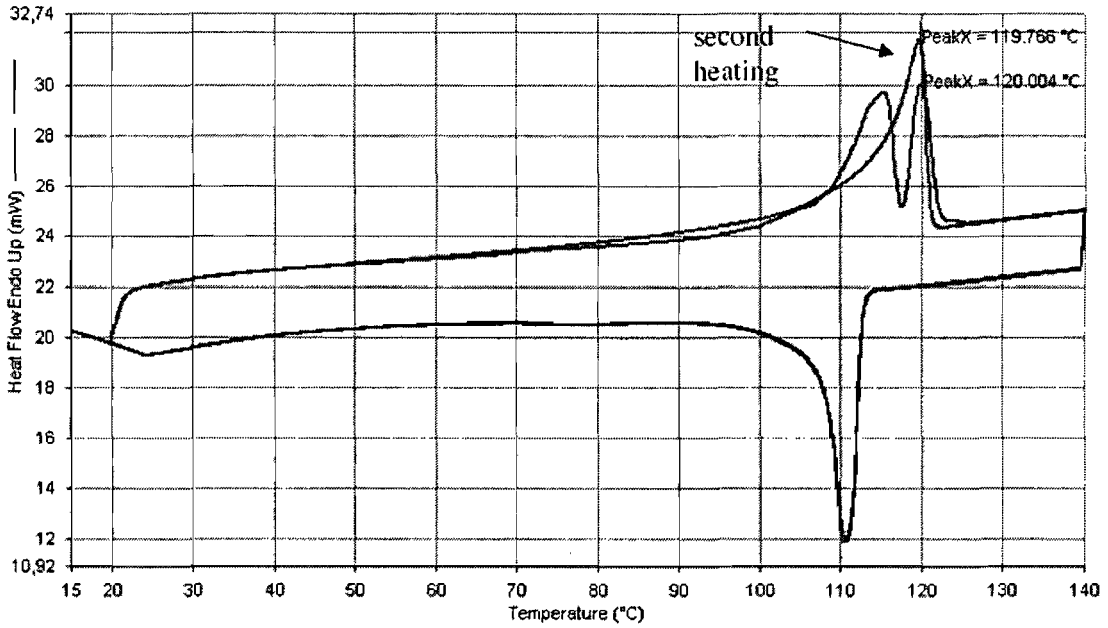

Figure B.1: DSC of expt.4 (PE-co-NVP).

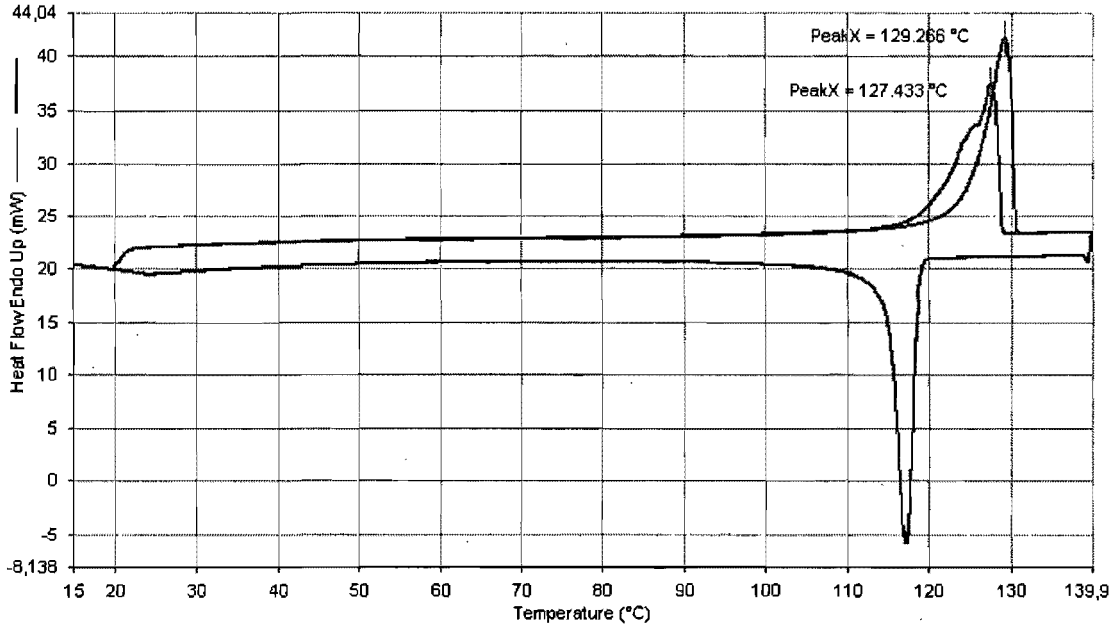

Figure B.2: DSC of expt.1 (pure PE).

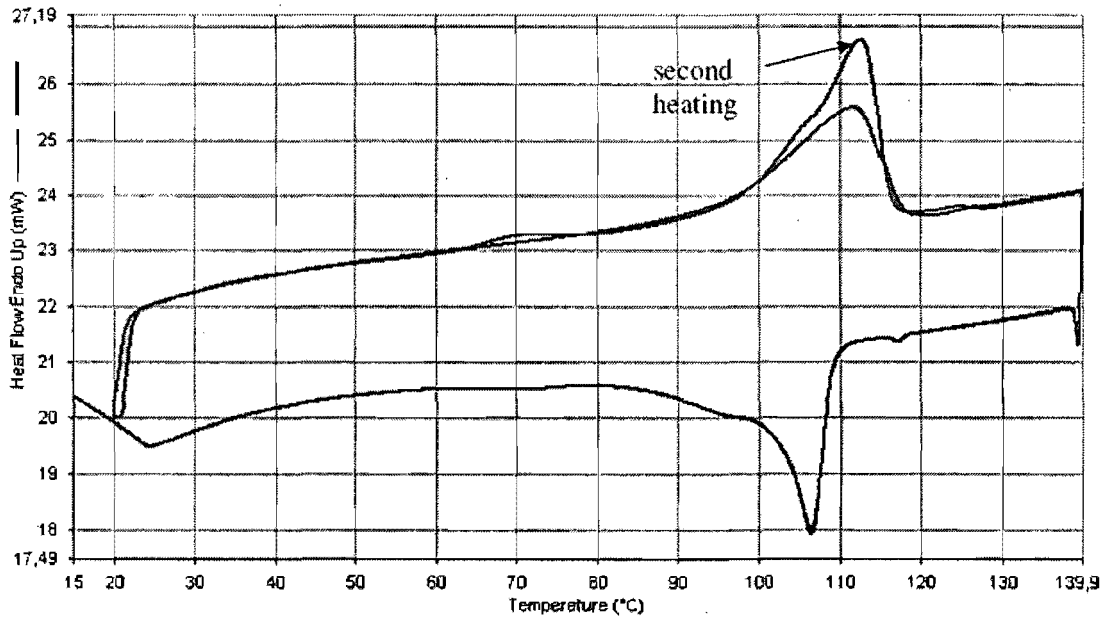

Figure B.3: DSC of expt. 7 (PE-co-NIPAM).

B.2.3 IR spectra

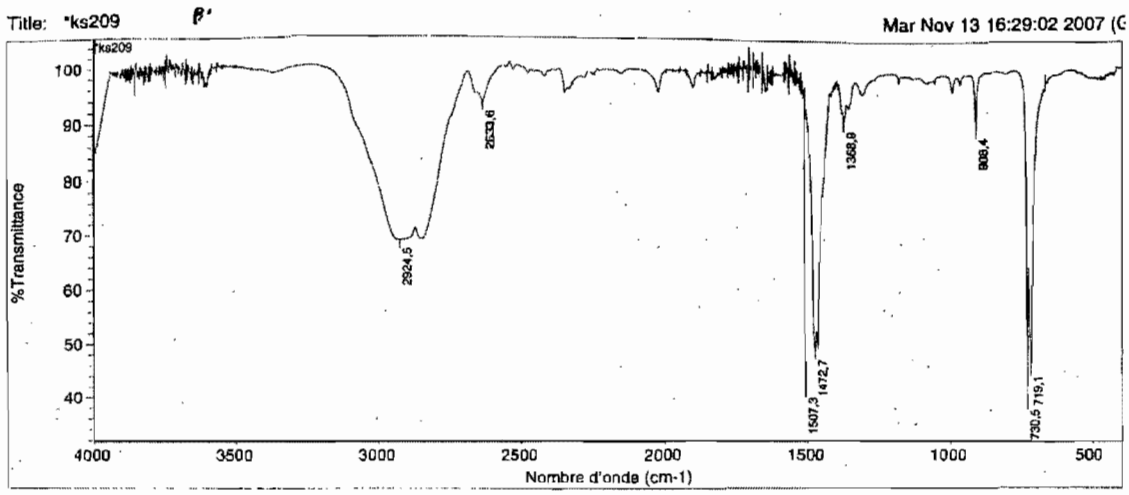

Figure B.4: IR of pure PE.

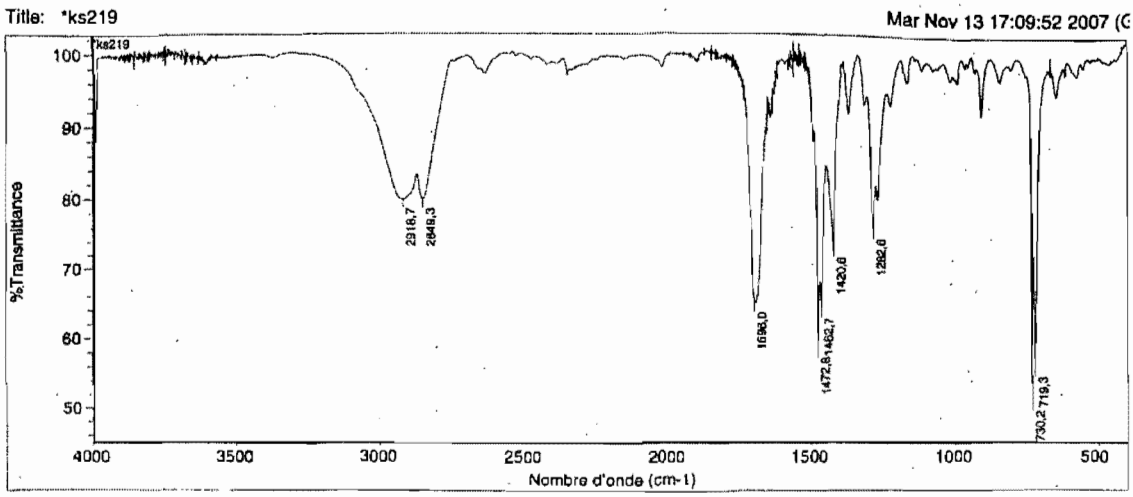

Figure B.5: IR of poly(E-co-NVP), expt. 5.

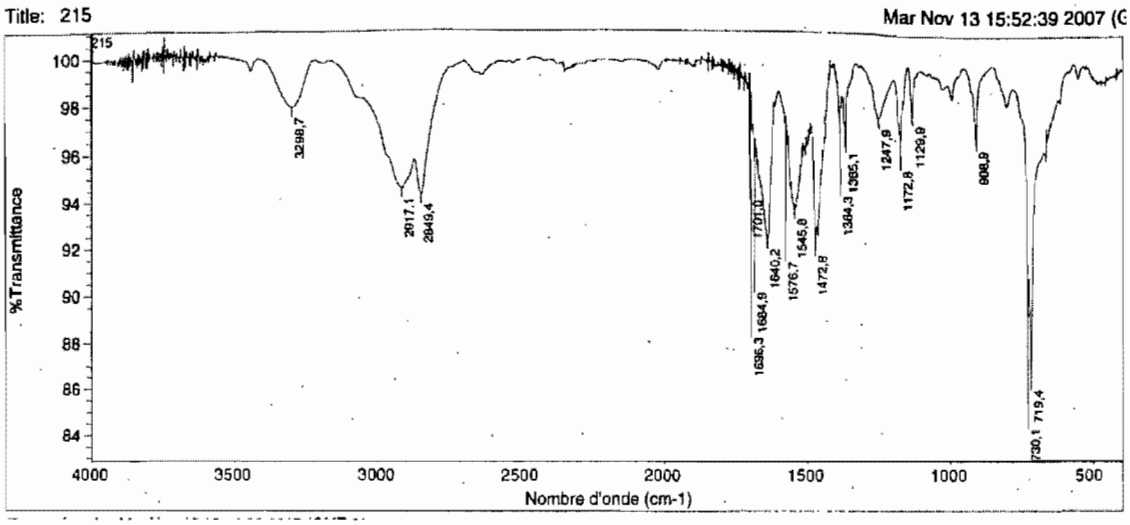

Figure B.6: IR of poly(E-co-NIPAM), expt. 7.

B.2.4 NMR Spectra

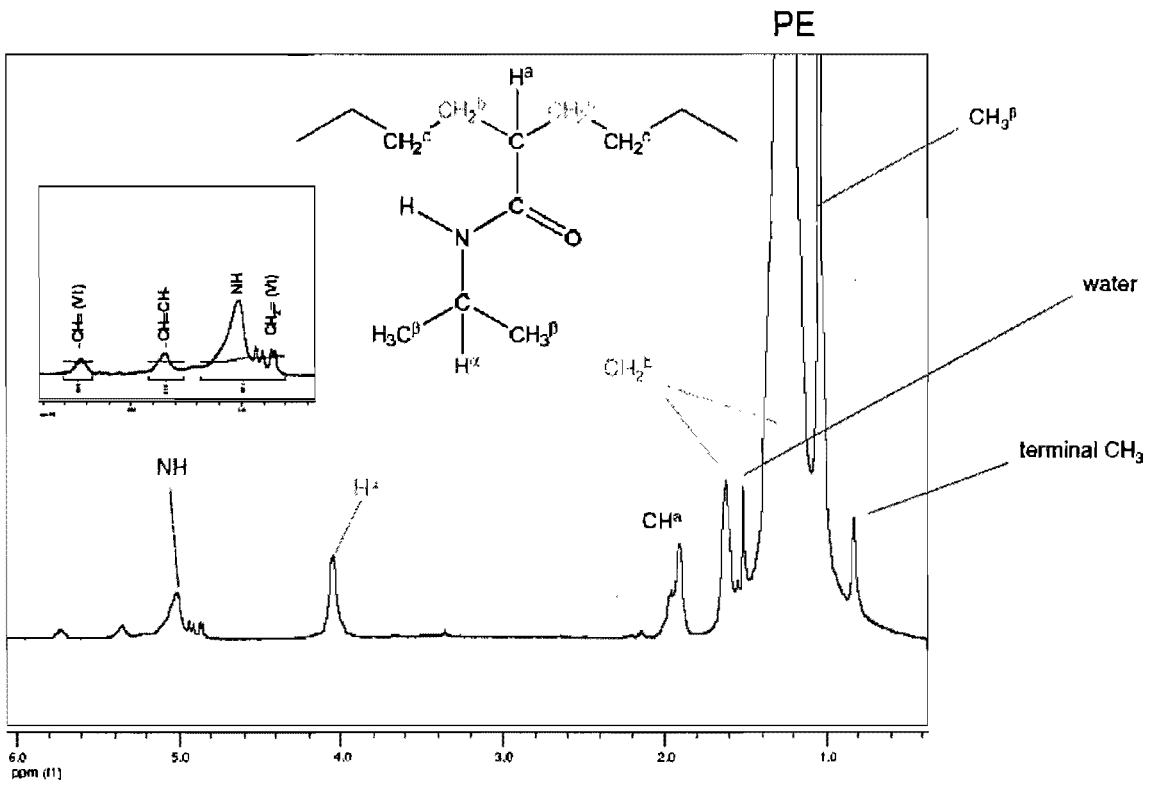

Figure B.7: Proton NMR of poly(ethylene-co-NIPAM) (experiment 7).

The $CH_2{}^b$ have 2 pairs of enantiotopic protons, one of which has a resonance masked under the PE peak and the second is partially overlapping with PE peak.

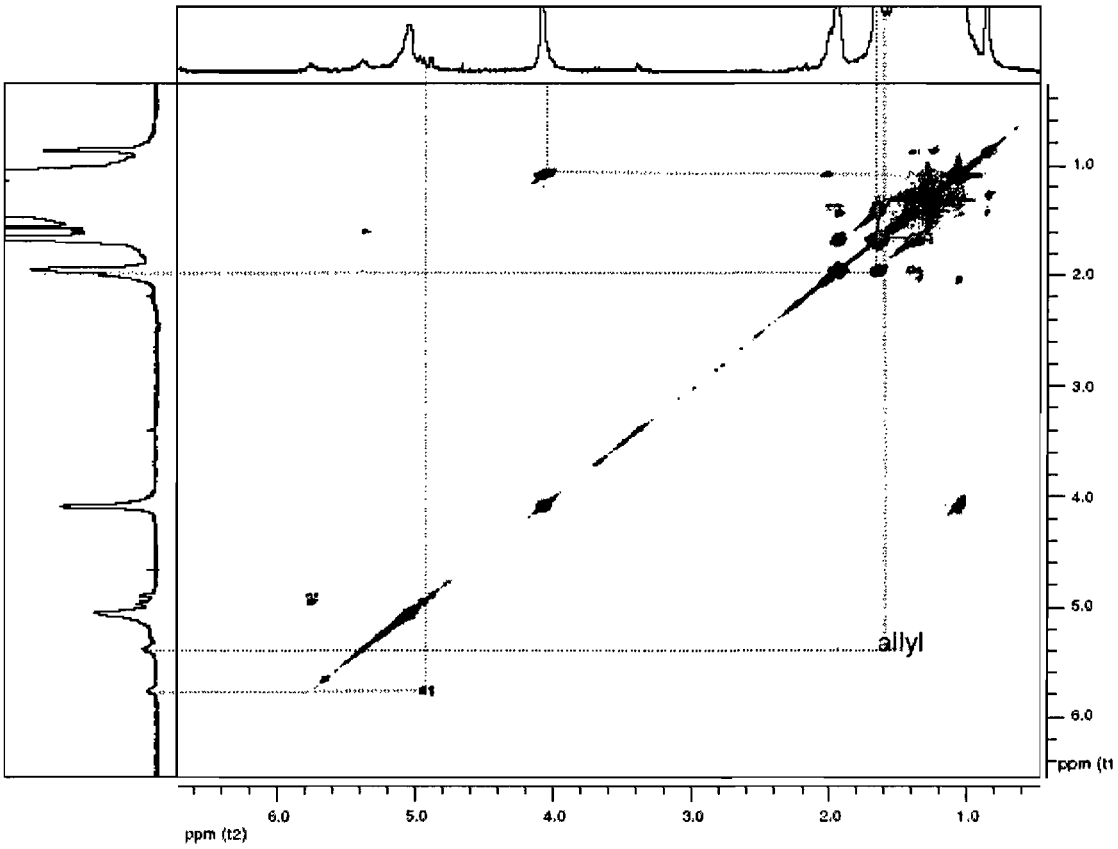

Figure B.8: COSY of poly(ethylene-co-NIPAM) (expt. 7).

Note the allyl peak is masked by the CH_2^b resonance.

Note the coupling between the two enantiotopic protons CH_2^b and $CH_2^{b'}$(red lines).

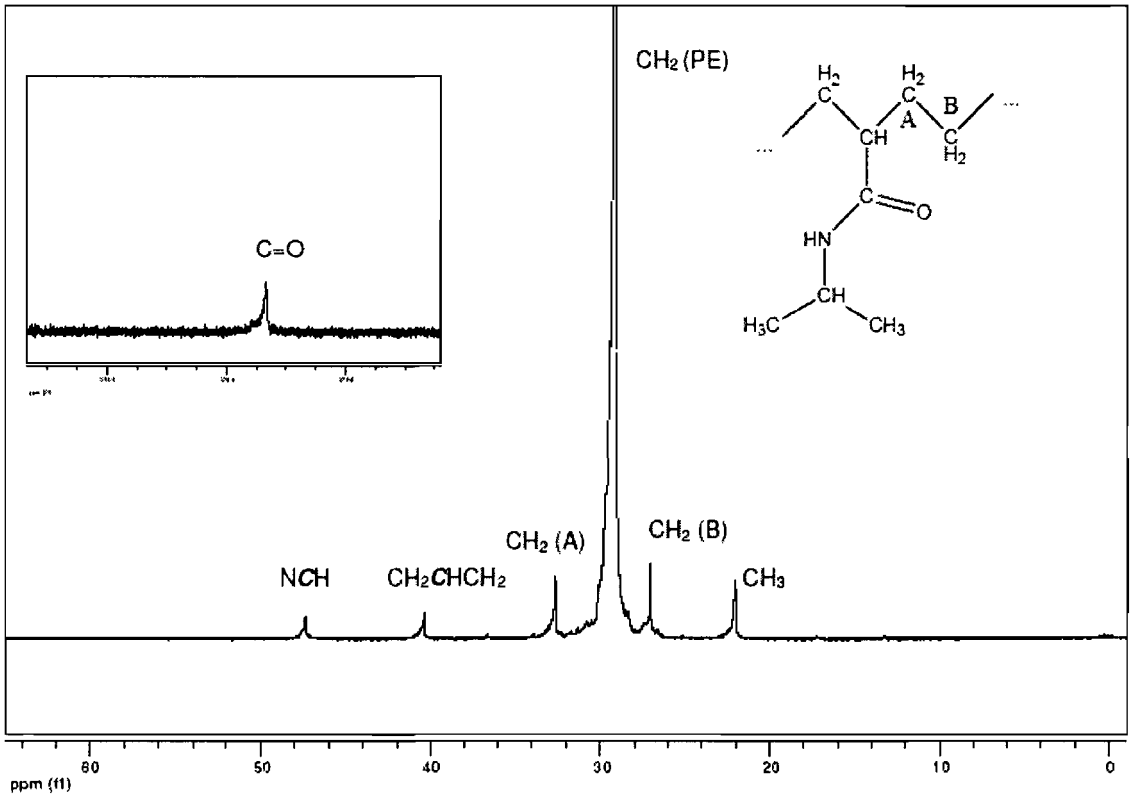

Figure B.9: ^{13}C NMR of poly(ethylene-co-NIPAM) (expt. 7).

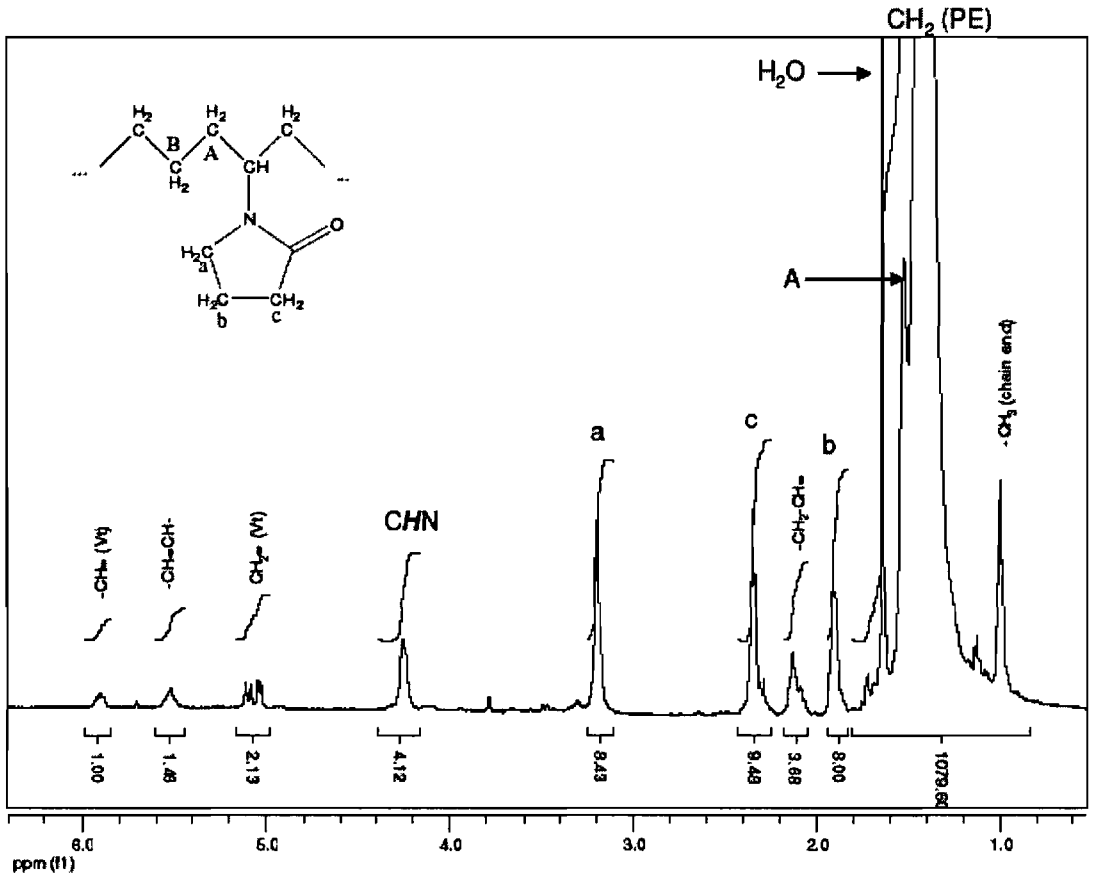

Figure B.10: Proton NMR of poly(ethylene-co-NVP) (experiment 5).

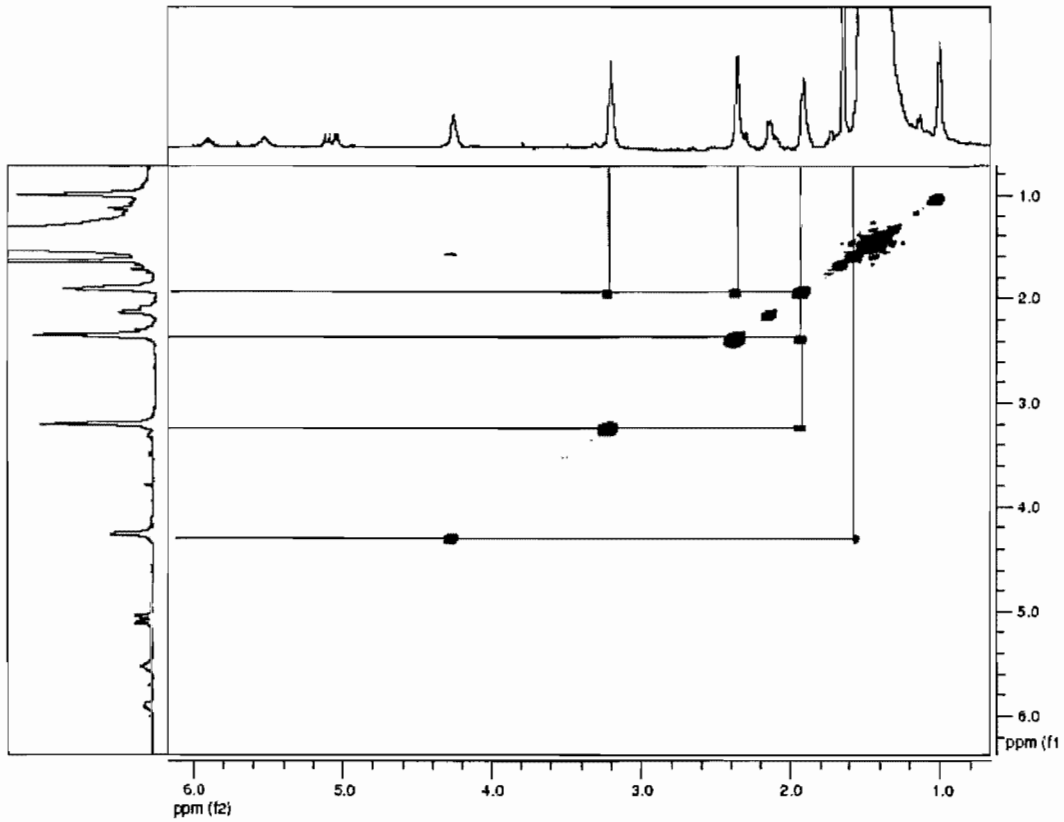

Figure B.11: COSY of poly(ethylene-co-NVP) (experiment 5).

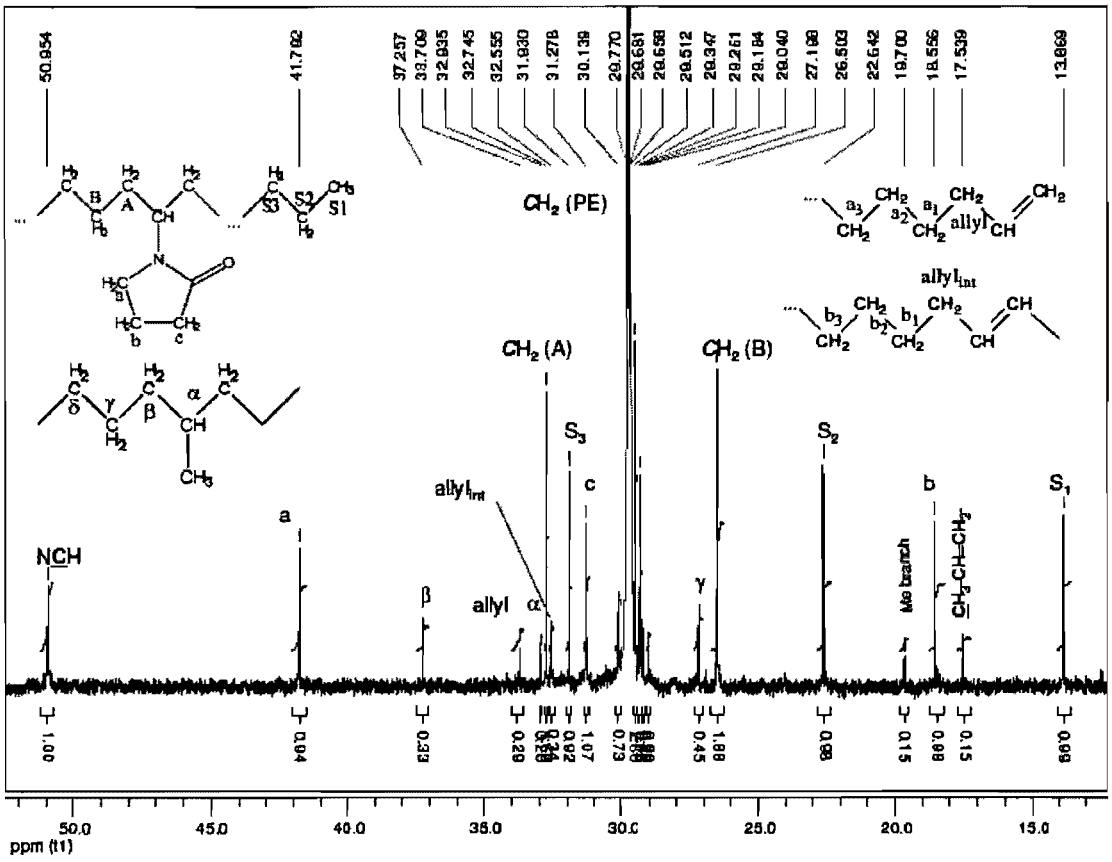

Figure B.12: ^{13}C NMR of poly(E-co-NVP) (polymer prepared at 95 ^{o}C, experiment 5).

Amount of Me branches : < 1 branch for 1000 C. For zoom of the "PE region" see below

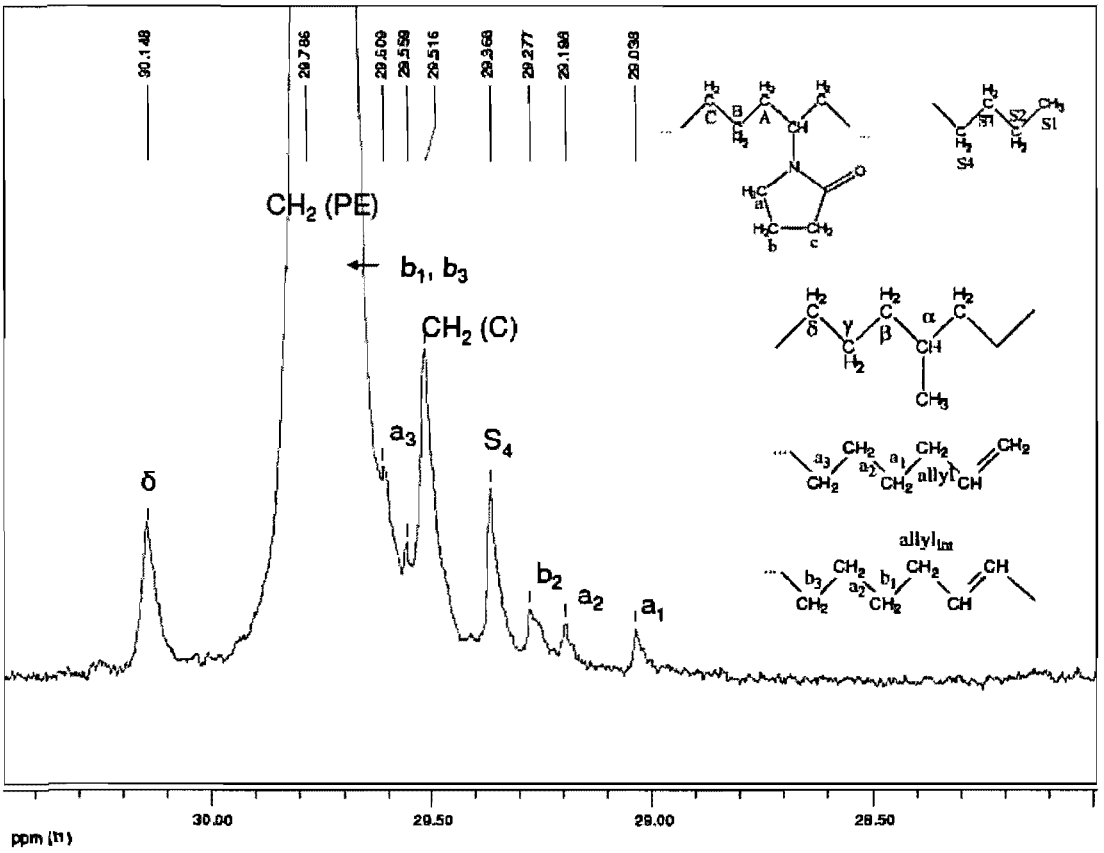

Figure B.13: Zoom of the "PE region" in ^{13}C NMR of poly(E-co-NVP) (expt. 5).

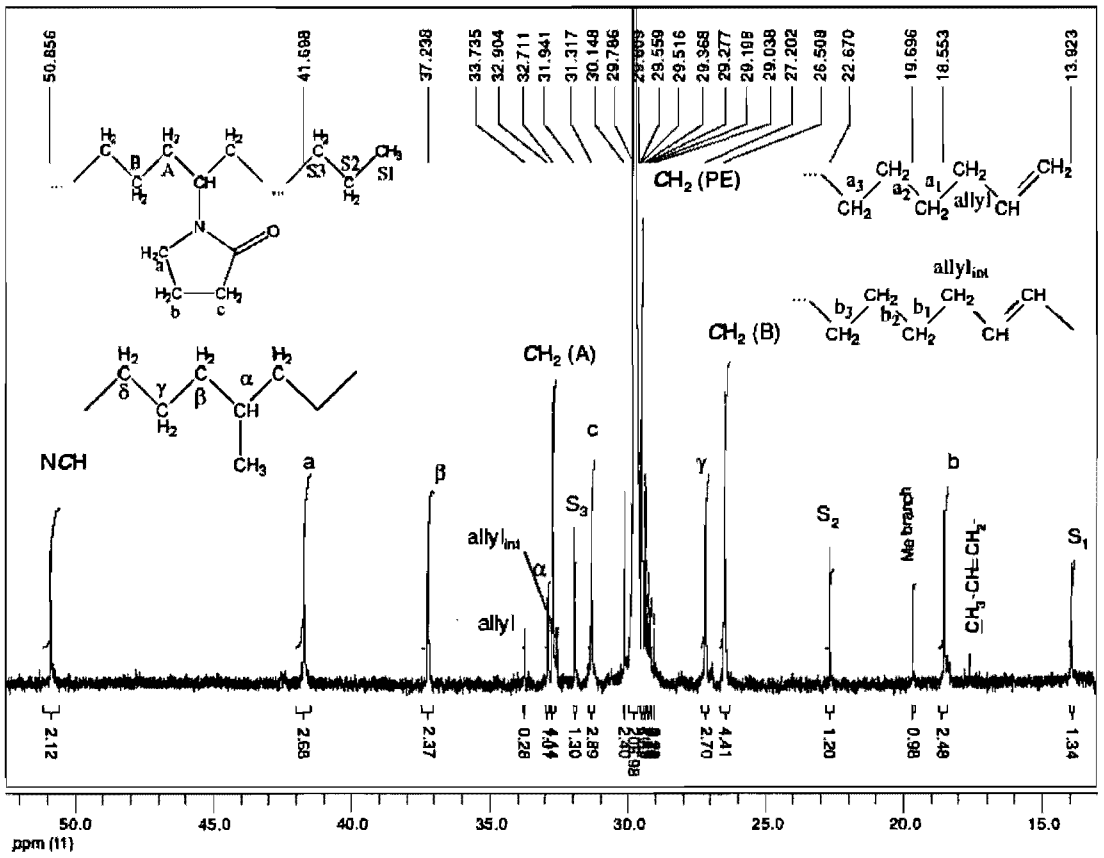

Figure B.14: ^{13}C NMR of poly(E-co-NVP), polymer prepared at 115 °C (Experiment 6).

5 Me branches for 1000 C (for zoom of the PE region, see below)

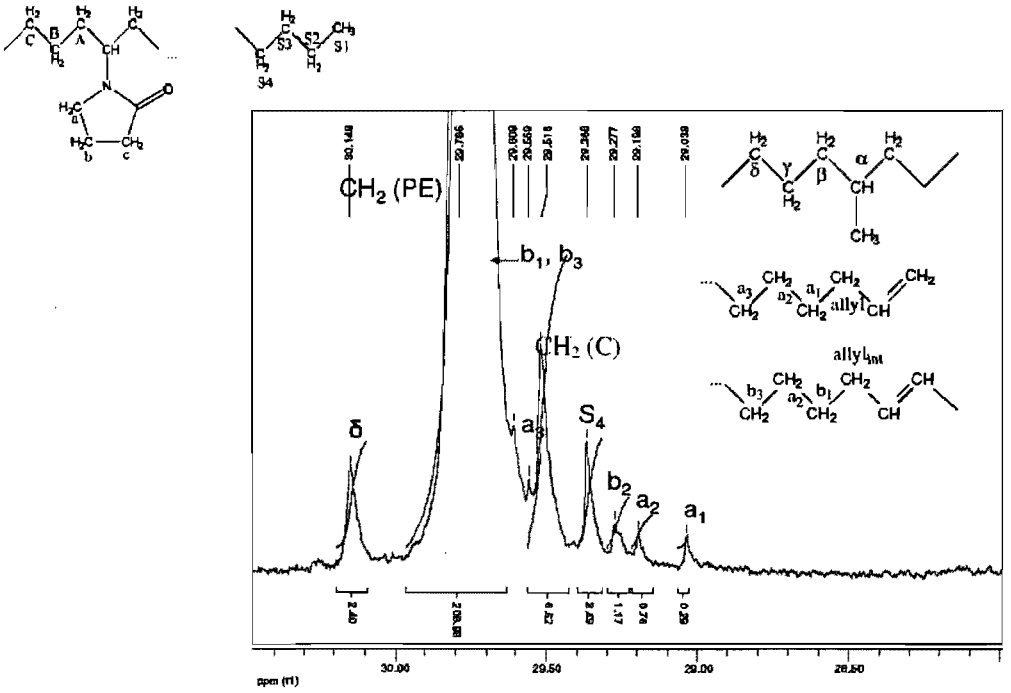

Figure B.15: Zoom of the "PE region" for polymer poly(E-co-NVP) prepared in expt. 6.

Appendix C

Supplementary Information

Kinetic and mechanistic aspects of ethylene and acrylates catalytic copolymerization in solution and in emulsion

K. M. Skupov, J. Hobbs, P. Marella, D. Conner, S. Golisz, B. L. Goodall, J. P. Claverie

Macromolecules, ASAP, doi: 10.1021/ma9o1210u.

C.1 Kinetic Analysis of Ethylene Homopolymerization

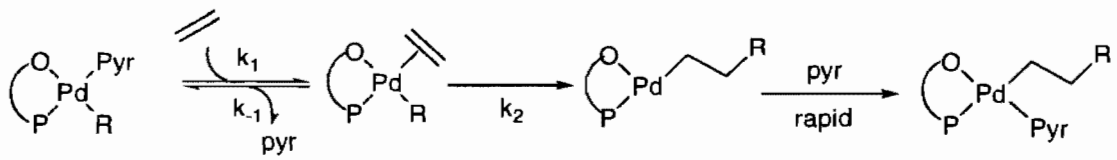

The rate of ethylene insertion is given by

$R = k_2 [PdE]$ where PdE is the palladium bound to ethylene. (C.1)

Quasi steady state approximation on PdE yields :

$$k_1 [Pdpyr][E] = k_2 [PdE] + k_{-1} [PdE][pyr] \quad (C.2)$$

which can be rewritten as

$$[PdE] = \frac{k_1 [Pdpyr][E]}{k_2 + k_{-1} [pyr]} \quad (C.3)$$

Using the mass conservation equations on Pd and pyr, on finds :

$[PdE] + [Pdpyr] = Pd_0$

$[pyr] + [Pdpyr] = Pd_0$ and therefore,

$[PdE] = [pyr]$ and $[Pdpyr] = Pd_0 - [pyr]$

Equation 3 can thus be written using [pyr] and [E] as sole concentration variables :

$$[pyr] = \frac{k_1 (Pd_0 - [pyr])[E]}{k_2 + k_{-1} [pyr]} \quad (C.4)$$

Knowing [E] (fixed under our experimental conditions), one can solve equation (C.4) :

$$[pyr] = \left(\frac{k_1[E]+k_2}{k_{-1}}\right)\frac{\sqrt{1+4\frac{k_1 k_{-1}[E]Pd_0}{(k_1[E]+k_2)^2}}-1}{2} \qquad (C.5)$$

Thus

$$R = k_2\left(\frac{k_1[E]+k_2}{k_{-1}}\right)\frac{\sqrt{1+4\frac{k_1 k_{-1}[E]Pd_0}{(k_1[E]+k_2)^2}}-1}{2} \qquad (C.6)$$

and

$$TOF = \frac{k_2}{Pd_0}\left(\frac{k_1[E]+k_2}{k_{-1}}\right)\frac{\sqrt{1+4\frac{k_1 k_{-1}[E]Pd_0}{(k_1[E]+k_2)^2}}-1}{2} \qquad (C.7)$$

Using equation (C.7), it is possible to calculate TOF and compare it to experimental values of TOF. This was done using a initial set of constants k_1, k_{-1} and k_2. This initial choice is important to ensure convergence of the non linear optimization. For k_1, our initial guess was based on the knowledge of the rate constant for pyridine displacement by pyridine ($k \sim 2.3\ 10^5$ L/mol/s at 100 °C, calculated from the activation parameters found by VT NMR, as described in the paper). For k_{-1}, we assumed that the reaction was diffusion controlled ($(k_{-1} \sim 10^9$ L/mol/s). For k_2, the initial value was chosen by assuming that K_m is constant, that is to say there exists a linear relationship between the inverse of the activity and the inverse of ethylene concentration:

$$\frac{1}{TOF} = \frac{1}{TOF_{max}} + \frac{K_m}{TOF_{max}} \frac{1}{(C_2H_4)} \qquad (C.8)$$

Determination of an initial value for k_2

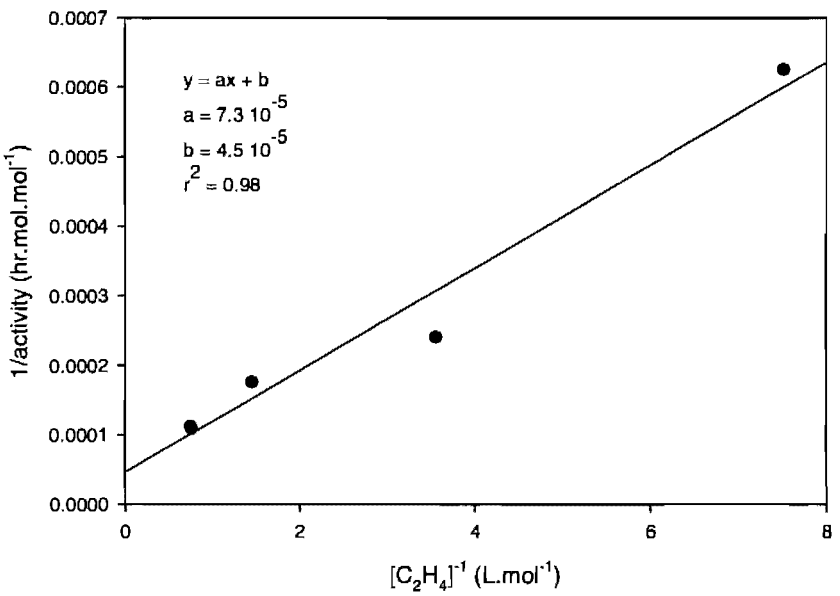

Inverse of the activity vs. inverse of the C_2H_4 concentration for C_2H_4 homopolymerization by catalyst **2b** (see experimental conditions in Table 2). The value of the maximum activity when all the catalyst molecules are bound to C_2H_4 is read at the y-intercept: TOF_{max} = 2.2 10^5 mol mol^{-1} hr^{-1}, therefore k_2 = 61 s^{-1}.

Figure C.1: Determination of an initial value for k_2.

Thus the initial choice for the constants was $k_2 = 61\ s^{-1}$, $k_{-1} \sim 10^9$ L/mol/s and $k_1 \sim 2.3\ 10^5$ L/mol/s. After optimization (Generalized Reduced Gradient, GRG2) one finds $k_2 = 102\ s^{-1}$, $k_{-1} = 10^8$ L/mol/s and $k_1 = 5.5$ L/mol/s.

Appendix D

Supplementary Information

Principal characterization methods used in this work.

For the completion of this research work, I have been exposed to numerous characterization techniques. Most of them are standard techniques (IR, NMR, GPC, microscopy, etc...) presented in elementary chemistry textbooks. Specific conditions of use for these methods can be found in the experimental sections of each article. The methods which are detailed below are those that require special care, or where the procedure used for this work departs from the usual procedure, for reasons explained within the text.

D.1 Quantitative analysis by NMR

Quantitative data on structural properties of the polymer, (such as information about stereochemical configuration or tacticity, geometrical isomerism, regioirregularity and monomer sequences in the polymer) can be obtained by analysis of NMR spectra. Many books and monographs on the NMR spectroscopy of polymers exist, starting with key textbook of Bovey[1] and other references.[2, 3] Spectra for quantitative analysis of polymers should be recorded with extremely high precision.

When the data is acquired by pulsed FT method, considerations of T_1 relaxation time become of importance for quantitative measurements. Factors such as the flip angle (pulse width) and the pulse repetition time must be considered. An example of this influence, the works of Hatada *et al.*[4] can be considered in which the effects of flip angle and pulse repetition time on relative NMR peak integrals was studied. For this purpose a series of ^1H NMR spectra were recorded for polymethylmethacrylate, prepared by radical

route in $CDCl_3$ at 55 °C. Flip angles of 16°, 45° and 90° were examined. At a flip angle 16°, the integrals of signals due to OCH_3 and CH_2 groups were very close to the theoretical value even at a low pulse repetition time (0.2 s). When the flip angle was 90° and the pulse repetition time was 6 s, a value about 5 times higher than T_1, the integral of the signal due to OCH_3 groups was at about 97 % of the theoretical value. However, the value reached the theoretical one with a repetition time of 10 s. With a flip angle of 45°, both values reaches almost theoretical level in 6 s. This work shows that for quantitative analysis a small flip angle as possible should be selected (but keeping signal to noise ratio high) with long pulse repetition times. Usually the optimal flip angle and pulse repetition time are found empirically. When the values of T_1 are very different for different protons in the same molecule, the longer repetition times, up to 5 times longer the highest T_1, may be required for accurate quantitative analysis of spectra. In general, small flip angles allow to work with short repetition time but decrease the signal intensity. Large flip angles would increase the peak intensity but longer pulse repetition times should then be applied.

For obtaining the fine structure of the spectrum (by ^{13}C NMR), the digital resolution should be optimized, by increasing the number of data points or reducing as much as possible the spectral width. Digital resolution and acquisition time are linked together (Nyquist theorem):

$$\text{Acquisition time, (s)} = N/2\Delta \qquad \text{(D.1)}$$

$$\text{Digital resolution (Hz)} = 2\Delta/N \qquad \text{(D.2)}$$

where N is the number of data points and Δ is the spectral width.

Worries about resolution tend to disappear with the use of NMRs of higher frequencies. For quantitative ^{13}C NMR, apodization techniques are usually avoided, as they can create artefacts. For example, zero filling tends to distort the baseline, generating 'oscillations' usually referred as sinc-wiggles. In addition, it is not always desirable to increase digital resolution and collection time. For many polymers the FID decays quite fast because of the very short T_2^* (broad peaks). Increasing the digital resolution results in collecting long sequences of FID with near zero signal, and therefore resulting in acquiring regions which contains only noise.

Another issue in quantitative polymer NMR (especially in ^1H NMR) is the ability to detect simultaneously and accurately large and small resonances. For example, ^1H NMR is often used for end-group analysis and for determining M_n. In this case, signal to noise is a key parameter, because M_n will be obtained via the ratio of the integral of main chain protons (large number) to end-group protons (small number). This parameter is related to signal over noise (S/N), as S/N is calculated from the ratio of the largest peak to baseline in NMR. Probes are characterized by their sensitivity, highly sensitive probes being instrumental for the detection of biological samples in low concentration. Most ^1H NMR sequences start by an adjustment of the gain. For polymer samples, the main chain protons being concentrated, the gain is set to a low value (i.e. low sensitivity mode), and the ability to detect the smallest resonances can be lost, even when the probe has a very high intrinsic sensitivity. This issue is an instrumental problem which cannot be improved by changing the sequence.

Routine procedures and parameters for quantitative ^{1}H and ^{13}C NMR of polymers have been exhaustively described in literature.[5-7] The relaxation delay is usually set to be 5 times the longest T_1 for a pulse of 90°. We most often used a pulse of approx 30°, which allows to work with shorter delays. For polyethylene, the T_1 in ^{13}C NMR was found to be 1050 ms at 116 °C.[6]

PARAMETERS FOR ^{1}H NMR :

Number of points: 16 K or 32 K

Pulse angle: 20 – 45°

Recycling delay: 10 s – 20 s

Number of scans: 16 – 128

Concentration of the polymer: 5 – 15 mg/mL

Temperature and solvent: 20 – 120 °C; chloroform, o-dichlorobenzene.

The ^{13}C analysis can be quantitative if one allows all carbon to relax completely, and if all carbons are decoupled without NOE enhancement using the same decoupling power. This can be achieved using a gated decoupling where the ^{1}H irradiation is turned off during the FID collection (see below). Care must be applied to irradiate uniformly across the ^{1}H range. With modern routine NMR instruments, this can be difficult. It is often necessary to set the decoupler frequency on the methylene peaks of polyethylene, resulting in a ^{13}C NMR spectrum which will be quantitative for methylene carbons (and often methyl and methyne carbons). Then, if necessary, another spectrum can be recorded

where the decoupler frequency is set in another region (for example aromatic region for poly(ethylene-co-styrene)), resulting in a quantitative analysis for the aromatic carbons.

PARAMETERS FOR ^{13}C QUANTITATIVE NMR:

Number of points: 16 K or 32 K

Pulse angle: 20 – 45°

Recycling delay: 10 s

Number of scans: 5000 - 10000

Decoupling power (turned off during acquisition): gated decoupling power

Concentration of the polymer: 5 – 50 mg/mL

Temperature and solvent: 20 – 120 °C; chloroform, o-dichlorobenzene

D.2 Differential scanning calorimetry

Differential scanning calorimetry (DSC) is an instrumental technique where a sample of interest is heated together with a reference sample in a controlled fashion. DSC analysis of polymers provides much information about its properties and structure in the bulk, yielding heat capacities (C_p), melting points (T_m), glass transition temperature (T_g), crystallization points (T_c) of the polymers. Evaluation of the kinetics of glass transition of polystyrene can be performed by modulated DSC.[8] The properties of the copolymers of ethylene with propylene,[9] octene,[10] etc. were studied by DSC. DSC can be applied to the studies of latexes,[11] or to dispersed polymers such as for example acrylic latexes.[12]

There exist two main different types of DSC: heat-flux and power compensated DSC. The schemes of two designs are shown in Figure D.1.

In power-compensated DSC, the sample and the reference are located in different furnaces. The difference in energy required to maintain equal temperature in both DSC capsules is measured. The heat-flux design of DSC includes only one furnace with sample and reference capsules connected by a heat-flow path. The change in heat capacity of the sample generates a temperature difference (ΔT) between the sample and the reference capsules. The temperature difference is measured and correlated with the enthalpy or heat capacity of the sample using calibration experiments. The DSC used for the completion of this work is a power compensated instrument with modulation.[13]

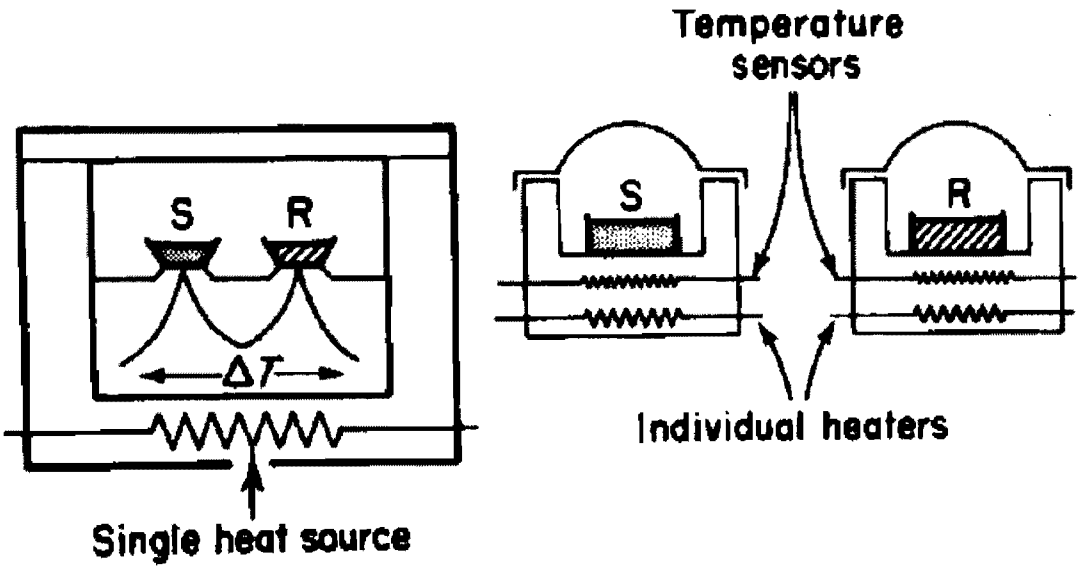

Figure D.1: Heat-flux (left) and power-compensated (right) designs of DSC.[14]

Glass transition is a second order transition, which translates into a step (and not a peak) into the DSC thermogram (heat flux vs temperature). Practically, when heating a sample at T_g, glassy parts of the polymer become "unfrozen", resulting in a subsequent relaxation toward the most stable conformation of the polymeric chain. Thus, enthalpic relaxations phenomena are often observed after heating past the T_g, especially on the first heating ramp. Sometimes, chains can start to crystallize after passage through the T_g, resulting in an exothermic crystallization peak.

Upon heating the sample further, the melting transition may appear when the entire polymer becomes a liquid phase. This process generates an inversed peak (comparatively to crystallization peak) on a DSC thermogram due to the endothermicity of the process.

Besides measuring T_g and T_m, DSC can be used to assess polymer crystallinity. A polyolefin is constituted of two distinct regions: amorphous and crystalline. If one considers a partially crystalline polymer, upon heating in the temperature interval from T_1 to T_2 which includes a melting point T_0 there then it is possible to calculate crystalline fraction (V) in the polymer. T_0 is taken as a point when the entire polymer is melted. A typical form of DSC thermogram is represented in Figure D.2. At first, both the amorphous and crystalline regions are heated and the enthalpy of heating can be represented as $H_a = Vc_c(T_0 - T_1) + (1 - V)c_a(T_0 - T_1)$, where c_c and c_a are the heat capacities for the amorphous and crystalline polymers. The value H_a should be subtracted from the total heat for calculation of V. At the temperature T_0 the crystalline fraction becomes amorphous and the heat of fusion can be represented as $H_b = VH_F$, where H_F is heat of fusion of crystalline fraction.

On the third part of heating in the interval from T_0 to T_2 the heat H_c can be represented as $H_c = c_a(T_2 - T_0)$ as only the amorphous fraction of the polymer is present at this point. The total enthalpy change measured is then $H_{tot}' = H_a + H_b + H_c$, and fraction of crystalline polymer would be $V = (H_{tot} - H_a - H_c)/H_F$.

In 1993, Reading described a new form of DSC called modulated differential scanning calorimetry.

By modulating the temperature during the experiment the information which can obtained from an experiment significantly increases. In this case the temperature does not increase linearly, but it is varies according to equation.

$$T = bt + B \sin(\omega t) \qquad (D.3)$$

where b - heating rate,

B - the amplitude of temperature variation,

ω - frequency of variation

t - time.

So that, the value of dQ/dt would be written as

$$dQ/dt = c_p\, dT/dt + f(t,T) \qquad (D.4)$$

$$dQ/dt = c_p\,(b + B\omega \cos(\omega t)) + f'(t,T) + C \sin(\omega t) \qquad (D.5)$$

where Q – amount of heat

c_p – heat capacity

T – absolute temperature

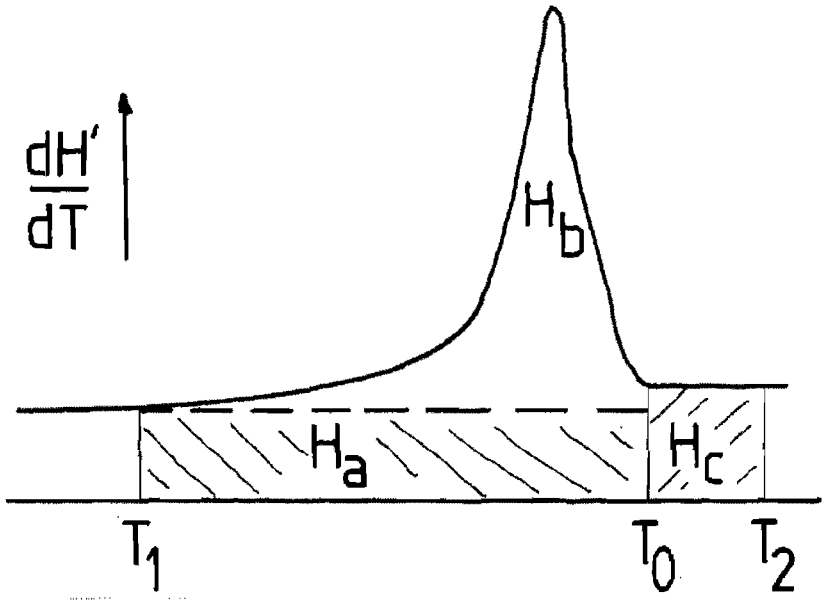

Figure D.2: Typical DSC curve of polymer melting point.[14]

f(t,T) – a function that governs the kinetic response of any physical or chemical transformation.

C – amplitude of the kinetic response to a sine wave modulation

f'(t,T) – a kinetic function after substraction of the sine wave modulation

In these calculations it is assumed that dT/dt is small and that the kinetic response on the sine wave modulation of temperature is linear in all the interval of T and is equal to C sin (ωt).

It is possible to rewrite this equation, considering that f(t,T) consists of 2 parts: the thermodynamic heat flow which depends on dT/dt and can be written as g'(t,T) dT/dt and the kinetically limited heat flow g''(t,T).

Then, the expression for dQ/dt out of sample can be written as:[15]

$$dQ/dt = -dT/dt\,[c_p + g'(t,T)] + g''(t,T) \qquad (D.6)$$

In this equation two contributions to the heat flow are present. One depends on heating rate and the other depends only on T. The heating rate dependent transitions become larger as the heating rate increases. They are reversing transitions (the transition appears by applying alternating heating and cooling). Temperature dependent transitions can not be reversed by heating/cooling and are called non-reversing. For example, heat capacity is a reversing process. The melting is frequency dependent (possesses two characteristics: reversing and non-reversing). Transitions such as cold crystallization, relaxation, decomposition are non-reversing. In heat-flux DSC curves these transitions are

combined. The modulated DSC allows one to separate reversing and non-reversing components of the transitions using a Fourier transformation. Modulated DSC has many useful applications For example, by using modulated DSC it is possible to separate relaxation phenomena from glass transition when the transitions coincide in heat-flux DSC.

For this work, a TA100 mDSC was used to measure melting points and amounts of crystallinity. In typical conditions, we used a heating rate of 5 °C/min with an amplitude of ± 1.5 °C each 60 s. These conditions were found to be favorable to 'remove' most if not all non-reversible phenomena.The amount of crystallinity was however calculated on the basis of the total heat flow, since the melting phenomenon is intrinsically frequency dependent.

D.3 Transmission electron microscopy

Transmission electron microscopy (TEM) is one of the essential tools for characterization of materials. Due to the ease of the electron focusing, the electron diffraction patterns are more widely used than x-ray diffraction patterns, despite the fact that the patterns produced by the X-ray method are more quantitative.

A diagram of the main parts of TEM is represented in Figure D.3. The electron gun producing a monochromatic electron beam is focused into a thin coherent beam by two condenser lenses. Condenser aperture is used to cut all the high-angle electrons, correcting the thickness of the beam. The resulting beam impinges on the surface of the sample. Some parts of the sample absorb electrons, another part of the electron beam is transmitted

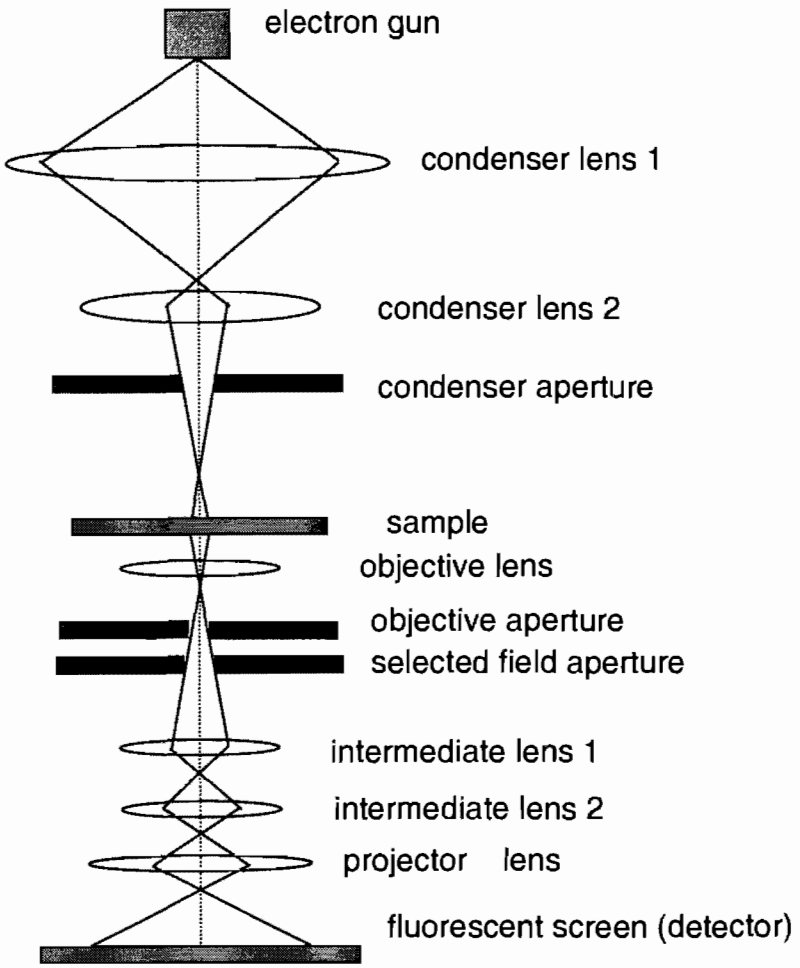

Figure D.3: Scheme of TEM optics.

producing a beam which contains information about the microstructure of the sample. The transmitted beam is focused on an image by the objective lens.

The contrast of the TEM image can be improved by the objective aperture, which restricts the beam and the electrons scattered on high angles are filtered out. The periodic diffraction of the electrons by the ordered structures formed by the atoms can be observed by selected field aperture. Then the beam passes through the column with intermediate lenses, allowing a significant enlarging of the image. Finally, the projector lens produces the resulting image which appears on a phosphorous screen (detector) or on a digital camera. On the screen or the camera, the dark areas correspond to the parts of the sample that have absorbed the electrons. The electron absorption takes place when the area of the sample is thick, dense, or due to the presence of heavy metals (which are used in the background staining in the sample). The light parts of the image correspond to the areas of the sample through which the electrons are transmitted. They correspond to regions in the sample of lower thickness or density. A TEM may operate in different modes, (Figure D.4) such as the dark-field and bright-field imaging. To describe these modes, it is necessary to assume that the illumination system consisting of the electron gun, the condenser lenses and the condenser aperture provides rays parallel to the optical axis. After hitting a specimen, all the diffracted and transmitted rays are collected to give an image on a screen. However, in this simple mode high contrast can not be achieved

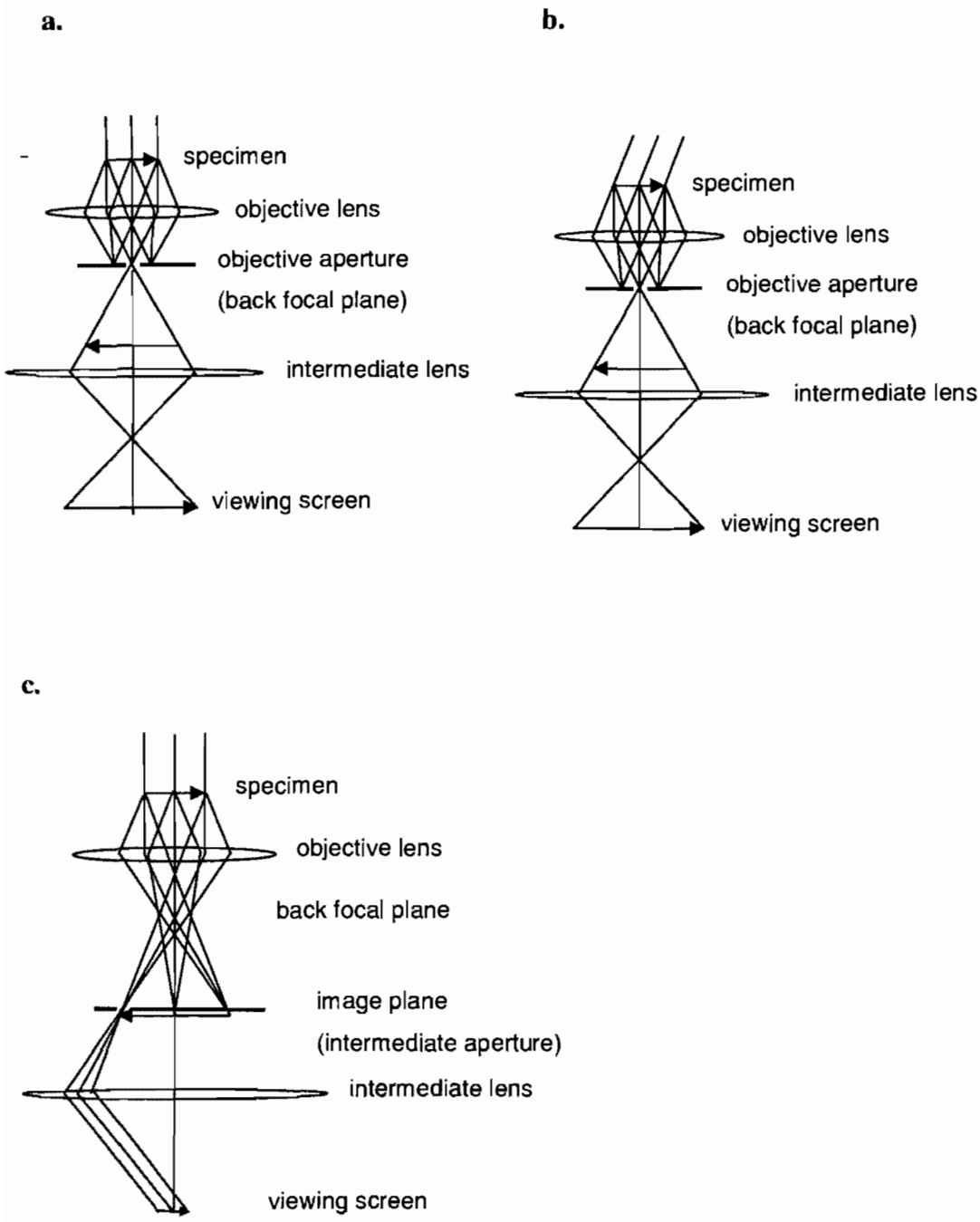

Figure D.4: TEM modes: a. bright-field mode (BF), b. axial dark-field mode (DF), c. selected area diffraction mode.

Due to diffraction, each point on the back focal plane contains all the information about the sample necessary to form an image. If the objective aperture is positioned at a specific point of the back focal plane, a picture formed only from the beams which were diffracted at the same angle is obtained. In this case of a bright-field image (BF) is formed when the aperture is positioned on the axis that only electrons transmitted through the sample would be registered and all the diffracted electrons do not pass the aperture. When the aperture is placed at a different location of the back focal place, only diffracted by a specific angle electrons would participate in image formation, in a case dark-field image (DF) is formed. Thus, diffraction contrast is obtained when the objective aperture is inserted. Both BF and DF images have a strong diffraction contrast. Without the objective aperture the diffracted intensity is combine with the transmitted intensity which leads to grey images with less contrast.

In practice, magnetic lenses are not ideal, so that in the DF mode, the more the rays are tilted from the optical axis, the more inaccurate image produced. Therefore it is advisable to keep the beam parallel to the optic axis when using magnetic lenses. When operating in diffraction mode, this can be achieved by tilting the incident beam, so that the electrons diffracted at a given angle are parallel to the optic axis. The nature of the BF and DF modes leads to the fact that objects appearing dark in the BF mode become bright in the DF mode, and vice versa. This is due to the fact that in the BF mode, only transmitted electrons form the image, so that the object which diffract electrons appears dark. In DF mode only diffracted electrons form the image, correspondingly, the image of the same object appears bright.

For example, heavy elements such as uranium or osmium (in the form of uranyl acetate and osmium tetraoxide) are used for staining, in view of their high ability to absorb electrons.

In addition to the technique of conventional imaging (BF and DF modes), the selective area electron diffraction (SAD) is also very important in TEM. In this mode a second aperture called intermediate aperture is introduced on the image plane of the objective lens. The intermediate aperture allows one to confine the diffraction pattern of a selected area of a specimen. Usually the specimen is observed in the image mode once the region of interest is found, then an intermediate aperture is inserted allowing the examination of the selected area.[16]

TEM is applied in to observe separate structures of micro- and nanoscale. Many research investigations are devoted to the characterization of latexes by TEM. Particularly, aqueous acrylic latexes and their coalescence,[17] rubber particles[18] and the films formed from them[19] have been examined by TEM.

In this study the TEM Leo 922 and Tecnai12 Biotwin equipped with a Morada digital camera of 13k pixels were used for obtaining the images. The images were prepared in the BF mode with negative staining by uranyl acetate. A typical preparation of a TEM sample is described below.

An ethylene – methyl acrylate or ethylene - norbornrne latex with solid content around 5 % was diluted 10 – 100 times with deionized water. Ten drops of this diluted dispersion were mixed with 3 drops of an aqueous solution of uranyl acetate dihydrate (1

wt. %) used as a negative stain agent. One drop of this mixture was placed on a gold or copper grid and dried at room temperature for 24 hours.

Changing the uranyl acetate content from 1 to 6 drops leads to acceptable results with more or less dark background correspondingly. The grid is overstained when the volume ratio of a diluted latex to the stain agent is 1 : 1. The 10 times dilution allows seeing many particles with some possible interactions. The 100 times dilution allows one to image separated particles. The dilution should be increased correspondingly when the solid content of the latex increases.

In order to clean the latex from SDS, the latex can be diluted 10 times and ultrafiltered with membrane Millipore Pellicon XL Ultracell-300k. Five to ten volumes of water containing 0.02 g/L of SDS are necessary for cleaning (the latex can flocculate if deionized water is used). Before examining the sample, sonication of the liquid may be needed in the case of "sticky" polymer particles, which may aggregate (without coalescence), in order to observe separate particles, further dilution of the sample also facilitates the observation of separate particles.

Copper or gold grids can be used. The grid has square holes with axial sizes of 50 – 300 μm. The grids are covered by a Formvar and a carbon layer.

D.4 Light scattering instrumentation

When light propagates through a medium, it mostly propagates into a straight line, however a small fraction of the light is scattered at all angles. The interpretation of the scattered light intensity can be accomplished according two methods. The time averaged distribution of scattered intensity is measured in static light scattering (SLS) while, the dynamic light scattering (DLS), measures the time-dependent scattered intensity is measured. In a continuous medium such as a liquid, the scattering appears when light interacts with objects of refractive index different from that of the liquid. The electromagnetic field of the light induces an oscillating polarization of electrons in the matter. These electrons serve as secondary sources of light and scattering appears.

In SLS, the average intensity of light scattered by a polymer particle at different angles is treated using the Zimm equation:

$$\frac{Kc}{R_\theta} = \left(\frac{1}{M} + 2Bc\right)\left[1 + \frac{16\pi^2 \overline{R}_g^2}{3\lambda^2}\sin^2\left(\frac{\theta}{2}\right)\right] \qquad \text{(D.7)}$$

where

K – optical constant

c – sample concentration

M – weight-average molecular weight

B – second virial coefficient

R_0 – Rayleigh ratio

λ – wavelength of light

θ – angle between light beam and horizontal plane

The major consequences of this equations are:

1) In the limit of $\theta = 0$, the equation reduces to

$$\frac{Kc}{R_\theta} = \frac{1}{M} + 2Bc \qquad (D.8)$$

So that, the interference effect is absent in this case

2) In the limit of $c = 0$, Kc/R_θ is proportional to $\sin^2(\theta/2)$.

3) If both c and θ are equal to 0 then Kc/R_θ equals 1/M

A Zimm plot can be constructed by plotting Kc/R_θ vs. $\sin^2(\theta/2) + c$ with points at different values of θ and c. From the plot, one can retrieve the values of the weight-average molecular weight, the second virial coefficient and radius of gyration of polymer particle.[20]

Practically, it is difficult to build a Zimm plot for polyolefins. However, with the use of on-line light scattering detectors, most of the practical difficulties are alleviated, and SLS can be used as a GPC detector. For most of this work, our industrial collaborator at Rohm and Haas performed the GPC work for us, due to the absence of a functional GPC at high temperature in the Claverie group. The Rohm and Haas GPC was a high temperature Alliance instrument which is not equipped with a SLS. Very recently, the Claverie group has acquired a Viscotek instrument equipped with both a viscometer and a SLS with detectors at two angles (90° and 7°). At an angle of 7°, the aforementioned equation can be exploited to give access to M_w and R_g.

Dynamic light scattering (DLS) allows the determination of the hydrodynamic radius (R_h) of any object, being dissolved or suspended in a continuous medium.[21] Due to the particle Brownian motion of the particles, the scattering intensity fluctuates. In a DLS experiment small fluctuations of the scattered intensity of a coherent and monochromatic light (for example a laser beam) is observed at time intervals τ typically comprised between 10^{-5} and 10^{-2} s, which is directly linked to the Brownian motion. To analyze quantitatively the particle mobility by light scattering, a Van Hove correlation functions $G(\mathbf{r},t)$ is used:

$G(\mathbf{r},t) = \langle n(\mathbf{0},t)n(\mathbf{r}, t+\tau)\rangle_{v,T}$; where $n(\mathbf{r},t)$ is the density of scattering particles in a small volume centered at **r** at time t.

In diluted solutions $G(\mathbf{r},\tau)$ gives the probability of finding a particle at a position **r** at time $t + \tau$ considering that at time t, the particle was at position **0**. The average $< >$ is taken over all the volume and measuring time. $G(r,\tau)$ does not depend on the absolute positions of the vectors **r** and **0**, or on time t, it depends only on the distance $r = |\mathbf{r}|$ and the time interval τ. The correlation function decays exponentially with an increase of time interval τ. The Fourier transform of the correlation function leads to the corresponding dynamic structure factor F :

$$F(q, \tau) = \exp(-Dq^2\tau) \qquad (D.9)$$

where D is the diffusion coefficient and $q = \frac{4\pi n_o}{\lambda}\sin\left(\frac{\theta}{2}\right)$ in which n_o is the refractive index of the continuous medium.

Finally the hydrodynamic radius (R_h) can be obtained from Stokes-Einstein equation:

$$R_h = \frac{kT}{6\pi\eta D} \qquad (D.10)$$

where

R_h – hydrodynamic radius of the particles

k – Boltzmann constant

D – diffusion coefficient

η – solvent viscosity

T – sample temperature

Thus, DLS allows the determination of the hydrodynamic radius of the scattering object provided the temperature, refractive index, and viscosity of the continuous medium are known. The hydrodynamic radius is calculated from the diffusion coefficient and represents a radius of an ideal sphere with the same diffusion coefficient. No specific knowledge about the scattering object is necessary.

The dynamic light scattering experiment should be carried out only with diluted solutions, since the Brownian motion is the process which is registered. When the sample is too concentrated, the interactions between particles may influence the particle mobility, introducing new factors into the theory and complicating the analysis.

The theory presented allows the determination of the diffusion coefficient, and through it, a hydrodynamic radius. Difficulties arise when the sample is polydisperse is size, and is characterized by a distribution of diffusion coefficients and hydrodynamic radii. The mathematical treatment of the correlation function can be mathematically demanding. The software of commercial instruments is not forthcoming about detailing what exact

treatment is applied to the correlation function. The so-called 'cumulant' method makes the assumption that the distribution of hydrodynamic radii is a log-normal distribution. The 'bimodal' method assumes that the distribution is the sum of two log-normal distributions. There exist other calculations such as the CONTIN method, developed by Provencher *et al.*[22] In all cases, a polydispersity index is obtained. This polydispersity index is the normalized variance of the hydrodynamic radius distribution. Thus, for a log-normal distribution, the width of the distribution, σ, is related to the polydispersity via :

$$\sigma = R_{h,average}\sqrt{PDI} \qquad \text{(D.11)}$$

Another difficulty arises for the treatment of polydisperse samples. Indeed, the resulting distribution is an 'intensity' distribution which relates the hydrodynamic radius to the intensity of the scattered light for objects having this hydrodynamic radius. It would be highly preferable to access a weight distribution or a number distribution. The transformation of an intensity distribution into a mass distribution requires information not only on the continuous medium but also on the scattering objects, especially knowledge of their complex refractive index (real and imaginary parts). To our knowledge, very few data exist about complex refractive indices of common polymers. Once again, commercial softwares readily perform this transformation, but without giving any details on how they perform it. A round-robin study has demonstrated that commercial instruments, even with multiangle detection, are not suitable to analyze accurately polydisperse distributions of latexes.[23]

Light scattering experiments are used in many applications for measurements of particle size. There are numerous applications of DLS for the characterization of different latexes, for example, for polystyrene latex,[24] poly(styrene-co-butadiene) latex,[25] acrylic latex and analysis of its aggregation,[26] etc.

D.5 Electrochemical Impedance Spectroscopy

Electrochemical impedance spectroscopy (EIS) is a very sensitive electrochemical technique which detects changes in the state of a coated metal, even when these changes may not be seen. EIS is based on the impedance measurement on a range of frequencies. The concept of resistance appears from Ohm's law:

$$R = V/I; \tag{D.12}$$

where R is the resistance, V is the voltage and I is the current.

In the case of an alternating current the impedance is defined as the complex number $Z = V_{ac}/I_{ac}$. For real systems, when an alternating voltage is applied to the system, the response of the current is not immediate. As a result, if a sine wave of voltage is applied, the current appears also as a sine wave, but shifted due to slow response of the system. In Figure D.5 the two sine waves are shown. As it can be seen from the picture, the shift can be expressed as the phase angle shift or phase angle Θ, considering that all the period of sine wave is $2\pi = 360^{\circ}$. The impedance can be obtained as the ratio of amplitudes

of the two sine waves. Yielding |Z|, which is magnitude of the magnitude of the impedance. To characterize the impedance it is necessary to know |Z| and Θ. The impedance is plotted in polar coordinates (|Z|, Θ), or, it can be expressed as a complex number Z = X + iY, and plotted with Re Z value on the x-axis and Im Z value on the y-axis, where Re Z = |Z| cos Θ,

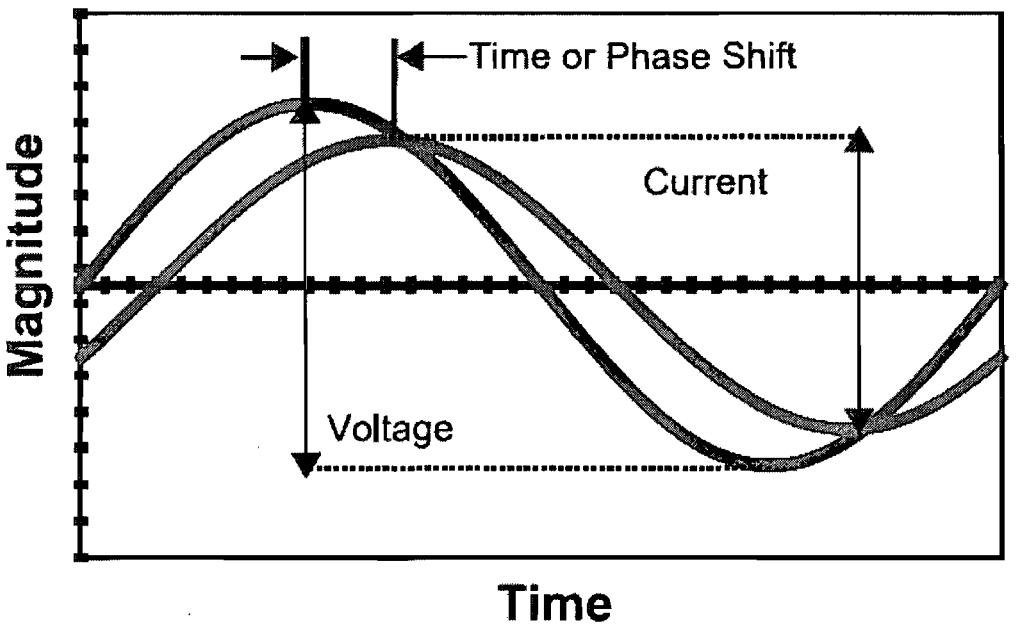

Figure D.5: Current and voltage as a function of time.[27]

and the Im $Z = |Z| \sin \Theta$; Consequently $|Z| = [(\text{Re } Z)^2 + (\text{Im } Z)^2]^{0.5}$ and $\Theta = \arctan (\text{Im } Z/\text{Re } Z)$.

The results of the measurements are usually represented on two plots: the Bode plot and the Nyquist plot. On the Bode plot, the impedance magnitude and the phase angle are plotted against the frequency of alternating current. The Nyquist plot is a plot of Im Z vs. Re Z.

A usual EIS cell contains a reference electrode (Saturated Calomel Reference electrode) and a counter (graphite) electrode. The metal part of the coating is connected to EIS and serves as working electrode.

The electrolyte (usually a NaCl aqueous solution) with two electrodes is placed on the top of the coated sample in the cell body with an area of contact with the coating of 10 – 30 cm^2. For studies of electrical resistance, the behavior of the coatings is modeled by one of several electrical circuits, depending on the condition of the coating (from excellent barrier coating to failed corroded coating),[28] from which one obtains the values of polarization resistance and the double layer capacitance. In the current study, two types of circuits were used (Figure D.6). Circuit a. was used to model a good barrier coating, the circuit b. for a coating in which water diffusion starts to develop.[29] In the first case the system can be represented with a circuit consisting from an uncompensated resistance (R_u) which is the resistance of the electrolyte solution, a polarization resistance (R_p) and a capacitor, the last two are modeling the behavior of the coating. The value of the polarization resistance should be corrected by multiplying by the contact area of the sample with the electrolyte. It is often considered that the lowest limit at which a coating can be

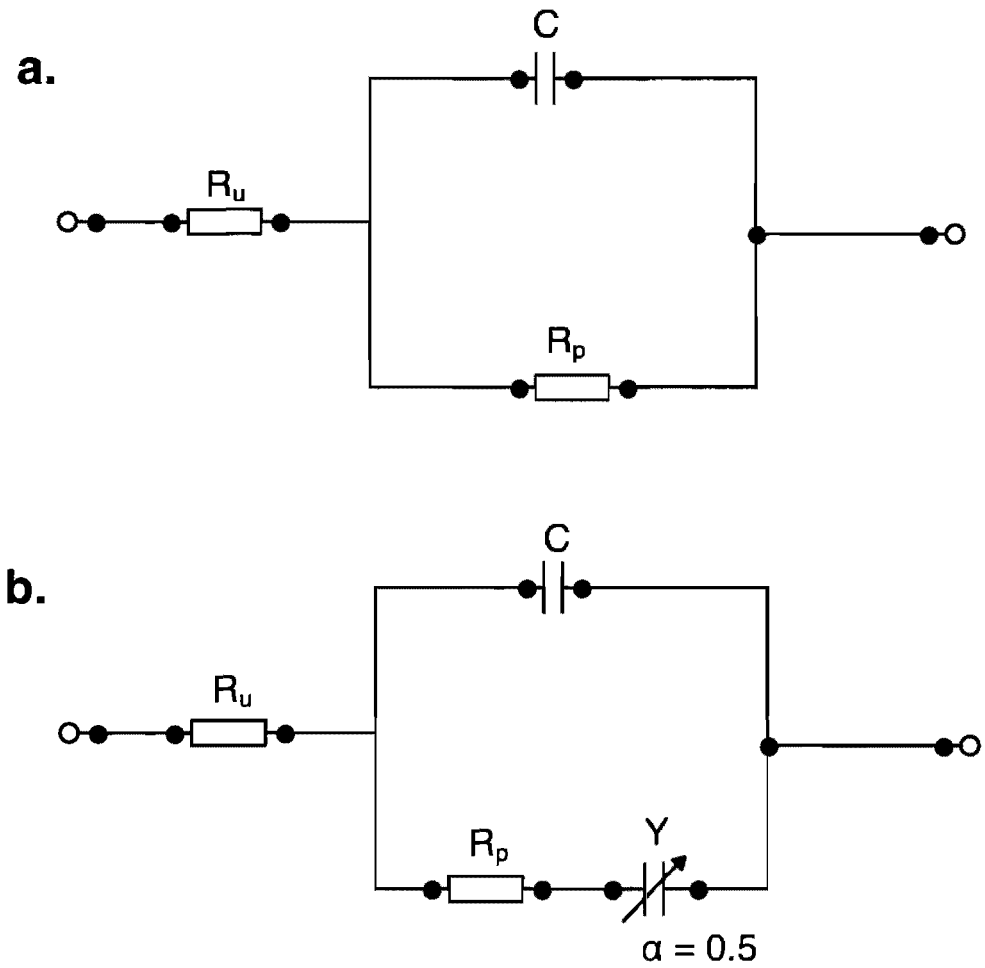

R_u – uncompensated resistance (electrolyte)

R_p – polarization resistance

C – double layer capacitance

Y – Warburg capacitance

Figure D.6: Circuit models for anticorrosion coatings. a. Simple coating. b. A degraded coating in which diffusion of water is occurring.

considered as resistive is $R_p = 1 \cdot 10^6\ \Omega\ cm^2$.[30] The EIS instrumentation can measure accurately very low R_p ($k\Omega\ cm^2$) to very high R_p ($G\Omega\ cm^2$), but cannot exceed the so-called 'open-circuit' resistance which is the resistance of the cell when the electrodes are not connected to the sample (air plays the role of insulator)

When a resistive coating begin to degrade, diffusion of water becomes important, and a Warburg element should be added to the electrical circuit used for the modeling. For resistor, the impedance is equal to the resistance and has only a real component $Z = R$. For a capacitor, the impedance is given by $Z = 1/(i\omega C)$ where C is the capacitance of the capacitor. The impedance of the capacitor has only an imaginary component. A Warburg element is a constant phase element with an impedance of $Z = (1/Y)\ (\omega C)^{-\alpha}$, where Y is the capacitance. The value of α is equal to 1 for a conventional capacitor. For a Warburg element, $\alpha = 0.5$ and the current is shifted by 45° compared to the voltage. Practically, the value of α increases from 0 to 0.5 as diffusion of water through the coating becomes more important.[31] More complex electrical circuit models can be used for coatings on the late stages of degradation, however, the characterization of the coatings which have completely lost their insulator properties is out of the scope of this study.

EIS is used in many applications. The method can as well be applied to the studies of electrochemical devices and processes such as batteries, fuel cells, semiconductors, electrocatalytic reactions, etc.[32, 33]

D.6 References

1. Bovey, F. A.; Mirau, P. A., *NMR of Polymers,* London, **1996**; p 459.
2. Bovey, F. A.; Schilling, F. C.; McCrackin, F. L.; Wagner, H. L. *Macromolecules* **1976,** 9, 76-80.
3. Bovey, F. A.; Mirau, P. A. *Makromolekulare Chemie-Macromol. Symp.* **1990,** 34, 1-16.
4. Hatada, K.; Kitayama, T., *NMR spectroscopy of polymers*. Springer-Verlag: Berlin, **2004**; p 43.
5. Pauli, G. F.; Jaki, B. U.; Lankin, D. C. *J. Nat. Prod.* **2005,** 68, 133-149.
6. Komoroski, R. A.; Maxfield, J.; Sakaguchi, F.; Mandelkern, L. *Macromolecules* **1977,** 10, 550-556.
7. Pauli, G. F.; Jaki, B. U.; Lankin, D. C. *J. Nat. Prod.* **2007,** 70, 589-595.
8. Boller, A.; Okazaki, I.; Wunderlich, B. *Thermochim. Acta* **1996,** 284, 1 - 19.
9. Gan, S. N.; Burfield, D. R.; Soga, K. *Macromolecules* **1985,** 18, 2684-2688.
10. Alizadeh, A.; Richardson, L.; Xu, J.; McCartney, S.; Marand, H.; Cheung, Y. W.; Chum, S. *Macromolecules* **1999,** 32, 6221 - 6235.
11. Henry, F.; Cansell, F.; Guillaume, J. L.; Pichot, C. *Colloid. Polym. Sci.* **1989,** 267, 167 - 178.
12. Tigli, R. S:; Evren, V. *Prog. Org. Coat.* **2005,** 52, 144 - 150.
13. Reading, M.; Elliott, D.; Hill, V. L. *J. Thermal. Anal.* **1993,** 40, 949-955.

14. Bhadeshia, H. K. D. H., *Differential Scanning Calorimetry*. University of Cambridge, http://www.msm.cam.ac.uk/phasetrans/2002/thermal.analysis.html as it is 14th May, 2009.

15. Gill, P. S.; Sauerbrunn, S. R.; Reading, M. *J. Therm. Anal.* **1993,** 40, 931-939.

16. Fultz, B.; Howe, J. M., *Transmission Electron Microscopy and Diffractometry of Materials*. Springer: Berlin, **2001**; p 72.

17. van Tent, A.; te Nijenhuis, K. *J. Colloid Interface Sci.* **2000,** 232 350 - 363.

18. Cornish, K.; Wood, D. F.; Windle, J. J. *Planta* **1999,** 210, 85 - 96.

19. Rippel, M. M.; Leite, C. A. P.; Galembeck, F. *Anal. Chem.* **2002,** 74, 2541-2546.

20. Hiemenz, P., *Principles of colloid and surface chemistry*. Marcel Dekker: New York, 1986; p 223.

21. Schartl, W., *Light Scattering from Polymer Solutions and Nanopartivle Dispersions*. Springler: Berlin, **2007**; p 16.

22. Provencher, S. W. *Comput. Phys. Commun.* **1982,** 27, 229-242.

23. Schneider, M.; McKenna, T. F. *Part. Part. Syst. Charact.* **2002,** 19, 28-37.

24. Eshuis, A.; Harbers, G.; Doorninck, D. J.; Mijnlieff, P. F. *Langmuir* **1985,** 1, 289 - 293.

25. Zhao, J.; Brown, W. *J. Colloid Interface Sci.* **1996,** 179, 255 - 260.

26. Hanus, L. H.; Hartzler, R. U.; Wagner, N. J. *Langmuir* **2001,** 17, 3136 - 3147.

27. Loveday, D.; Peterson, P.; Rodgers, B. *J. Coat. Technol., Coat. Tech.* **2004,** 8, 46-52.

28. Loveday, D.; Peterson, P.; Rodgers, B. *J. Coat. Technol., Coat. Tech.* **2004,** 10, 88-93.

29. Gamry Instruments, Application Note, **2007**, Rev 4.

30. Singh, S. K.; Tambe, S. P.; Raja, V. S.; Kumar, D. *Prog. Org. Coat.* **2007,** 60, 186-193.

31. Loveday, D.; Peterson, P.; Rodgers, B. *J. Coat. Technol., Coat. Tech.* **2005,** 2, 23-27.

32. Conway, B. E.; Bockris, J.; White, R. E., *Electrochemical Impedance Spectroscopy and Its Applications, Modern Aspects of Electrochemistry.* Kluwer Academic/Plenum Publishers: New York, **1999**; vol. 32, pp. 143-248.

33. Grisolia, J.; Assayag, G. B.; Claverie, A.; Aspar, B.; Lagahe, C.; Laanab, L. *Appl. Phys. Lett.* **2000,** 76, 852 - 854.